Distribution Agreement

In presenting this thesis or dissertation as a partial fulfillment of the requirements for an advanced degree from Emory University, I hereby grant to Emory University and its agents the non-exclusive license to archive, make accessible, and display my thesis or dissertation in whole or in part in all forms of media, now or hereafter known, including display on the world wide web. I understand that I may select some access restrictions as part of the online submission of this thesis or dissertation. I retain all ownership rights to the copyright of the thesis or dissertation. I also retain the right to use in future works (such as articles or books) all or part of this thesis or dissertation.

Signature:

_____ _____

James A. Simmons Date

Conformational Exchange: A Common Mechanism for Amyloid Assembly

By

James A. Simmons
Doctor of Philosophy

Chemistry

_____

David G. Lynn, Ph.D.
Advisor

_____

Vince P. Conticello, Ph.D.
Committee Member

_____

Dale E. Edmondson, Ph.D.
Committee Member

Accepted:

_____

Lisa A. Tedesco, Ph.D. Dean of the James T. Laney School of Graduate Studies

_____

Date

Conformational Exchange: A Common Mechanism for Amyloid Assembly

By

James A. Simmons
B.S. Davidson College, 2003

Advisor: David G. Lynn, Ph.D.

An abstract of
A dissertation submitted to the Faculty of the
James T. Laney School of Graduate Studies of Emory University
in partial fulfillment of the requirements for the degree of
Doctor of Philosophy
in Chemistry
2011

Abstract

Conformational Exchange: A Common Mechanism for Amyloid Assembly

By James A. Simmons

Amyloid fibrils cause disease and serve functional roles. The formation of these structures follows an amyloid assembly pathway which involves the aggregation of peptide monomers into oligomers that later transition into β-sheet fibrils. The mechanism responsible for this transition is currently unknown. Using amyloid peptide truncations, the monomeric and assembled states of amyloid fibril formation share a common secondary structure, a polyproline II helix, which is often observed for unordered peptides. This process can occur in the presence of phospholipid membranes. Phospholipid membrane vesicles are used to mimic the peptide oligomers observed during amyloid assembly. Using Aβ(13-21), a peptide derived from the full-length amyloid-β (Aβ) peptide and whose assembly is controllable, the mechanism of amyloid assembly in the context of membranes is shown to occur on the membrane surface. This solvent microenvironment likely mimics that of the oligomer-water interface and strengthens this location as the site that initiates assembly. A novel mechanism for amyloid assembly – conformational exchange – is proposed in which solvent polarity microenvironments dictate a secondary structural change that initiates the formation of amyloid fibrils. This new insight allows thermodynamics and kinetics to control amyloid peptide orientation, registry, and mixing.

Conformational Exchange: A Common Mechanism for Amyloid Assembly

By

James A. Simmons
B.S. Davidson College, 2003

Advisor: David G. Lynn, Ph.D.

A dissertation submitted to the Faculty of the
James T. Laney School of Graduate Studies of Emory University
in partial fulfillment of the requirements for the degree of
Doctor of Philosophy
in Chemistry
2011

Acknowledgements

First, I want to thank Professor David G. Lynn for his guidance during my graduate training. He excitement about and dedication to science is truly inspiring. He gave me the freedom to pursue my own research interests and take my project to places I did not think were possible. He allowed me to make mistake and to learn from them as well. He also took a huge risk my allowing a student with no previous research experience to join his lab and to explore science. I can think critically and independently and have the confidence to face any future challenges. I also would like to thank my committee members, Professor Vince P. Conticello and Professor Dale E. Edmondson. These two professors gave me great advice during my graduate career and always had an open door to speak with me about my research and career.

I want to thank the Drs. James T. Kindt, Fred M. Menger and Khalid Salaita for their suggestions and guidance. Without their knowledge of lipids and phospholipid membranes, my project would not have progressed to this level. I thank Drs. Ricardo Delgado, Bing Wang and Shaoxiong Wu for their help with the NMR experiments. Additional thanks are extended to Dr. Pappannan Thiyagarajan, Dr. Sai Venkatesh Pingali, and Denis Wozniak for their help with the small angle neutron scattering experiments performed at Argonne National Laboratory's (ANL) Intense Pulsed Neutron Source. I also would like to thank Dr. Stefan Lutz for allowing me to work as the Bioanalytical Instruments and AFM Service Instructor.

I especially would like to thank Patti Barnett and Steve Krebs for all the hard work they labored to ensure that my research ran smoothly. I want to also thank Ann Dasher for always having an open door and kind heart. I would also like to thank Jeannette

Taylor and Hong Yi in the Robert P. Apkarian Integrated Electron Microscopy Core Facility for assistance in using the transmission electron microscope.

I am grateful to have worked with numerous people in the laboratory of Professor David G. Lynn. I enjoyed learning from the lab members of this diverse and enriching group. I want to thank you all for the opportunity to enjoy science together. I wish you all the best with your careers wherever they may take you. I want to thank Yi-han Lin and Yue Liu for sharing this journey together. I wish you both the best in life.

I am extremely grateful for Dr. Virginia Shadron. Without her constant support throughout my graduate career, I would not have been able to finish. She has been very supportive and encouraging. I greatly enjoyed our conversations about life, and I value her wisdom dearly. She is truly a lifelong friend and mentor.

I would also like to extend my gratitude to my friends – Shawn Reynolds, Susy Reynolds, Wang Yi, Hailey Dong, Sammy Lee, Erin Schuler, Kevin Yehl, Ashley Bagwell Daugherty and the rest for you. Thank you for the great stories and for sharing your life with me.

Most importantly, I want to thank my family. I am extremely grateful for my father Tommy Simmons, mother Katie Simmons, sister Elizabeth Simmons, grandmother Ocie Wilkie, uncle Fred Wilkie and cousin Carson Wilkie. Thank you for your support, encouragement and love. I am happy to be able to celebrate this time with you all. I am deeply thankful for my wife Yichen Liu. You are my lifelong friend, my protector, my lover, and my inspiration. Thank you for sharing this journey with me. I love you.

List of frequently used abbreviations

Abbreviation	Full name
Aβ	amyloid-β
AFM	atomic force microscopy
APP	amyloid precursor protein
ATR	attenuated total reflectance
Abu	amino butyric acid
CD	circular dichroism
DC	dicapryl
DL	dilauroyl
DLS	dynamic light scattering
DM	dimyristoyl
DO	dioleoyl
DP	dipalmitoyl
DSC	differential scanning calorimetry
ΔG	Gibb's free energy
Fcn	*para*-cyano-phenylalanine
FT-IR	Fourier transform infrared spectroscopy
HEPES	4-(2-hydroxyethyl)-1-piperazineethanesulfonic acid
LUV	large unilamellar vesicle
MES	2-(*N*-morpholino)ethanesulfonic acid
Nle	norleucine
NMR	nuclear magnetic resonance

Nva	norvaline
P_{II}	polyproline II helix
PA	phosphatidic acid
PC	phosphatidylcholine
PE	phosphatidylethanolamine
PG	phosphatidylglycerol
PO	palmitoyl oleoyl
PS	phosphatidylserine
R_g	radius of gyration
SANS	small angle neutron scattering
TEM	transmission electron microscopy
UV	ultraviolet and visible spectroscopy

Table of Contents

List of Figures

List of Tables

Chapter 1

Mechanisms of Amyloid Fibril Formation

1.1 Amyloid Peptide Fibrils – the Good, the Bad, and the Characteristics

Peptide sequences able to form amyloid can serve functional roles in biology. *E. coli* biofilm formation and cell adhesion are assisted by curli fibers (Chapman, Robinson et al. 2002), and fungi produce hydrophobin, an amyloid forming peptide that protects its cell surface (Wosten and de Vocht 2000). *P. anserine* utilizes the [Het-s] prion to aid in heterokaryon incompatibility (Saupe 2007), while Pmel17 assembles into amyloid structures that appear to be required for the synthesis and accumulation of melanin (McGlinchey, Shewmaker et al. 2011). Other amyloid forming peptides, derived directly from human proteins, are associated with human diseases. Amyloidosis diseases, including Alzheimer's, Parkinson's, Huntington's and diabetes mellitus type 2, involve protein misfolding and self-aggregation into amyloid structures (Dong, Canfield et al. 2007; Haataja, Gurlo et al. 2008). The proteins, amyloid-β, α-synuclein, huntingtin, and amylin, involved in these disease states have vastly different sequences yet they all result in the formation of amyloid fibrils. These aggregated structures possess many common features: form fibrils that are 5-10 nm in diameter, bind various histochemical stains (*i.e.*, Congo red, thioflavin T), assemble into structures that cannot be degraded, and consist of stacked pleated β-sheets arranged in a cross-β pattern. The increased prevalence of these amyloid diseases continues to drive scientific interest in this area of research.

The most studied and widespread of these diseases is Alzheimer's disease, which is clinically diagnosed by the progressive loss of neuronal functions involved in memory. The histology of the diseased brain consists of extracellular amyloid plaques and intracellular neurofibirillary tangles. The plaques are composed of amyloid-β (Aβ), which is produced from the sequential cleavage of a single-pass membrane protein labeled APP

(amyloid precursor protein), (Thinakaran and Koo 2008) (Figure 1.1). In non-pathogenic cases, α-secretase cleaves APP producing an extracellular diffusible peptide and an intracellular component that is degraded. In Alzheimer's disease, APP is cleaved by β- and then γ-secretases producing peptide lengths that range between 38-43 amino acids (Thinakaran and Koo 2008). Additional Aβ fragments have been isolated in Alzheimer's disease which consist of *N*-terminal truncations starting at positions 2, 4, 8, 11, and 17 (Seubert, Vigo-Pelfrey et al. 1992; Naslund, Schierhorn et al. 1994; Saido, Iwatsubo et al. 1995; Mattson 1997; He and Barrow 1999). Aβ(1-40) and Aβ(1-42) are the predominant Aβ peptides *in vivo* (Thinakaran and Koo 2008).

Despite the length heterogeneity, Aβ is believed to be the causative agent in neuronal toxicity observed in Alzheimer's disease according to the amyloid hypothesis; however, the precise mechanism of amyloid assembly remains unclear (Bossy-Wetzel, Schwarzenbacher et al. 2004). Aβ toxicity has been linked to membrane pores, metal induced oxidative stress, receptor binding, and membrane leakage (Lashuel, Hartley et al. 2002; Dong, Canfield et al. 2007; LaFerla, Green et al. 2007; Friedman, Pellarin et al. 2009). More recently, Aβ oligomers have emerged as the leading contributory factor of toxicity (Kayed, Head et al. 2003), and it appears that the assembly is associated with the disease state.

1.2 Amyloid Fibril Structural Characterization

Traditionally, amyloid fibrils have been characterized using low resolution approaches due to their large size and non-crystallinity. Transmission electron microscopy (TEM) and atomic force microscopy (AFM) reveal the presence of the fibril structure and

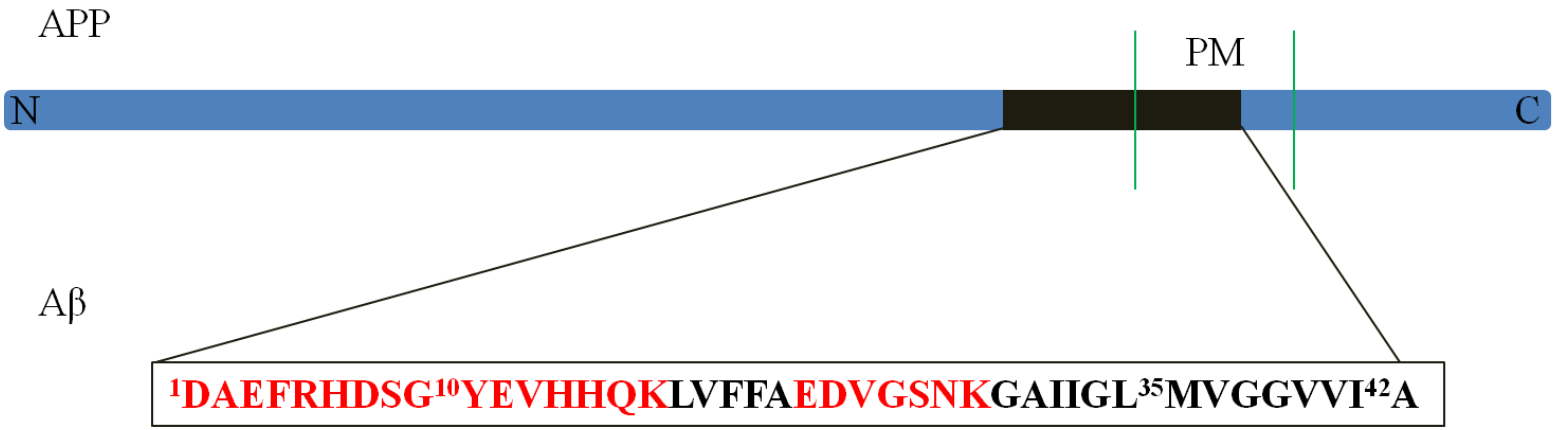

Figure 1.1 Aβ presented as the single letter code with the approximate placement in the plasma membrane (PM).

provide a precise measurement of the fibril dimensions. Circular dichroism (CD) and Fourier transform infrared spectscopy (FT-IR) provide information about the β-sheet secondary structure. Diffraction techniques have offered information about the cross-β fold, establishing that the β-strands (5 Å apart) form β-sheets that run parallel to the fibril length and these sheets (10 Å apart) laminate perpendicular to the fibril length giving the fibril width/height. The same structural characteristics have been reported for many different amyloid fibrils; however, high resolution fibril structures have been difficult to solve due to the aforementioned amyloid properties – precipitation and non-crystallinity.

By manipulating several experimental conditions, higher resolution structures of amyloid fibrils has been published over the past fifteen years. This has predominately been performed using synthetically derived full-length and truncated Aβ peptides that assemble into fibrils which are similar in every aspect to *ex vivo* fibrils. The first structurally characterized amyloid structure was obtained for Aβ(10-35) (Benzinger, Gregory et al. 1998; Burkoth, Benzinger et al. 2000) (Figure 1.2). This structure, determined using DRAWS which is a solid-state NMR (ssNMR) experiment, consists of parallel in-register extended β-sheets, which were previously thought to be anti-parallel. The structure of Aβ(1-40) fibrils has since been solved (Petkova, Ishii et al. 2002). These fibrils consist of individual peptides that possess two stretches of β-sheets that are connected by a turn. Continued truncations of these Aβ peptides again produce amyloid fibrils that display the same structural, histochemical, and toxic characteristics as the longer counterparts. These similarities in the secondary structure of the fibril structures and the fact that many peptides form similar amyloid fibrils suggest that amyloid assembly may be governed by a similar mechanism.

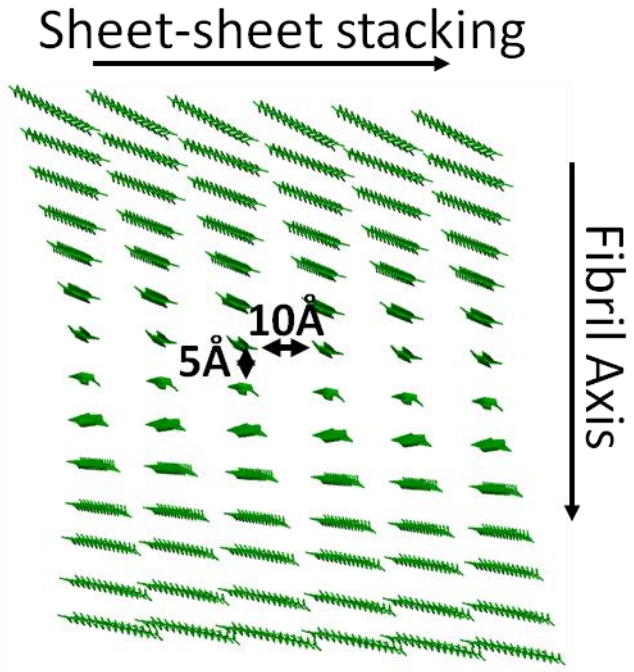

Figure 1.2 Structural model for Aβ(10-35).

1.3 Amyloid Fibril Formation – Kinetic Mechanisms

The amyloid assembly mechanism is unknown. However, the rate of assembly has been studied by several groups. Because seeding experiments have been shown to accelerate fibril formation, it is currently proposed that amyloid fibril assembly begins with unordered monomeric peptides that self-assemble in a nucleation-dependent manner. This mechanism is believed to result from the formation of a nucleus. This species is the smallest assembled structure that promotes β-sheet formation. In these assembly mechanisms, it is commonly postulated that the formation of the nucleus is rate limiting (initiation) while fibril growth is rapid (propagation). Investigating the exact mechanism for amyloid initiation has proven difficult, however several models have been proposed.

The proposed kinetic models are as follows in order of literature appearance: 1) Templated Assembly (TA), 2) Monomer-Directed Conversion (MDC), 3) Nucleated Polymerization (NP), 4) Nucleated Conformational Conversion (NCC), and 5) Off-Pathway Micelle Model (OPMM) (Figure 1.3A-E). All of these mechanisms share two different peptide structures – unassembled (U) and assembled (A) peptide conformations. In the TA mechanism, the A fibril structure templates a U to A conformational conversion, which is rate-limiting (Griffith 1967; Uratani, Asakura et al. 1972). For MDC, U peptides convert into an A state conformation which then assembles (Prusiner 1982). This conversion is again rate-limiting. Model 3 (NP) entails the coexistence of U and A conformations which exist at an equilibrium state shifted towards the U conformation making the A state extremely rare (Jarrett and Lansbury 1993). The A state conformation is stabilized by forming a nucleus which is rate-limiting. The next two mechanisms involve the formation of micelle-like structures that are either on-pathway or

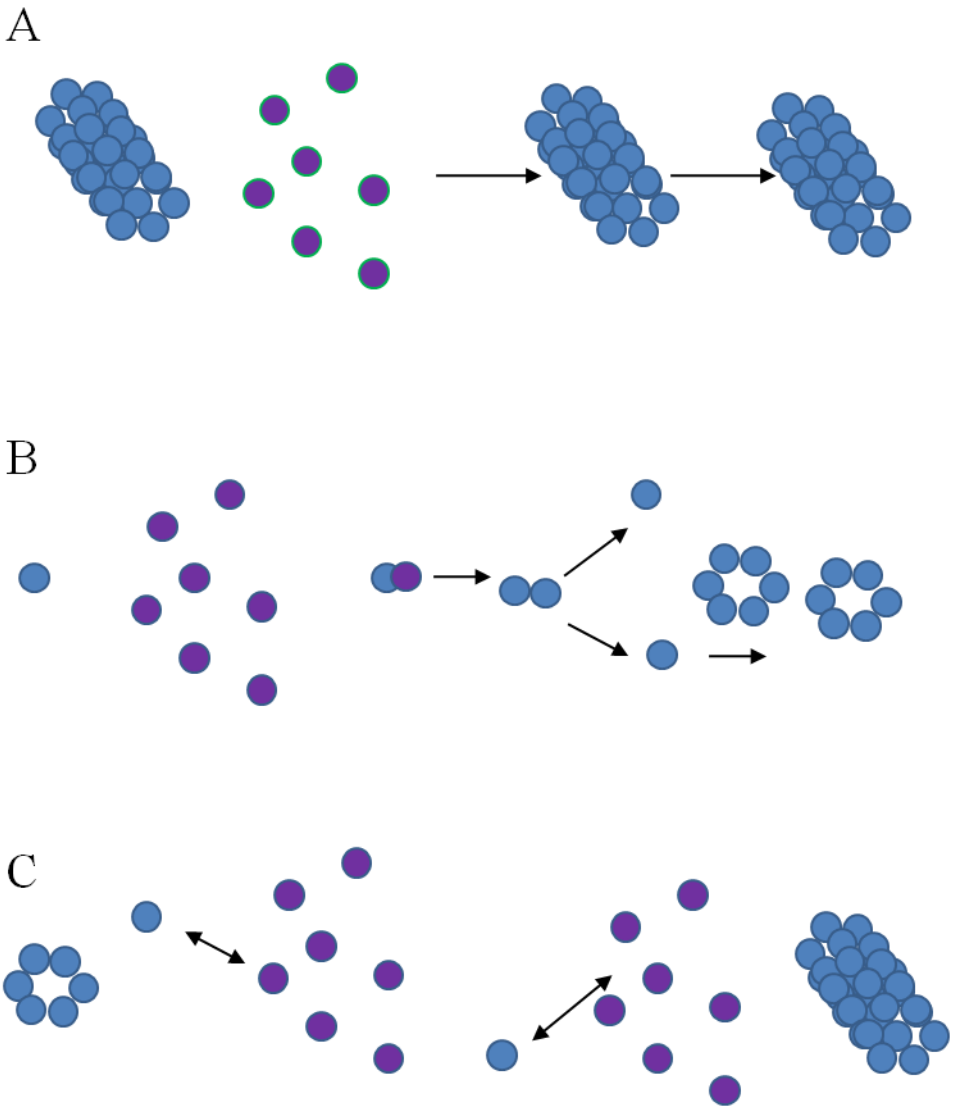
A
B
C

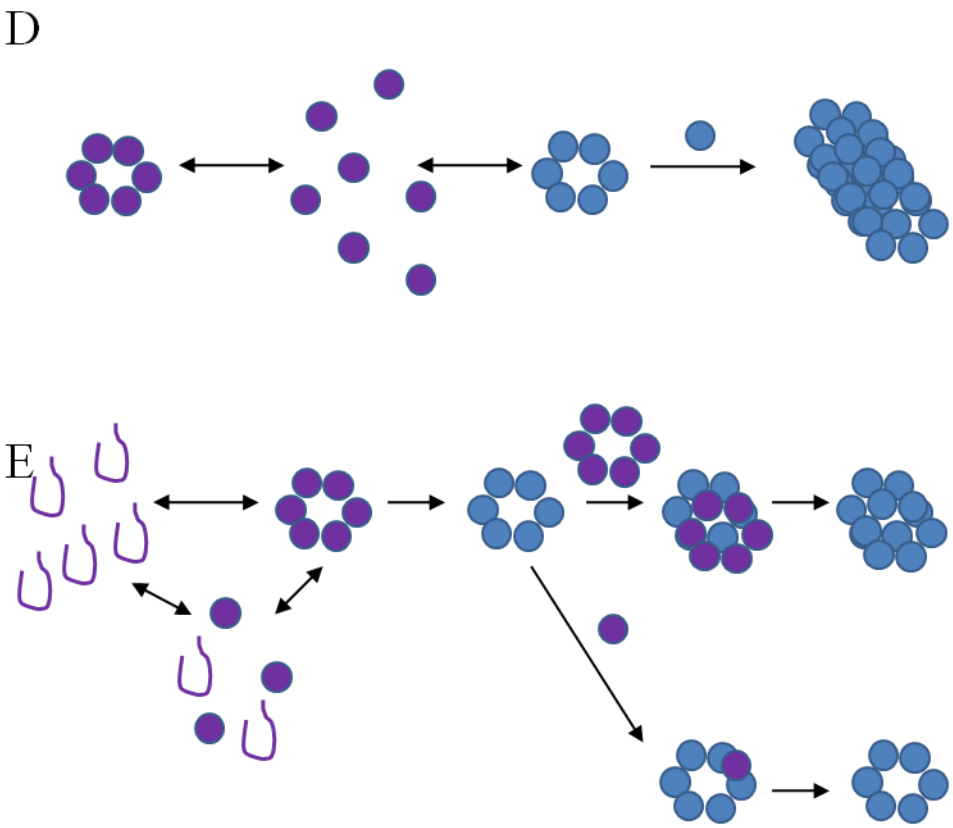

Figure 1.3 Proposed Kinetic Mechanisms for Amyloid Assembly. A) Templated Assembly, B) Monomer-Directed Conversion, C) Nucleated Polymerization, D) Off-pathway Micelle Model, E) Nucleated Conformational Conversion. Blue circle = aggregated conformation, Purple circle = unassembled conformation.

off-pathway. In NCC, U monomers and U aggregates exist in solution with the formation of an A nucleus stemming from the conformational conversion of a U aggregate thereby forming an A aggregate (Serio, Cashikar et al. 2000). Fibril growth proceeds via addition of U monomers to A aggregates or the fusion of A aggregates with other A aggregates. In this mechanism, the A state aggregate possesses micelle-like properties and therefore is on-pathway. Conversely, the micelle-like structures for the OPMM are off-pathway (Souillac, Uversky et al. 2002). This mechanism also has U monomers and U aggregates in equilibrium; the A aggregate gives rise to the nucleus which forms by the addition of U monomers that subsequently change conformation with the U aggregates being off-pathway. These kinetic models suggest that a rate-limiting step is dictating amyloid assembly. These mechanisms suggest that there are independent assembly mechanisms for amyloid formation; however, similar structures are formed during the assembly (*i.e.*, oligomers, fibrils) which suggests there may be a common assembly mechanism.

1.4 Amyloid Fibril Formation – Thermodynamic Mechanism

Even though the kinetic models above do not suggest a common mechanism for amyloid assembly, the presence of oligomeric species has been observed across a wide range of amyloid forming peptides (Harper, Wong et al. 1999; Kowalewski and Holtzman 1999; Serio, Cashikar et al. 2000; Parbhu, Lin et al. 2002; Poirier, Li et al. 2002; Kim and Lee 2004). The binding of an oligomeric specific antibody to oligomers composed of different amyloid peptides has been shown (Kayed, Head et al. 2003). This result suggests that the oligomer structure is similar even when it is composed of different amyloid peptides. But, the oligomer structure and it role in assembly remain unknown.

The formation of oligomers is believed to stem from the hydrophobic collapse of monomeric peptides in solution, a process governed by thermodynamics. They have been detected by AFM and TEM, and experiments have been shown them to be composed of a wide range of peptide monomers (Santini, Wei et al. 2004; Bernstein, Dupuis et al. 2009; Eichner and Radford 2009; Ahmed, Davis et al. 2010; Smith, Radford et al. 2010; Matsumura, Shinoda et al. 2011). Then through an unknown mechanism, amyloid peptides undergo a conformational change from an unordered peptide (U) to form an amyloid fibril (A). Literature precedence suggests that this conversion involves the oligomeric structure (Ahmed, Davis et al. 2010); however, a recent report suggests that this conformational change does not involve the oligomer, which is believed to be an off-pathway species (Lee, Culyba et al. 2011). Clearly, the role of the oligomer is amyloid assembly is unresolved, but their presence among all amyloid forming peptides suggests they play a role in amyloid assembly.

1.5 Aβ Interactions with Phospholipid Membranes

Since the human body is composed of cells encapsulated by the plasma membrane and contains numerous membrane organelles, amyloid peptides are produced in an environment in which they are constantly exposed to phospholipids. The phospholipid membrane is often ignored with respect to amyloid fibril formation. However, amyloid peptides can interact with membranes, and these associations may compromise cellular function.

Two types of peptide-membrane associations have been reported – surface and hydrophobic (Murphy 2007). Surface association places the peptide at the membrane-

water interface. The peptide may also insert in the lipid tail environment. And, different conformations have been reported for both associations. The potential for various peptide-membrane associations requires a detailed investigation of the role membranes play in amyloid assembly.

Added to the two types of membrane associations, the two conformational (U vs. A) and aggregational (monomer vs. aggregate) states make deciphering the peptide-membrane interactions difficult thus clouding our understanding of the influence membranes have on the assembly of amyloid peptides. Peptide monomers and aggregates can bind to membranes, and aggregates were shown to bind irreversibly to membranes at a slow rate while monomers display a quick reversible membrane binding (Kremer and Murphy 2003). Additionally, amyloid oligomers potentially possess a hydrophobic domain that promotes membrane association and that fibrils do not have such domains (Kremer, Pallitto et al. 2000).

Interestingly, phospholipid membranes have been shown to affect the kinetics of amyloid fibrils assembly, and membranes are even believed to be a necessary component for accelerated fibril growth (Cox, Sing et al. 2006). However, lipid membranes may also inhibit fibril assembly (Sharp, Forrest et al. 2002). In other reports, lipids shift the assembly rate constants (Sabate, Gallardo et al. 2005), and it has been proposed that insertion of the amyloid peptide into a hydrophobic environment slows or inhibits assembly while a surface association may hasten fibril formation (Bokvist, Lindstrom et al. 2004). However, these amyloid peptides were mixed with the phospholipid mixtures before vesicle preparation, thereby completely changing the environment under which the peptide is exposed and drastically altering the assembly and/or conformation (Figure 1.4).

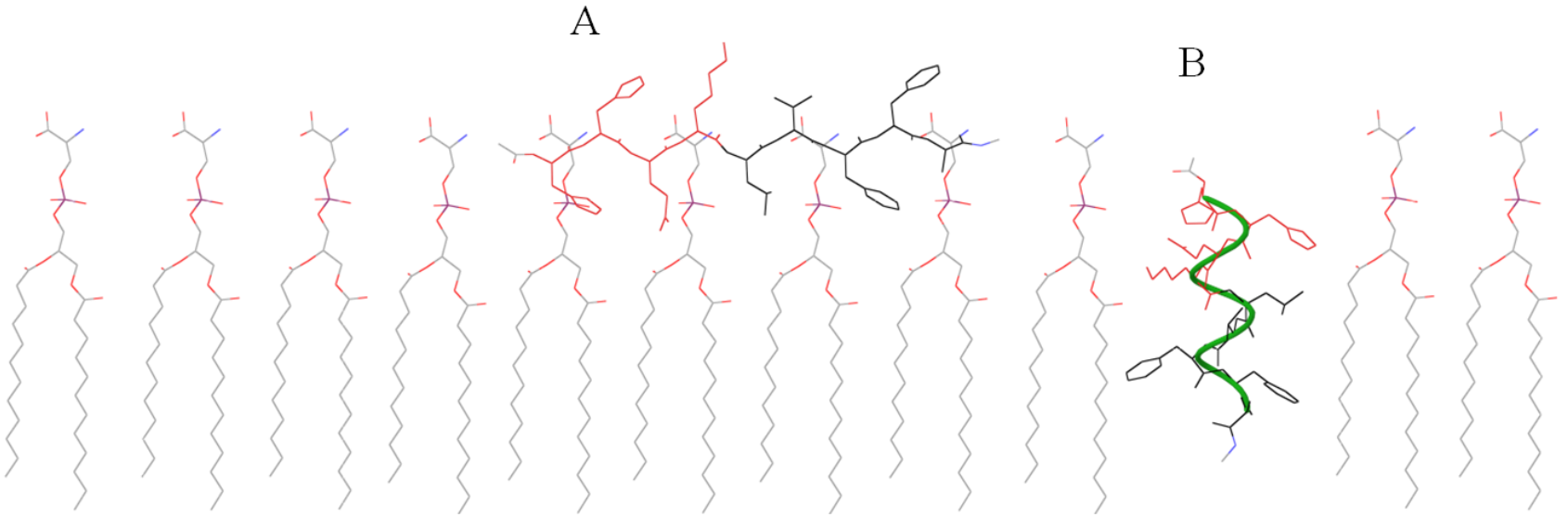

Figure 1.4 Proposed Amyloid-Membrane Associations. A) Membrane-water interface association suggests β-sheet, B) Hydrophobic association via insertion with a helical structure proposed.

Because a dynamic interplay between the peptide and the membrane often exists, it has been shown that the composition of the membrane can have drastic effects on peptide location, secondary structure, and assembly. The amount of cholesterol in the membrane can dictate Aβ-membrane association. At high cholesterol concentrations, Aβ inserts into the membrane and adopts a helical structure while Aβ remains associated with the membrane surface at low cholesterol concentrations (Ji, Wu et al. 2002). Additionally, membrane and peptide charge have been shown to dictate these dynamic interactions (Volles, Lee et al. 2001).

1.6 Summary

Amyloid peptides assemble into fibrils that share a common structure – the cross-β fold. The existing literature suggests that this process is controlled either though different assembly mechanisms or even through a common assembly mechanism that accesses very different phases. Structural models have offered insight into fibrillogenesis, but the mechanism of fibrillogenesis remains elusive. Using a combination of truncated amyloid-β peptides and phospholipid membranes, this dissertation aims to decode the amyloid assembly mechanism.

Chapter 2

Characterization of an Unassembled Amyloid Derived Peptide Monomer: Aβ(13-21)

2.1 Introduction

The self-assembly propensity of amyloid-forming peptides complicates a detailed study of the pathway because the starting point cannot be definitively controlled by experimentation (Gorman and Chakrabartty 2001). Added to this lack of control is that initiation is thought to occur in a heterogeneous fashion through random events (Dos Santos, Chandravarkar et al. 2005). A third limiting factor often observed during amyloid formation is precipitation of the amyloid structure (Hill, Miti et al. 2011). Despite the inherent difficulties in deciphering the mechanism of amyloid assembly, researchers still attempt to define the different events that promote this process by manipulating experimental conditions and synthesizing peptides with amino acid substitutions or truncations that can be exploited to probe the pathway (Lu, Jacob et al. 2003; Dong, Canfield et al. 2007).

Broadly, all amyloid assembly mechanisms proceed through two steps – initiation and elongation. Initiation is the event that promotes the structural conversion into a β-sheet-like nucleus. Elongation simply refers to the further templated growth of the amyloid structure. Assembly mechanims begin with unassembled peptide monomers and end with amyloid structures, which are commonly fibrils but can also be sheets, ribbons, or tubes (Figure 2.1), all of which are characterized as having a high content of pleated, β-sheets arranged in a cross-β orientation and possessing an affinity for Congo red (Gorman and Chakrabartty 2001; Lu, Jacob et al. 2003; Dong, Canfield et al. 2007; Childers, Mehta et al. 2009). Amyloid fibrils are generally considered to have fibril diameters of 5-10 nm. The progression towards amyloid structures from peptide monomers has been heavily

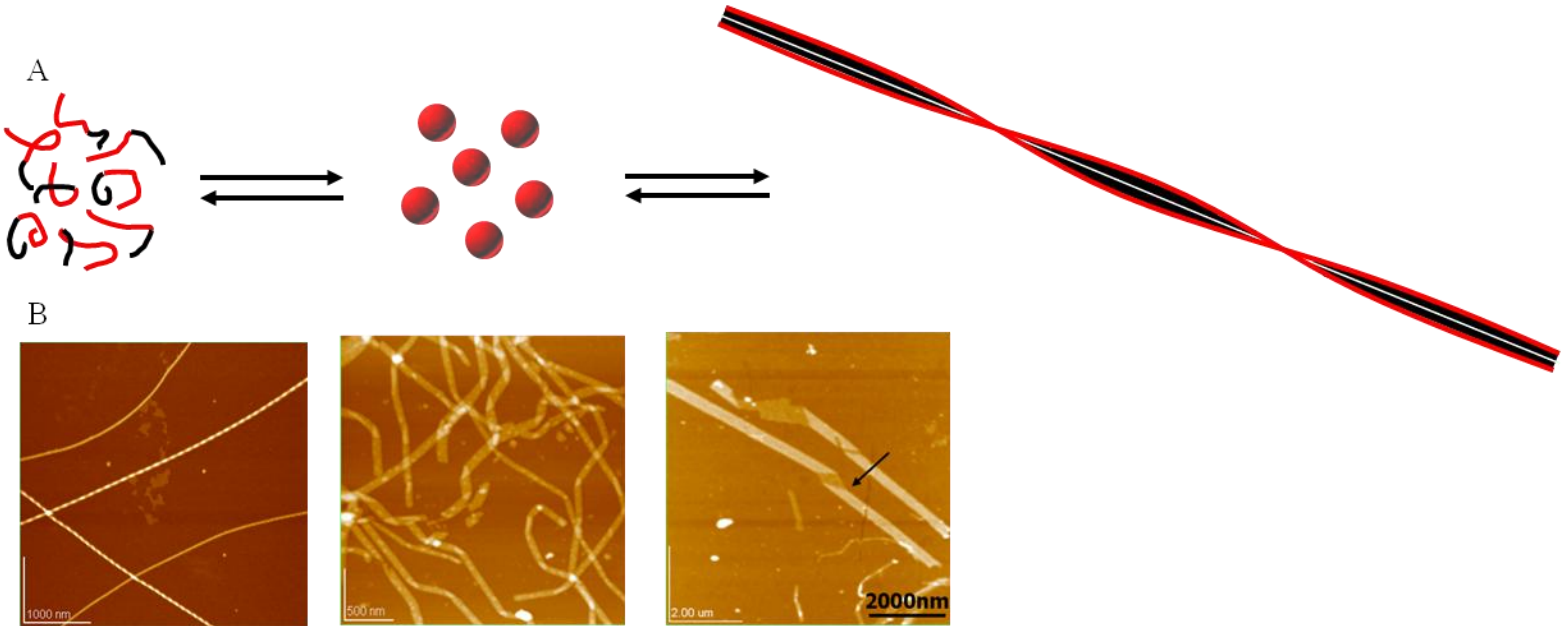

Figure 2.1 Amyloid Assembly Pathway. A) Simplistic model for amyloid assembly proceeds from peptide monomers through oligomeric micelle-like intermediates (oligomers) to fibrils. B) Representative structures accessible to Aβ(13-21)K161A, an amyloid forming peptide, imaged by AFM – left: fibrils in the absence of Zn^{2+}, middle: sheets and ribbons in the presences of Zn^{2+}, right: nanotubes in the presence of Zn^{2+}.

debated for decades (Griffith 1967; Uratani, Asakura et al. 1972; Prusiner 1982; Jarrett and Lansbury 1993; Serio, Cashikar et al. 2000; Souillac, Uversky et al. 2002).

In this lab, the formation of amyloid structures has been probed using peptide truncations, substitutions, time, temperature, pH, and metals – all of which are believed to affect initiation and/or elongation (Lu, Jacob et al. 2003; Dong, Canfield et al. 2007). Still, the main limiting factor that is difficult to control in the self-assembly pathway is initiation. To thoroughly investigate the pathway of amyloid assembly, the following conditions must be met: 1) the peptide should remain in an unassembled state, 2) this state must be fully characterized, 3) an initiation event capable of starting the assembly is required, and 4) the mature amyloid structure needs to be characterized. In this chapter, conditions 1 and 2 are addressed and is placed in context of the subsequent steps.

2.2 Results and Discussion

2.2.1 Structural Analysis of Aβ(13-21) with CD

Amyloid assembly is thought to be influenced by physical properties that shift equilibrium constants (O'Nuallain, Thakur et al. 2006). Concentration is known to shift equilibrium constants according to Le Chatelier's principle. To test the effect of concentration on Aβ(13-21) assembly, the peptide was monitored at 1 mM concentrations in 25 mM HEPES pH 7.5 at room temperature by circular dichroism (CD). The 1 mM samples show a negative ellipticity at 195 nm and a positive ellipticity at 220 nm (Figure 2.2A). This CD signature has recently been assigned to a polyproline II helix (P_{II}) (Rucker and Creamer 2002; Shi, Chen et al. 2006; Shi, Chen et al. 2006).

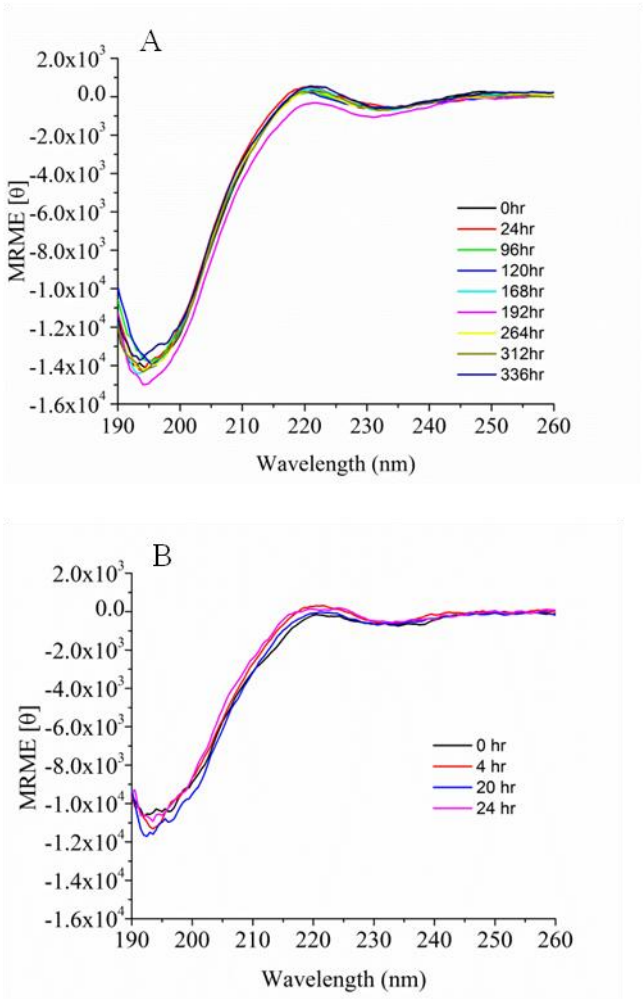

Figure 2.2 CD Spectra of Aβ(13-21) Wild-type. A) Aβ(13-21) – 1 mM, B) Aβ(13-21) – 0.5 mM. All samples were prepared in 25mM HEPES at pH 7.5.

Aβ(13-21) was studied at lower concentrations as well and the peptides do not assemble at 0.5 mM and below (Figure 2.2B). The CD spectra at 0.5 mM have the same characteristics as the 1 mM sample, but with less intensity due to the lower concentration.

2.2.2 Effects of pH on Aβ(13-21)

The charge carried by the peptide melittin is known to affect its aggregation (Bello, Bello et al. 1982). Since Aβ(13-21) contains several protonatable residues (H13, H14, K16), pH could potentially affect the assembly of this peptide. In order to understand the impact charge has on amyloid assembly, Aβ(13-21) was evaluated at various pH values above and below the pK_a values of these protonatabled residues.

To address the effect of protonating the histidine residues, CD spectra of Aβ(13-21) at 1 mM in 25 mM MES pH 5.5 were acquired. The CD spectra of this sample have a negative minimum at 195 nm and a positive maximum at 220 nm (Figure 2.3A). The pH 5.5 sample has a stronger negative ellipticity at 195 nm and a stronger positive ellipticity at 220 nm (Figure 2.3B), most characteristic of an unassembled peptide, and the peptide conformation at these two pH units is nearly identical. Therefore, the protonation states of these two histidine residues (H13 and H14) do not affect the global secondary structure of Aβ(13-21). The observed spectral changes, however, do most likely reflect the percentage of the P_{II} conformation, but, this percentage is difficult to estimate on CD alone (Shi, Chen et al. 2006).

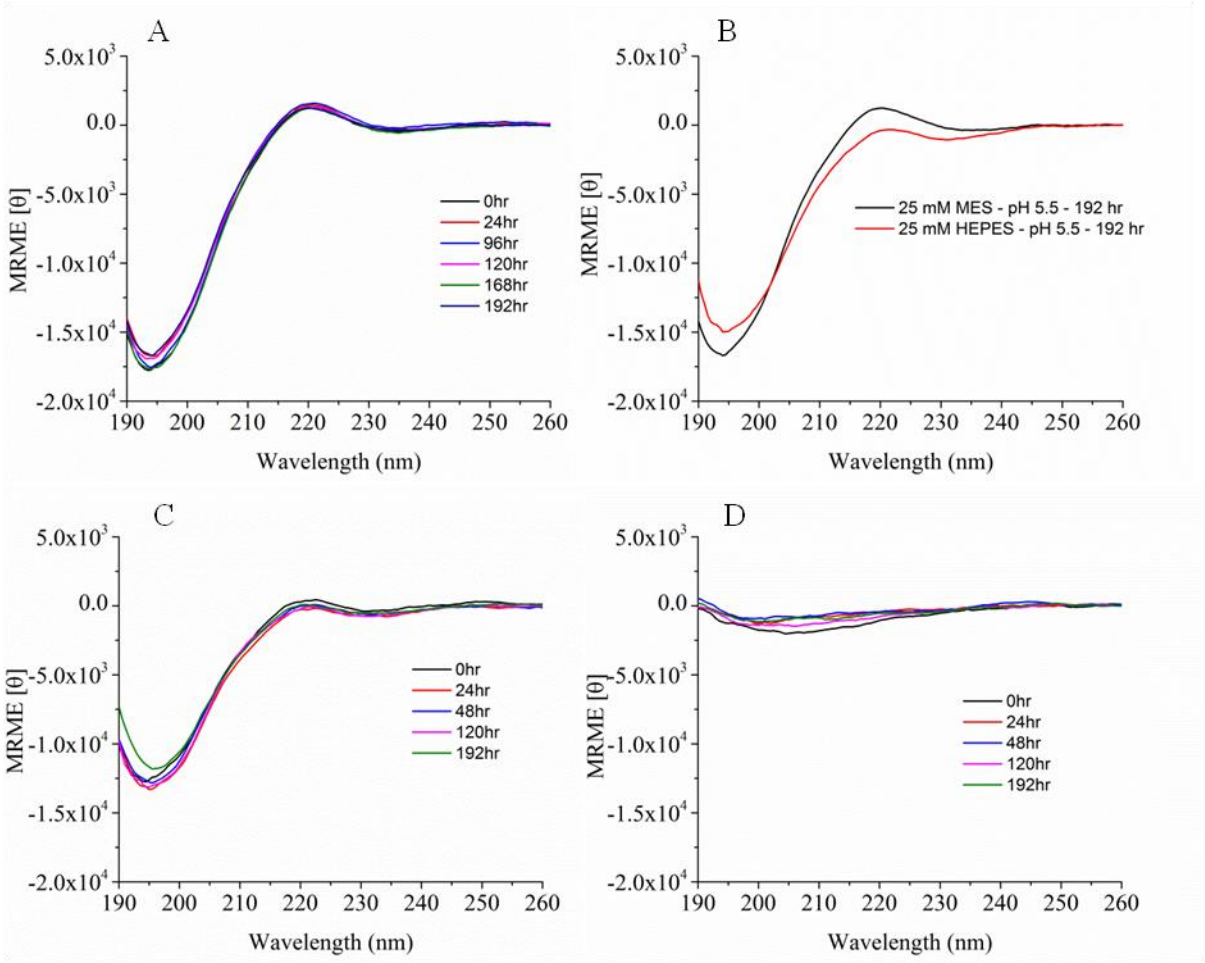

Figure 2.3 Effects of pH on Aβ(13-21). A) CD spectra of Aβ(13-21) – 1 mM in 25 mM MES at pH 5.5, B) Overlay of Aβ(13-21) CD spectra in 25 mM HEPES at pH 7.5 (black) and 25 mM MES at pH 5.5 (red), C) CD spectra of Aβ(13-21) - 1 mM in 25 mM CAPS at pH 9.5, D) CD spectra of Aβ(13-21) – 1 mM in 25 mM CAPS at pH 11.5.

Since the *N*-terminus is not acetylated and the sequence contains a lysine residue, Aβ(13-21) was subjected to pH values of 9.5 and 11.5 in 25 mM CAPS buffer. At pH 9.5, the CD spectra of Aβ(13-21) are consistent with spectra at pH 5.5 and pH 7.5 (Figure 2.3C). At pH 11.5, the sample precipitated due to *N*-terminus and lysine side chain deprotonation leaving the peptide completely uncharged (Figure 2.3D).

2.2.3 Structural Analysis of Aβ(13-21) with FT-IR

Fourier-transform infrared spectroscopy (FT-IR) also probes the secondary structure of proteins, and the amide backbone has several distinct transitions that are commonly used to analyze protein structure (*i.e.*, amide I region, amide II region). The most common frequencies used for protein structural analysis is the C=O stretch (1600-1700 cm^{-1}). Typical stretching frequencies for the commonly assigned secondary structure are 1620-1640 cm^{-1} (β-sheet), 1644 cm^{-1} random coil, and 1650-1658 cm^{-1} (α-helix) (Haris and Severcan 1999).

FT-IR spectra of Aβ(13-21) in two different buffers (25 mM HEPES, pH 7.5; 25 mM MES, pH 5.5) were acquired to investigate secondary structure. Several transitions stand out in the pH 7.5 spectrum (Figure 2.4A). The ~1673 cm^{-1} band has been assigned to trifluoroacetate, which is used for peptide cleavage as well as HPLC purification (Roux, Zekri et al. 2008). The two other transitions present in the spectrum at 1650 cm^{-1} and 1643 cm^{-1} can be assigned as random coil and either -OH bending, helical structures, and random coil, respectively (Bruque, Martinez-Lara et al. 1987; Haris and Severcan 1999; Torrent, Rubens et al. 2001). The same transitions are also present in the pH 5.5 sample

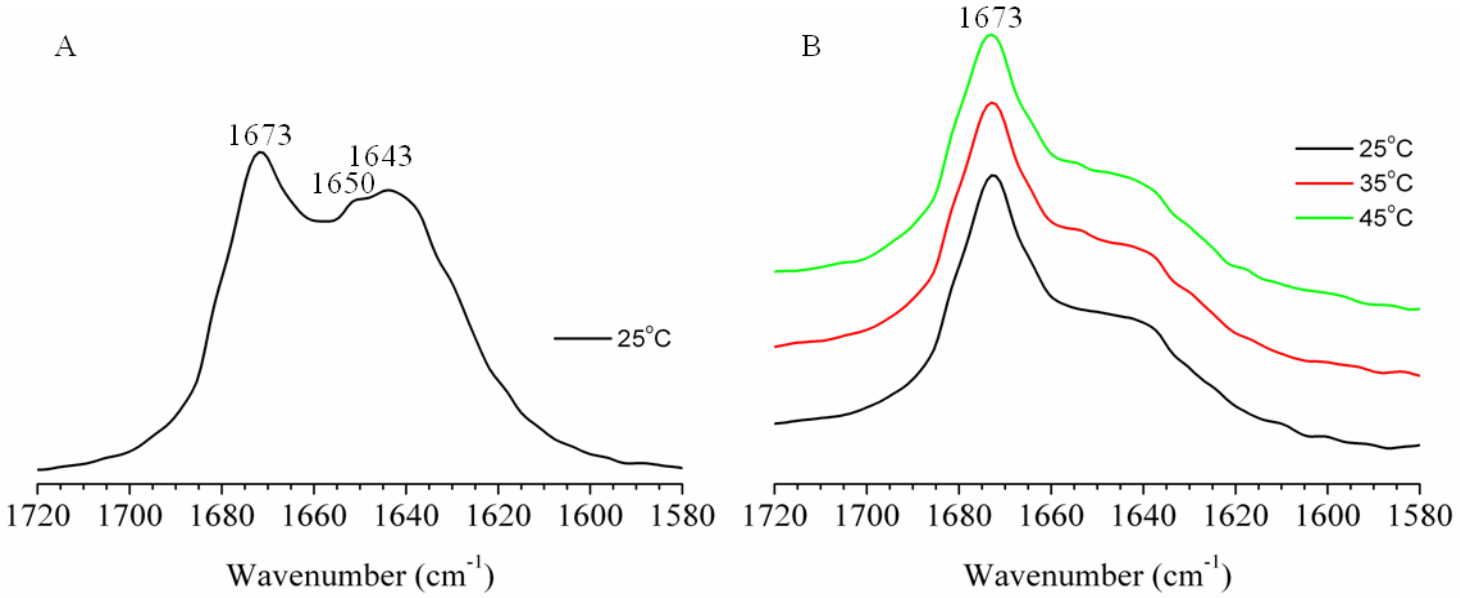

Figure 2.4 Structural analysis Aβ(13-21) using FT-IR. A) FT-IR spectra of Aβ(13-21) – 5 mM in 25 mM HEPES at pH 7.5 – 0 hr, B) FT-IR spectra of Aβ(13-21) – 5 mM in 25 mM MES at pH 5.5 – 0 hr. (temperatures as indicated)

although the stretching frequencies for the protein conformation are not as clearly resolved (Figure 2.4B).

2.2.4 Effects of Temperature on Aβ(13-21)

Temperature has been shown to have differing effects on peptide assembly (Wright and Conticello 2002; Kim, Hardcastle et al. 2006; Lu 2006; Childers 2010). To determine the influence temperature, Aβ(13-21) at 0.5 mM in 25 mM HEPES was followed by CD for 24 hours at different temperatures (Figure 2.5). Temperatures of 35 ^{o}C and 55 ^{o}C do not promote assembly, consistent with the IR data (Figure 2.4B).

Although the change in temperature did not promote the assembly of Aβ(13-21), temperature increases did alter CD ellipticity. Increasing the temperature from 1 ^{o}C to 65 ^{o}C increased ellipiticity at ~195 nm and decreased ellipticity at ~220 nm (Figure 2.6A). Subtraction of the spectrum at 1 ^{o}C from the spectrum at 65 ^{o}C results in a net β-sheet signature (Figure 2.6B). This CD spectral change supports the existence of a P_{II} conformation existing in solution (Shi, Olson et al. 2002; Shi, Chen et al. 2006; Shi, Chen et al. 2006).

2.2.5 Structural Analysis of Aβ(13-21) with NMR

The relatively low molecular weight of Aβ(13-21) makes this peptide amenable to solution NMR studies (Jacobsen 2007). The amide protons of Aβ(13-21) in the 1D spectrum are all between 7.8 ppm and 8.4 ppm at 25 ^{o}C (Figure 2.7A), most consistent

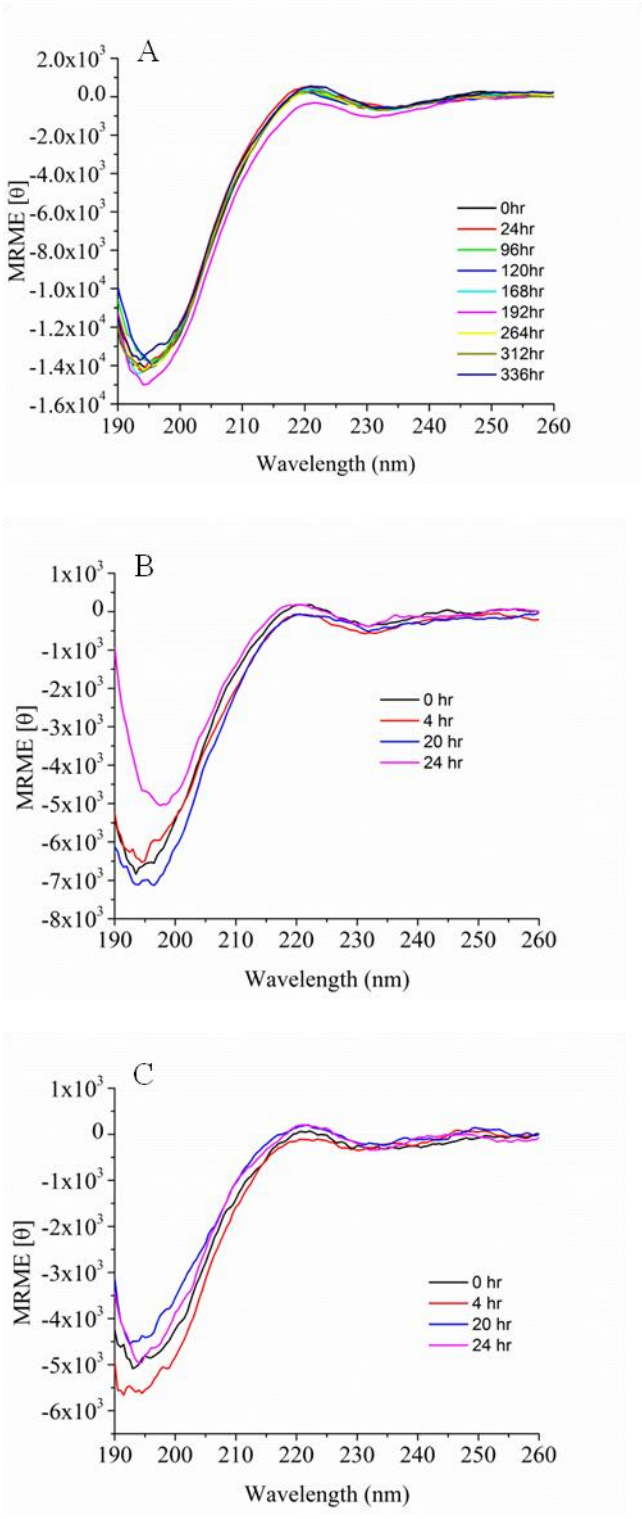

Figure 2.5 Effects of Temperature on Aβ(13-21). A) CD spectra of 1 mM Aβ(13-21) – room temperature, B) CD spectra of 0.5 mM Aβ(13-21) – ~35 ^{o}C, C) CD spectra of 0.5 mM Aβ(13-21) – ~55 ^{o}C. All spectra in 25 mM HEPES pH 7.5.

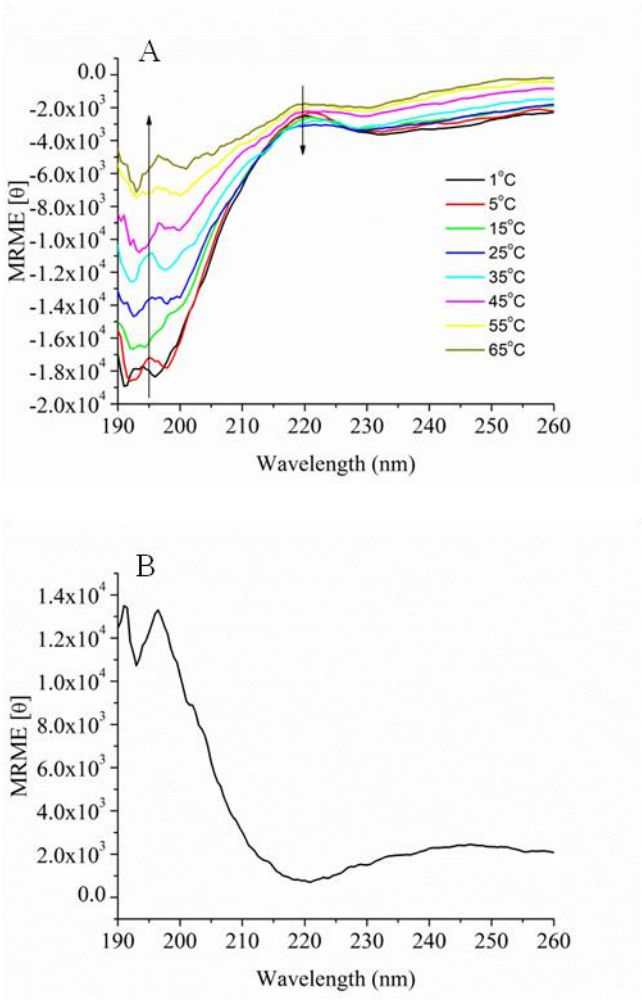

Figure 2.6 Thermal Melting of Aβ(13-21) Followed by CD. A) Differential temperature CD spectra of 1 mM Aβ(13-21), B) Difference spectra of 1 mM Aβ(13-21) at 65 ^{o}C and 1 ^{o}C. Buffer conditions are 25 mM HEPES pH 7.5.

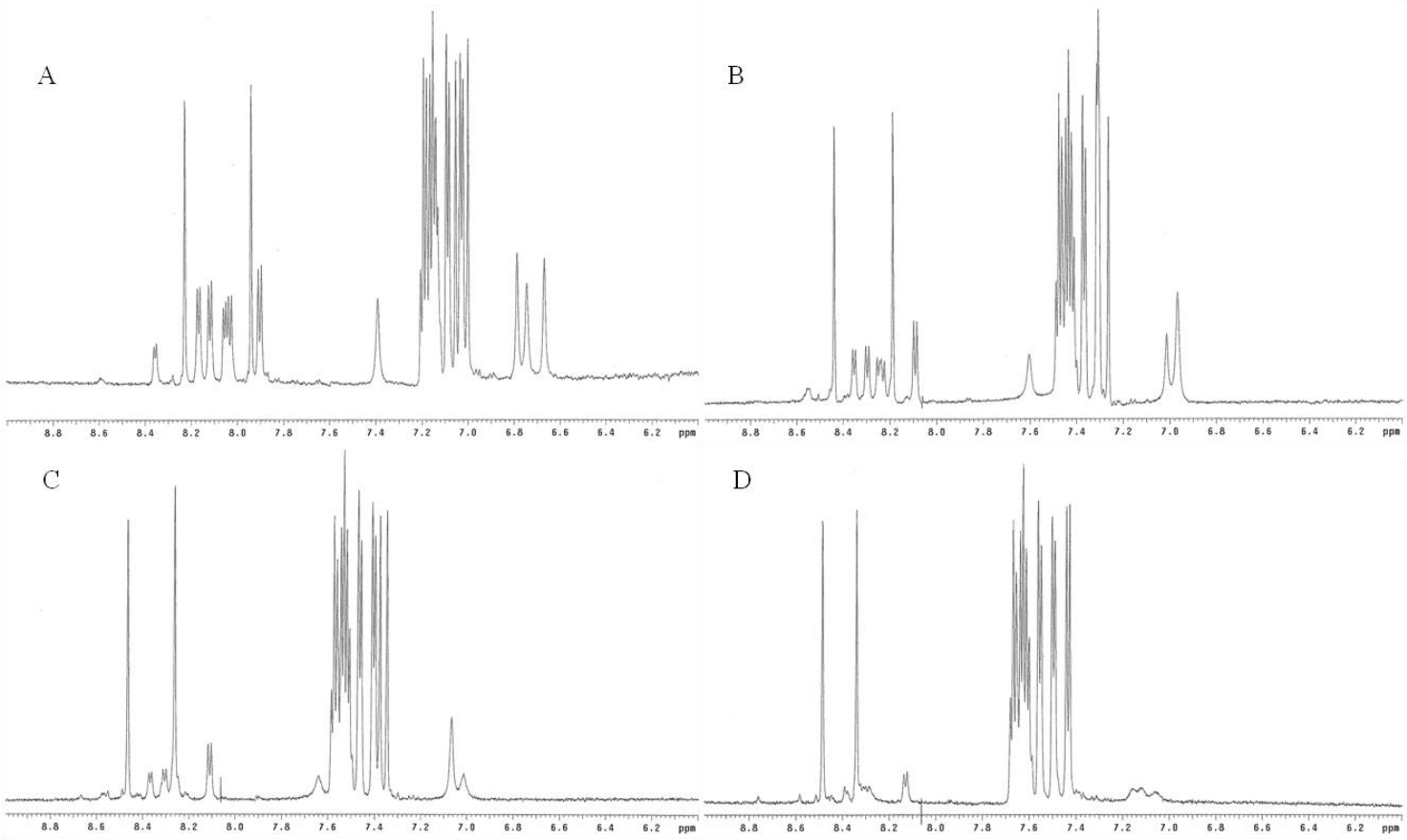

Figure 2.7 Thermal Analysis of 1mM Aβ(13-21) Followed by NMR. All spectra are in deuterated acetate pH 5.5. A) 25 ^{o}C, B) 35 ^{o}C, C) 45 ^{o}C, D) 55 ^{o}C.

with a highly unstructured peptide backbone with P_{II} character (Shi, Olson et al. 2002). There are 6 clearly defined transitions in the amide region of this nine residue peptide that should have eight backbone amide protons. The two missing protons are likely due to presaturation transfer from water suppression. Further, the amide proton resonances decrease significantly in intensity relative to the aromatic region of the spectrum when the sample was heated at 10 ^{o}C increments from 25-55 ^{o}C (Figure 2.7A-D). This decrease in intensity is further consistent with presaturation spin transfer from suppression of the large water signal. The fact that all the signals decrease at the same rate suggests that all the amide protons have similar exchange rates, a situation possible with the P_{II} conformation where all of these protons freely exchange with solvent (Shi, Olson et al. 2002; Shi, Woody et al. 2002; Ding, Chen et al. 2003).

2.2.6 Effects of Ionic Strength on Aβ(13-21)

Hypothesizing that the amount of charge relative to the amount of hydrophobic character of Aβ(13-21) may retard self-assembly, the ability for this peptide to assemble by varying the ionic strength was investigated with 50 mM, 100 mM, 250 mM, and 500 mM salt concentrations. If the lack of assembly of this peptide is prevented by the initial hydrophobic side-chain burial not taking place, then solutions with high ionic strength could result in amyloid assembly (Hill, Miti et al. 2011). Also, assuming that amyloid formation occurs via the fusion of hydrophobically collapsed species (Liang, Lynn et al. 2010), the charge-charge micelle repulsion in the case of Aβ(13-21) could also be overcome at high salt concentrations (Gomez, Clack et al. 2009).

Aβ(13-21) at a 1 mM concentration in 25 mM HEPES buffer at pH 7.5 was prepared with the above salt concentrations of sodium chloride (NaCl), tetramethylammonium chloride ($N(CH_3)_4Cl$), ammonium chloride (NH_4Cl), and sodium acetate ($NaCH_3COO$) salts. The samples were analyzed by CD over 30 days and evidence for changes in the secondary structure is present at higher salt concentrations (Figure 2.8A-D).

2.2.7 Aβ(13-21) Assembly by NMR

Deuterium exchange has been used to analyze the exchange rate of amide protons along the peptide backbone (Feng, Orlando et al. 2006). Accordingly, Aβ(13-21) was prepared in 100% D_2O and resulted in complete amide proton exchange suggesting that the peptide is monomeric because all of the amide proton transitions disappear due to their exchange with deuterium. However, if spherical particles exist, the monomer exchange in and out of the particle would have to occur faster than the amount of time required to acquire the 1D NMR spectra. To further analyze the exchange rates, titrations of D_2O are necessary in order to determine whether these exchange rates correlate to monomeric peptides or are slowed due to oligomeric species in solution. Further characterization of Aβ(13-21) is necessary in order to determine the position of Aβ(13-21) along the assembly pathway.

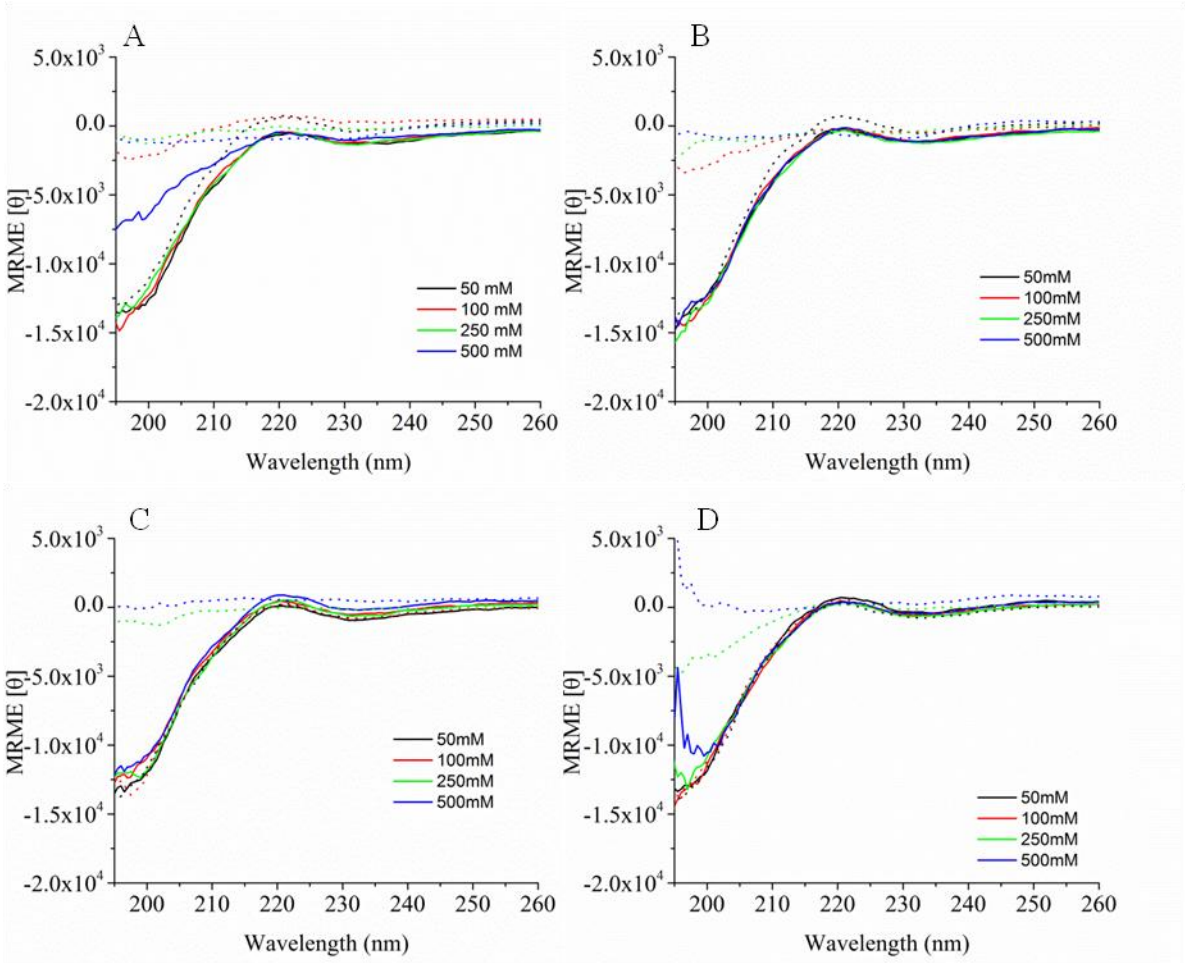

Figure 2.8 Effects of Ionic Strength Aβ(13-21). A) sodium chloride, B) ammonium chloride, C) tetramethylammonium chloride, D) sodium acetate. (solid lines = 0 d, dashed lines = 30 d)

2.2.8 Characterizing Aβ(13-21) Position on the Assembly Pathway with SANS

Although pH and temperature do not promote the assembly of Aβ(13-21), the ionic strength dependence of this peptide suggests that Aβ(13-21) may exist in spherical micelles that are unable to fuse or are simply unable to form spherical particles. However, both pH and temperature result in a change in the CD spectra of Aβ(13-21) suggesting this peptide could exist as a monomer or incorporated in a spherical micelle-like structure along the assembly pathway. To further characterize the assembly pathway, small angle neutron scattering (SANS) was utilized to probe for particles on the order of 1-100 nm in diameter. If small spherical particles exist in solution, the scattering curve should have an intensity drop of ~2-3 orders of magnitude as seen with dihexanoylphosphatidylcholine (DHPC), sodium dodecyl sulfate (SDS), and dodecyltrimethylammonium bromide (DTAB) micelles (Griffiths, Paul et al. 2005). The scattering curve Aβ(13-21) does not show any loss in intensity (Figure 2.9A), arguing against any homogeneous population of spherical species below 100 nm in diameter. The sample was further heated from room temperature to 65 ^{o}C at 10 ^{o}C increments and again no change in the scattering curves could be resolved (Figure 2.9A).

Guiner analysis of SANS data produces a radius of gyration ($R_g = \sqrt{(I/A)}$; I – second moment of area, A – total cross-sectional area). This number is then compared to various structural models. This experiment reveals that the species in solution is monomeric (Figure 2.9B). The Guiner fit results in a R_g of 10.3 +/- 1.8 Å, consistent with either a Debye Gaussian coil (random coil) with a predicted R_g of 9.4 +/- 2.3 Å or a cylinder (P_{II}) with an R_g of 8.9 +/- 2.9 Å (Figure 2.9B).

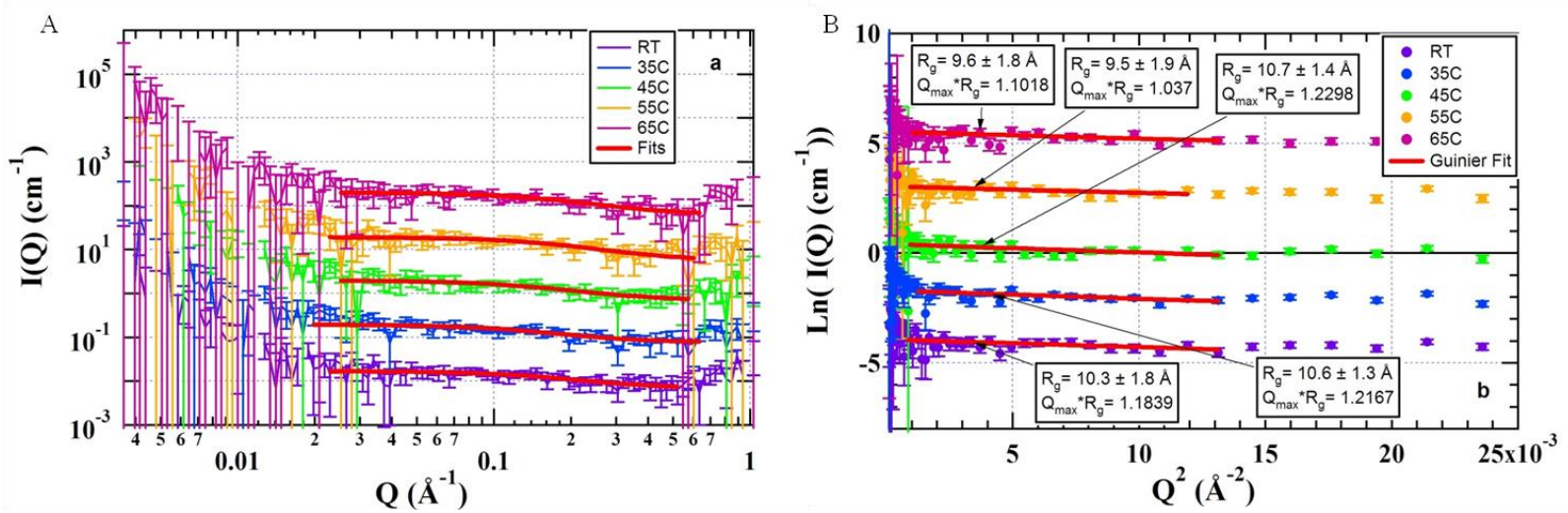

Figure 2.9 SANS Analysis of Aβ(13-21). A) SANS scattering curves of Aβ(13-21) from room temperature to 65 ^{o}C incremented by 10 ^{o}C (curves are offset for clarity), B) Guiner plots of scattering profiles from A with fitted radii of gyration (R_g) at each temperature is fit for both a Debye flexible gaussian coil (random coil) and a solid cylinder (polyproline II helix and type-II β-turn).

2.2.9 Characterizing Aβ(13-21) Position on the Assembly Pathway with DLS

The SANS data proves that Aβ(13-21) does not consist of a homogeneous population of spherical micelle-like particles in the range of 1-100 nm, but the peptide could exist in a spherical species that is larger than this range. Dynamic light scattering (DLS) on 1 mM Aβ(13-21) in 25 mM HEPES pH 7.5 revealed no spherical species in this range (Figure 2.10A). The scattering data could not be fit to a homogeneous particle size on three consecutive acquisitions (Figure 2.10A), even though the scattering for a sample of polystyrene beads with a 47 nm diameter produced the expected size (Figure 2.10B). These results all support that Aβ(13-21) does not assemble as a homogeneous population of spherical particles but rather exists as a single peptide conformation, a P_{II} conformation.

2.2.10 Analyzing Aβ(13-21) Position on the Assembly Pathway with Fluorescence

Aβ(13-21) contains two phenylalanine residues, however this particular amino acid has an extremely low fluorescence quantum yield (Lakowicz 2006). For this reason, several aromatic peptide substitutions were generated and analyzed including Aβ(13-21)F19W, Aβ(13-21)F20W, Aβ(13-21)F19WF20W, Aβ(13-21)F19Fcn, and Aβ(13-21)F20Fcn (Fcn - cyanophenylalanine). These single substituted peptides display similar CD characteristics as Aβ(13-21) when analyzed at 1 mM in 25 mM HEPES pH 7.5 at room temperature (Figure 2.11A-E). The double tryptophan substitution displays the same negative ellipticity, but at 198 nm the spectrum possesses a positive band near 215

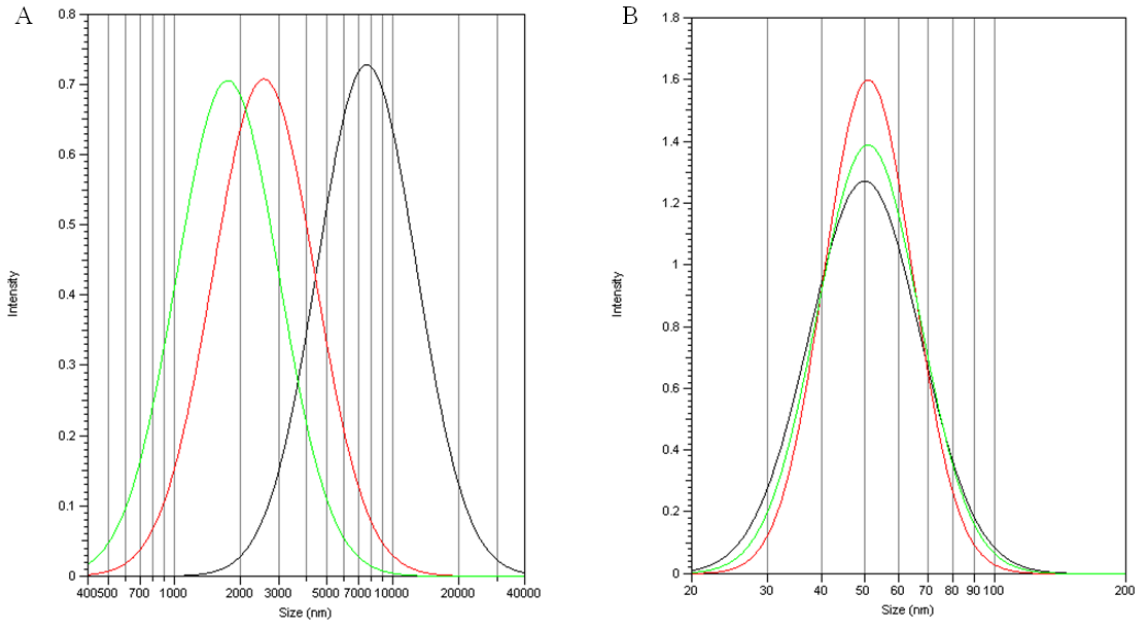

Figure 2.10 DLS Analysis of Aβ(13-21). A) Irreproducible scattering fits of Aβ(13-21), B) Fitted scattering profile of 47 nm polystyrene standard.

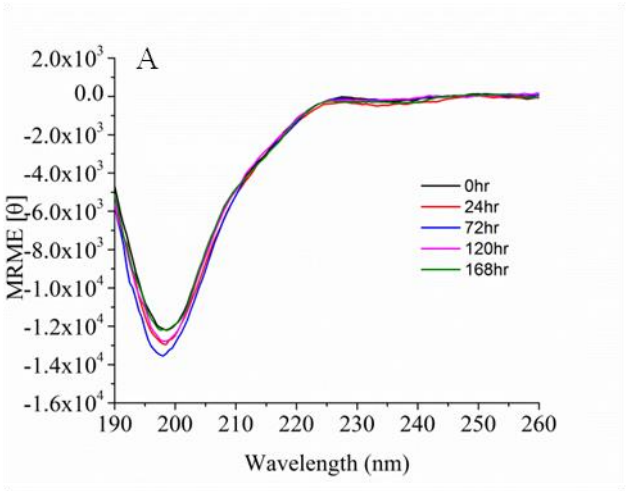
A
2.0x10^3
0.0
-2.0x10^3
-4.0x10^3
-6.0x10^3
-8.0x10^3
-1.0x10^4
-1.2x10^4
-1.4x10^4
-1.6x10^4
MRME [θ]
190 200 210 220 230 240 250 260
Wavelength (nm)
0hr
24hr
72hr
120hr
168hr

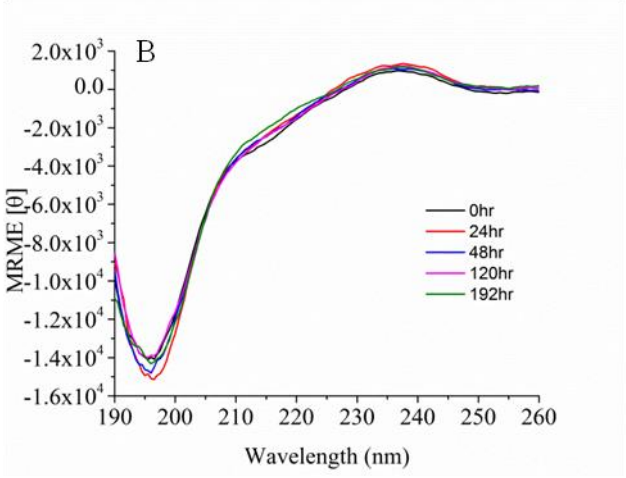
B
2.0x10^3
0.0
-2.0x10^3
-4.0x10^3
-6.0x10^3
-8.0x10^3
-1.0x10^4
-1.2x10^4
-1.4x10^4
-1.6x10^4
MRME [θ]
190 200 210 220 230 240 250 260
Wavelength (nm)
0hr
24hr
48hr
120hr
192hr

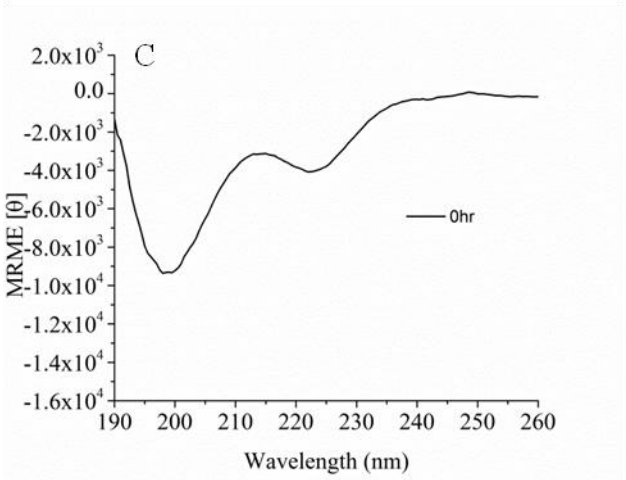
C
2.0x10^3
0.0
-2.0x10^3
-4.0x10^3
-6.0x10^3
-8.0x10^3
-1.0x10^4
-1.2x10^4
-1.4x10^4
-1.6x10^4
MRME [θ]
190 200 210 220 230 240 250 260
Wavelength (nm)
0hr

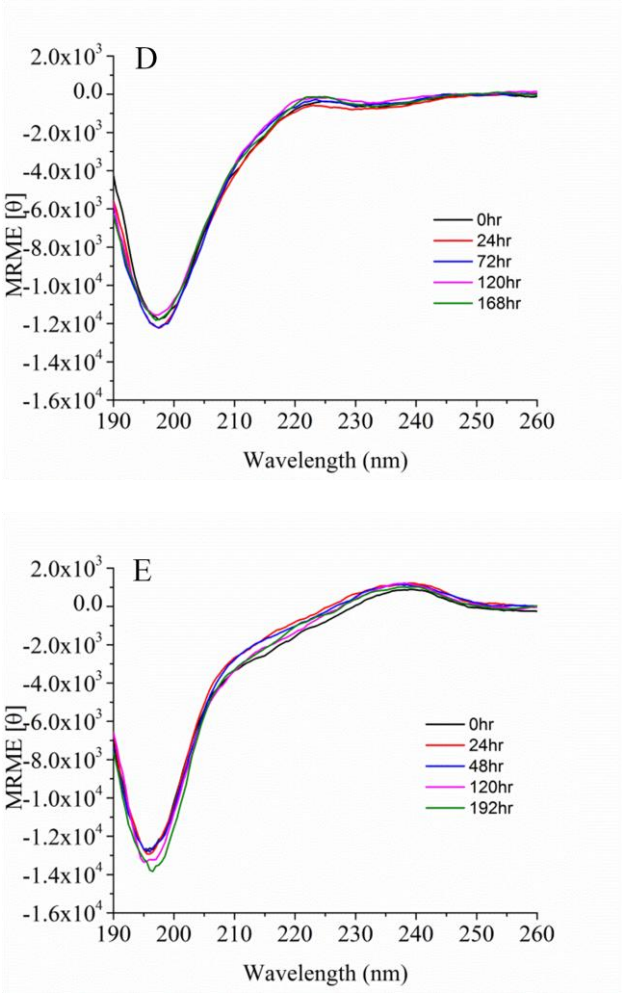

Figure 2.11 CD Signature of Aβ(13-21) Wild-type and F19/F20 Substitutions. A) Aβ(13-21)F19W – 1 mM, B) Aβ(13-21)F19Fcn – 1 mM, C) Aβ(13-21)F19WF20W – 1 mM, D) Aβ(13-21)F20W – 1 mM, E) Aβ(13-21)F20Fcn – 1 mM. All samples were prepared in 25mM HEPES at pH=7.5.

nm. These two transitions again suggest a P_{II} conformation (Rucker and Creamer 2002; Shi, Olson et al. 2002; Shi, Woody et al. 2002; Ding, Chen et al. 2003; Shi, Chen et al. 2006; Shi, Chen et al. 2006). The Fcn substituted peptides show a positive band at 240 nm, at the absorbance maximum for this side chain.

2.2.10.1 Fluorescence Emission

If the tryptophan residue is buried in a hydrophobic environment, then the tryptophan fluorescence should blue shift relative to individual tryptophan derivatives in buffer. The blue shift results from a change in the local environment of the solvent polarity, but a change in hydrogen bonding capability also influences the indole ring emission (Lakowicz 2006). When indole is dissolved in cyclohexane, the fluorescence curve consists of three maxima resulting from fluorescence emission from the ^1L_b transition, but when a small amount of ethanol is added to this indole solution, the multiple maxima disappear as a result of fluorescence emission from the ^1L_a transition (Gryczynski, Wiczk et al. 1988). As the solvent polarity increases, the tryptophan fluorescence emission continues to red shift (Lakowicz 2006).

Aβ(13-21)F19W, Aβ(13-21)F20W, and Aβ(13-21)F19WF20W fluorescence emission spectra were acquired at 1 mM 25 mM HEPES pH 7.5 from 25 ^oC to 65 ^oC at 10 ^oC increments (Figure 2.12A-C). The fluorescence emission spectra contain a single maximum at 359 nm, 361 nm, and 360 nm respectively. As positive controls, tryptophan (H_3N^+-Trp-COO^-) and two derivatives (Ac-Trp-COO^-, H_3N^+Trp-NH_2) were analyzed under identical conditions (Figure 2.12D-F). The fluorescence emission spectra of the

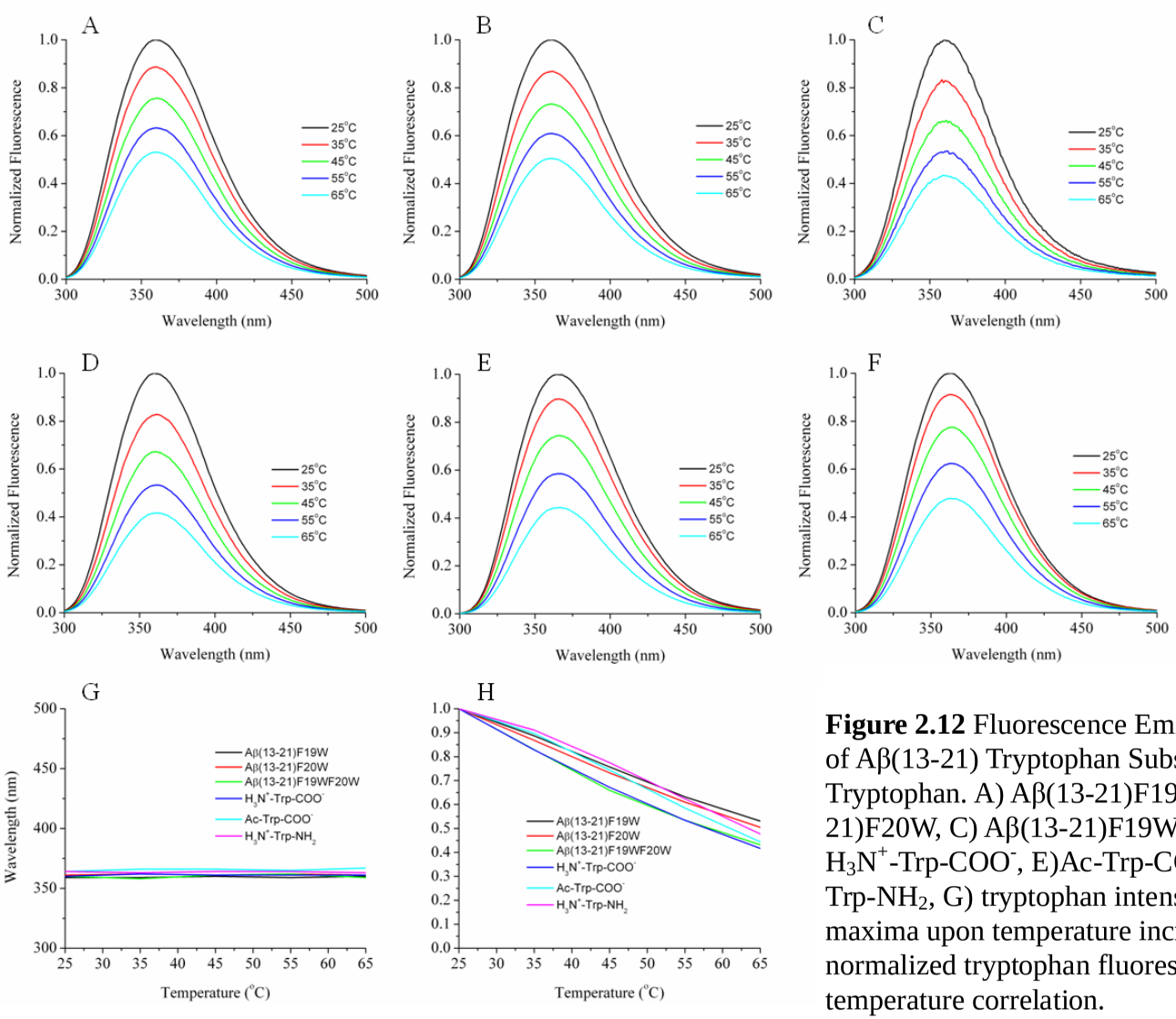

Figure 2.12 Fluorescence Emission Spectra of Aβ(13-21) Tryptophan Substitutions and Tryptophan. A) Aβ(13-21)F19W, B) Aβ(13-21)F20W, C) Aβ(13-21)F19WF20W, D) H_3N^+-Trp-COO^-, E)Ac-Trp-COO^-, F) H_3N^+-Trp-NH_2, G) tryptophan intensity lambda maxima upon temperature increases, H) normalized tryptophan fluorescence intensity temperature correlation.

compounds consist of a single maximum at 360 nm (H_3N^+-Trp-COO^-), 363 nm (Ac-Trp-COO^-), and 362 nm (H_3N^+Trp-NH_2). The fluorescence of these compounds behaved exactly as Aβ(13-21)F19W, Aβ(13-21)F20W, and Aβ(13-21)F19WF20W, and the tryptophan emission maximum signifies that the tryptophan residue is completely solvated and monomeric at all temperatures (Figure 2.12G). Further support is seen in the linear dependence of the tryptophan emission maximum with respect to a temperature increase (Figure 2.12H), attributable to a decrease in the quantum yield with increasing temperature (Robbins, Fleming et al. 1980). Since these substitutions make each sequence more hydrophobic yet still reflect a completely solvated indole ring, it is highly likely that the wild-type sequence is monomeric as well.

2.2.10.2 Fluorescence Quenching

To determine whether Aβ(13-21) is a monomer or incorporated in larger aggregates that do not display any β-strand characteristics, Aβ(13-21)F19W and Aβ(13-21)F20W were analyzed by fluorescence quenching using acrylamide and cesium chloride (Figure 2.13A-D). Both compounds should quench the free monomer and display a linear Stern-Volmer plot. If all the peptide strands in solution are buried, then acrylamide should quench the fluorescence because this compound is uncharged and can penetrate the hydrophobic core of a spherical micelle, thus resulting in a linear Stern-Volmer plot. However, the tryptophan side chain should not be accessible to cesium chloride quenching due to the positive charge of the cesium ion. If there are two populations of tryptophans (*i.e.*, peptide monomers and peptide micelles), then the Stern-Volmer plot for

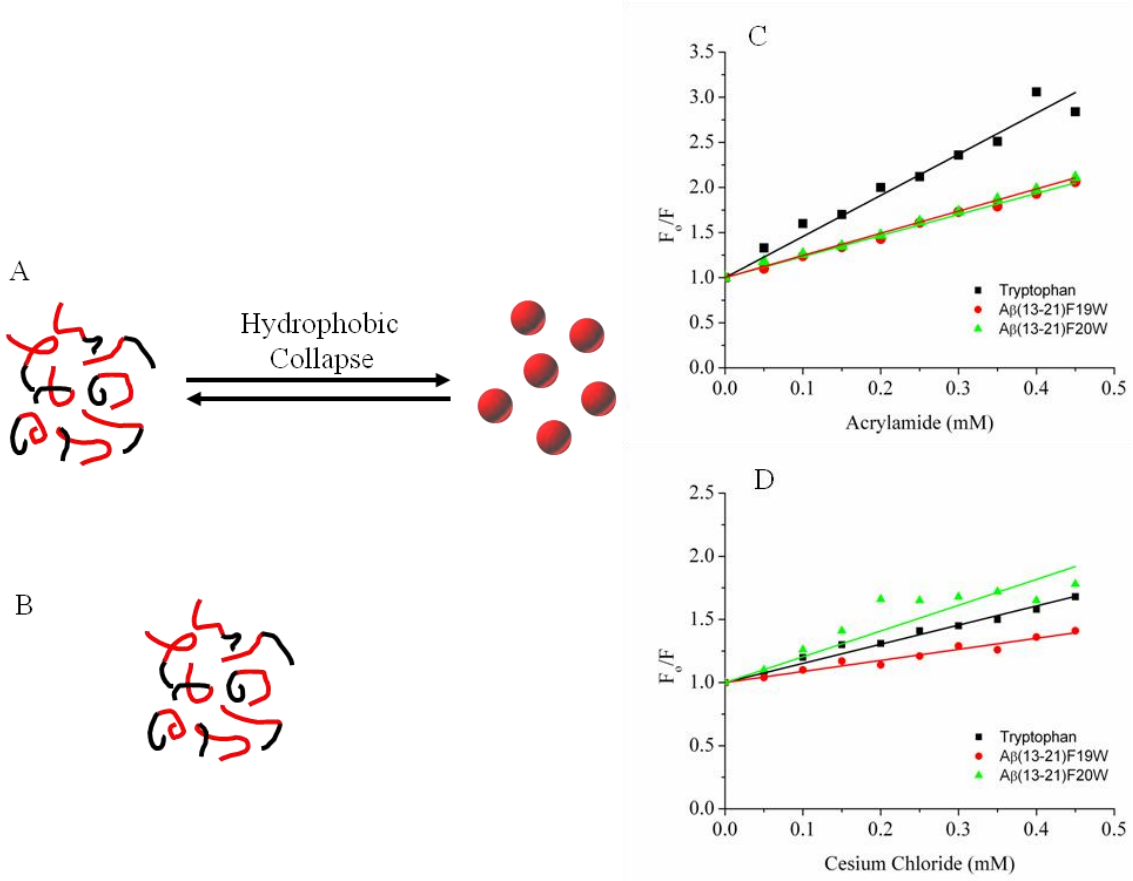

Figure 2.13 Fluorescence Quenching of Aβ(13-21) Tryptophan Substitutions. A) Scenario 1: monomers and oligomers within positively charged aggregates, B) Scenario 2: only monomers, C) Tryptophan acrylamide quenching, D) Tryptophan cesium chloride quenching.

acrylamide should be linear because this quencher can access both fluorophore environments; however, the cesium chloride Stern-Volmer plot should have a negative curvature.

Both acrylamide and cesium chloride quench Aβ(13-21)F19W and Aβ(13-21)F20W fluorescence. The Stern-Volmer plots for these peptide substitutions and quencher combinations are analyzed best with a linear fit. Cesium chloride does not quench the indole fluorescence as well as acrylamide relative to the free amino acid. In these sequences (HHQKLVWFA and HHQKLVFWA), the tryptophan residue is surrounded by hydrophobic residues which likely can impact quenching efficiency. The Aβ(13-21)F20W does show a slight downward curvature, however this sample precipitates at higher quencher concentrations for the salt cesium chloride which dramatically affects the fluorescence intensity and thus the quenching efficiency. The two tryptophan populations are the soluble form and the aggregated form. Higher salt concentrations were previously shown to affect the assembly state. Interestingly the higher salt concentrations do not affect the slope of Aβ(13-21)F19W further proving its monomeric state.

2.2.10.3 Fluorescence Anisotropy

Finally, fluorescence anisotropy is used to determine the molecular motions of fluorophores. Anisotropy values are only valid between -0.2 and 0.4. Any value outside of this range is theoretically impossible and thus deemed an artifact (*i.e.*, light scattering). If the molecular motions are reduced (*i.e.*, as the fluorophore environment becomes more

rigid), then the anisotropy value will increase. The opposite is true for increasing molecular motions.

The measured anisotropy values for Aβ(13-21)F19W and Aβ(13-21)F20W were 0.02 and 0.03, respectively. The anisotropies for Aβ(13-21)F19Fcn and Aβ(13-21)F20Fcn were both 0.00. The value for the Fcn substitutions reflects the smaller side chain which has the potential for greater ring mobility. This technique can probe whether any oligomeric species exist in solution (Figure 2.14), and if oligomeric species exist in solution, then the fluorescence anisotropy should decrease on sample dilution (Figure 2.14). The four Aβ(13-21) substitutions (Aβ(13-21)F19W, Aβ(13-21)F20W, Aβ(13-21)F19Fcn, Aβ(13-21)F20Fcn) reveal that the steady-state anisotropy remains constant from 1 mM to 1 μM, further supporting a monomeric Aβ(13-21) peptide in aqueous solution.

2.3 Conclusions

Studying Aβ(13-21) under several conditions that are known to affect chemical equilibrium constants did not result in Aβ(13-21) assembly. The biophysical data presented in this chapter strongly support that Aβ(13-21) is monomeric in solution without the presence of any spherical particles. Unassembled Aβ(13-21) is fully characterized using CD, SANS, DLS, FT-IR, and NMR. It was found that this peptide is monomeric and possesses a P_{II} conformation. The fluorescently substituted peptides, which also do not assemble into amyloid structures, are also monomeric in solution. Aβ(13-21)F20W precipitates under with the addition of higher concentrations of cesium

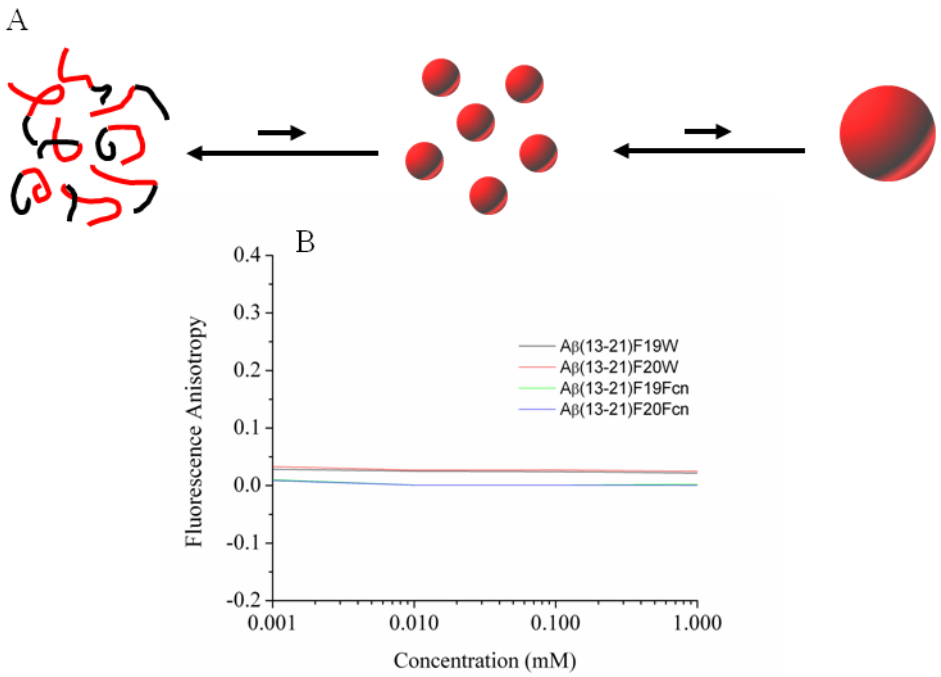

Figure 2.14 Fluorescence Anisotropy of Serially Diluted Aβ(13-21) Fluorescent Substitutions. A) Equilibrium shift towards monomer upon serial dilution, B) Fluorescence anisotropy values upon serial dilution of fluorescently labeled peptides.

chloride, but all other bioanalytical analysis suggests that this peptide is in fact monomeric. This chapter provides a complete characterization of the left side of the proposed amyloid assembly pathway. This complete characterization of monomeric Aβ(13-21), as well as its fluorescent substitutions, now allows the amyloid assembly pathway to be probed to the following chapters. Does increasing the concentration of Aβ(13-21) promote assembly? Does increasing the hydrophobic nature of Aβ(13-21) promote assembly? These questions will be addressed in the following chapter because the final assembly state needs characterization before addressing the complexities that will arise when analyzing amyloid assembly pathway in the context of membranes.

2.4 Methods

2.4.1 Materials

Solid-phase peptide synthesizer reagents (*i.e.*, FMOC-amino acids, peptide resins) were obtained from Anaspec, Inc. (San Jose, CA). Distilled deionized water (ddH_2O) was purchased from EMD Chemicals, Inc. (Gibbstown, NJ) for sample preparations. All other reagents were acquired from Sigma-Aldrich Chemical Co. (Milwaukee, WI).

2.4.2 Peptide Synthesis and Purification

Peptide synthesis was performed using standard FMOC solid-phase peptide chemistry on a FMOC Rink-amide polystyrene resin (AnaSpec, Inc., sub. 0.4-0.6 meq/g) by a Rainin Symphony Quartet multiplex solid-phase peptide synthesizer (Protein

Technologies, Tucson, AZ) or a Liberty Microwave solid-phase peptide synthesizer (CEM, Matthews, NC).

On the Rainin Symphony Quartet, HBTU and NMM were the coupling reagents. Each amino acid was coupled for 2 hours. His13, His14, Gln15, Lys16, Leu17, Val18 and Phe19 were double coupled. An acetylation reaction was performed after every coupling reaction to eliminate deletion peptides. On the CEM Liberty, HBTU and NMP/DIEA were the coupling reagents. Each amino acid was single coupled following the standard coupling reaction conditions from CEM. An acetylation reaction was performed after every coupling reaction to eliminate deletion peptides.

The cleavage/deprotection reaction was carried out with trifluoroacetic acid/thiolanisole/EDT/anisole (95/5/3/2, v/v). The crude peptide was precipitated using cold ethyl ether and centrifuged at 6,500 rpm for 10 min at 4 ^{o}C. The crude product was then washed with cold ethyl ether and centrifuged four additional times. The crude peptide was kept under vacuum until purified.

All peptides were purified by RP-HPLC using a Waters Delta 600 and a Jasco LC2000 HPLC with a Zorbax 300SB-C18 preparative HPLC column (21.2mm x 25cm) and eluted at 10 mL/min. The peptide was dissolved in H_2O with 0.1% TFA. If the solution was cloudy, the crude mixture was filtered though a 0.2 μm filter (Whatman). A linear gradient from 15%/85% MeCN/H_2O with 0.1% TFA to 45%/55% MeCN/H_2O with 0.1% TFA was used. The HPLC peak was collected, condensed, frozen at -80 °C, and lyophilized (ATR FD3.0 freeze dryer or a Labconco FreeZone 12Plus freeze dryer). Lyophilized peptides were stored at -20 or -80 °C. MALDI-TOF MS analysis (Voyager-

DE™ STR Biospectrometry Workstation; 2,5-dihydroxybenzoic acid matrix) was collected on each peptide.

2.4.3 Peptide Sample Preparation

Peptide stock solutions were prepared by dissolving a known amount of peptide in ddH_2O at twice the desired concentration, sonicating for 10 min, and centrifuging at 13,200 x g for 10 min. The supernatant was collected and used as the peptide stock solution. 1 mM samples were prepared by diluting a 2 mM stock solution with 50 mM of the desired buffer and pH. 0.5 mM samples were further diluted with 25 mM of the desired buffer solution.

2.4.4 Circular Dichroism (CD)

CD spectra were collected using a Jasco J-810 CD spectropolarimeter (Easton, MD). Three spectra were recorded from 260 nm to 190 nm (step size = 0.2 nm, speed = 100 nm/s) using a 0.1 mm path length quartz slides at room temperature and averaged automatically. Each spectrum was background subtracted (using the same acquisition protocol) from the same conditions without peptide. Samples were heated using a peltier controller. Each sample was equilibrated at the desired temperature for 5 min before data acquisition.

2.4.5 NMR (1D, variable temperature)

Aβ(13-21) was prepared at 2 mM in a 10%D_2O/90%H_2O d_3-acetate buffer pH 5.5 or at 1 mM in 100% D_2O without buffer. ^1H spectra were acquired on a Bore Oxford INOVA 600 MHz spectrometer with a 5 mm pulsed field gradient (PFG) indirect detection probe. All one-dimensional ^1H spectra were acquired with 32 K complex data points by averaging 128 scans. Solvent was suppressed with presaturation. Spectra were referenced to water at 4.78 ppm. Variable temperature one-dimensional spectra were collected from 25 – 55 ^oC in 10 ^oC increments (30 min wait for temperature equilibration). Temperature was controlled with the software and is presented without correction. Data was processed using the NMR acquisition software.

2.4.6 Small Angle Neutron Scattering (SANS)

Data was collected at the Intense Pulsed Neutron Source of Argonne National Laboratory on the time-of-flight small-angle diffractometer (SAD). The 64 x 64 array position sensitive gas filled 20 x 20 cm^2 area detector was fixed 1.54 m from the sample. Pulsed neutrons with wavelengths of 0.5-14 Å were collected which provides a scattering vector ($Q = 4\pi \sin(\theta)/\lambda$) ranging from 0.005-0.25 Å in one experiment, where θ = half the scattering angle and λ = neutron wavelength. Aβ(13-21) was investigated at 1 mM in 100% D_2O 25 mM HEPES buffer pH 7.5 in 1 mm quartz cells and measured for greater than 4 hours at each temperature. Data were corrected for background scattering.

2.4.7 Dynamic Light Scattering (DLS)

Data was collected on a N4 particle sizer (Beckman-Coulter, Miami, FL). A 1 mM sample of peptide was added to a square cuvette. Using a He-Ne laser (wavelength = 632.8 nm) and a 90^{o} detection angle, data were collected and averaged for 5 minutes 3 times at room temperature. The resulting decay curves were automatically analyzed by the instrumental program using unimodal distribution algorithms.

2.4.8 Fluorescence Emission Measurements

Fluorescence emission measurements were acquired on a SPEX FluoroMax-3 and analyzed using DataMAX (Horiba Jobin Yvon, Edison, NJ). The excitation wavelength was 295 nm for tryptophan and 241 nm for Fcn. Tryptophan emission spectra were collected from 300 nm to 600 nm. Fcn emission spectra were acquired from 250 nm to 350 nm. The data pitch was 1 nm. The integration time was 0.5 sec. Data displayed is the average of three scans.

2.4.9 Fluorescence Quenching

A stock solution of 1 mM peptide was diluted with a stock solution of acrylamide or CsCl to the desired quencher concentration. The samples were thoroughly mixed and the emission spectra was acquired using the same parameters

2.4.10 Fluorescence Anisotropy

Fluorescence anisotropy measurements were acquired on a SPEX FluoroMax-3 and analyzed using DataMAX (Horiba Jobin Yvon, Edison, NJ). The excitation wavelength was 295 nm, and the emission wavelength was at the emission maxima was determined for each peptide at each individual concentration before anisotropy data was collected. The anisotropy values represent the average of 100 acquisitions.

2.4.11 Fourier Transform Infrared Spectroscopy (FT-IR)

Solution FT-IR spectra were collected on a Jasco FT-IR 4100 spectrophotometer. Samples were loaded into a 0.1 mm fused quartz cell. Using a digitally controlled heating element (Pike Technologies, Madison, WI), samples were heated to the desired temperature and allowed to equilibrate for 15 min before data collection.

Chapter 3

Solvent Polarity Microenvironments Induce Amyloid Peptide Conformational Exchange – A Common Mechanism of Amyloid Assembly using Tightly Controlled Amyloid Assemblies

3.1 Introduction

The previous detailed biophysical characterization of a monomeric peptide provides a starting point for the analysis of amyloid assembly. Aβ(13-21) is monomeric in solution with a secondary structure best defined by CD as populating predominately a polyproline II helix (P_{II}). In order to fully understand amyloid assembly, the initiation and the end point of assembly need characterization. To do this, a controllable switch for assembly must be developed.

Several labs, including ours, have gone to extensive lengths to provide detailed structural information for assembled amyloid forming peptides (Benzinger, Gregory et al. 1998; Burkoth, Benzinger et al. 2000; Lu, Jacob et al. 2003; Dong, Lu et al. 2006; Dong, Canfield et al. 2007; Liang, Pingali et al. 2008). These structures have proven invaluable in formulating hypotheses for the mechanism responsible for amyloid formation. The first structural characterization for the arrangement of amyloid peptides within amyloid fibrils was conducted by Benzinger *et al.* on Aβ(10-35) (Benzinger, Gregory et al. 1998). Using DRAWS, this work proved that the amyloid fibril consists of parallel, in-register β-sheets. However, further detailed biophysical characterization of amyloid peptide systems has been plagued by the inability to control the assembly process.

Previous members of our lab generated Aβ peptide truncation and substitution variants to simplify the biophysical characterization and overcame the precipitation complications. Using Aβ(16-22), Lu *et al.* discovered that this peptide formed structures similar to the full-length peptide assembly at pH 6 (Lu 2006). Aβ(16-22) also generated a new amyloid structure – a peptide nanotube – under acidic and basic pH conditions (Lu,

Jacob et al. 2003). Additional substitutions expanded the structural elements to include sheets and ribbons. Using Aβ(10-21), Ac-Aβ(13-21)H14A and Aβ(13-21)16A, Dong and coworkers probed the effects of metals on amyloid assembly (Morgan, Dong et al. 2002; Dong, Shokes et al. 2006; Dong, Canfield et al. 2007). These peptides too formed similar structures as the full-length peptide. Aβ(13-21)K16A in the presence of Zn^{2+} formed ribbons and tubes while Cu^{2+} was found to inhibit assembly. With the structural information obtained on these peptides, hypotheses were generated for the contributing factors responsible for amyloid assembly; however, these hypotheses remain limited by the inability to control amyloid assembly initiation and to probe the assembly in real time.

Liang *et al.* generated a fluorescently labeled Aβ(16-22) and investigated amyloid nanotube assembly using fluorescence microscopy of mixed peptide assemblies (Liang, Lynn et al. 2010). This peptide variant allows the assembly to be followed in real time when added to the wild-type peptide at ratios of 1:250. When Aβ(16-22) was doped with this fluorescently labeled peptide, it was found that this peptide mixture formed the same structures as Aβ(16-22) alone – nanotubes. Fluorescence images reveal large spherical species from which the amyloid structures grow. This analysis suggests that amyloid formation proceeds through large aggregates and peptides add to the end of the growing amyloid structure. This data strengthens the amyloid assembly hypothesis that proposes that assembly proceeds through spherical species. However, this analysis is limited only to amyloid nanotube because amyloid fibrils are smaller than the diffraction limit of light thus making them irresolvable using this technique.

In order to probe the amyloid assembly pathway for fibril formation, assembly initiation must be controlled and the assembly end point must be characterized thereby bracketing the right side of the assembly pathway. This chapter focuses on the generation of amyloid peptides whose assembly is tightly controlled and whose assembly can be investigated with the incorporation of small less perturbing fluorescent probes. This analysis addresses several unknown questions with respect to amyloid assembly. What controls amyloid assembly? Can amyloid assembly be consistently initiated? Is amyloid assembly reversible? What are the secondary structural elements present along the assembly pathway?

3.2 Results and Discussion

3.2.1 Concentration Dependent Amyloid Assembly

Aβ(13-21) does not assemble at 1 mM or lower concentrations (Chapter 2), however a 4 mM peptide sample in 25 mM HEPES pH 7.5 does assemble as fibrils. The CD spectrum for the 4 mM Aβ(13-21) sample contains a positive maximum at 190 nm, a negative minimum at 203 nm, and a negative shoulder at 215 nm (Figure 3.1A). Specific spectral assignments are inconclusive in this sample because of the non-classical nature of the spectrum, however the shoulder at 215 nm can be assigned to a β-strand peptide conformation. Additional evidence in the literature suggests that this CD spectrum is best characterized as a mixture of β-sheet and P_{II} (Sreerama and Woody 2003). When the sample is analyzed using atomic force microscopy (AFM), fibrils approximately 4 nm in height are present (Figure 3.1B).

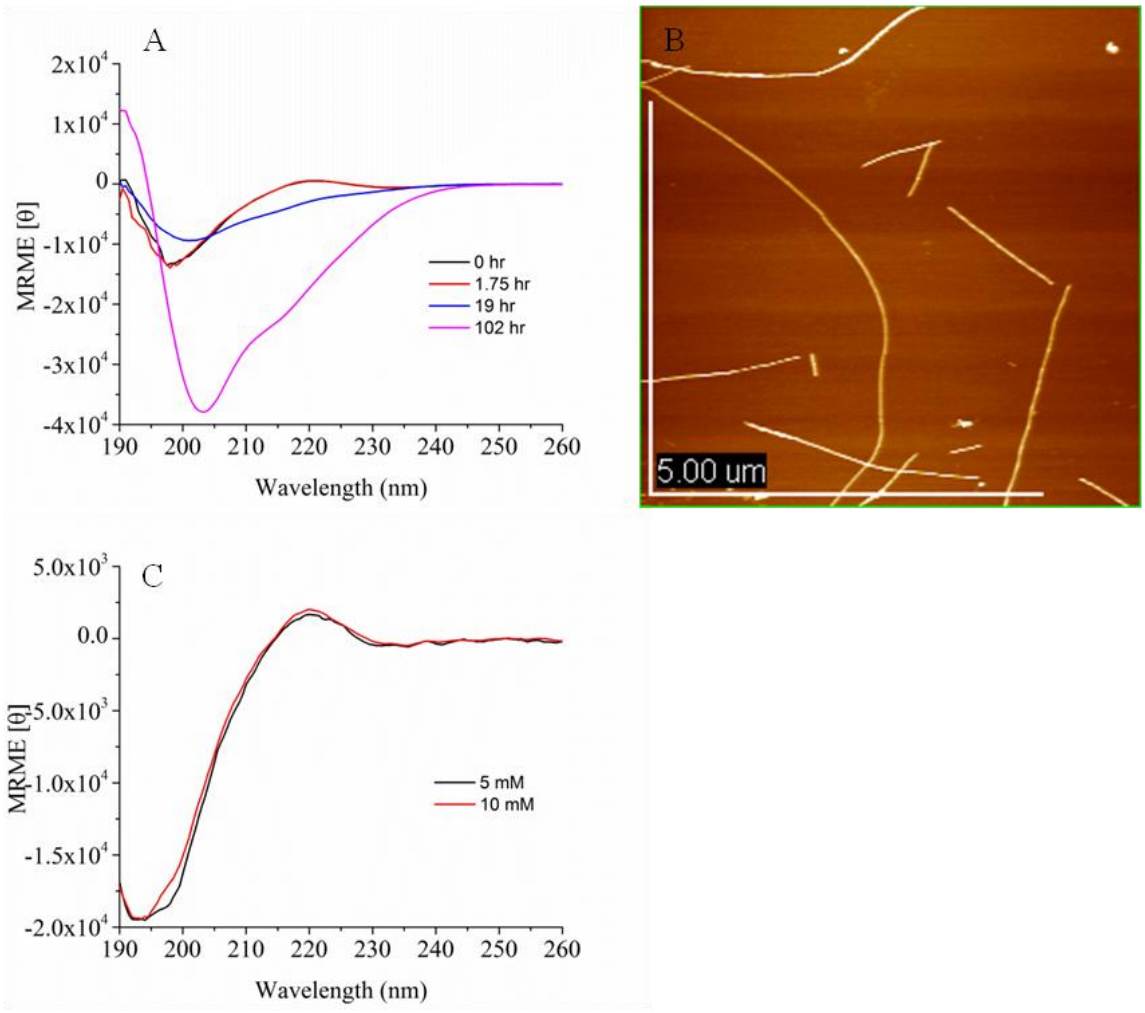

Figure 3.1 Effects of Concentration on the Self-Assembly Propensity of Aβ(13-21). A) CD spectra of 4 mM Aβ(13-21) in 25 mM HEPES pH 7.5, B) AFM image of 4 mM Aβ(13-21), C) CD spectra of 5 mM and 10 mM Aβ(13-21) in 25 mM MES pH 5.5.

Concentration increases for Aβ(13-21) in 25 mM MES pH 5.5 were characterized as well. The CD spectra for 5 mM and 10 mM Aβ(13-21) appear the same as the CD spectra presented in Figure 3.1C. Thus, concentration increases of Aβ(13-21) on this order of magnitude at this lower pH do not promote assembly. At pH 5.5, Aβ(13-21) has two additional positive charges which makes the peptide more hydrophilic. These results suggest that the balance between the hydrophilicity and hydrophobicity of amyloid peptides influences their assembly propensity.

3.2.2 Promoting Aβ(13-21) Assembly by C-terminal Substitution

One possible explanation for the 1 mM Aβ(13-21) not assembling at pH 7.5 is that the balance between peptide charge and hydrophobic character destabilizes assembly. To test this hypothesis, a series of natural and non-natural substitutions were synthesized to investigate whether small increases in hydrophobic surface can drive self-assembly.

Using Karplus' derived energetic gain of hydrophobic burial of amino acid side chains, A21 was selected as the position to substitute amino acid side chains that have a greater energetic gain from side-chain burial (Karplus 1997). Aβ(13-21)A21V, Aβ(13-21)A21L, and Aβ(13-21)A21I were synthesized, and indeed while all produced fibers (Figure 3.2D-I), not every sample produced the classical β-sheet CD signature when allowed to assemble at 1 mM (Figure 3.2A-C). Aβ(13-21)A21V and Aβ(13-21)A21L give CD signatures consistent with the spectrum of β_{II} proteins while Aβ(13-21)A21I produces a β_I assembly (a typical β-sheet). Further support for amyloid assembly comes from the Congo red spectral shift assay (Figure 3.2J-L). Therefore, increasing

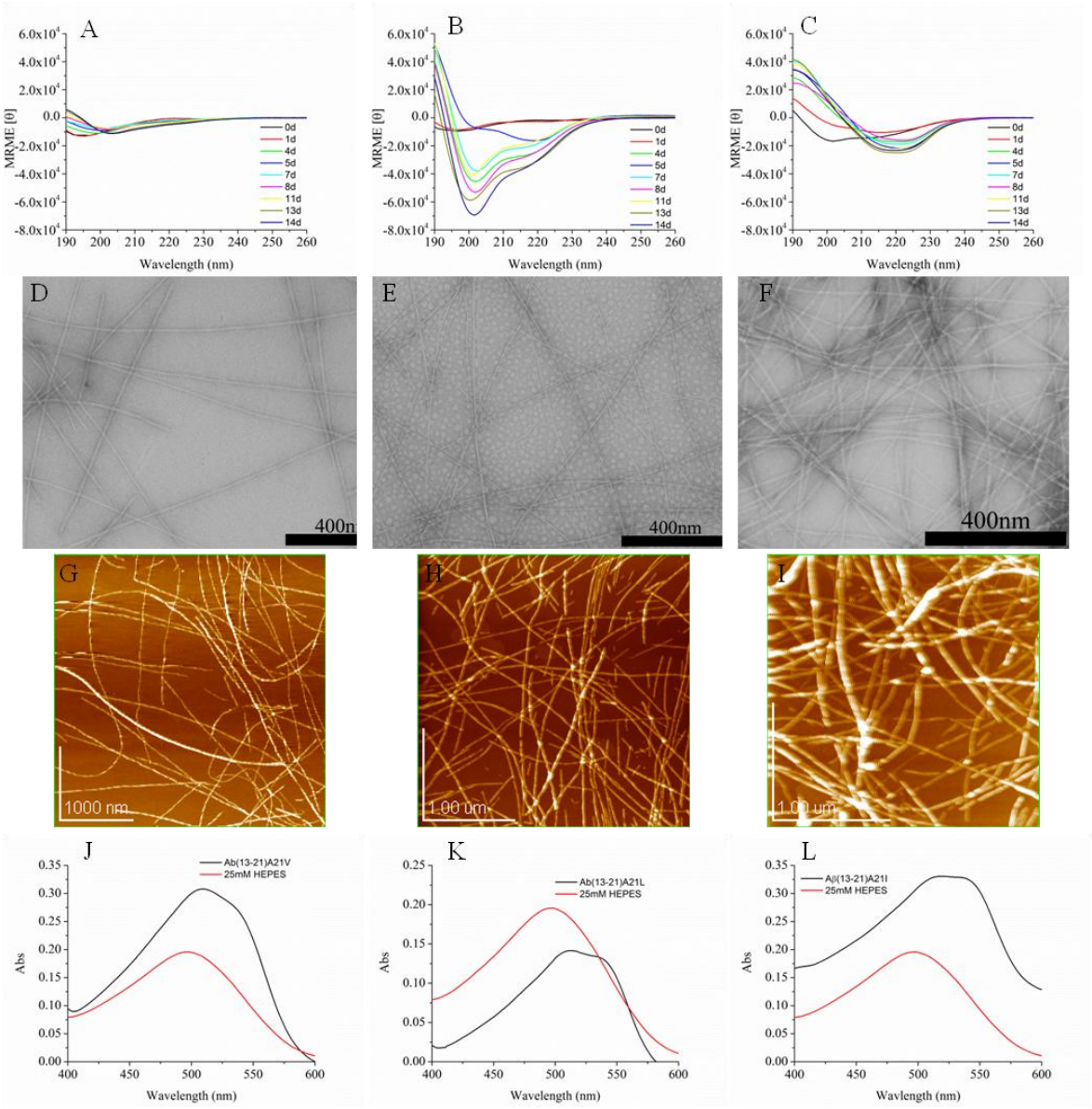

Figure 3.2 Increases in the *C*-terminal Hydrophobicity of Aβ(13-21) Promotes Amyloid Assembly at pH 7.5. A) CD spectra of Aβ(13-21)A21V, B) CD spectra of Aβ(13-21)A21L, C) CD spectra of Aβ(13-21)A21I, D) TEM image of Aβ(13-21)A21V, E) TEM image of Aβ(13-21)A21L, F) TEM image of Aβ(13-21)A21I, G) AFM image of Aβ(13-21)A21V, H) AFM image of Aβ(13-21)A21L, I) AFM image of Aβ(13-21)A21I, J) CR assay of Aβ(13-21)A21V, K) CR assay of Aβ(13-21)A21L, L) CR assay of Aβ(13-21)A21I. All samples were prepared at 1 mM in 25 mM HEPES pH 7.5.

hydrophobicity can regulate amyloid assembly. These two CD spectra for β-sheets are classified as β_I- and β_{II}-proteins (Wu, Yang et al. 1992). After correlating the CD spectra with crystal structures, the difference between β_I and β_{II} proteins is the ratio of two different amide conformations: β-sheet and P_{II} (Sreerama and Woody 2003). According to Sreerama and Woody 2003, most β_I proteins (Figure 3.2C) have a P_{II} to β-sheet ratio lower than 0.3 while a ratio greater than 0.4 is observed for β_{II} proteins (Figure 3.2B). These data suggest that Aβ(13-21)A21L is best characterized as a β_{II}-protein with the band at 203 nm indicative of a P_{II} secondary structure and the shoulder at 215 nm representing β-sheet while Aβ(13-21)A21I is best characterized as a β_I-protein. Therefore, the difference between the CD spectra for Aβ(13-21)A21L and Aβ(13-21)A21I is the extent of assembly; Aβ(13-21)A21I assembles to a greater extent given the lower percentage of P_{II} content which has been shown to exist at earlier stages in assembly.

To evaluate the role of varying degree of β-branching (Sreerama and Woody 2003; Liang, Pingali et al. 2008), a series of unbranched alkyl chain lengths were synthesized, including Aβ(13-21)A21Abu [A21Abu – ethyl side chain], Aβ(13-21)A21Nva [A21Nva – propyl side chain], and Aβ(13-21)A21Nle [A21Nle – butyl side chain]. The intensity of the 203 nm transition suggests that these peptides have different degrees of assembly (Sreerama and Woody 2003), but fibril formation and Congo red binding was present in each sample (Figure 3.3). This approach was not position dependent as Aβ(13-22)E22L also assembled into fibrils and sheets (Figure 3.4). The increase in the hydrophobic nature possibly allows for an increase in the number of laminates due to a thermodynamic driving force to bury the larger hydrophobic surface area created by the addition of the

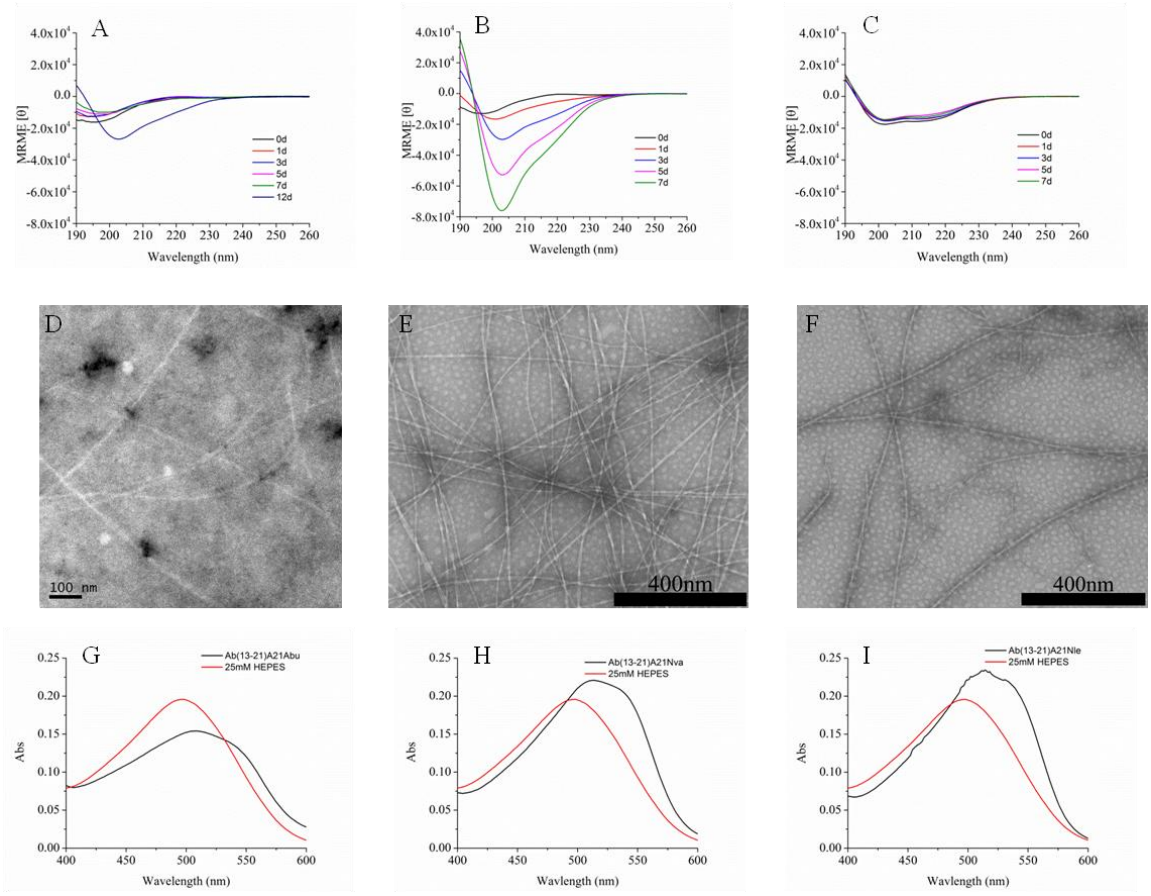

Figure 3.3 Increases in the *C*-terminal Hydrophobicity of Aβ(13-21) Promotes Amyloid Assembly at pH 7.5. A) CD spectra of Aβ(13-21)A21Abu, B) CD spectra of Aβ(13-21)A21Nva, C) CD spectra of Aβ(13-21)A21Nle, D) TEM image of Aβ(13-21)A21Abu, E) TEM image of Aβ(13-21)A21Nva, F) TEM image of Aβ(13-21)A21Nle, G) CR assay of Aβ(13-21)A21Abu, H) CR assay of Aβ(13-21)A21Nva, I) CR assay of Aβ(13-21)A21Nle. All samples were prepared at 1 mM in 25 mM HEPES pH 7.5.

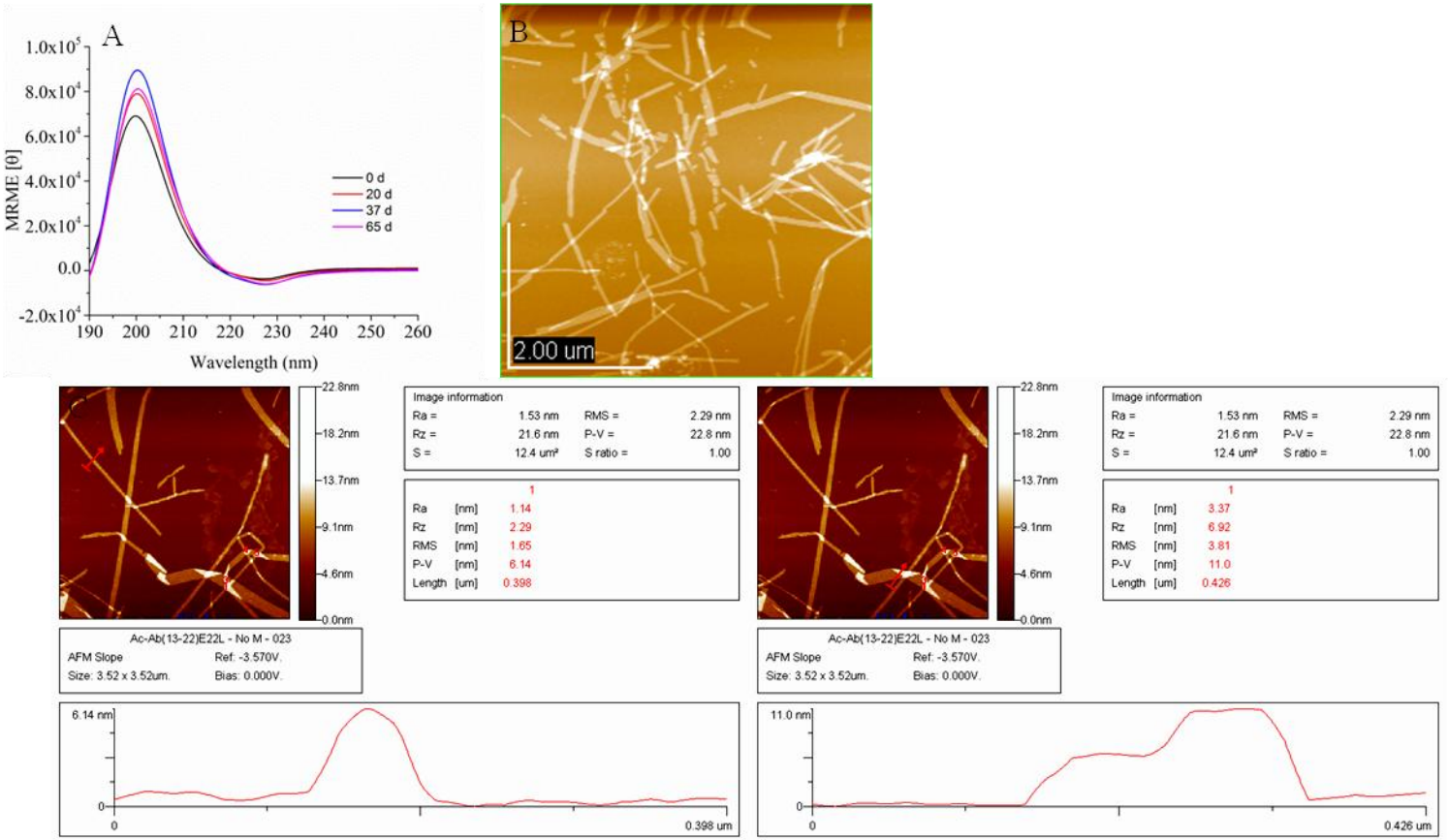

Figure 3.4 Increases in the C-terminal Hydrophobicity of Ac-Aβ(13-21) by Adding an Additional Amino Acid Promotes Amyloid Assembly at pH 7.5. A) CD spectra of Ac-Aβ(13-22)E22L, B) AFM image of Ac-Aβ(13-22)E22L highlighting a fibril with a red arrow. The height of this fibril is approximate 6 nm, C) AFM image of Ac-Aβ(13-22)E22L highlighting a sheet with a red arrow. The height of this sheet is approximate 5.5 nm as well but this structure folds onto itself with an approximate height of 11 nm. Sample prepared at 1 mM in 25 mM HEPES pH 7.5.

leucine residue (Liang, Pingali et al. 2008). Collectively, this data suggests that the transition to amyloid can be dominated by the degree of hydrophobicity at the *C*-terminus.

3.2.3 Incorporating Probes for Aβ(13-21) Assembly

Tryptophan was incorporated at several positions in this peptide to give Aβ(13-21)L17W, Aβ(13-21)V18W, Aβ(13-21)F19W, Aβ(13-21)F20W). Aβ(13-21)F19W and Aβ(13-21)F20W do not assemble at 1 mM while Aβ(13-21)L17W and Aβ(13-21)V18W at a concentration of 1 mM did assemble (Figure 3.5A-B, D-E, G-H). The *buriability*, a measurement of the driving force of side-chain burial in proteins (cal/mol/$Å^2$), of these residues likely explains observed results (Zhou and Zhou 2004). Tryptophan, phenylalanine, leucine, and valine have *buriability* values of 24.5, 23.9, 20.8, and 19.5, respectively. Tryptophan substitutions at L17 and V18 will result in an increased hydrophobic nature of Aβ(13-21) while the F19 and F20 substitutions do not result in such a change. Tryptophan substitutions at these positions affect the hydrophilic/hydrophobic ratio of Aβ(13-21) to differing degrees.

Previous work has shown that substituting the lysine residue with an alanine results in amyloid fibril assembly again consistent with the overall hydrophilicity/hydrophobicity balance (Dong, Shokes et al. 2006). At pH 7.5, Aβ(13-21)K16W assembles but later precipitates. Previous studies using Aβ(13-21)K16A were performed at pH 5.5 to avoid precipitation, and Aβ(13-21)K16W also assembles into sheets at this pH (Figure 3.6B-C). Previous work suggested that Aβ(13-21)K16A needs Zn^{2+} to form sheets due to the

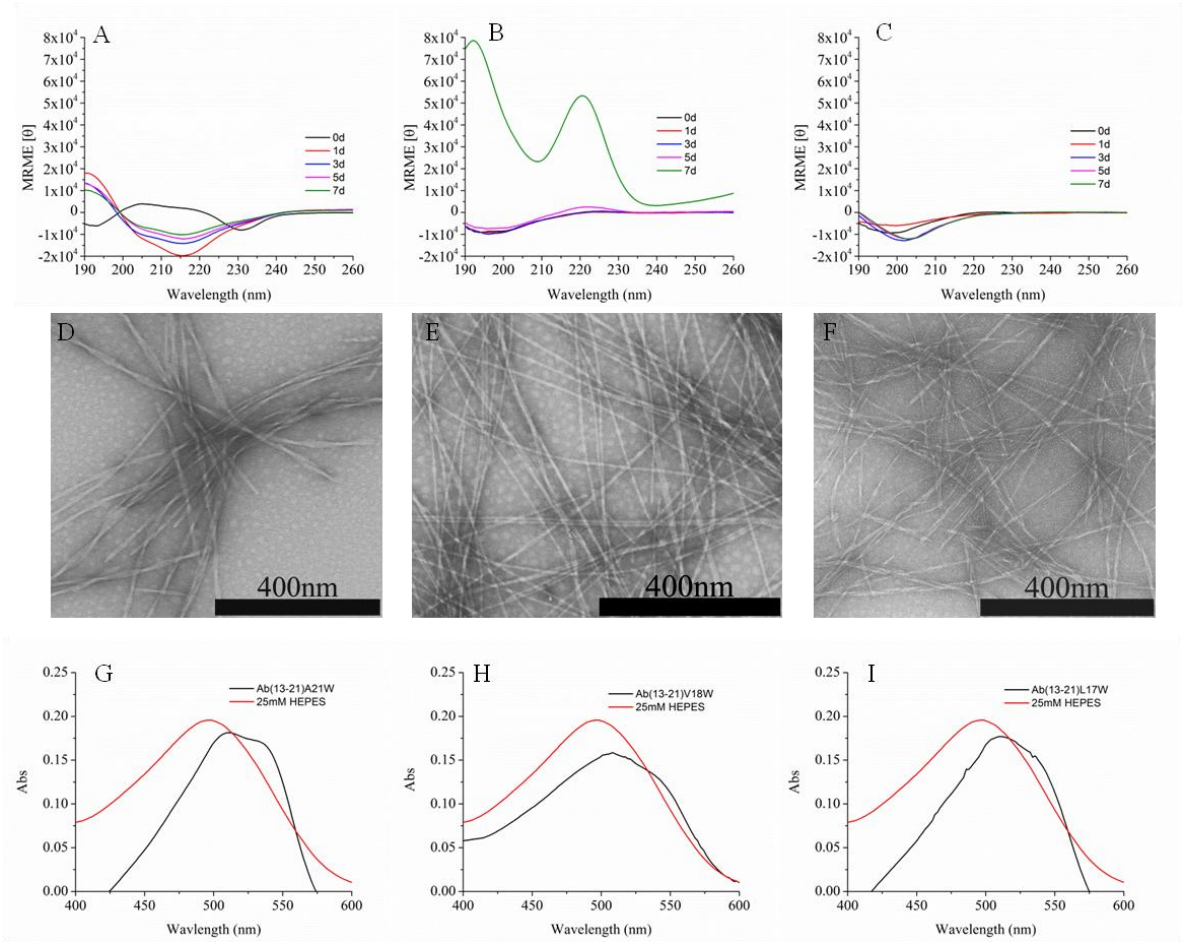

Figure 3.5 Increases in the non-*C*-terminal Hydrophobicity of Aβ(13-21) Promotes Amyloid Assembly at pH 7.5. A) CD spectra of Aβ(13-21)A21W, B) CD spectra of Aβ(13-21)V18W, C) CD spectra of Aβ(13-21)L17W, D) TEM image of Aβ(13-21)A21W, E) TEM image of Aβ(13-21)V18W, F) TEM image of Aβ(13-21)L17W, G) CR assay of Aβ(13-21)A21W, H) CR assay of Aβ(13-21)V18W, I) CR assay of Aβ(13-21)L17W. All samples were prepared at 1 mM in 25 mM HEPES pH 7.5.

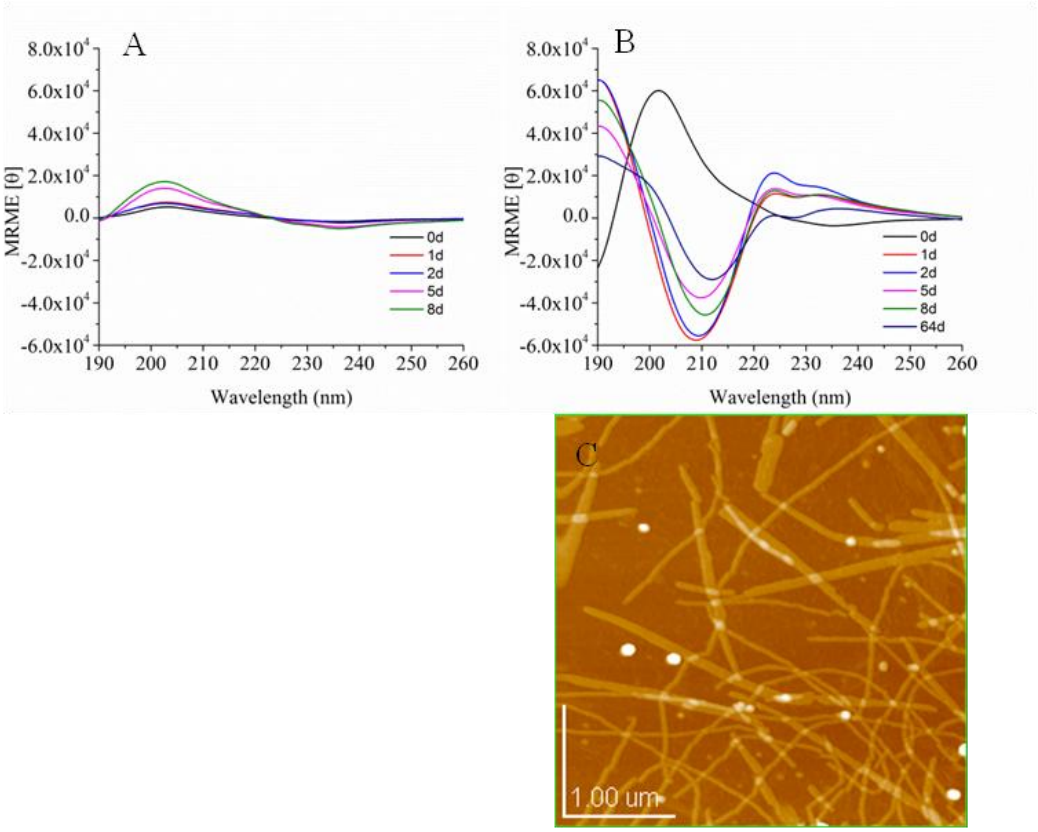

Figure 3.6 Aβ(13-21)K16W Assembly is Dependent on pH. A) CD spectra of 1 mM Aβ(13-21)K16W in 25 mM HEPES pH 7.5, B) CD spectra of 1 mM Aβ(13-21)K16W in 25 mM MES pH 5.5, C) AFM image of 1 mM Aβ(13-21)K16W in 25 mM MES pH 5.5.

increased stability that the metal coordination provides to lamination (Dong, Shokes et al. 2006), and aromatic base stacking may provide similar stabilization. These fluorescent substitutions now present an opportunity to probe amyloid assembly optically.

3.2.4 pH Dependent Aβ(13-21) Assembly

The hydrophilic/hydrophobic balance in the peptide sequence can be controlled around neutral pH because of the two histidine residues. Indeed 1 mM Aβ(13-21) peptides with a free *N*-terminus, two histidine residues, and a lysine residue do not assemble in 25 mM MES at pH 5.5 (Figure 3.7).

These two pH values account for protonation changes involving histidine; however, they do not cover deprotonation of the *N*-terminus or the lysine residue. Although these two positions are primary amines which suggest that they have a similar pK_a, calculated literature values indicated that these values can be different (Zhu, Kemple et al. 1995). If Aβ(13-21) is investigated at pH 11.5 in 25 mM CAPS, the sample precipitates immediately. If the sample is studied at pH 9.5 in 25 mM CAPS, the sample remains in an unassembled state with no observed precipitation. Therefore, it is concluded that these two amines have a similar pK_a. The charge state of the peptide controls whether these peptides assemble, but it does not answer the question of whether pH changes can influence the extent of assembly.

To determine whether amyloid assembly can be pushed towards more fibrils, Aβ(13-21)A21Nle and Aβ(13-21)A21Nva were used given their fast assembly rates at 1 mM. At pH 5.5, these two peptides do not assemble. At pH 7.5, the CD spectra of these two

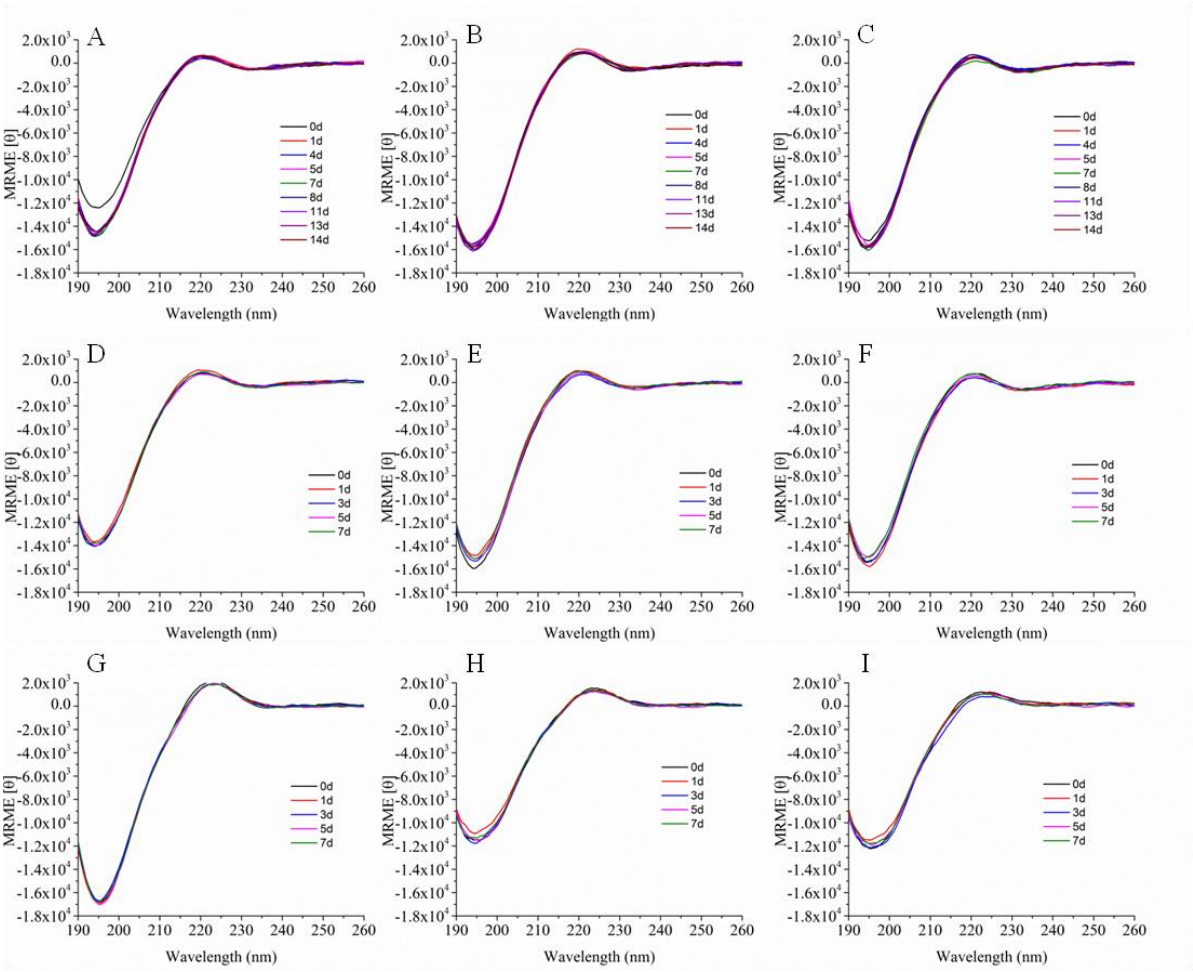

Figure 3.7 pH Affects the Assembly State of Amyloid Forming Peptides Derived from Aβ(13-21). A) CD spectra of Aβ(13-21)A21V, B) CD spectra of Aβ(13-21)A21L, C) CD spectra of Aβ(13-21)A21I, D) CD spectra of Aβ(13-21)A21Abu, E) CD spectra of Aβ(13-21)A21Nva, F) CD spectra of Aβ(13-21)A21Nle, G) CD spectra of Aβ(13-21)A21W, H) CD spectra of Aβ(13-21)V18W, I) CD spectra of Aβ(13-21)LL17W. All samples were prepared at 1 mM in 25 mM MES pH 5.5.

peptides have a negative peak at 203 nm and a shoulder at 215 nm. The shoulder at 215 nm suggests β-sheet secondary structure. TEM confirms the appearance of fibrils for both peptides. The 203 nm transition most likely indicates P_{II} structure (Schneider, Schneider et al. 1970; Sreerama and Woody 2003). If this secondary structural element does exist, then increasing the pH should cause this band to disappear as assembly is pushed further to the formation of fibrils. For Aβ(13-21)A21Nva, the 203 nm transition is weakened significantly pH 9.5 and pH 10.5 after assembly has reached an equilibrium (Figure 3.8). For Aβ(13-21)A21Nle, the 203 nm is also weakened between pH 7.5 and pH 8.5 (Figure 3.9). At higher pH values, these peptides begin to precipitate.

3.2.5 Probing the Side Chain Environment in Amyloid Fibrils by Fluorescence

Tryptophan fluorescence is sensitive to the polarity of it surrounding environment and provides an opportunity to evaluate assembly through the side chain in addition to the backbone signature (Lakowicz 2006). The λ maximum wavelength shifts are often used as a reporter for the side-chain environment (Lakowicz 2006). As seen above, 1 mM Aβ(13-21)F19W and 1 mM Aβ(13-21)F20W do not assemble and have λ maxima ~360 nm. This wavelength indicates a completely solvated tryptophan residue (Lakowicz 2006). Aβ(13-21)L17W, Aβ(13-21)V18W, and Aβ(13-21)A21W all assembled into amyloid fibrils at the same concentration, and Aβ(13-21)V18W had a single λ maximum at ~340 nm while Aβ(13-21)L17W and Aβ(13-21)A21W had maxima at ~320 nm and ~450 nm (Figure 3.10). The blue shifted maxima are diagnostic of less polar

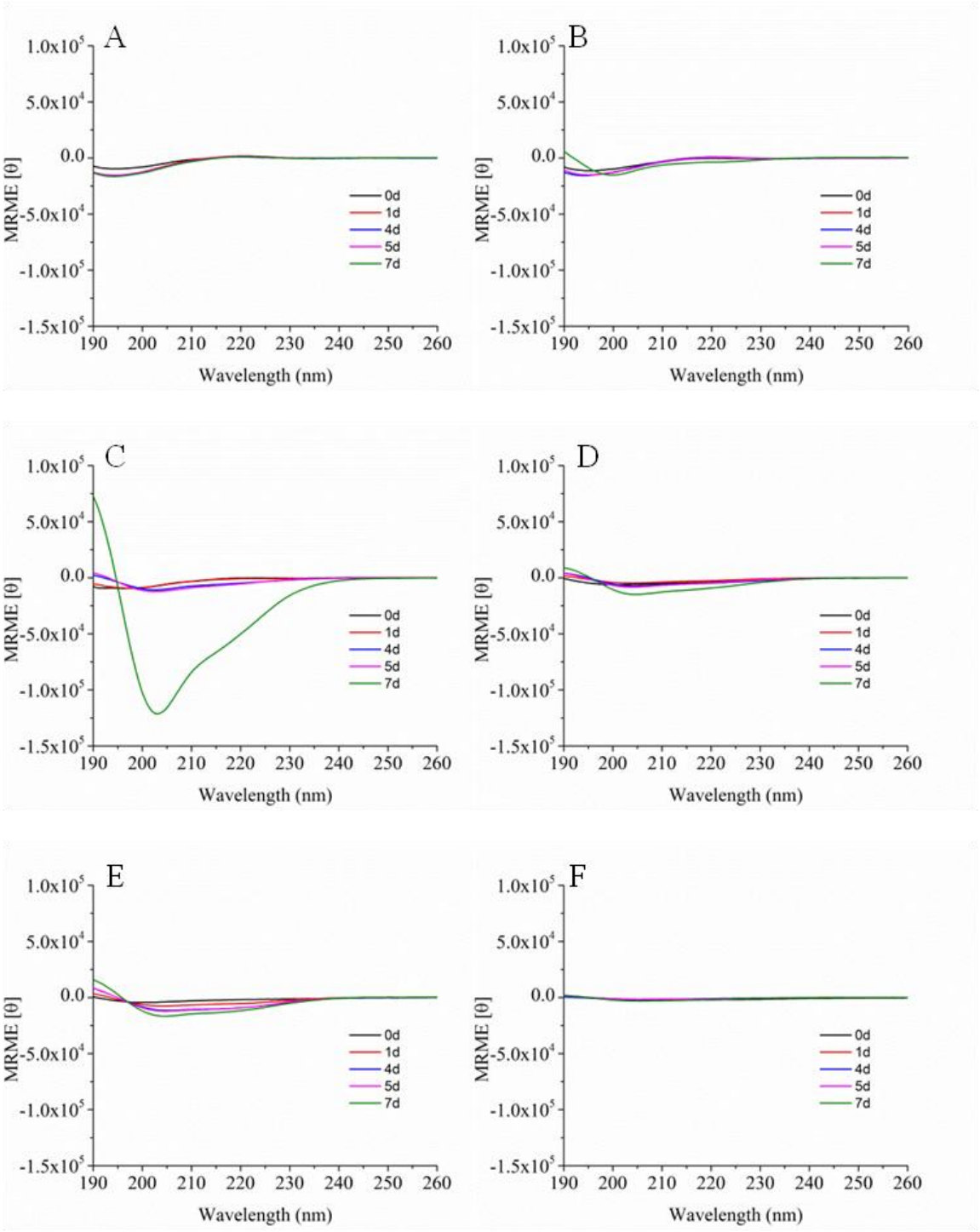
A
B
C
D
E
F
MRME [θ]
Wavelength (nm)
0d
1d
4d
5d
7d
1.0x10^5
5.0x10^4
0.0
-5.0x10^4
-1.0x10^5
-1.5x10^5
190
200
210
220
230
240
250
260

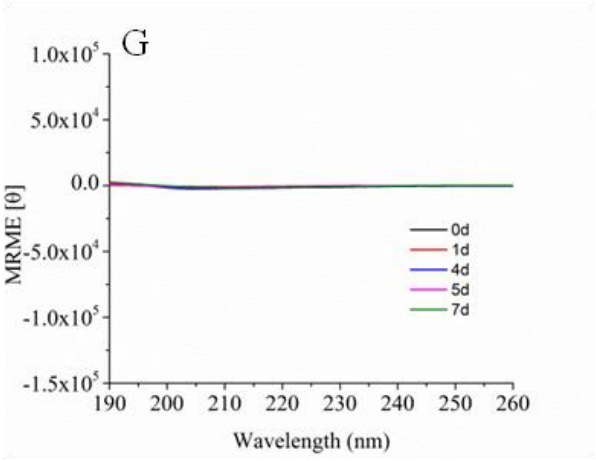

Figure 3.8 pH Increases Promotes Amyloid Assembly Changes as Demonstrated by CD for Aβ(13-21)A21Nva. A) pH 5.5 25 mM MES, B) pH 6.5 25 mM MES, C) pH 7.5 25 mM HEPES, D) pH 8.5 25 mM Bicine, E) pH 9.5 25 mM CAPS, F) pH 10.5 25 mM CAPS, G) pH 11.5 25 mM CAPS.

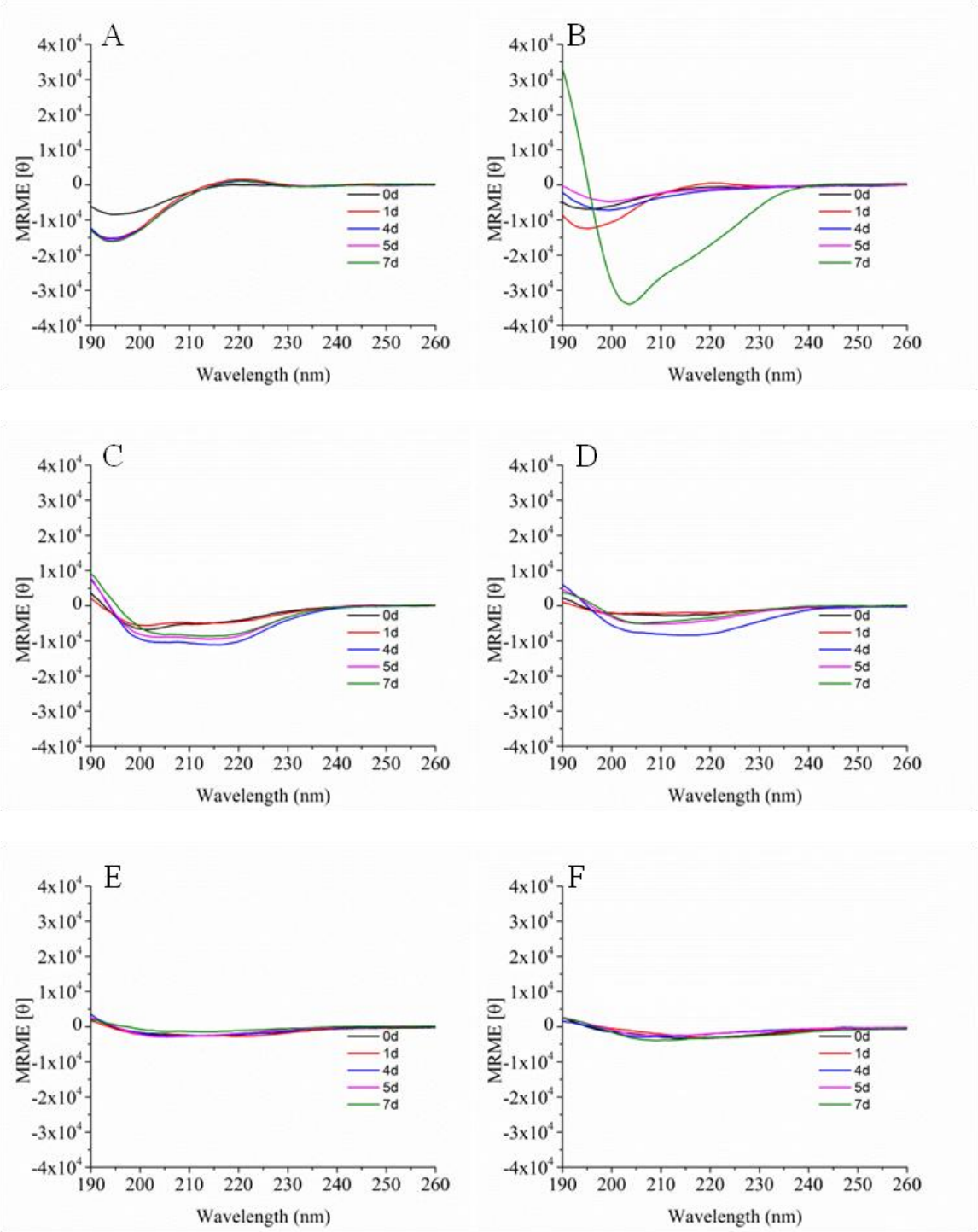
A
B
C
D
E
F
MRME [θ]
Wavelength (nm)
0d
1d
4d
5d
7d

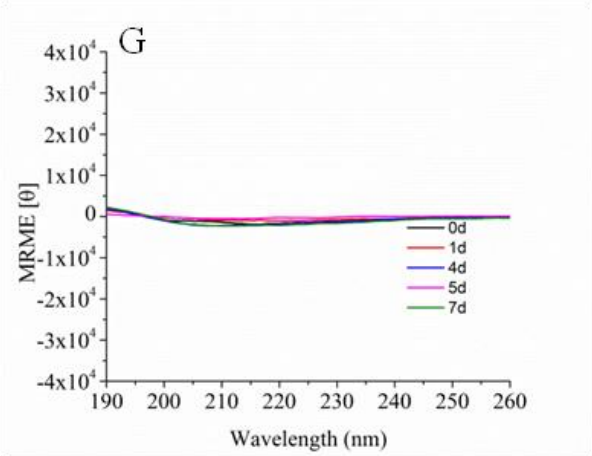

Figure 3.9 pH Increases Promotes Amyloid Assembly Changes as Demonstrated by CD for Aβ(13-21)A21Nle. A) pH 5.5 25 mM MES, B) pH 6.5 25 mM MES, C) pH 7.5 25 mM HEPES, D) pH 8.5 25 mM Bicine, E) pH 9.5 25 mM CAPS, F) pH 10.5 25 mM CAPS, G) pH 11.5 25 mM CAPS.

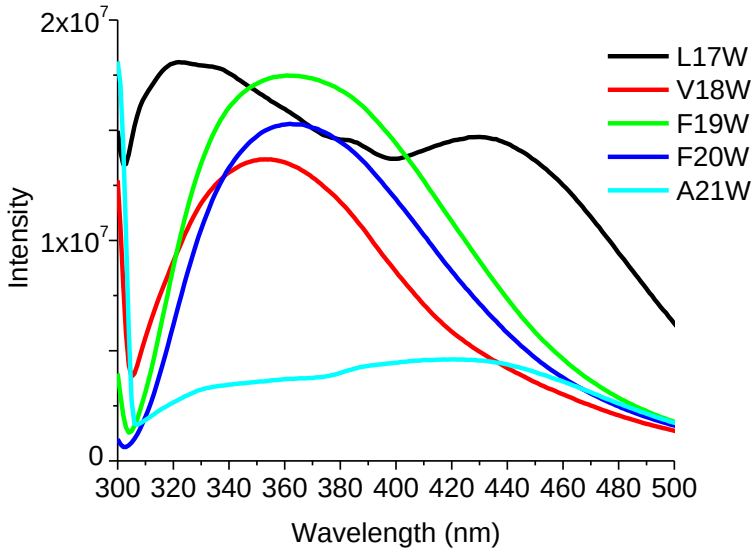

Figure 3.10 Emission Spectra of Tryptophan Substituted Aβ(13-21) Peptides.

environments and the double maxima can be attributed to excimer formation between the tryptophan residues (Keleti 1970).

Because Aβ(13-21)L17W and Aβ(13-21)A21W precipitated and due to the slow assembly of Aβ(13-21)V18W, the doubly substituted peptide, Aβ(13-21)F20WA21I, was investigated. This peptide assembles at pH 7.5 (Figure 3.11A), but in 25 mM MES at pH 5.5, the peptide does not assemble (Figure 3.11B). The assemblies display the classical Congo red UV shift (Figure 3.11C), and ATR FT-IR shows rich β-sheet structure (Figure 3.11D). The tryptophan emission maximum at 358 nm in the assembled state at pH 7.5 indicates a buried indole ring while the unassembled peptide fluoresces at 362 nm at pH 5.5 indicative of a solvated tryptophan (Figure 3.11D) (Lakowicz 2006). Also, it is noted that emission intensity increases, indicating the motion of the tryptophan residue is more restricted relative to the monomeric peptide (Tang, Yin et al. 2009). Fluorescence anisotropy measurements support this conclusion with a value is 0.09 for the assembled case and 0.02 for the unassembled state. Fibrils are seen when imaged by TEM and AFM (Figure 3.11F-G).These tryptophan fluorescence emission spectra show that the tryptophan is in a different environment depending on it location in the sequence.

To control the side-chain size, the para-cyano-phenylalanine (Fcn) was investigated. The fluorescence emission intensity of this probe is also sensitive to the solvent polarity (Serrano, Troxler et al. 2010). Aβ(13-21)F20FcnA21I, Aβ(13-21)F20FcnA21Nle, Aβ(13-21)F19FcnA21I, Aβ(13-21)F19FcnA21Nle were all prepared and found to be equally sensitive to pH (Figure 3.12A-D and 3.13A-D). The fluorescence emission spectra of these peptides are however distinct. Aβ(13-21)F20FcnA21I and Aβ(13-21)F20FcnA21Nle fluorescence intensities decrease relative to the unassembled state

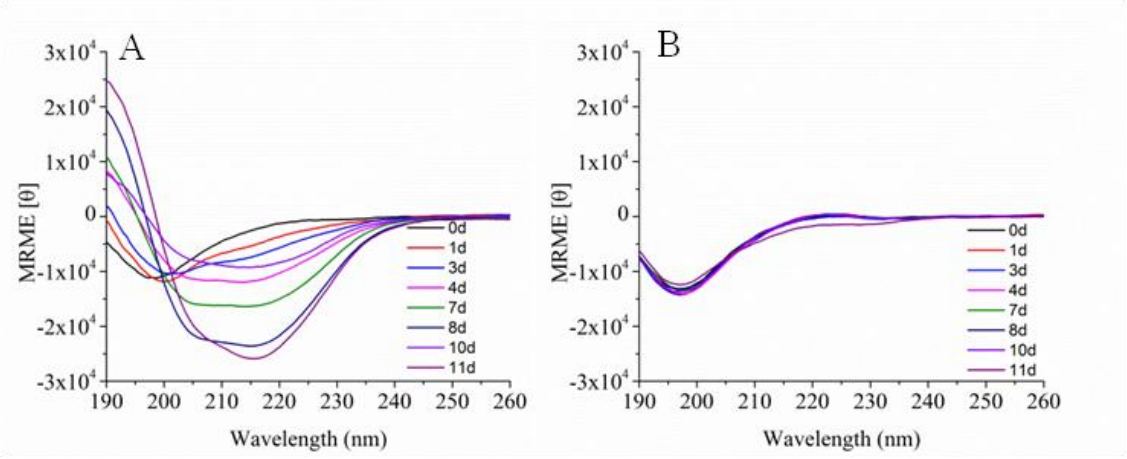
A
B
MRME [θ]
Wavelength (nm)
0d
1d
3d
4d
7d
8d
10d
11d

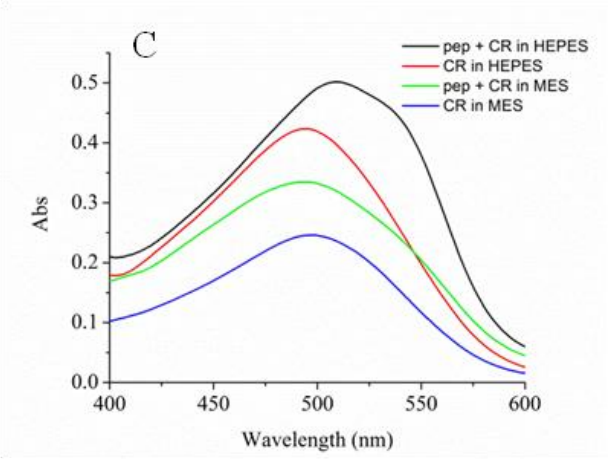
C
pep + CR in HEPES
CR in HEPES
pep + CR in MES
CR in MES
Abs
Wavelength (nm)

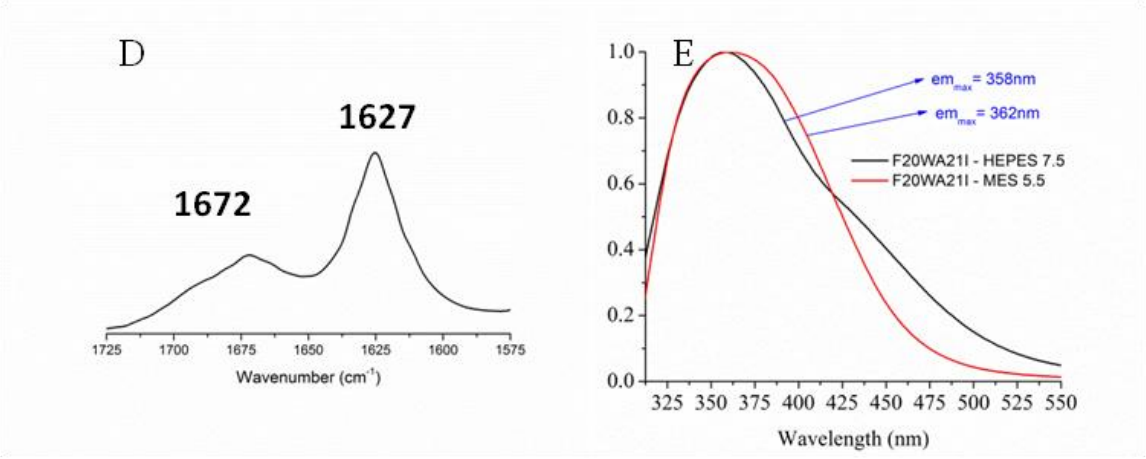
D
1627
1672
Wavenumber (cm-1)
E
emmax = 358nm
emmax = 362nm
F20WA21I - HEPES 7.5
F20WA21I - MES 5.5
Wavelength (nm)

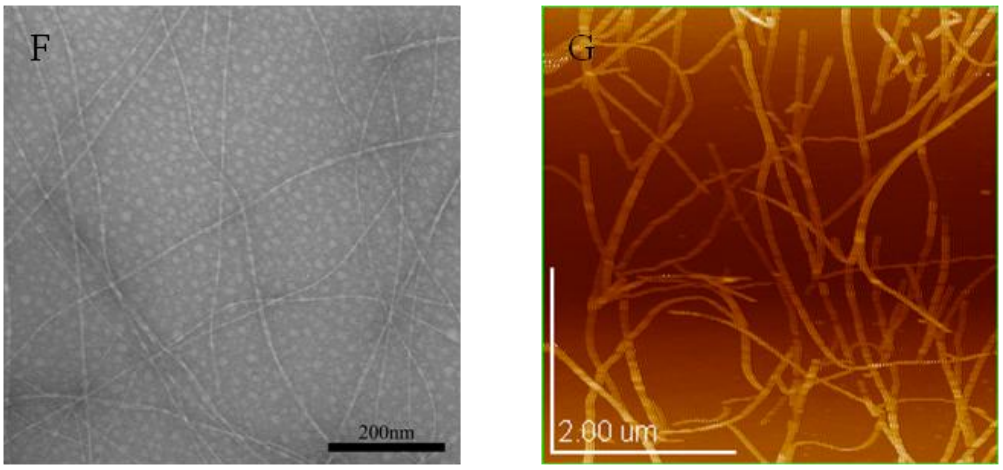

Figure 3.11 Characterization of Aβ(13-21)F20WA21I. A) CD spectra at 1 mM in 25 mM HEPES pH 7.5, B) CD spectra at 1 mM in 25 mM MES pH 5.5, C) CR binding assay, D) ATR FT-IR spectra of sample assembled at 1mM in 25 mM HEPES pH 7.5, E) Normalized tryptophan fluorescence emission spectra at different pH values, F) Fibrils revealed in TEM image, G) Fibrils revealed in AFM image.

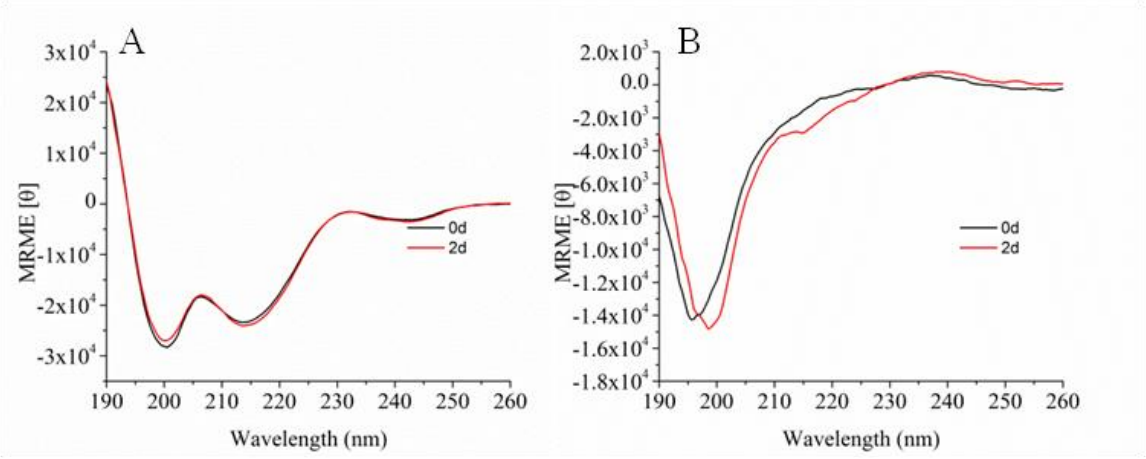
A
B
MRME [θ]
Wavelength (nm)
0d
2d

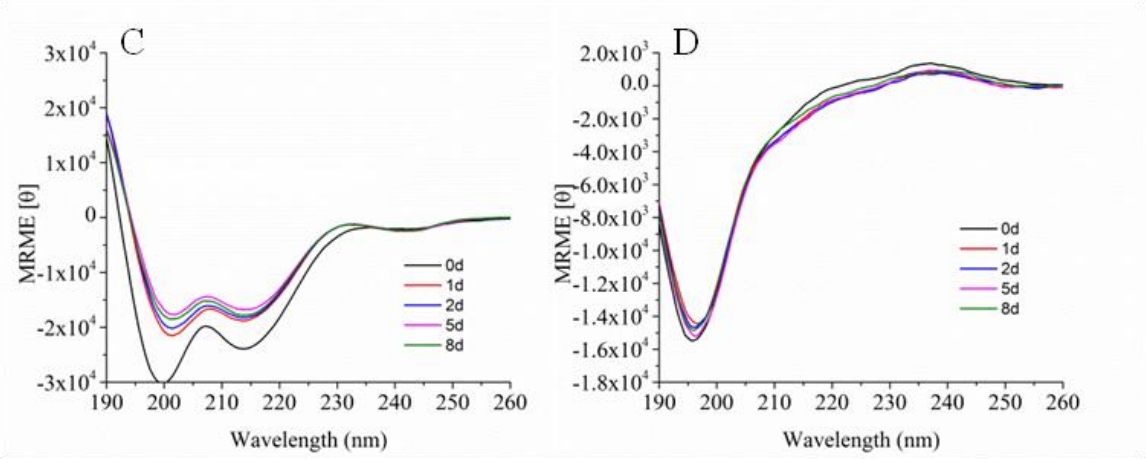
C
D
MRME [θ]
Wavelength (nm)
0d
1d
2d
5d
8d

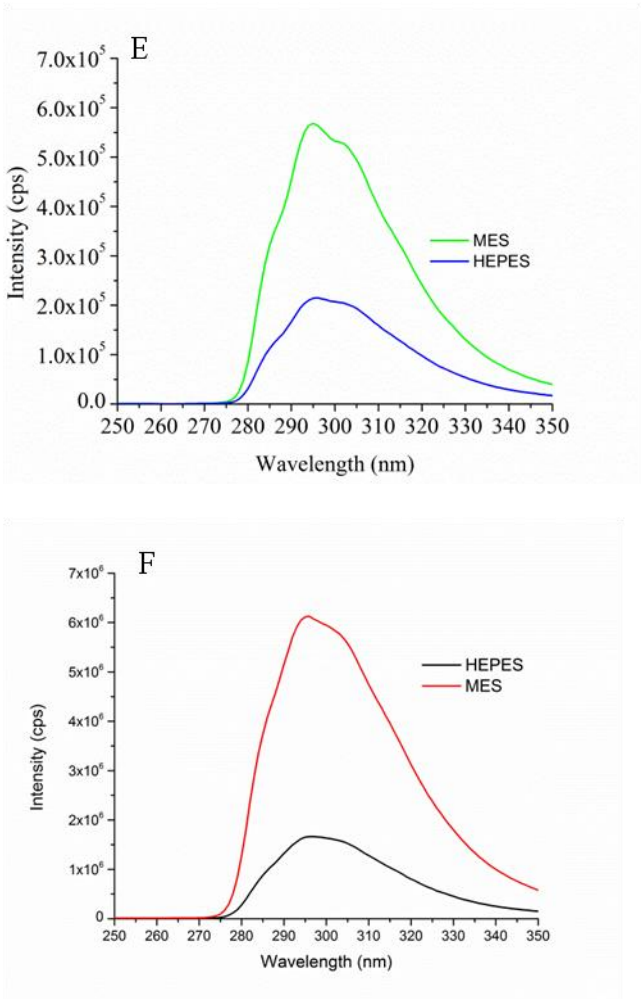

Figure 3.12 Characterization of Aβ(13-21)F20FcnA21I and Aβ(13-21)F20FcnA21INle. A) Far-UV CD of 1 mM Aβ(13-21)F20FcnA21I in 25 mM HEPES pH 7.5, B) Far-UV CD of 1 mM Aβ(13-21)F20FcnA21I in 25 mM MES pH 5.5, C) Far-UV CD of 1 mM Aβ(13-21)F20FcnA21Nle in 25 mM HEPES pH 7.5, D) Far-UV CD of 1 mM Aβ(13-21)F20FcnA21Nle in 25 mM MES pH 5.5. E) Fluorescence emission of 1 mM Aβ(13-21)F20FcnA21I, F) Fluorescence of 1 mM Aβ(13-21)F20FcnA21Nle.

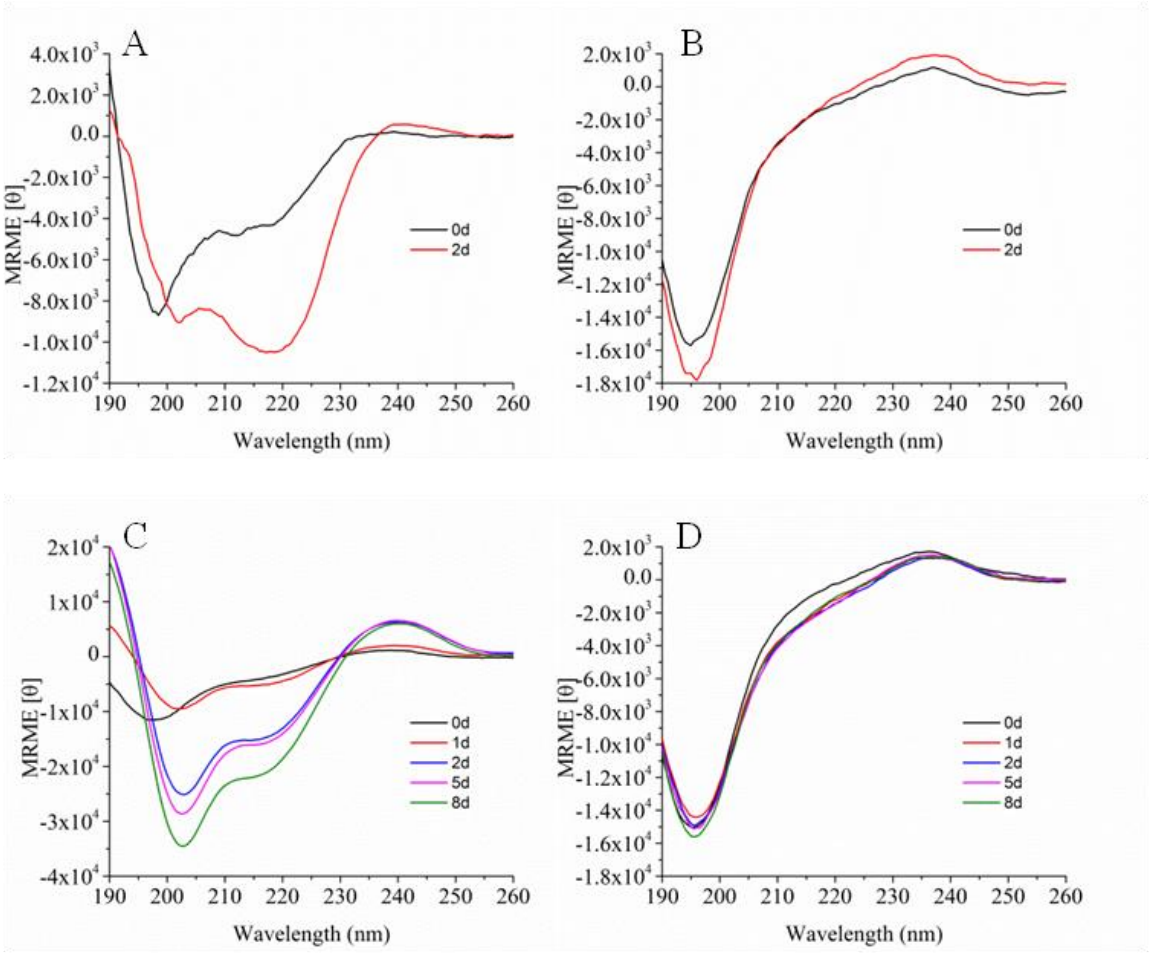
A
B
C
D
MRME [θ]
Wavelength (nm)
0d
1d
2d
5d
8d

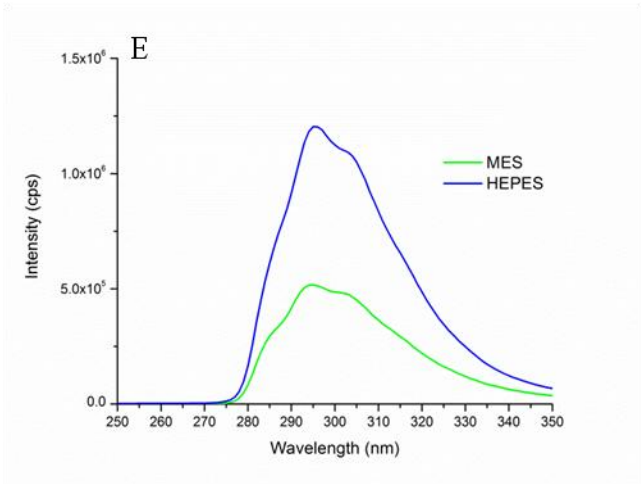

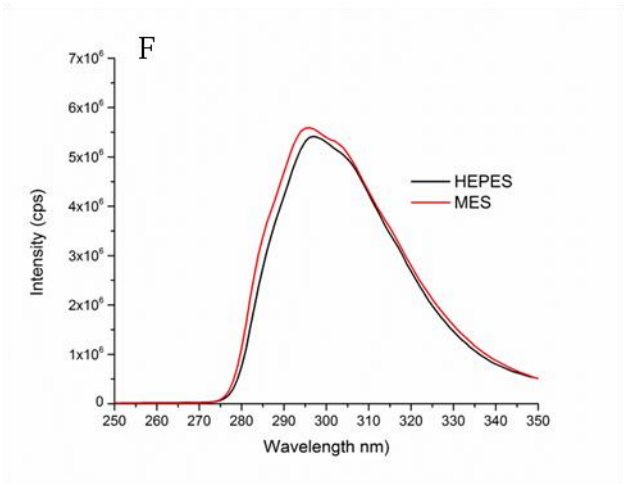

Figure 3.13 Characterization of Aβ(13-21)F19FcnA21I and Aβ(13-21)F19FcnA21INle. A) Far-UV CD of 1 mM Aβ(13-21)F19FcnA21I in 25 mM HEPES pH 7.5, B) Far-UV CD of 1 mM Aβ(13-21)F19FcnA21I in 25 mM MES pH 5.5, C) Far-UV CD of 1 mM Aβ(13-21)F19FcnA21Nle in 25 mM HEPES pH 7.5, D) Far-UV CD of 1 mM Aβ(13-21)F19FcnA21Nle in 25 mM MES pH 5.5. E) Fluorescence emission of 1 mM Aβ(13-21)F19FcnA21I, F) Fluorescence of 1 mM Aβ(13-21)F19FcnA21Nle.

(Figure 3.12E-F) while the intensity of Aβ(13-21)F19FcnA21I increases relative to the unassembled state (Figure 3.13E). In contrast, the Fcn emission intensity for Aβ(13-21)F19FcnA21Nle does not change dramatically (Figure 3.13F), and there are no wavelength shifts for the emission maxima. The intensity variation of Fcn has been attributed to several different phenomena including quenching and differences in the cyano group hydrogen-bond partner (Serrano, Troxler et al. 2010), so these emission intensity fluctuations are most consistently used as a reporter for the degree of hydrogen bonding with the cyano group (Serrano, Troxler et al. 2010).

Clearly, tryptophan and Fcn fluorescence establish that the side-chain environments of the 19^{th} and 20^{th} positions are different. From these fluorescence emission changes, it is postulated that the laminate stacking of these peptide assemblies are different. This difference could arise from differing intra-β-strand (β-sheet) contacts that orient the side chain differently in space or from difference in the inter-β-strand (lamination) contacts. Another more plausible explanation for these observed differences is that the orientation of the aromatic side chain places the ring structure in a different environment even though the lamination is the same by changes in the side-chain bond angle.

3.2.6 Probing the Side Chain Environment in Amyloid Fibrils by Near-UV CD

Near-UV CD analysis can probe the position of aromatic side chains (Strickland 1974; Barth, Martin et al. 1998; Gasymov, Abduragimov et al. 2003), and the near-UV CD of tryptophan is dominated by the ^1L_a and ^1L_b vibronic transitions (Figure 3.14A). The ^1L_a transition is broad and lacks vibronic structure while spectra containing predominantly

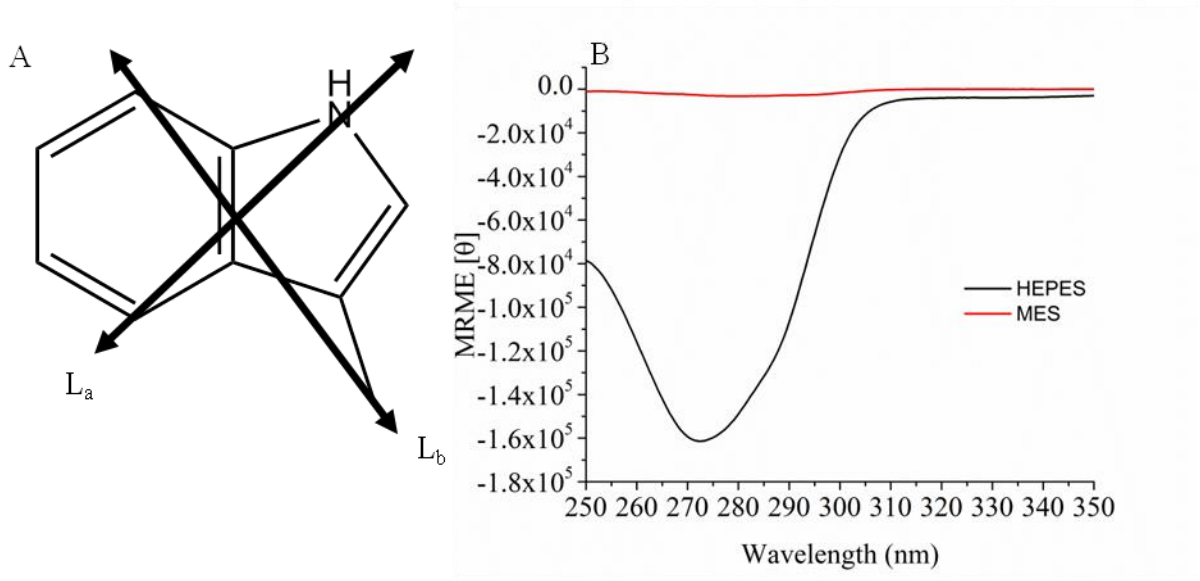

Figure 3.14 Near-UV CD of Aβ(13-21) Tryptophan Fluorescent Substitutions. A) Tryptophan transition moments for the near-UV region. B) Aβ(13-21)F20WA21I.

the ^1L_b transition possess well defined vibronic bands. Because these transitions overlap in this spectral region, the spectra have been grouped into four types: Type 1 spectra resembles the ^1L_b transition, Type 2 resembles the ^1L_a transition, Type 3 is a combination of both ^1L_a and ^1L_b transitions, and Type 4 do not display any characteristics of either or of a combination of a ^1L_a or ^1L_b transition. The near-UV CD for Aβ(13-21)F20WA21I most resembles that of Type 2 spectra – the ^1L_a transition – in the unassembled and assembled states (Figure 3.14B), which predominately occurs in polar solvents or in the presence of hydrogen-bonding partners and displays several other changes upon assembly. At pH 5.5 a condition under which the peptide does not assembly, the ellipticity is positive, which likely stems from μ-μ coupling with the adjacent phenylalanine (Strickland 1974; Barth, Martin et al. 1998; Gasymov, Abduragimov et al. 2003).

Upon assembly, the tryptophan ellipticity becomes negative, adopts a stronger negative ellipticity, and is red shifted (Figure 3.14B). The change from positive to negative ellipticity suggests that the residue adopts a different rotamer conformation. The negative ellipticity intensity change correlates to a reduction in the indole mobility and suggests more aromatic ring interactions are present. The red shift suggests that the indole ring is buried. All of these scenarios are expected in an assembled amyloid fibril and support the fluorescence data.

The cyano-Phe (Fcn) has a smaller side-chain perturbation and again the far-UV CD of Aβ(13-21)F20FcnA21I and Aβ(13-21)F19FcnA21I confirmed assembly. Further, the near-UV CD spectra again reveal two different trends for the 20th and 19th positions; Aβ(13-21)F20FcnA21I has a negative transition, similar to Aβ(13-21)F20WA21I, while

for Aβ(13-21)F19FcnA21I the transition is positive (Figure 3.15A,C). Two additional peptides were synthesized to confirm whether these trends for the 20th and 19th positions exist in other peptides. Aβ(13-21)F20FcnA21Nle and Aβ(13-21)F19FcnA21Nle behave similarly to the A21I substitutions (Figure 3.15B,D).

Previous studies employing molecular modeling have shown that the conformation of F19 and F20 are similar (Liang, Pingali et al. 2008; Mehta, Lu et al. 2008; Senguen, Lee et al. 2011); however, these results suggest that amyloid assemblies can have different F19 and F20 conformations. Although the peptides presented above display differences with respect to the side-chain environment, they all contain similar CD characteristics regardless of fluorophore or position. The strong 203 nm transition in the far-UV CD probably stems from the presence of the P_{II} transition (Sreerama and Woody 2003).

3.2.7 Revisiting Concentration Dependent Amyloid Assembly

Taken together and to avoid the complications stemming from branched amino acid side-chains, bulky aromatic side chains, pH changes, sample viscosity and peptide mixing experiments, the previously substituted Aβ(13-21)A21Abu peptide was selected for further study. The CD spectrum of this peptide assembly at 1 mM does not display the characteristic β-sheet bands (Figure 3.16A). The classical CD signature of a model β-sheet contains a positive band at 196 nm and a negative band at 216 nm (Brahms, Brahms et al. 1977). However, a second CD signature is commonly assigned as β-sheet, which contains a positive band at 190 nm, a negative band around 200 nm, and a negative shoulder around 220 nm (Sreerama and Woody 2003). These two predominating CD

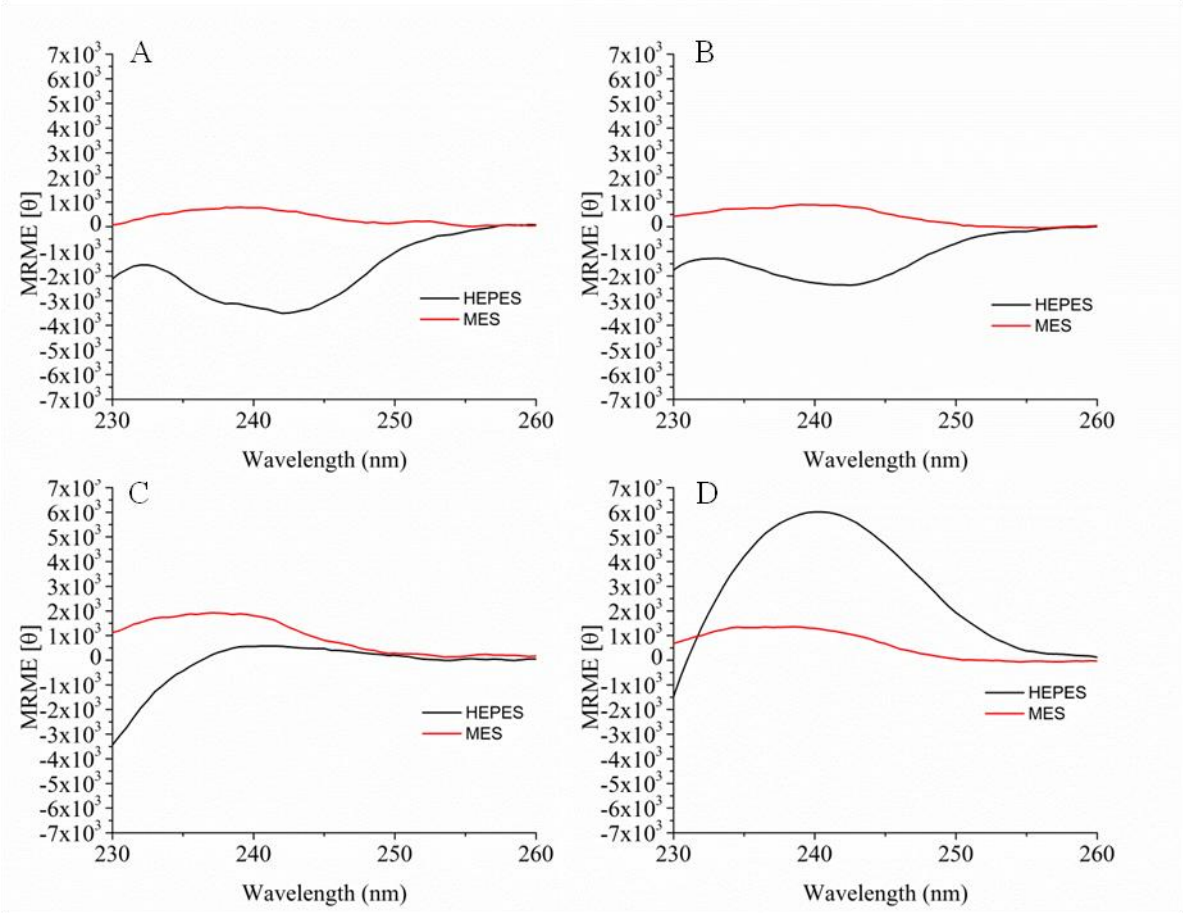

Figure 3.15 Near-UV CD of Aβ(13-21) Cyanophenylalanine Fluorescent Substitutions. A) Aβ(13-21)F20FcnA21I. B) Aβ(13-21)F20FcnA21Nle. C) Aβ(13-21)F19FcnA21I. D) Aβ(13-21)F19FcnA21Nle.

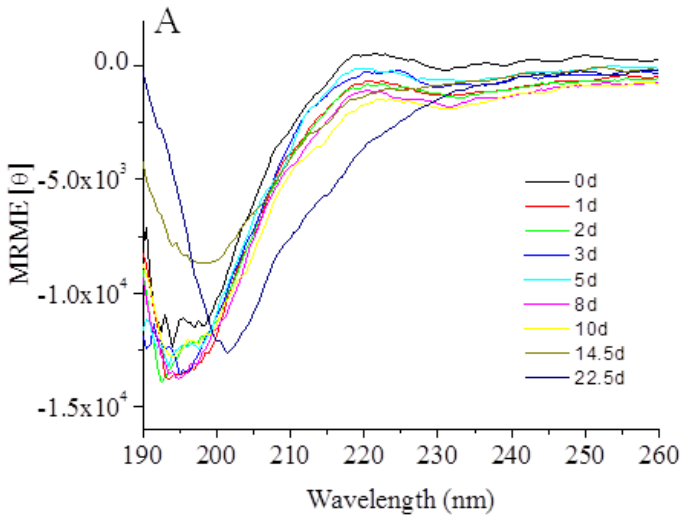
A
0.0
-5.0x10^3
-1.0x10^4
-1.5x10^4
MRME [θ]
190
200
210
220
230
240
250
260
Wavelength (nm)
0d
1d
2d
3d
5d
8d
10d
14.5d
22.5d

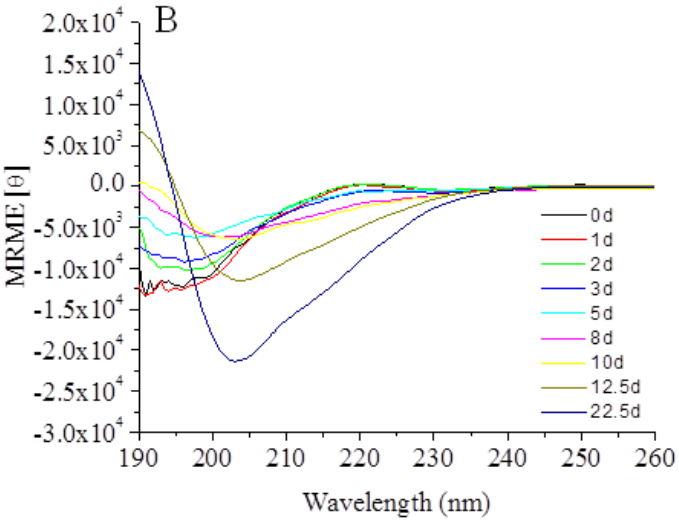
B
2.0x10^4
1.5x10^4
1.0x10^4
5.0x10^3
0.0
-5.0x10^3
-1.0x10^4
-1.5x10^4
-2.0x10^4
-2.5x10^4
-3.0x10^4
MRME [θ]
190
200
210
220
230
240
250
260
Wavelength (nm)
0d
1d
2d
3d
5d
8d
10d
12.5d
22.5d

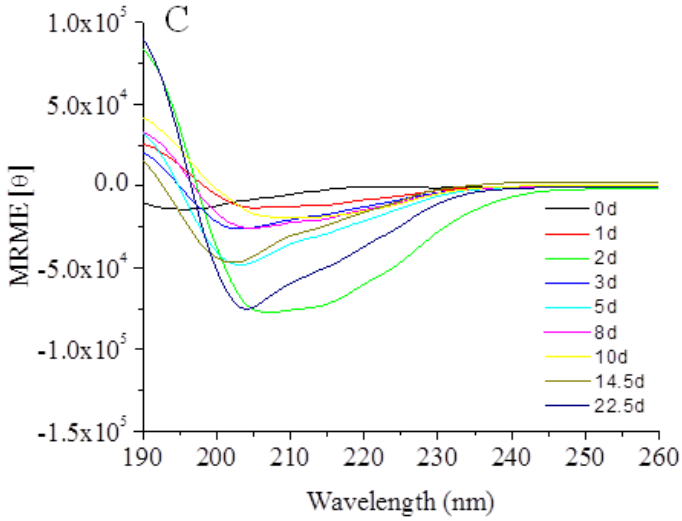
C
1.0x10^5
5.0x10^4
0.0
-5.0x10^4
-1.0x10^5
-1.5x10^5
MRME [θ]
190
200
210
220
230
240
250
260
Wavelength (nm)
0d
1d
2d
3d
5d
8d
10d
14.5d
22.5d

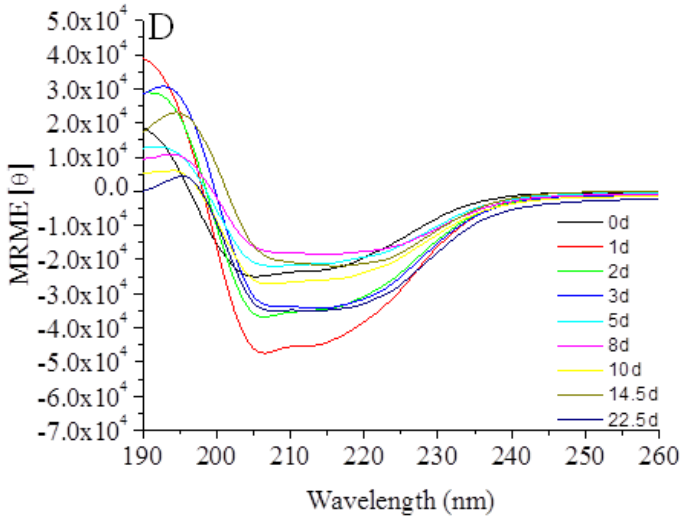
D
5.0x10^4
4.0x10^4
3.0x10^4
2.0x10^4
1.0x10^4
0.0
-1.0x10^4
-2.0x10^4
-3.0x10^4
-4.0x10^4
-5.0x10^4
-6.0x10^4
-7.0x10^4
MRME [θ]
190
200
210
220
230
240
250
260
Wavelength (nm)
0d
1d
2d
3d
5d
8d
10d
14.5d
22.5d

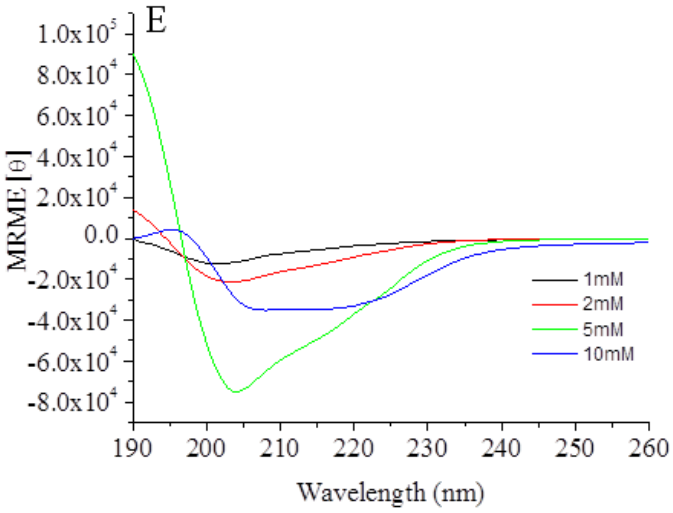

Figure 3.16 Secondary Structural Characterization Aβ(13-21)A21Abu by CD. A) 1 mM, B) 2 mM, C) 5 mM, D) 10 mM, E) Combine CD spectra of each concentration on the 22.5 d.

spectra for β-sheets have been classified as β_I- and β_{II}-proteins (Wu, Yang et al. 1992). After correlating the CD spectra with crystal structures, the difference between β_I and β_{II} proteins is the ratio of two different amide conformations: β-sheet and P_{II} (Sreerama and Woody 2003). Most β_I proteins have a P_{II} to β-sheet ratio lower than 0.3 while a ratio greater than 0.4 is observed for β_{II} proteins (Sreerama and Woody 2003). These data suggest that Aβ(13-21)A21Abu is best characterized as a β_{II}-protein with the band at 203 nm indicative of a P_{II} secondary structure and the shoulder at 215 nm representing β-sheet. Fibrils are observed in the TEM and AFM images (Figure 3.17A-B), and this sample gives the classic Congo red UV shift (Figure 3.18A). The P_{II} conformation is now conclusively present in both unassembled and assembled amyloid states, however it is unclear whether the P_{II} is an on- or off-pathway element.

If a P_{II} is associated with the formation of amyloid assembly, then concentration increases of Aβ(13-21)A21Abu should result in the growth and eventual disappearance of the transition responsible for this secondary structure. Samples of this peptide prepared at 2 mM, 5 mM, and 10 mM, prepared from the same 20 mM stock solution support this conclusion (Figure 3.16B-D). The 203 nm transition increases as the concentration increases from 1 mM to 2 mM to 5 mM, and then decreases in the 10 mM sample. Interestingly, the 1 mM, 2 mM, and 5 mM spectra contain a positive band at 190 nm while the 10 mM sample possesses a positive band at 195 nm. Fibrils are observed by TEM and AFM (Figure 3.17C-H). To determine whether the differences observed in the CD spectra stem from differences in the degree of secondary structure or difference in the β-sheets, an aliquot of the assembled samples was removed, lyophilized and analyzed by ATR FT-IR (Figure 3.18B). Collecting spectra at a resolution of 2 cm^{-1}, ATR FT-IR

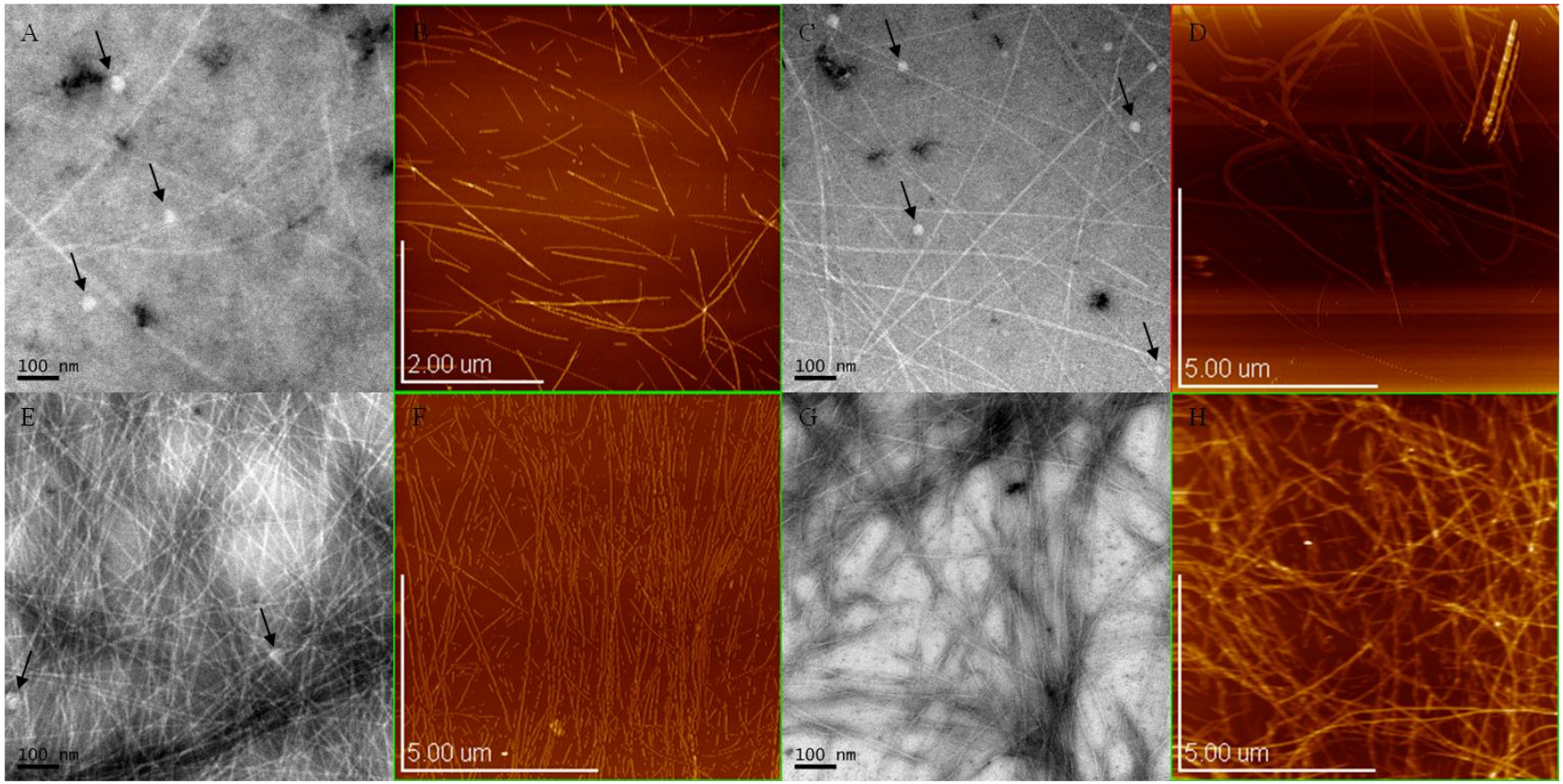

Figure 3.17 TEM and AFM images of Aβ(13-21)A21Abu reveals the presences of peptide oligomers and fibrils. A) 1 mM. B) 2 mM. C) 5 mM. D) 10 mM.

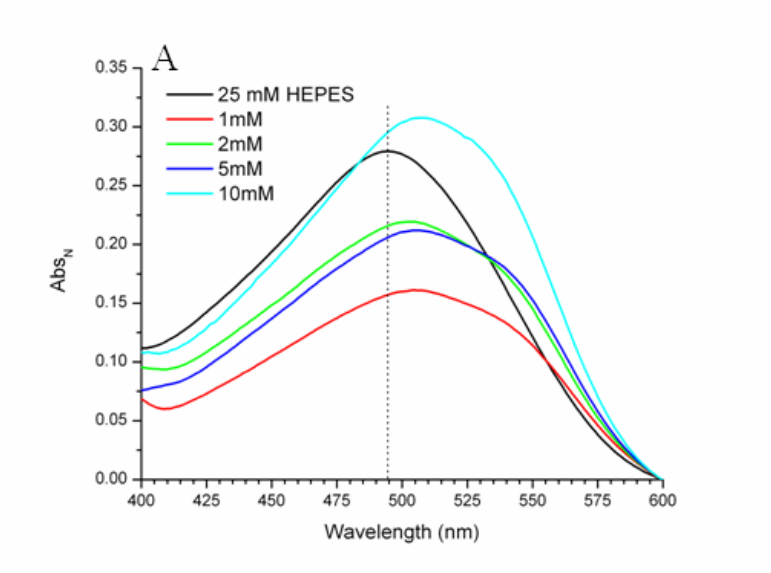
A
25 mM HEPES
1mM
2mM
5mM
10mM
Abs$_N$
Wavelength (nm)

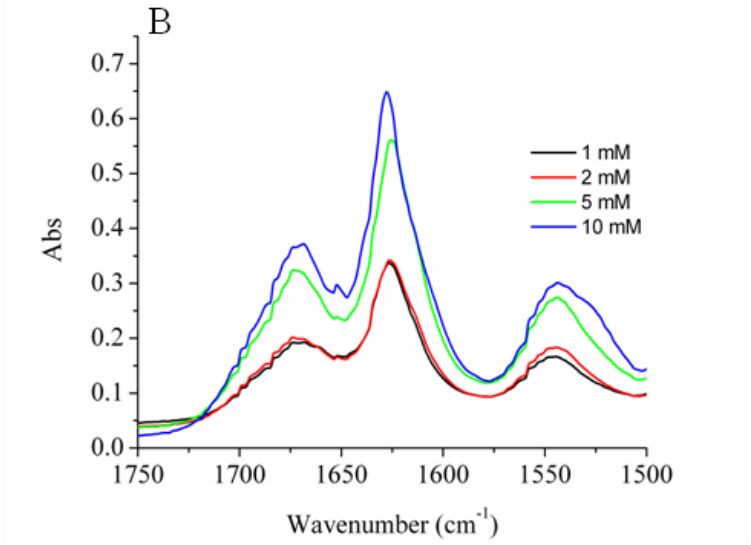
B
1 mM
2 mM
5 mM
10 mM
Abs
Wavenumber (cm^{-1})

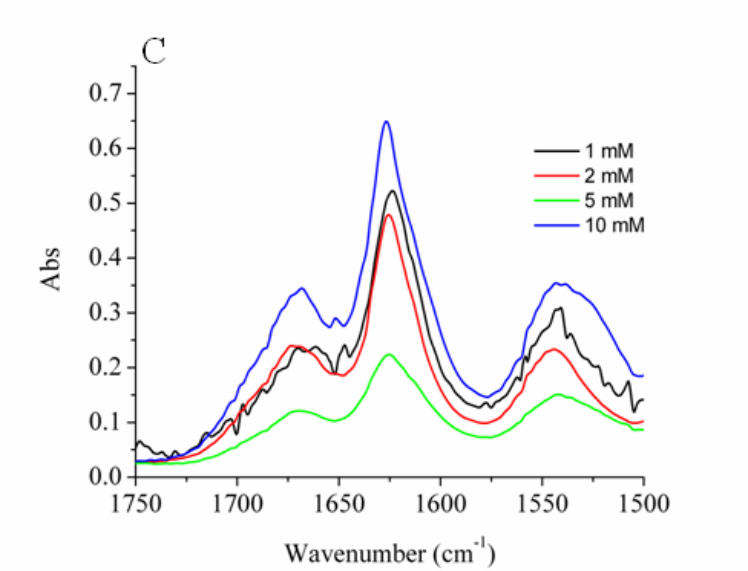

Figure 3.18 Biophysical characterization of Aβ(13-21)A21Abu at different concentrations reveals the same amyloid characteristics. A) CR spectral shift assay of 1 mM, 2 mM, 5 mM, 10 mM Aβ(13-21)A21Abu. B) ATR FT-IR spectra of Aβ(13-21)A21Abu at 1 mM, 2 mM, 5 mM, 10 mM. C) ATR FT-IR spectra of 1 mM, 2 mM, 5 mM, 10 mM Aβ(13-21)A21Abu supernatant after centrifugation.

analysis reveals that the β-sheets are identical. ATR FT-IR spectra of pelleted samples that were centrifuged at 12,000 x g, which has been reported to remove aggregated peptide structures, gave similar results, further strengthening the argument that the fibrils contain the same β-sheet core structure (Figure 3.18C) (Dewald, Hodges et al. 2011). The classical Congo red spectral shift assay further confirms the formation of amyloid structures (Figure 3.18A). These data show that the final assembled fibril structure for all four concentrations contain the same β-sheet secondary structure and thus the secondary structural analysis by CD implies that these four samples exist at different percentages of amyloid assembly and share the P_{II} conformation in the unassembled fraction.

Careful analysis of the TEM images of these samples revealed further insight into the assembly (Figure 3.17). All four samples contain fibrils of similar dimensions, but a noticeable difference in the lower concentration samples (1 mM, 2 mM, and 5 mM) is the appearance of spherical particles similar in structure to previously observed peptide oligomers (Ahmed, Davis et al. 2010). These oligomeric species appear as different phases (Liang, Lynn et al. 2010) and form different microenvironments with dynamic properties similar to those for lipid micelles and phospholipid membranes (Safarzadeh-Amiri, Thompson et al. 1989).

Clearly, these peptide assemblies are sensitive to their environment (Lu, Jacob et al. 2003; Dong, Shokes et al. 2006; Lu 2006; Dong, Canfield et al. 2007) and can form different structures at pH 2 and pH 6 (Lu, Jacob et al. 2003; Lu 2006). Additionally, amyloid assembly is sensitive to metals (Dong, Shokes et al. 2006; Dong, Canfield et al. 2007), and the Aβ truncations and substitutions in this chapter are also sensitive to the solvent polarity and the pH. When Aβ(13-21) was dissolved in a 50:50 mixture of

TFE:water, the CD signature closely represents that of a 3_{10}-helix (Figure 3.19) (Andersen, Liu et al. 1996; Maekawa, Toniolo et al. 2006; Crisma, Saviano et al. 2007) while it adopts a P_{II} conformation in water. The most striking difference between a P_{II} and a 3_{10}-helix is the twist handedness. P_{II} have a left-handed twist while the 3_{10}-helices have a right-handed twist (Figure 3.20) (Manning and Woody 1991; Toniolo, Polese et al. 1996), suggesting that amyloid peptides can adopt very different helical twists as a function of solvent polarity.

3.3 Conclusions

A complete biophysical characterization of unassembled and assembled amyloid forming peptides of Aβ(13-21) has allowed for the construction of a model for amyloid assembly. The data presented in this chapter gives details for tightly controlling amyloid assembly experimentally using pH and concentration. Amyloid assembly is a concentration dependent process that involves the aggregation of monomeric peptides that transition into fibrils. This transition involves a P_{II} that undergoes a conformational change when experiencing different polarity microenvironments. The common features of all the peptides studied here suggest a general assembly model for the formation of amyloid structures.

Interpreting the present data presents a molecular mechanism responsible for amyloid assembly initiation (Figure 3.21). The data in this section supports that a P_{II} is a secondary structure that exists along the amyloid assembly pathway. Chapter 1 supports that this structure is present in the absence of any oligomeric species. Since these amyloid

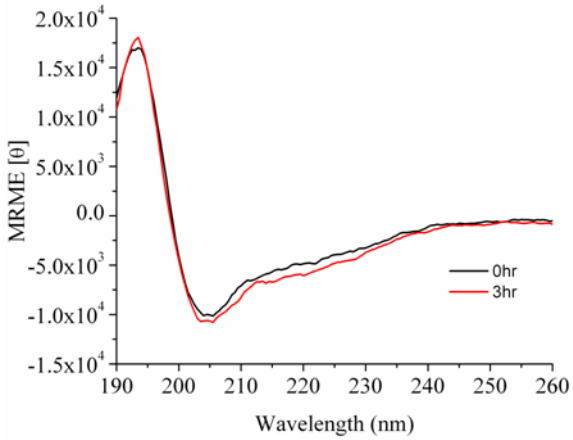

Figure 3.19 Conformational plasticity of Aβ(13-21). A) CD spectra of 0.5 mM Aβ(13-21) in 50:50 TFE:water in 25 mM HEPES.

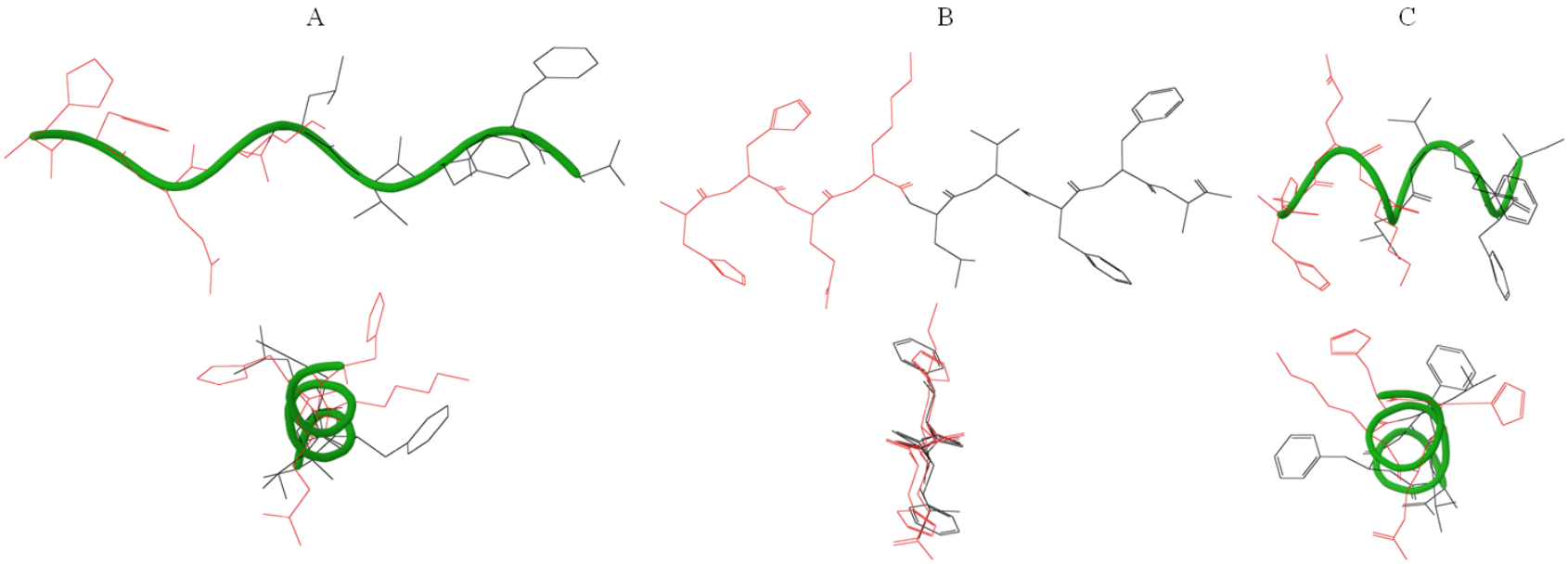

Figure 3.20 –Secondary Structures Present as Observed by CD at Various Concentrations of Aβ(13-21)A21Abu. A) P_{II} B) β-strand, C) 3_{10}-helix.

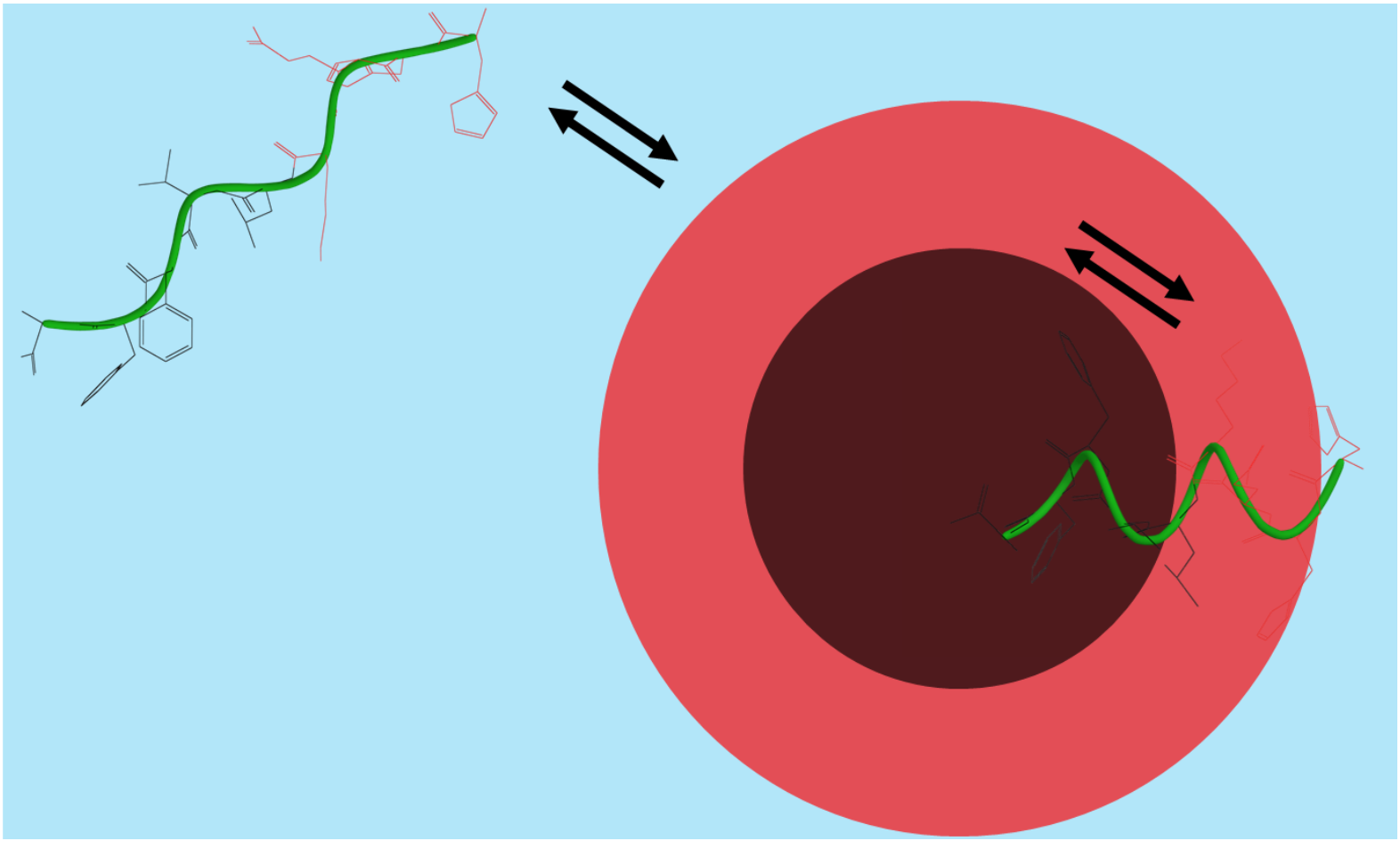

Figure 3.21 Proposed Amyloid Assembly Initiation Proceeds by Conformational Exchange. In solution the peptide adopts a P_{II} secondary structure. When the peptide associated with the surface of the oligomer, it adopts a β-strand secondary structure and can associated with other β-strand monomers to initiate amyloid assembly. If the peptide inserts into the hydrophobic core of the oligomer, then the secondary structure resembles a 3_{10}-helix. Blue = solution, Red = hydrophilic, Black = hydrophobic.

peptide truncations can adopt different secondary structures solely dictated by solvent polarity, a conformational exchange mechanism is proposed as an initiator of amyloid assembly since solvent polarity can change the handedness of these helical structures. Hydrophobic side-chain burial is believed to promote amyloid assembly by driving oligomer formation. It is therefore proposed that the peptide monomers exchange in and out of these spherical particles causing the amide backbone to adopt a change in helical handedness. This change requires that the peptide untwist potentially through an extended (β-strand) conformation. The most likely position for this conformational exchange to occur is at the oligomer-water interface. With the peptide in an extended conformation, it is able to hydrogen bond with other β-strands thereby initiating amyloid formation.

Further dynamic interactions between oligomers result in fibril propagation (Figure 3.22). The β-strands located at the oligomer-water interface can hydrogen bond with other β-strands at this same location to form β-sheets by the fusion of additional oligomers to the end of the fibril. This results in β-sheet growth in the hydrogen bonding dimension. The β-strands and/or β-sheets located at the interface of the oligomers can also associate with other β-sheets on different oligomers for growth in the lamination dimension. Higher order fibril associations (fibril dimers, fibril trimers, *etc.*) stem from collisions of oligomers containing β-strands and or β-sheets that result in peptide termini associations. These dynamic interactions will be transient. They also do not bias the peptide towards a specific β-strand orientation or registry within the fibril not does it control the number of laminated β-sheets, but rather lets kinetics and thermodynamics to control amyloid assembly.

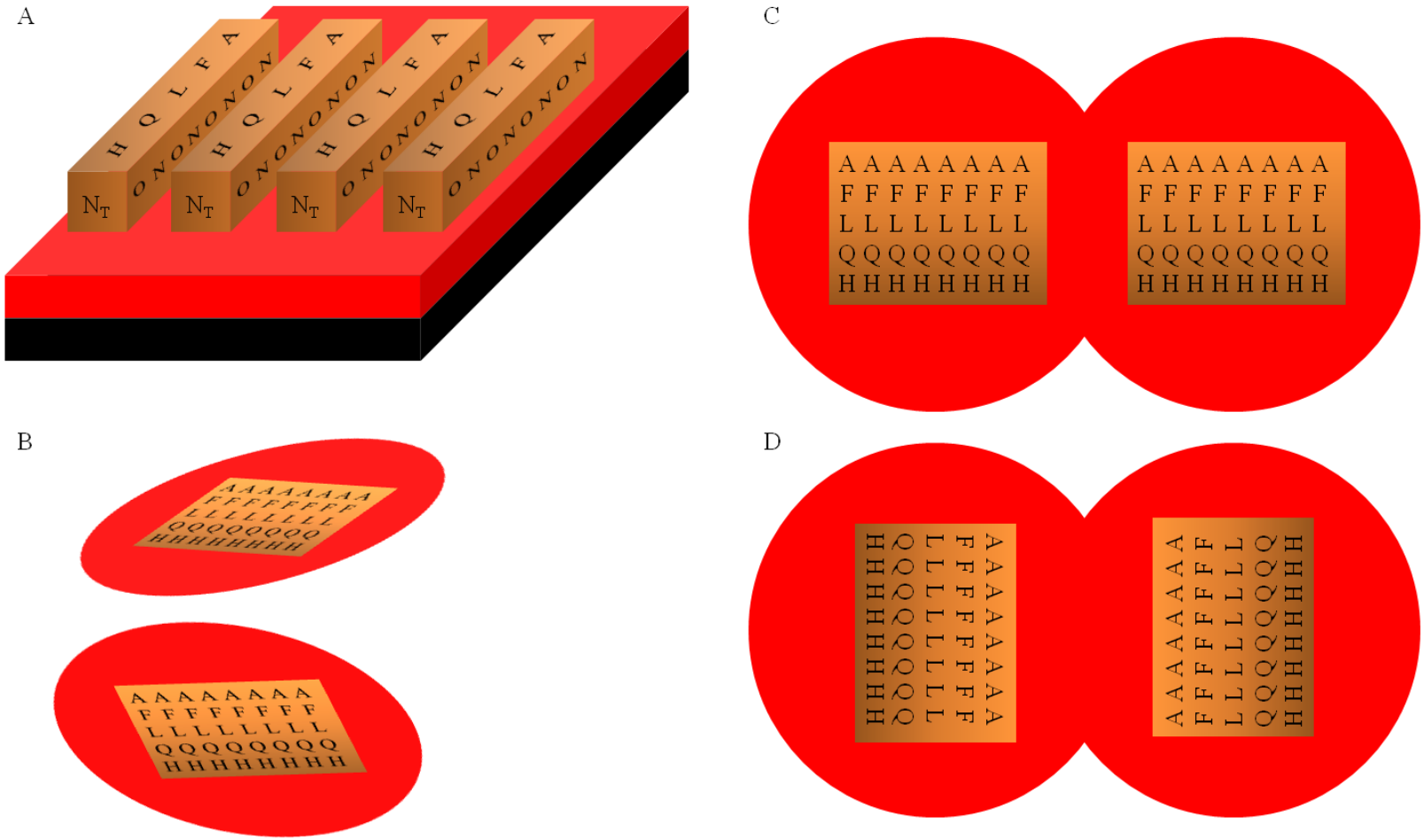

Figure 3.22 Proposed Amyloid Assembly Pathway Propagation Proceeds by Conformational Exchange. A) β-strand association to form β-sheets on oligomer surface, B) Oligomer fusion that orients the β-sheets that allows for the propagation of the β-sheet, C) Oligomer fusion that propagates fibril growth in the lamination dimension, D) Oligomer fusion that results in the N- and/or C-terminal association that results in fibril dimers.

This amyloid forming peptide possesses macromolecular structural characteristics similar to that of lipid molecules which self-assemble into micelles and membranes. Micelles closely resemble the oligomeric species observed along the amyloid assembly pathway. The lipid-solvent or membrane-solvent interface offers a similar polarity microenvironment that can potentially initiate amyloid assembly by mimicking the environment at the oligomer-water interface. The physical similarities suggest that membranes can influence the dynamic interactions predicted for conformational exchange mechanism of amyloid assembly. However, membranes posses several different experimentally controllable characteristics that need investigation to determine the role these properties play in amyloid formation before any mechanistic investigation.

3.4 Methods

3.4.1 Materials

Solid-phase peptide synthesizer reagents (*i.e.*, FMOC-amino acids, peptide resins) were obtained from Anaspec, Inc. (San Jose, CA). Distilled deionized water (ddH_2O) was purchased from EMD Chemicals, Inc. (Gibbstown, NJ) for sample preparations. All other reagents were acquired from Sigma-Aldrich Chemical Co. (Milwaukee, WI).

3.4.2 Peptide Synthesis and Purification

Peptide synthesis was performed using standard FMOC solid-phase peptide chemistry on a FMOC Rink-amide polystyrene resin (AnaSpec, Inc., sub. 0.4-0.6 meq/g) by a

Rainin Symphony Quartet multiplex solid-phase peptide synthesizer (Protein Technologies, Tucson, AZ) or a Liberty Microwave solid-phase peptide synthesizer (CEM, Matthews, NC).

On the Rainin Symphony Quartet, HBTU and NMM were the coupling reagents. Each amino acid was coupled for 2 hours. His13, His14, Gln15, Lys16, Leu17, Val18 and Phe19 were double coupled. An acetylation reaction was performed after every coupling reaction to eliminate deletion peptides. On the CEM Liberty, HBTU and NMP/DIEA were the coupling reagents. Each amino acid was single coupled following the standard coupling reaction conditions from CEM. An acetylation reaction was performed after every coupling reaction to eliminate deletion peptides.

The cleavage/deprotection reaction was carried out with trifluoroacetic acid/thiolanisole/EDT/anisole (95/5/3/2, v/v). The crude peptide was precipitated using cold ethyl ether and centrifuged at 6,500 rpm for 10 min at 4 ^{o}C. The crude product was then washed with cold ethyl ether and centrifuged four additional times. The crude peptide was kept under vacuum until purified.

All peptides were purified by RP-HPLC using a Waters Delta 600 and a Jasco LC2000 HPLC with a Zorbax 300SB-C18 preparative HPLC column (21.2mm x 25cm) and eluted at 10 mL/min. The peptide was dissolved in H_2O with 0.1% TFA. If the solution was cloudy, the crude mixture was filtered though a 0.2 μm filter (Whatman). A linear gradient from 15%/85% MeCN/H_2O with 0.1% TFA to 45%/55% MeCN/H_2O with 0.1% TFA was used. The HPLC peak was collected, condensed, frozen at -80 °C, and lyophilized (ATR FD3.0 freeze dryer or a Labconco FreeZone 12Plus freeze dryer).

Lyophilized peptides were stored at -20 or -80 °C. MALDI-TOF MS analysis (Voyager-DE^{TM} STR Biospectrometry Workstation; 2,5-dihydroxybenzoic acid matrix) was collected on each peptide.

3.4.3 Peptide Sample Preparation

Peptide stock solutions were prepared by dissolving a known amount of peptide in ddH_2O at twice the desired concentration, sonicating for 10 min, and centrifuging at 13,200 x g for 10 min. The supernatant was collected and used as the peptide stock solution. 1 mM samples were prepared by diluting a 2 mM stock solution with 50 mM of the desired buffer and pH. 0.5 mM samples were further diluted with 25 mM of the desired buffer solution.

3.4.4 Circular Dichroism (CD)

CD spectra were collected using a Jasco J-810 CD spectropolarimeter (Easton, MD). Three spectra were recorded from 260 nm to 190 nm (step size = 0.2 nm, speed = 100 nm/s) using a 0.1 mm path length quartz slides at room temperature and averaged automatically. Each spectrum was background subtracted (using the same acquisition protocol) from the same conditions without peptide. Samples were heated using a peltier controller. Each sample was equilibrated at the desired temperature for 5 min before data acquisition.

3.4.5 Congo red Binding Assay

To the 1 mM samples was added Congo red to a final concentration of 7 mM. UV-Vis spectra were collected in a 1 cm path length quartz cuvette using a Jasco V-530 UV/Vis spectrometer.

3.4.6 Transmission Electron Microscopy (TEM)

Approximately 5 μL of the sample solution was placed on a Formvar/Carbon-coated 300 mesh copper grid (Electron Microscopy Science, Hatfield, PA) for 3 min. The excess solution was wicked away using triangular filter paper. 5 μL of 2% uranyl acetate or ammonium tungstate staining solution was applied to the TEM grid for 1.5 min, and the excess staining solution was wicked away. All grids were stored in a desiccator overnight. A Philips transmission electron microscope operating at 80 kV or a Hitachi H-7500 transmission electron microscope operating at 75 kV in the Robert P. Apkarian Integrated Electron Microscopy Core facility was used to obtain electron micrographs. Micrographs were digitally imaged used a Gatan BioScan 1K CCD camera with the accompanying imaging software (Gatan Inc., Pleasanton, CA).

3.4.7 Atomic Force Microscopy (AFM)

Approximately 5 μL of the sample solution was placed on a silicon chips (Ted Pella, Redding, CA). The sample was forcefully washed away with 1000 μL of ddH_2O. Images

were acquired on a JEOL JSPM-4210 AFM operating in tapping mode under dry conditions with ultra-sharp silicon cantilevers.

3.4.8 Fluorescence Emission

Fluorescence emission measurements were acquired on a SPEX FluoroMax-3 and analyzed using DataMAX (Horiba Jobin Yvon, Edison, NJ). The excitation wavelength was 295 nm for tryptophan and 241 nm for Fcn. Tryptophan emission spectra were collected from 300 nm to 600 nm. Fcn emission spectra were acquired from 250 nm to 350 nm. The data pitch was 1 nm. The integration time was 0.5 sec. Data displayed is the average of three scans.

3.4.9 Fluorescence Anisotropy

Fluorescence anisotropy measurements were acquired on a SPEX FluoroMax-3 and analyzed using DataMAX (Horiba Jobin Yvon, Edison, NJ). The excitation wavelength was 295 nm, and the emission wavelength was at the emission maxima was determined for each peptide at each individual concentration before anisotropy data was collected. The anisotropy values represent the average of 100 acquisitions.

3.4.10 Attenuated Total Reflectance Fourier Transform Infrared Spectroscopy (ATR FT-IR)

ATR FT-IR spectra were collected on a Jasco FT-IR 4100 spectrophotometer (Jasco, MD) attached with a Gladiator ATR attachment with a diamond crystal (Pike Technologies, Madison, WI). 1024 scans at a 2 cm^{-1} resolution were acquired.

Chapter 4

Biophysical Membrane Properties and Amyloid Assembly:

Electrostatic, Hydrophobic, Fluidity, Curvature Effects

4.1 Introduction

Amyloid-β (Aβ) is produced naturally from the amyloid precursor protein (APP), a single pass transmembrane protein. The *N*-terminus is produced by β-secretase while the *C*-terminus generated by γ-secretase (Thinakaran and Koo 2008). The histidine residue at position 14 is believed to influence how Aβ interacts with membranes (Smith, Ciccotosto et al. 2010), but several charged residues in the full-length amyloid peptide may also influence electrostatic interactions with the membrane, interactions that have been shown to control many amyloid peptide membrane associations (Lee, Pollard et al. 2002; Simakova and Arispe 2007).

The repeating hydrophilic and hydrophobic nature of Aβ is proposed to be responsible for amyloid assembly. Hydrophobic interactions have been shown to influence amyloid association with membranes (Tsai, Lee et al. 2010), however the exact influence hydrophobic membrane properties have on amyloid assembly is complicated by the hydrophobic collapse responsible for amyloid assembly in the absence of membranes. Hydrophobic mismatch is believed to influence peptide/protein-membrane interactions (Killian 1998), and Aβ(13-21) possesses the same hydrophobic character and position as the full-length peptide, and this region has been suggested to be the nucleating core of Aβ (Liang, Lynn et al. 2010).

Two largely uninvestigated membrane properties have yet to be explored with respect to amyloid assembly – membrane fluidity and curvature. Changes in membrane fluidity have been show to direct specific peptide binding as well as control peptide membrane binding and insertion (Pande, Qin et al. 2005). Additionally, peptide interactions with

these different phases can have dramatic effects on membranes. Further membrane curvature has been proposed to influence peptide assembly by dictating the size distribution and orientation of peptide aggregates (Bohinc, Iglič et al. 2005).

Aβ(13-21) possesses two histidine residues as well as a free *N*-terminus and a lysine residue, all of which have the ability to dictate the electrostatic association of this peptide with membranes. These interactions will be addressed by varying the phospholipid head group charge as well as the overall membrane charge. The truncated peptide also has five hydrophobic residues which can interact with the membrane hydrophobic core. Membrane fluidity and curvature will also be investigated in order to understand its influence on amyloid assembly. The model developed in Chapter 3 for Aβ(13-21) assembly provides an opportunity to investigate the influence of the membrane, however before a mechanistic investigation of amyloid assembly in the presence of membranes is attempted, several membrane properties need to be defined.

4.2 Results and Discussion

4.2.1 Calculations of Aβ(13-21) Membrane Associations

Wimbley and White generated free energies of transfer (ΔG) for amino acid side chains from water to the bilayer (Wimley and White 1996). These scales are often used to predict the location of peptides/proteins associated with membranes as either interfacial or insertional. These numbers are based on the Ac-WLxLL peptide in the context of 1-palmitoyl-2-oleoyl-phosphatidylcholine (POPC) membranes. Further development lead to the construction of the Membrane Protein Explorer (MPEx), a membrane protein

prediction program. The values calculated in Table 4.1 for various peptides were determined using MPEx.

Using the protonation state at pH=7.5, H_3N^+-hhQKLVFFA-NH_2 (h – deprotonated histidine, H – protonated histidine) gives a ΔG = -2.84 kcal/mol for an interfacial membrane association (water to bilayer transfer) and a ΔG = 3.46 kcal/mol for an inserted peptide into the hydrophobic core of the membrane. Since it is proposed that the hydrophilic and hydrophobic nature of Aβ is responsible for assembly, Aβ(13-21) was analyzed for interfacial membrane association with respect to the *N*- and *C*-termini. H_3N^+-hhQKL-NH_2 results in a ΔG of -0.82 kcal/mol while a value of -5.13 kcal/mol is calculated for Ac-LVFFA-NH_2. The values calculated for these peptide fragments for an insertional membrane association are 6.84 kcal/mol and -2.63 kcal/mol, respectively. For the bilayer to water free energy transfers, all values above are of opposite sign but equal in magnitude. The values calculated for Aβ(13-21) using MPEx and the Wimbley-White hydropathy calculations suggest that this peptide has a favorable transfer from water to the membrane in an interfacial association and an unlikely transfer from water to the hydrophobic core of the membrane (unlikely insertional event). Since the actual protonation state of the peptide is unknown, the values for various protonation states were also determined in Table 4.1.

4.4.2 POPC LUVs Do Not Promote Amyloid Assembly

Several biophysical parameters are known to promote the assembly of peptides in membranes. However, when POPC large unilamellar vesicles (LUVs) and Aβ(13-21)

	A) Interfacial (ΔG)	B) Insertional (ΔG)
Ac-LVFFA-NH_2	-5.13	-2.63
H_3N^+-hhQKLVFFA-NH_2	-2.84	3.46
H_3N^+-HhQKLVFFA-NH_2	-2.05	5.68
H_3N^+-hHQKLVFFA-NH_2	-2.05	5.68
H_3N^+-HHQKLVFFA-NH_2	-1.26	7.9
H_3N^+-hhQKL-NH_2	-0.82	6.84
H_3N^+-HhQKL-NH_2	-0.03	9.06
H_3N^+-hHQKL-NH_2	-0.03	9.06
H_3N^+-HHQKL-NH_2	0.76	11.28

Table 4.1 Wimbley-White Free Energy Transfers from Water to the Bilayer. A) MPEx calculations for peptide and peptide fragments from water to the bilayer interface [interfacial], B) MPEx calculations for peptide and peptide fragments from water to the bilayer hydrophobic core [insertional].

were mixed, the CD signature did not suggest that assembly occurs to a significant extent (Figure 4.1). However there is a slight red shift in the negative band below 200 nm, suggesting a slight shift in the secondary structure. To further explore the association, variations in lipid chain length could cause a greater mismatch between the peptide and phospholipid hydrophobic core and promote assembly (Killian 1998). Aβ(13-21) assembly was surveyed with various phosphotidylcholine (PC) phospholipid LUVs (Figure 4.2), but none of these PC LUVs promoted assembly. I attributed the absence of assembly to either peptide binding to the membrane in such a manner that does not initiate assembly (*i.e.*, not penetrating the hydrophobic core of the membrane) or simply to not binding to the PC LUVs. An additional membrane property that affects the assembly of peptides in the context of membranes is the membrane curvature. This biophysical property influences the size distribution of peptide assemblies and their orientation with the membrane. The PC LUVs composed of saturated lipid tails did not promote assembly when the curvature is varied by changing the vesicle diameter (Figure 4.2). These data suggest that the predominant biophysical properties of membrane architecture have little impact on amyloid assembly. The MPEx calculations suggest that this peptide should bind to PC membranes, and more information is required to understand why the PC membranes do not promote assembly.

4.2.3 Aβ(13-21) Does Not Affect Phosphatidylcholine Membrane Fluidity

A possible reason for the lack of assembly observed for PC LUVs is that Aβ(13-21) is sequestered inside the membrane's hydrophobic core and bound in such a way as to

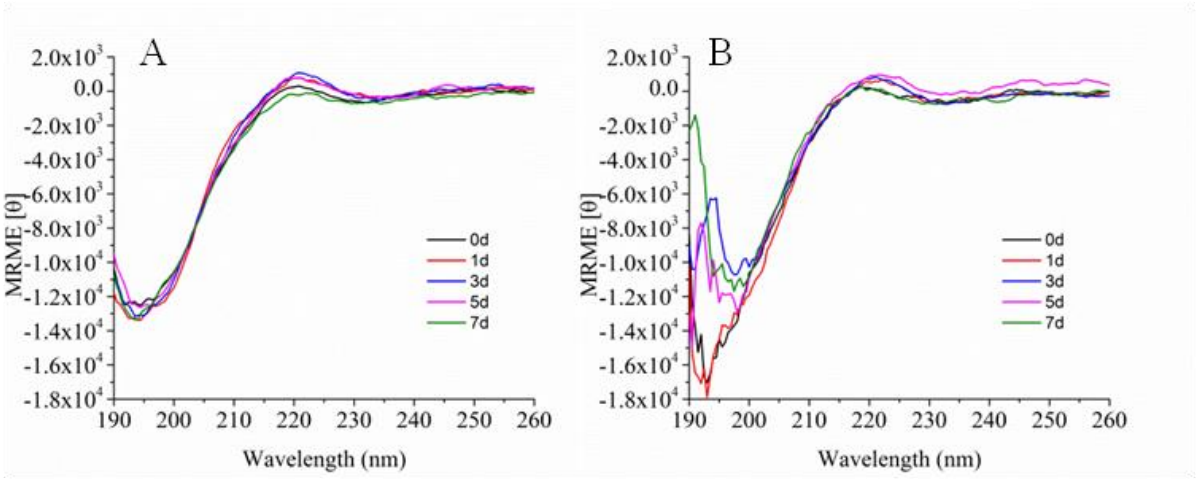

Figure 4.1 POPC does not promote the assembly of Aβ(13-21). A) no POPC, B) 100 nm POPC LUVs.

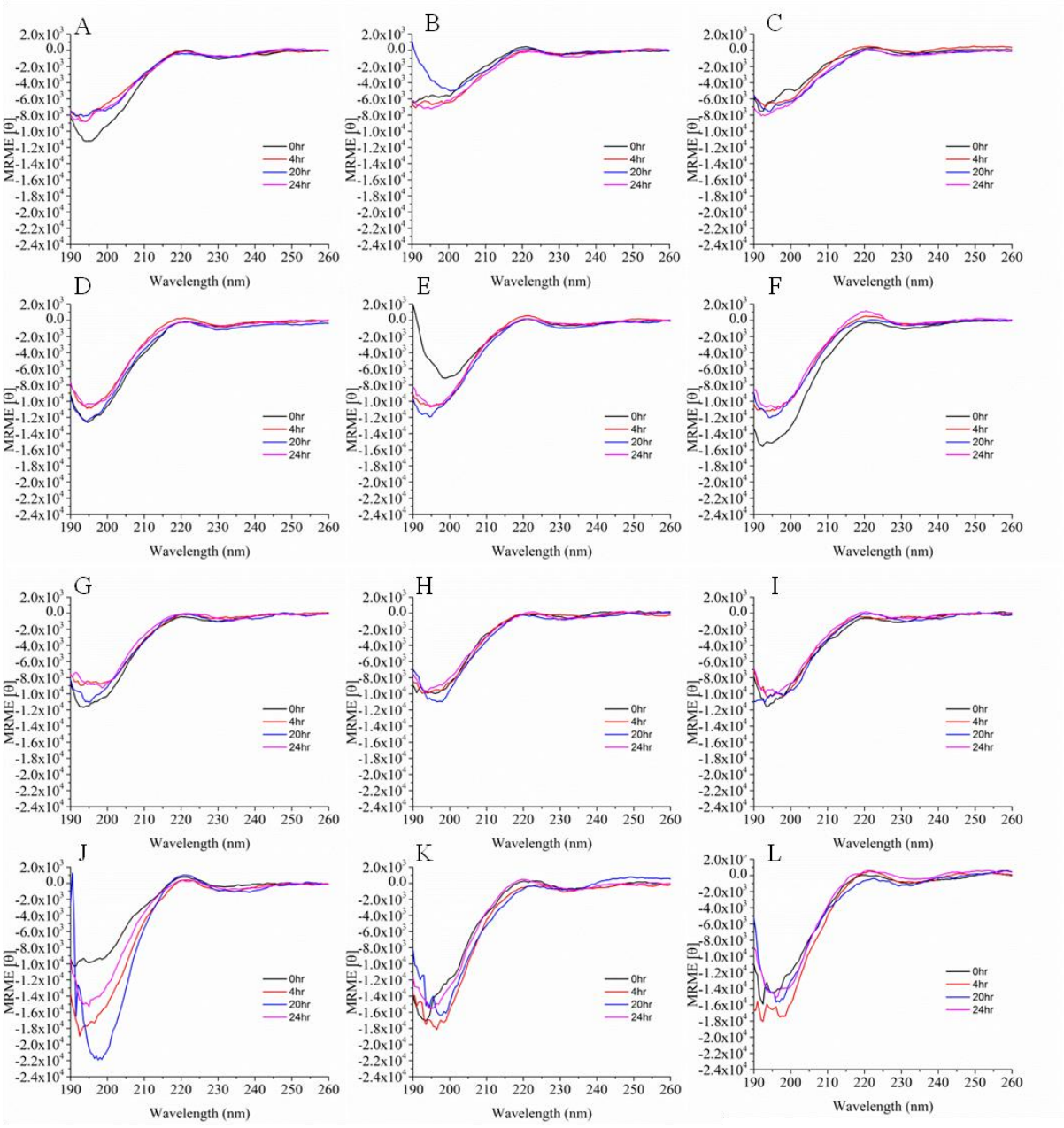

Figure 4.2 Varying the chain length and curvature of the PC LUV membranes does not promote the assembly of Aβ(13-21). A) 50 nm DCPC, B) 100 nm DCPC, C) 200 nm DCPC, D) 50 nm DLPC, E) 100 nm DLPC, F) 200 nm DLPC, G) 50 nm DMPC, H) 100 nm DMPC, I) 200 nm DMPC, J) 50 nm DPPC, K) 100 nm DCPC, L) 200 nm DPPC.

prevent assembly. To probe whether this is in fact the case, fluorescence anisotropy was used to investigate changes in bulk membrane transitions. Incorporation of a high concentration of peptide into the hydrophobic region of the membrane should either shift the anisotropy to higher or lower values as dictated by the interaction between the peptide and the membrane. Membrane stiffening results in a higher anisotropy value whereas membrane disruption leads to lower anisotropy values. Fluorescence anisotropy, using a fluorescence probe, can monitor these lipid phase transitions.

Diphenylhexatriene is a common probe used to detect changes in membrane fluidity where the fluorescence anisotropy of this probe depends on the membrane phase. A gel phase membrane produces a higher anisotropy value, but the addition of Aβ(13-21) does not affect DPPC's anisotropy nor does the peptide affect the phospholipid phase transition (Figure 4.3). Since the graphs overlap nicely, the data suggests that Aβ(13-21) is not in the hydrophobic core of the membrane as expected from the calculations.

4.2.4 Aβ(13-21) May Bind to the Surface of Phosphatidylcholine Membranes

When Aβ(13-21)F19W and Aβ(13-21)F20W were mixed with POPC, the fluorescence emission maxima do not shift significantly, and the emission spectra indicate that the fluorophore environment does not change (Figure 4.4). The hydrophobic core of the membrane has a lower dielectric constant than water which should result in an appreciable blue shift of the fluorescence emission maximum for each peptide. Even, the membrane-water interface has a dielectric constant closer to that of the hydrophobic core, and the tryptophan located in this region should show a blue shifted emission.

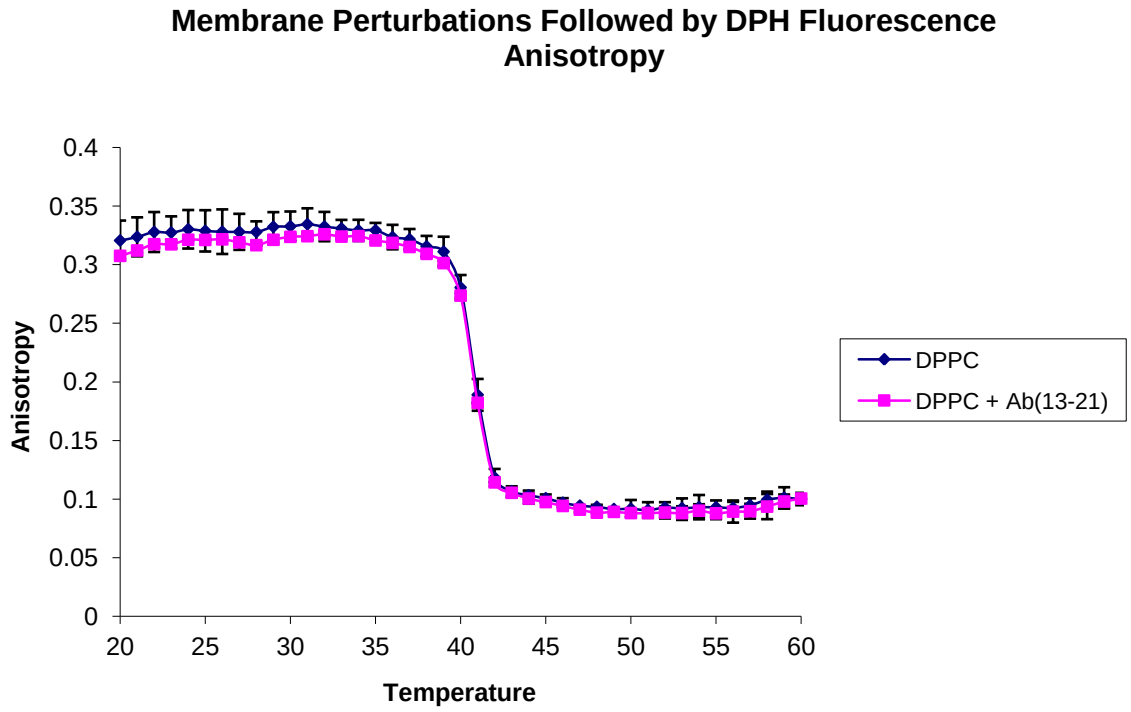

Figure 4.3 DPH Fluorescence Anisotropy in Aβ(13-21)-DPPC Mixtures. Probe:peptide:lipid = 1:55:1100.

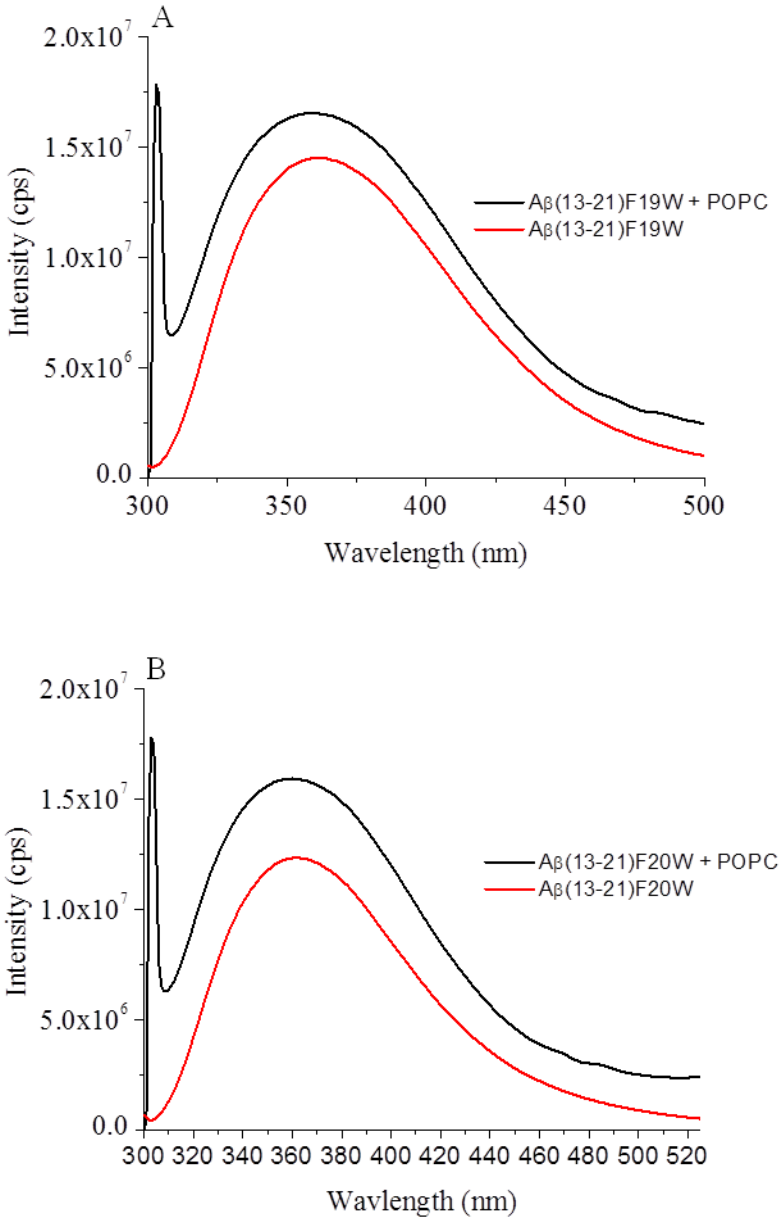

Figure 4.4 Tryptophan Fluorescence Emission Offers Insight into the Interaction between Aβ(13-21) and POPC LUVs. A) Aβ(13-21)F19W in the presences and absence of 100 nm POPC, B) Aβ(13-21)F20W in the presences and absence of 100 nm POPC.

One interesting difference between the tryptophan fluorescence emission in the presence and absence of POPC vesicles is the increased intensity, suggesting that the peptide is binding to the membrane and limiting the mobility of the indole ring (Lakowicz 2006). If the peptide does bind to the membrane, then the lack of assembly can be attributed to either the low concentration of peptides at the membrane or to ordered binding that prevents assembly.

4.2.5 Net Negatively Charged Membranes Promote Aβ(13-21) Assembly

Membrane electrostatics do influence peptide-membrane associations (Lee, Pollard et al. 2002; Simakova and Arispe 2007), and given that Aβ(13-21) is a positively charged peptide, then membrane association and potential assembly can be dependent on the phospholipid headgroup. Naturally occurring phospholipid membranes are composed of various lipids, and to investigate the role membrane electrostatics in amyloid assembly, the three naturally occurring net negative phospholipids (phosphatidylglycerol – PG, phosphatidylserine – PS, and phosphatidic acid – PA) were screened for the ability to promote amyloid formation.

LUVs composed of POPG phospholipids produce a change in the CD signature of Aβ(13-21) that then grows into a β-sheet CD signature (Figure 4.5A). Addition of Aβ(13-21) to POPS membranes gives a similar result (Figure 4.5B), although these LUVs produce a weak CD signature.

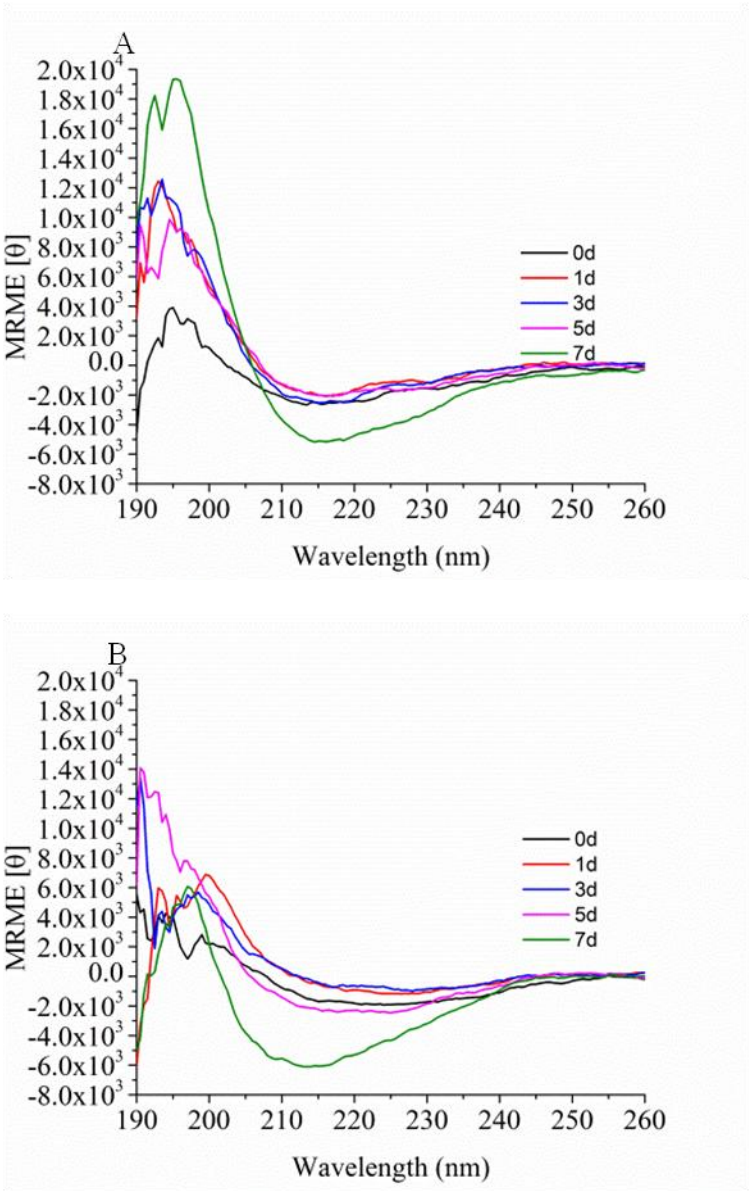

Figure 4.5 Net Negative LUVs Result in CD Spectral Changes for Aβ(13-21). A) POPG, B) POPS.

4.2.6 Probing Peptide-Membrane Insertion through Hydrophobic Mismatch

Hydrophobic matching is critical to peptide-membrane interactions (Killian 1998). To probe the effects on amyloid assembly of Aβ(13-21), various hydrocarbon chain lengths were explored. As seen in Figure 4.6, all of the chain lengths used show differences in promoting the assembly. DCPG and DLPG display distinctly different CD signatures (Figure 4.6A-F), possibly because these phospholipids are not vesicles but are micelles, and micelles have very different lipid packing and/or curvatures.

4.2.7 Effects of Membrane Curvature on Amyloid Assembly

Phospholipid membrane curvature is thought to affect the assembly of linear aggregates by controlling the size and orientation of the linear aggregates (Bohinc, Iglič et al. 2005). More specifically, curvature may possibly affect the length of the β-sheet fibril and/or the number of laminates or multimers (*i.e.*, fibril dimers, fibril trimers). To probe the effects of membrane curvature on amyloid assembly, Aβ(13-21) was added to 50 nm, 100 nm, and 200 nm diameter vesicles of various negatively charged LUVs (Figure 4.6-4.8), and none have definitive differences by CD. A more conclusive investigation of these interactions may be achieved using planar lipid bilayers. The lack of observed differences possibly stems from the similarities in the membrane curvatures among 50 nm, 100 nm, and 200 nm. These membrane curvatures may be too similar and not result in any differences in amyloid assembly. To achieve a drastically different membrane curvature, lipid micelles were explored.

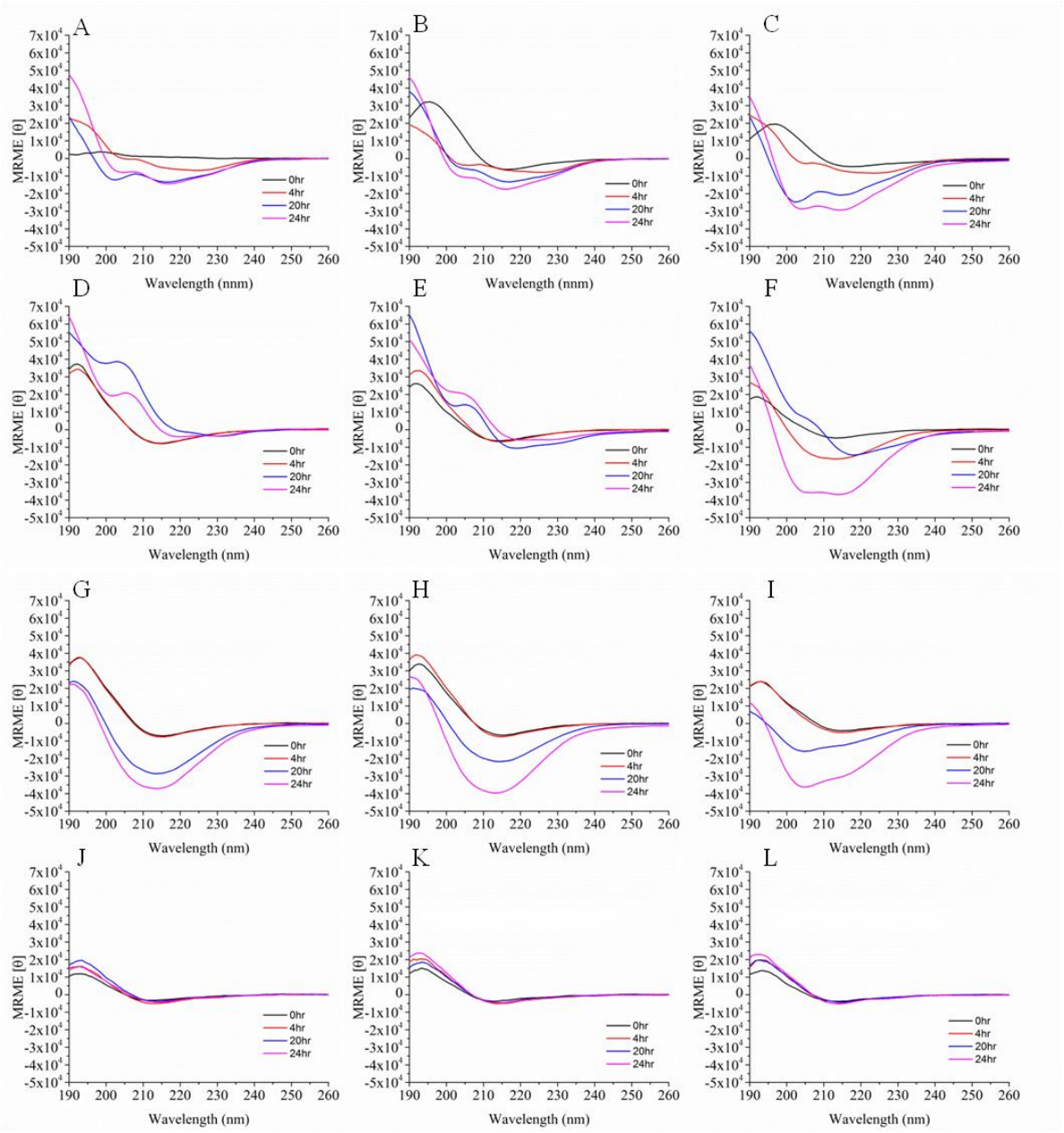

Figure 4.6 Varying the chain length and curvature of the PG LUV membranes affect the assembly of Aβ(13-21) differently. A) 50 nm DCPG, B) 100 nm DCPG, C) 200 nm DCPG, D) 50 nm DLPG, E) 100 nm DLPG, F) 200 nm DLPG, G) 50 nm DMPG, H) 100 nm DMPG, I) 200 nm DMPG, J) 50 nm DPPG, K) 100 nm DCPG, L) 200 nm DPPG.

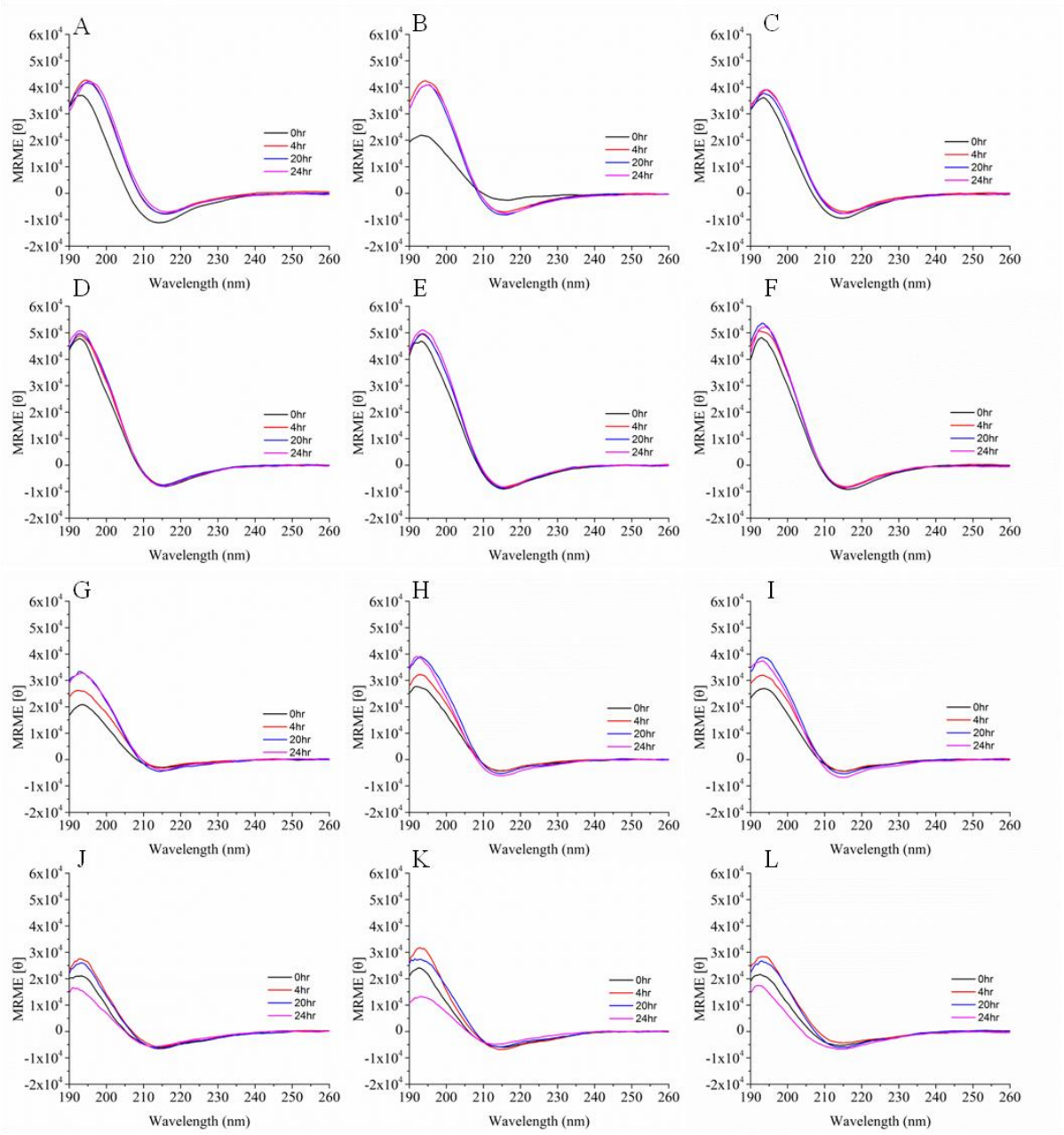

Figure 4.7 Varying the chain length and curvature of the PS LUV membranes does not promote the assembly of Aβ(13-21). A) 50 nm DCPS, B) 100 nm DCPS, C) 200 nm DCPS, D) 50 nm DLPS, E) 100 nm DLPS, F) 200 nm DLPS, G) 50 nm DMPS, H) 100 nm DMPS, I) 200 nm DMPS, J) 50 nm DPPS, K) 100 nm DCPS, L) 200 nm DPPS.

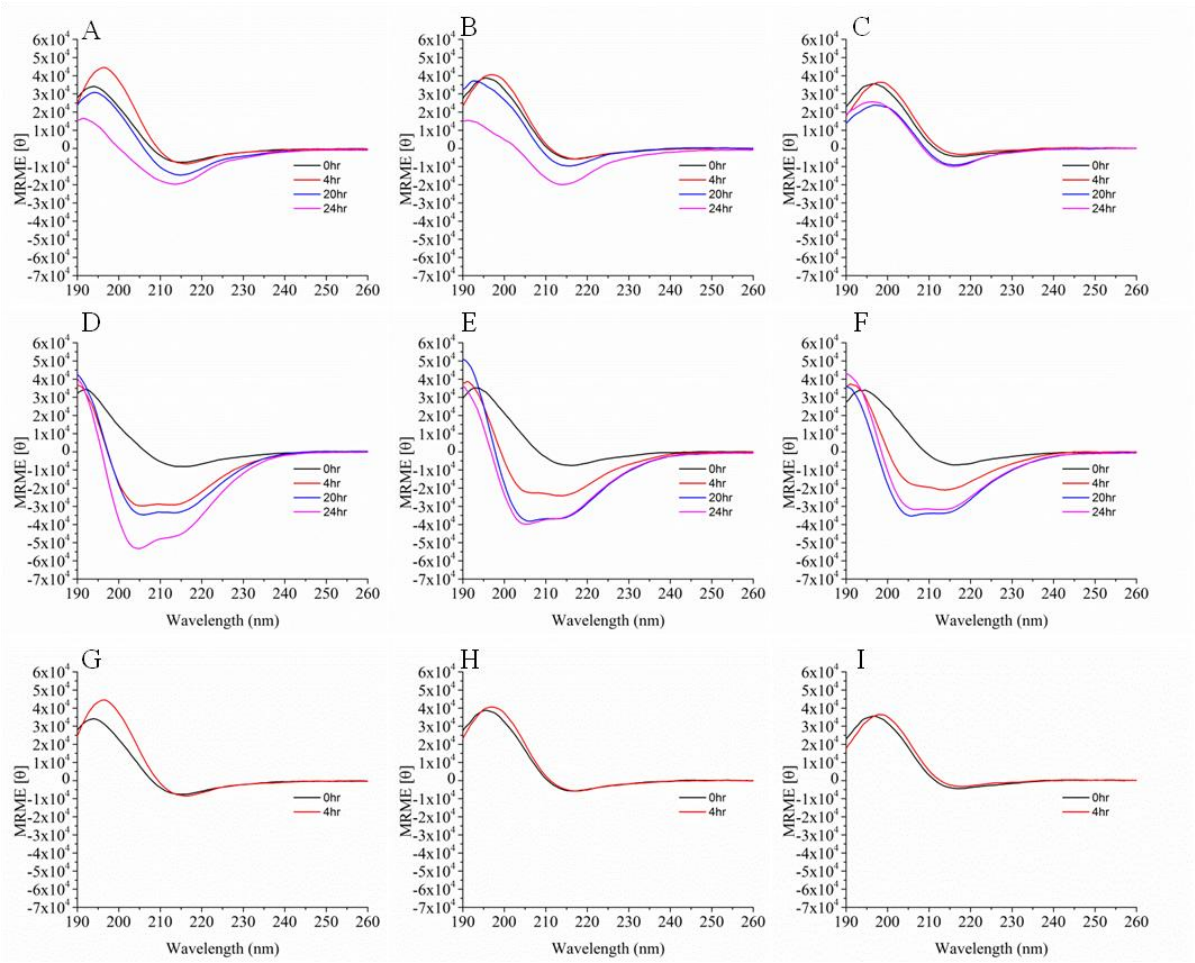

Figure 4.8 Varying the chain length and curvature of the PA LUV membranes does not promote the assembly of Aβ(13-21). A) 50 nm DCPA, B) 100 nm DCPA, C) 200 nm DCPA, D) 50 nm DLPA, E) 100 nm DLPA, F) 200 nm DLPA, G) 50 nm DMPA, H) 100 nm DMPA, I) 200 nm DMPA.

Using dodecyltrimethylammonium bromide (DTAB) as a mimic for a positively charged lipid, Aβ(13-21) did not assemble as indicated by CD (Figure 4.9A). However, when the peptide was added to dodecylphosphocholine (DPC), which is also a positively charged lipid, the CD signal did change surprisingly (Figure 4.9B). A new band near 200 nm appears and the band at 220 nm changes as well. These two bands decrease over time which implies assembly, but remain globally similar.

When Aβ(13-21) is added to sodium lauroylsarcosinate (NLS), the peptide undergoes an immediate structural change (Figure 4.9C), and at 2 d and 7 d, the spectra resemble that of a β-sheet with some portion of P_{II} (β_{II}-protein). Addition of the same peptide to sodium dodecylsulfate (SDS) and sodium octylsulfate (SOS), two negatively charged detergents, produces similar CD spectra (Figure 4.9D-E). The SOS spectra immediately resembles that of a β-sheet but transitions into a P_{II} type spectra at 2 d and then transitions again into a non-classical CD spectra at 7 d. SDS also induce a structural change to β-sheet character with a negative band at 215 nm but changes over the experimental time frame.

In order to keep similar properties as that of phospholipid headgroups, two lyso-phospholipids were used to analyze the effects on the secondary structure of Aβ(13-21). Lyso-phosphatidylcholine (LPC-C14) and lyso-phosphatidylglycerol (LPG-C14) have the same headgroups at PC and PG, but the molecule only contains one lipid chain instead of two as is the case for phospholipids. These two lipids produce similar effects on Aβ(13-21) (Figure 4.9F-G) to resemble a P_{II} secondary structure.

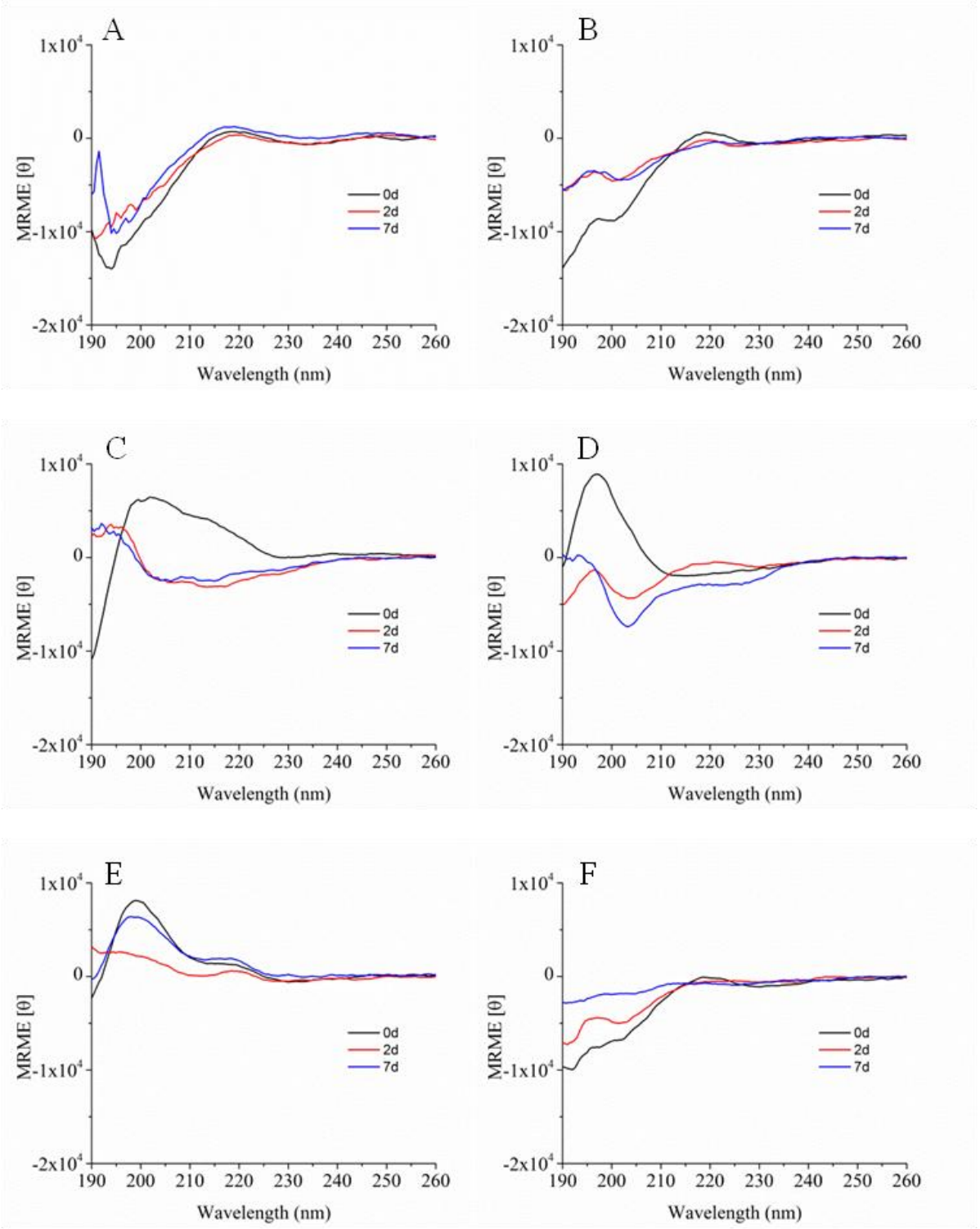
A
B
C
D
E
F
MRME [θ]
Wavelength (nm)
0d
2d
7d
1x10⁴
0
-1x10⁴
-2x10⁴
190
200
210
220
230
240
250
260

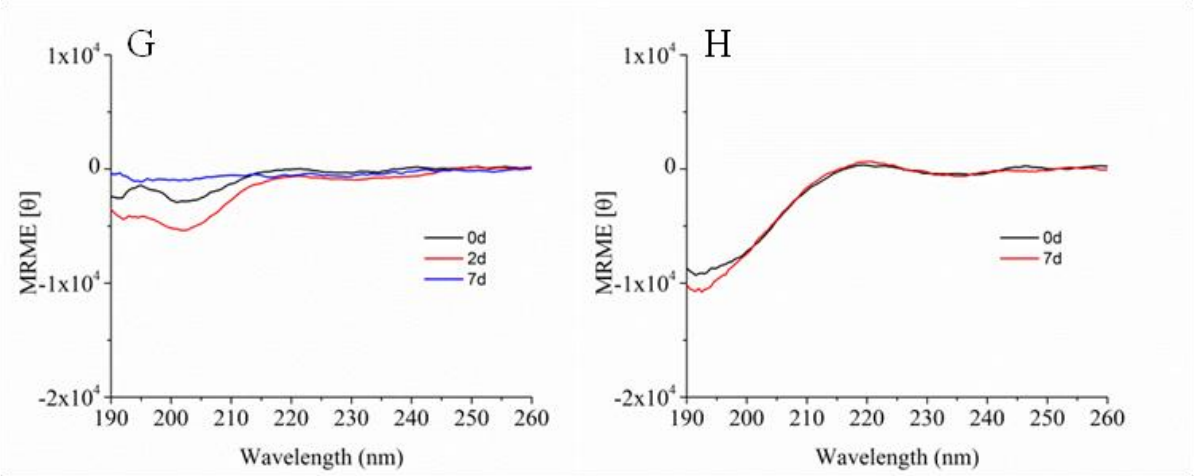

Figure 4.9 Varying the lipid packing density using lipid micelles drastically affects the assembly of Aβ(13-21). A) DTAB, B) DPC, C) NLS, D) SDS, E) SOS, F) LPC-C14, G) LPG-C14, H) Ab(13-21).

Accessibility to negatively charged lipids (electrostatics) appears to have a greater influence on the assembly than does lipid curvature. However, the changes observed for zwitterionic lipids, which have been shown not to affect assembly, appear to have a small affect on peptide assembly in this section. This difference may be due to the accessibility of the negative charge which may not be accessible when studying PC LUVs.

4.2.8 Varying Peptide-Membrane Interactions through Various Peptide-Lipid Ratios

Phospholipid membranes and peptide interactions are best explained by a dynamic interplay between the two components. This essentially means that peptides affect the membrane and that the membrane affects the peptide. Cytochrome c has been shown to associate on the surface of negatively charged membranes; however, it was found that under certain conditions protein insertion can happen at high protein concentrations on the membrane surface (Zuckermann and Heimburg 2001). This paper suggests that surface associated proteins apply a lateral pressure on the membrane bilayer and that at high binding concentrations and large surface coverage this pressure may become high enough to overcome the protein insertion energy barrier. Therefore when Aβ(13-21) interacts with the membrane, two potential interactions can exist that may produce different secondary structures or assembly states.

To probe whether different membrane associations occur when using Aβ(13-21), the peptide was mixed with dimyristoylphosphatidylglycerol (DMPG) at various ratios. All the ratios tested result in CD spectral changes that predominately resemble that of a β-sheet (Figure 4.10) at 33 ^{o}C. It was found that as the ratios approach peptide:phospholipid

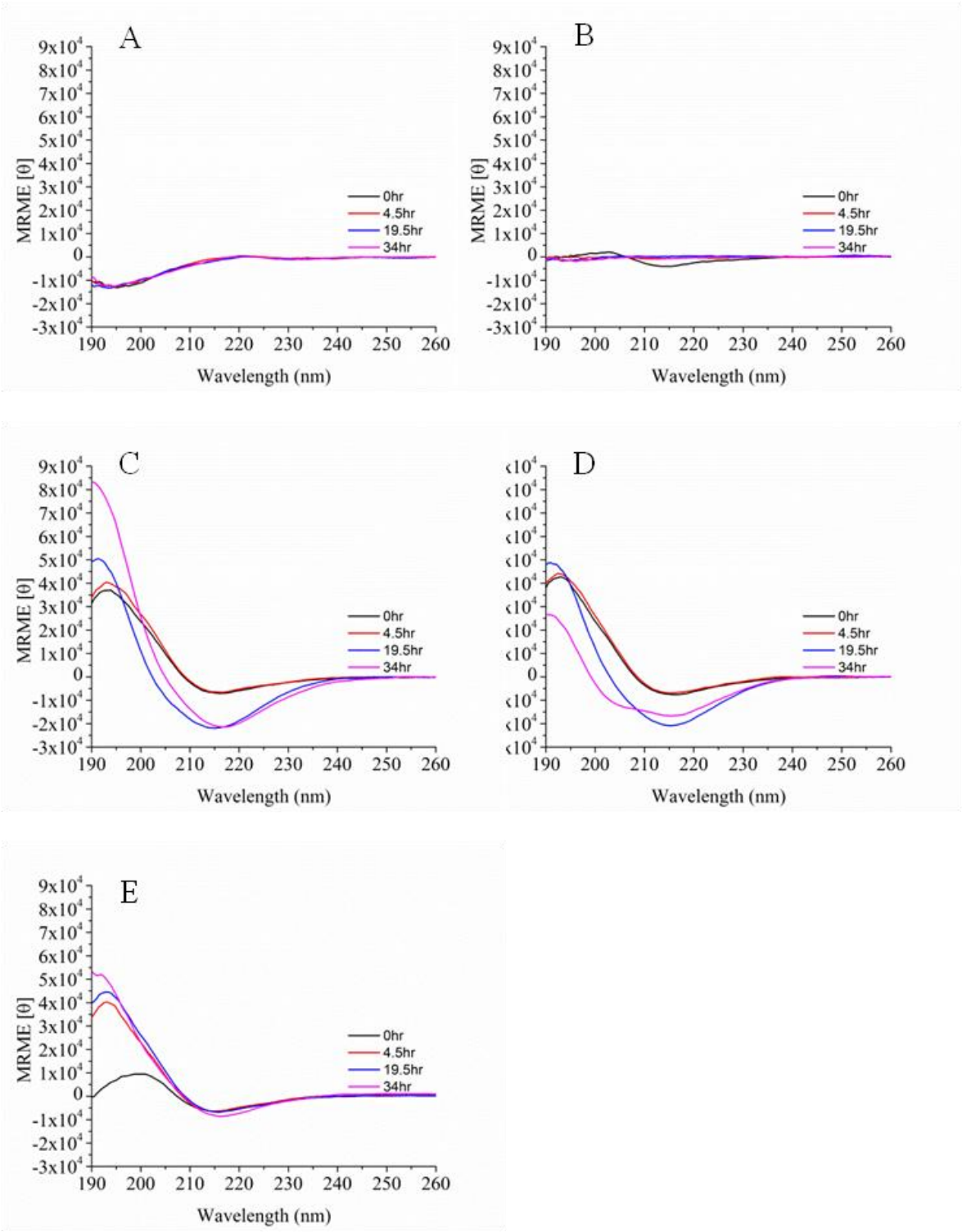

Figure 4.10 Varying the Peptide-Lipid Ratio produces the same CD spectral changes for Aβ(13-21)-DMPG. A) 1:0, B) 1:1, C) 1:5, D) 1:10, E) 1:20.

of 1:1, the mixture precipitates. As phospholipid concentration decreases more of the lipid membrane is covered by peptide, and thus neutralizing the charge ratios may result in sample precipitation. Another explanation is that the increased surface coverage stresses the membrane to the point of rupture. With the exception of the 1:1 ratio, the various peptide-lipid ratios used here gave similar results.

When the same experiment was performed using dipalmitoylphosphatidylglycerol (DPPG) at 33 ^{o}C, the ratio at which precipitation was observed was the same but the secondary structural changes by CD were drastically different with the CD spectral change closely resembling that of a 3_{10}-helix (Figure 4.11). Here, the membrane fluidity is different because the DPPG membrane is in a different phase than the DMPG LUV at this temperature and warrants further investigation. The gel phase is more rigidly packed when compare to the fluid phase. Therefore, peptide binding could exert a greater stress on the membrane and cause the peptide to change its membrane association by inserting into the membrane or adopting a different secondary structure or both. Understanding the dynamic interplay between the lipid membrane and Aβ(13-21) is critical before investigating the assembly mechanism further.

4.2.9 Membrane Phase Influences Peptide Secondary Structure

Changes in membrane fluidity are known to direct specific peptide binding as well as control peptide membrane binding and insertion (Pande, Qin et al. 2005). This scenario reinforces the dynamic interplay between peptides and membranes. To determine the effect that membrane fluidity has on the peptide secondary structure, Aβ(13-21) was

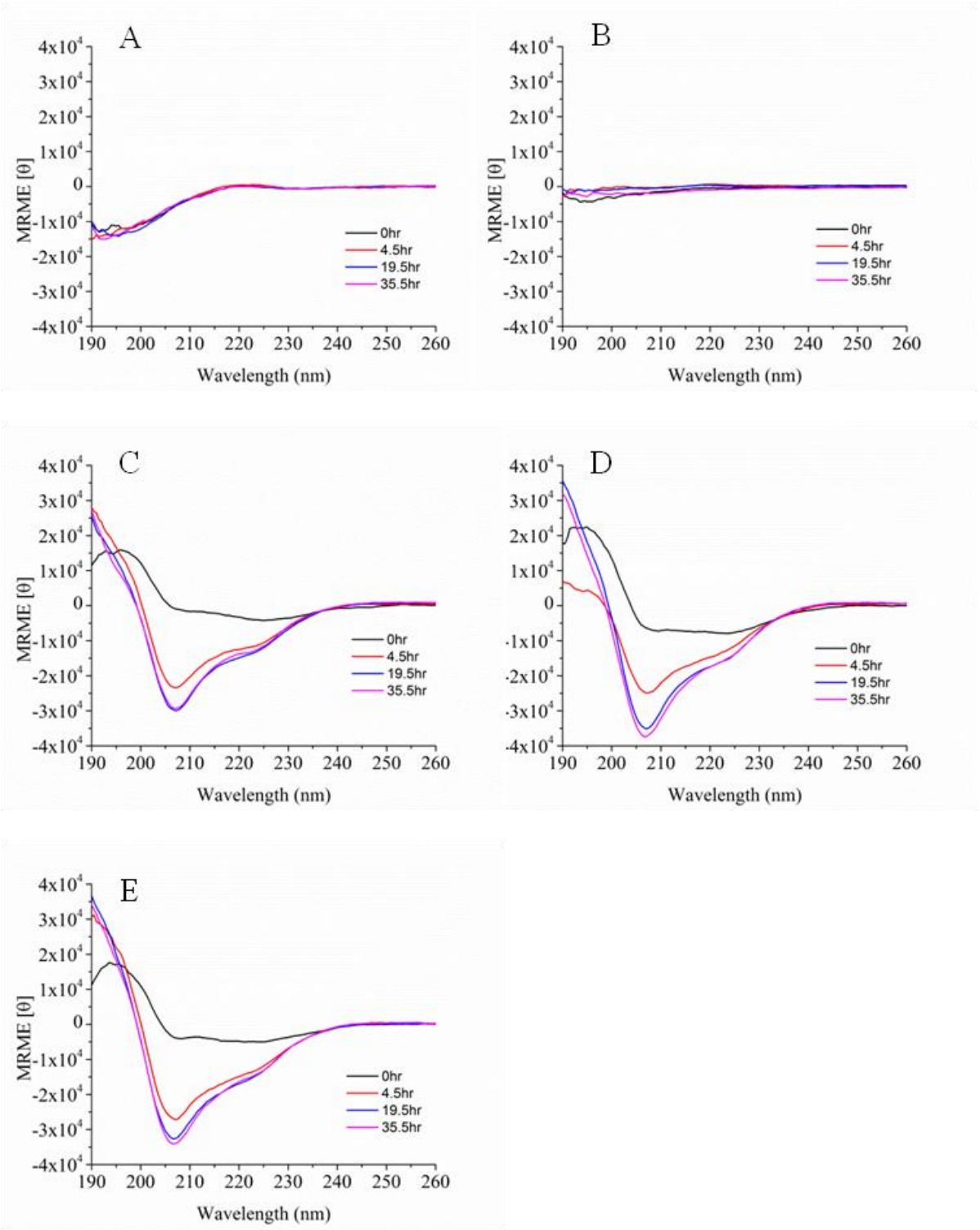

Figure 4.11 Varying the Peptide-Lipid Ratio produces the same CD spectral changes for Aβ(13-21)-DPPG. A) 1:0, B) 1:1, C) 1:5, D) 1:10, E) 1:20.

added to negatively charged membranes in different phases. When Aβ(13-21) is mixed with LUVs of DPPG in the gel phase, precipitation is observed immediately. When Aβ(13-21) is added to ripple phase DPPG LUVs, the spectrum has a double minimum at 208 nm and 222 nm at 0 hr (Figure 4.12A), and both bands become more intense over the first four hours, but the 208 nm band becomes more intense than the 222 nm band. TEM images of this sample do not show the appearance of fibrils. Aβ(13-21) in the presence of fluid phase DPPG LUVs however gives the classical β-sheet CD signature with a maximum at 192 nm and a minimum at 215 nm (Figure 4.12B). Fibrils associated with LUVs are present in the TEMs and the sample displays the typical red shift upon Congo red binding.

When Aβ(13-21) was added to dilaurylphosphatidylserine (DLPA) in the gel or fluid phase, both phases produced the classical β-sheet CD signature immediately (Figure 4.12C-D). The gel phase DLPA CD signature became more intense at 3 d, however the fluid phase DLPA sample changed continually over the 5 d period. The initial change has a reduced intensity below 200 nm and a red shifted negative band to 230 nm. The 5 d sample is a flat line due to precipitation. It is difficult to determine whether this change is due to the peptide alone because of the elevated temperature (50 ^{o}C) required to keep the DLPA in the fluid phase. These elevated temperatures also accelerate the hydrolysis rate of the phospholipid. Given the lipid dependences of Aβ(13-21), these lipid changes are the likely cause of the CD spectral changes. Clearly, the behavior of Aβ(13-21) with different membrane phases depends strongly on the phospholipid.

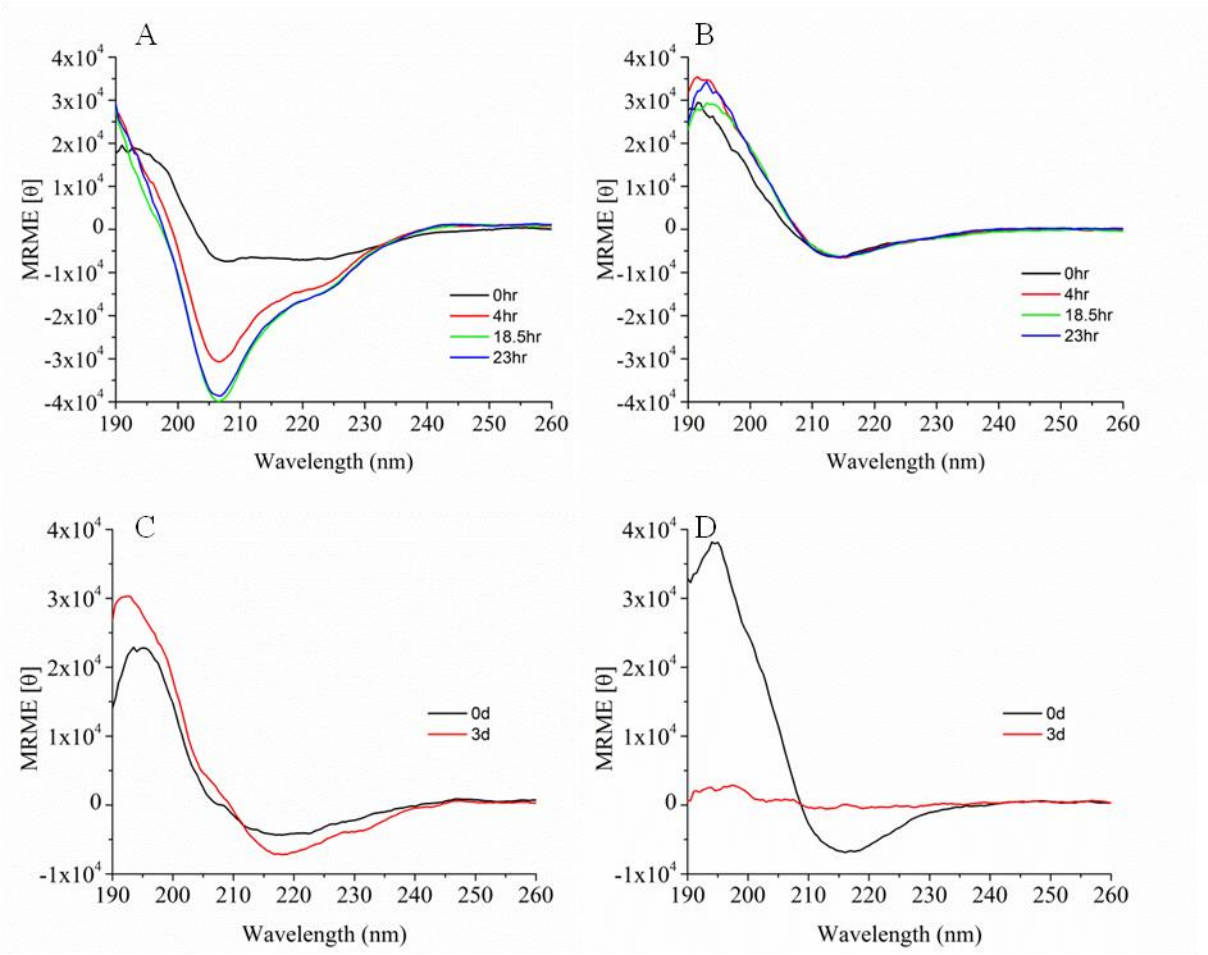

Figure 4.12 Varying the Membrane Phase Produces Phospholipid dependent results for the assembly of Aβ(13-21). A) ripple phase DPPG, B) fluid phase DPPG, C) gel phase DLPA, D) fluid phase DLPA.

4.2.10 Varying Peptide-Membrane Interactions through Various Surface Charge Density

Although varying the peptide-to-lipid ratio did not produce any observable differences, interpretation of the results is limited by the experimental technique in that the degree of peptide coverage on a particular membrane cannot be controlled. This lack of control could result in coverage of some vesicles while leaving others uncovered. Additionally, the effects negatively charged gel phase membranes has on the secondary structure of Aβ(13-21) cannot be explored due to DPPG-Aβ(13-21) precipitation when mixed in this phase. To overcome these experimental limitations, Aβ(13-21) was added to membranes composed of various ratios of DPPC and DPPG. These two lipids form an ideal mixture and thus can be used to probe the effects of electrostatics in peptide-membrane interactions which controls the degree of peptide adsorption (Mansour, Wang et al. 2001).

Mixtures of Aβ(13-21) and DPPC:DPPG were followed for five days by CD. Samples were prepared with a final peptide concentration of 0.5 mM and a final phospholipid concentration of 5 mM. Since these membranes have three different phases, then the different membrane phases (gel, ripple, fluid) were also used to determine the effect the membrane phase has on amyloid assembly. As a control, Aβ(13-21) was also investigated at the temperatures used for the experiment (RT, 35 ^{o}C, 50 ^{o}C). These elevated temperatures caused the secondary structure as followed by CD to change. This is most likely due to the accelerated evaporation at these temperatures which will concentrate the peptide and increase the salt concentration (Figure 4.13A, 4.14A, 4.15A). Both of these changes have already been shown to affect the assembly of Aβ(13-21). However, it is worth exploring to determine if these changes are in fact due to these experimental

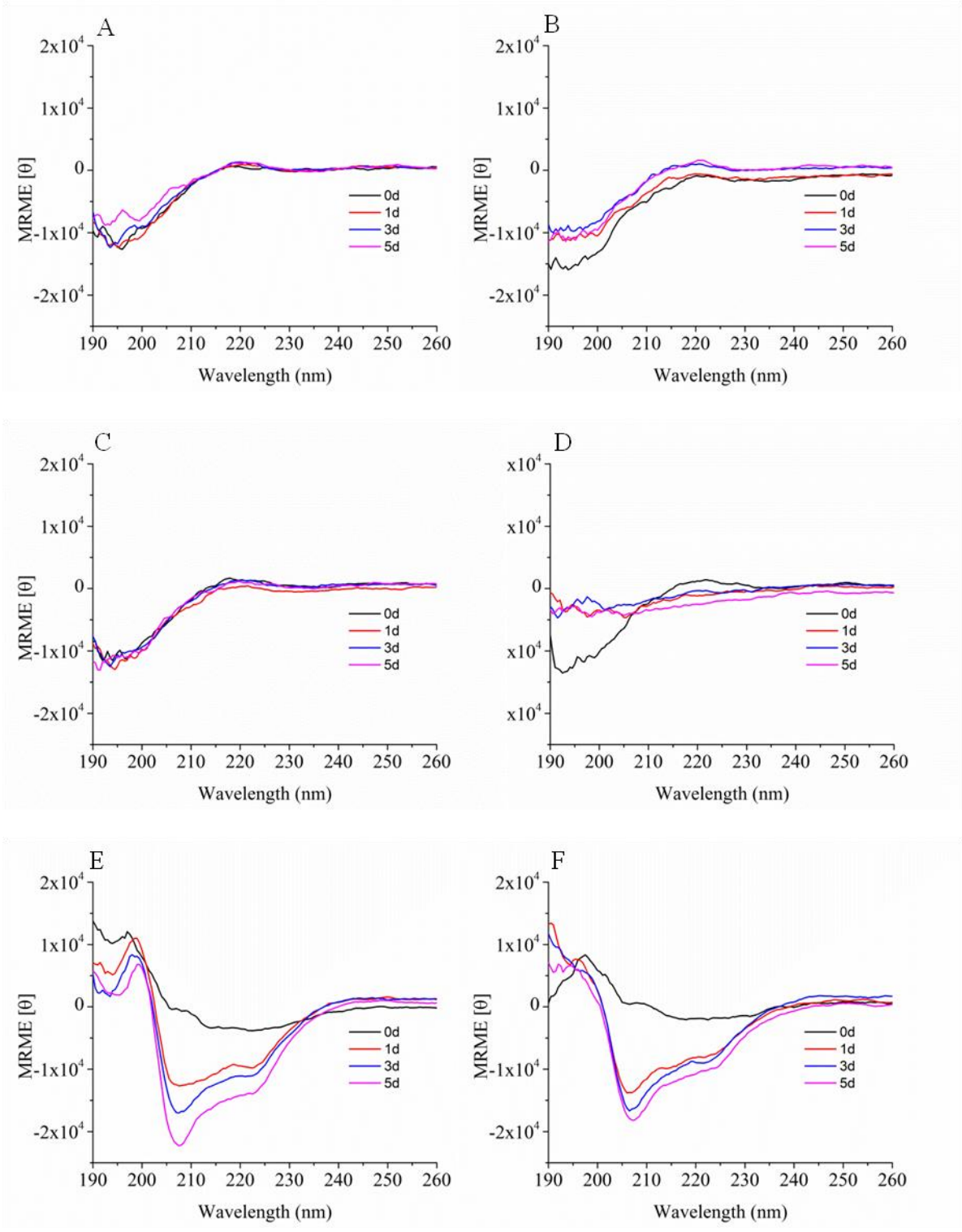

Figure 4.13 Varying the surface charge density affects the assembly of Aβ(13-21) when using mixtures of DPPC:DPPG in the gel phase. A) Ab(13-21), B) 99.9:0.1, C) 99:1, D) 90:10, E) 50:50, F) 10:90.

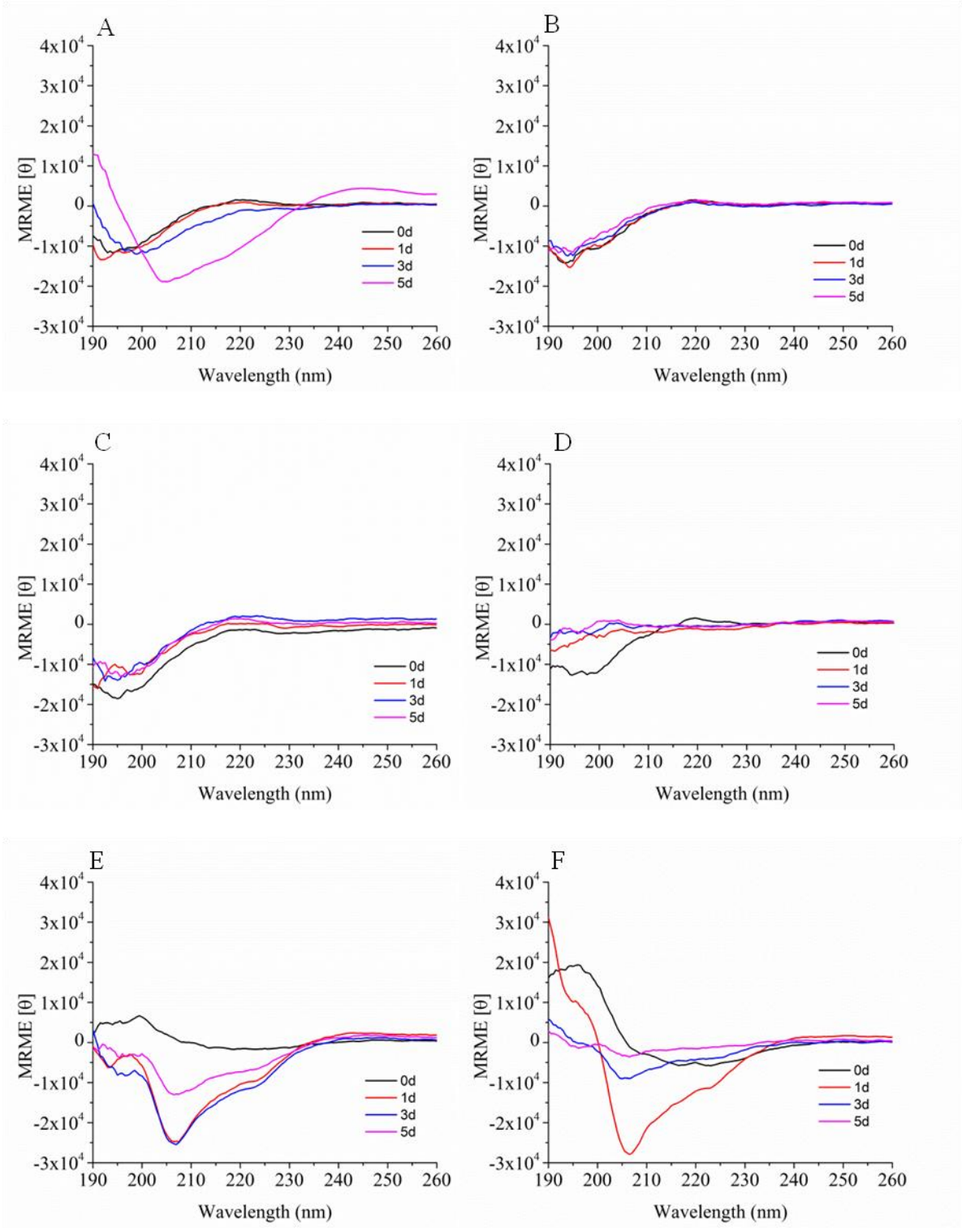

Figure 4.14 Varying the surface charge density affects the assembly of Aβ(13-21) when using mixtures of DPPC:DPPG in the ripple phase. A) Ab(13-21), B) 99.9:0.1, C) 99:1, D) 90:10, E) 50:50, F) 10:90.

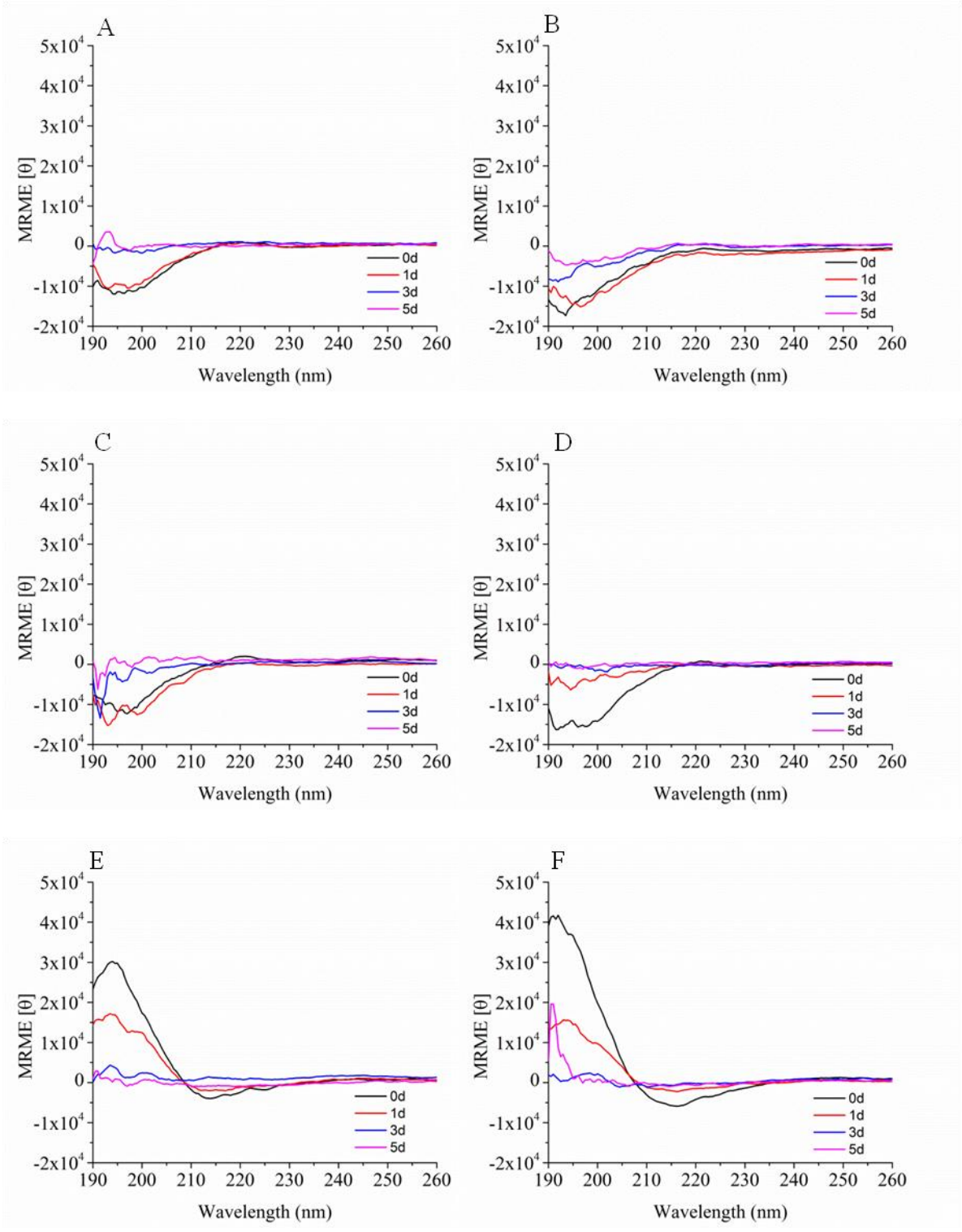

Figure 4.15 Varying the surface charge density affects the assembly of Aβ(13-21) when using mixtures of DPPC:DPPG in the fluid phase. A) Ab(13-21), B) 99.9:0.1, C) 99:1, D) 90:10, E) 50:50, F) 10:90.

variables changing or due to an inverse temperature dependence with this particular peptide. The changes in the presences of the various lipid compositions and phases used were much slower and different.

DPPC:DPPG at ratios of 99.9:0.1 and 99:1 do not promote assembly (Figure 4.13B-C, 14B-C, 15B-C). The changes observed for these two ratios at 50 ^{o}C were due to sample concentration due to evaporation. Therefore, not all negatively charged membranes promote assembly because the 1% negatively charged PG should produce negative surface potential at this ionic strength yet it did not promote assembly within the time frame of the experiment. However, when Aβ(13-21) is mixed with the following ratios, 90:1, 50:50, and 10:90, the CD signatures change (Figure 4.13D-F, 4.14D-F, 4.15D-F). The 90:10 samples slowly changes over the time course of the experiment. The negative band at 195 nm disappears into the noise. This is most likely due the assembly of Aβ(13-21) followed by sample precipitation. The 50:50 and 10:90 phospholipid ratios produce dramatically different results. The gel and ripple phase membranes composed of these ratios results in a CD spectral change for Aβ(13-21) that can most easily be assigned to a 3_{10}-helix. On the other hand, these two ratios in the gel phase produce CD spectra that are classically assigned to a β-sheet. The signals decrease over time due to sample precipitation. Again, phospholipid hydrolysis is accelerated at high temperatures which could be the cause of the sample precipitation over the experimental timeframe. Nevertheless, the results are similar to the various peptide-to-lipid ratios presented previously in that the secondary structure of Aβ(13-21) can be controlled.

4.3 Conclusions

The lipid surrounding membrane proteins can drastically change their structure and function (Sachs and Engelman 2006). Membrane charge clearly influences amyloid assembly. The net membrane charge necessary for a structural change cannot be accurately determined due to the limited lifetime of phospholipid LUVs; however, as the amount of negative charge increases so does the rate of β-sheet formation. Approximately 10% DPPG in DPPC membranes is required to initiate a structural change by CD in the timeframe of the experiment, and the percentage is likely to change based on the particular membrane phospholipid used. This percentage is also likely to change if the negatively charge component of the membrane has a higher effective concentration.

Membrane phase also affects the secondary structure of Aβ(13-21). Amyloid assembly of Aβ(13-21) in the presence of gel or ripple phase membranes containing at least 10% DPPG result in a CD signal that can be attributed to the presence of a 3_{10}-helix while all negatively charged fluid phase membranes produce the classical β-sheet appearance. An unresolved question is the specific orientation of the amyloid assembly in the context of negatively charged membranes.

Cells regulate the type and location of phospholipids located within the different membranes of the cell. Since Aβ has been shown to result in mitochondrial damage, protein sorting malfunctions, lysosome dysfunction, and excitotoxicity (Cataldo, Peterhoff et al. 2000; Nixon and Cataldo 2006; Minkeviciene, Rheims et al. 2009; Müller, Eckert et al. 2010) and since all of these cellular processes involve negatively charged phospholipids, this correlation may be important for disease etiology.

Mitochondria also contain elevated levels of both phosphatidylglycerol and phosphatidic acid, both of which promote amyloid assembly. Endosomes, lysosomes, and synaptic vesicles all contain phosphatidylserine, which is shown here to promote amyloid assembly. Therefore, not only do these negatively charged surfaces seem to sequester amyloid, but the cellular activity may be driven by this association. And, a detailed understanding of the location of the amyloid structure, both of which are likely controllable by changing the membrane properties, is necessary in order to understand the assembly mechanism.

While biophysical evidence presented connects several membrane properties (membrane charge and membrane phase) with Aβ mediated etiology, insight into Alzheimer's disease will require a detailed mechanism of membrane-mediated assembly. Recent literature points to both hydrophobic and electrostatic interactions (Murphy 2007), and the ability to experimentally control peptide structure (P_{II}, 3_{10}-helix, β-sheet) by manipulating specific experimental lipid parameters has this system poised to explore the mechanism responsible for amyloid assembly in the presence of membranes. The chapter outlines the ability to control the occurrence of the highlighted secondary structures proposed to be involved in amyloid assembly, and understanding amyloid assembly in the context of membranes may also reinforce the mechanism of peptide assembly developed in Chapter 3. This observation is most significant for the oligomers that have been proposed to possess micelle like properties and possibly similar microenvironments. Specifically, understanding the membrane association when Aβ(13-21) forms β-sheets is necessary in order to determine the mechanism of amyloid formation.

4.4 Methods

4.4.1 Materials

Solid-phase peptide synthesizer reagents (i.e., FMOC-amino acids, peptide resins) were obtained from Anaspec, Inc. (San Jose, CA). Distilled deionized water (ddH_2O) was purchased from EMD Chemicals, Inc. (Gibbstown, NJ) for sample preparations. All other reagents were acquired from Sigma-Aldrich Chemical Co. (Milwaukee, WI).

4.4.2 Peptide Synthesis and Purification

Peptide synthesis was performed using standard FMOC solid-phase peptide chemistry on a FMOC Rink-amide polystyrene resin (AnaSpec, Inc., sub. 0.4-0.6 meq/g) by a Rainin Symphony Quartet multiplex solid-phase peptide synthesizer (Protein Technologies, Tucson, AZ) or a Liberty Microwave solid-phase peptide synthesizer (CEM, Matthews, NC).

On the Rainin Symphony Quartet, HBTU and NMM were the coupling reagents. Each amino acid was coupled for 2 hours. His13, His14, Gln15, Lys16, Leu17, Val18 and Phe19 were double coupled. An acetylation reaction was performed after every coupling reaction to eliminate deletion peptides. On the CEM Liberty, HBTU and NMP/DIEA were the coupling reagents. Each amino acid was single coupled following the standard coupling reaction conditions from CEM. An acetylation reaction was performed after every coupling reaction to eliminate deletion peptides.

The cleavage/deprotection reaction was carried out with trifluoroacetic acid/thiolanisole/EDT/anisole (95/5/3/2, v/v). The crude peptide was precipitated using cold ethyl ether and centrifuged at 6,500 rpm for 10 min at 4 ^{o}C. The crude product was then washed with cold ethyl ether and centrifuged four additional times. The crude peptide was kept under vacuum until purified.

All peptides were purified by RP-HPLC using a Waters Delta 600 and a Jasco LC2000 HPLC with a Zorbax 300SB-C18 preparative HPLC column (21.2mm x 25cm) and eluted at 10 mL/min. The peptide was dissolved in H_2O with 0.1% TFA. If the solution was cloudy, the crude mixture was filtered though a 0.2 μm filter (Whatman). A linear gradient from 15%/85% MeCN/H_2O with 0.1% TFA to 45%/55% MeCN/H_2O with 0.1% TFA was used. The HPLC peak was collected, condensed, frozen at -80 °C, and lyophilized (ATR FD3.0 freeze dryer or a Labconco FreeZone 12Plus freeze dryer). Lyophilized peptides were stored at -20 or -80 °C. MALDI-TOF MS analysis (Voyager-DE^{TM} STR Biospectrometry Workstation; 2,5-dihydroxybenzoic acid matrix) was collected on each peptide.

4.4.3 Peptide Sample Preparation

Peptide stock solutions were prepared by dissolving a known amount of peptide in ddH_2O at twice the desired concentration, sonicating for 10 min, and centrifuging at 13,200 x g for 10 min. The supernatant was collected and used as the peptide stock solution. 1 mM samples were prepared by diluting a 2 mM stock solution with 50 mM of

the desired buffer and pH. 0.5 mM samples were further diluted with 25 mM of the desired buffer solution.

4.4.4 Multilamellar Vesicle (MLV) Preparation

Multilamellar vesicles were prepared using two different protocols. (1) Phospholipids were dissolved in buffer solution, vortexed for 1 min, and then stored at 4 ^{o}C until used. (2) Phospholipids were purchased pre-dissolved as monomers in a solution containing various ratios of chloroform, methanol, and water that is specific to the phospholipid as determined by Avanti Polar Lipids and dried on a rotary evaporator ≥12 hrs to form a thin lipid film. To hydrate the phospholipids, buffer solution, 10-15 ^{o}C above the phospholipid main transition temperature, was added to the thin lipid film to obtain the desired phospholipid concentration. The solution was spun on a rotary evaporator for agitation for >30 min while keeping the water bath above the main transition temperature of the phospholipid. The sample was then frozen by submerging the round bottom flask in an acetone-dry ice bath and was followed by melting the sample to a temperature above the main transition temperature of the phospholipid using the rotary evaporator as an agitator. Five cycles of this process (freeze-thaw) were completed.

4.4.5 Large Unilamellar Vesicles (SUV or LUV) Preparation by Extrusion

After the 5 freeze-thaw cycles, the sample was passed 19 times through a 100 nm single track-etch polycarbonate membrane (Avanti Polar Lipids) above the phospholipid

main transition temperature using a mini-extruder (Avanti Polar Lipids, Alabaster, AL) to achieve the desired size (size = vesicle diameter).

4.4.6 Peptide-Vesicle Mixing

Peptide stock solutions were prepared as stated previously. Phospholipid vesicle stock solutions were prepared as stated in Phospholipid Vesicle Preparation. The peptide solution was added to the phospholipid vesicle solution by slowly ejecting the peptide stock solution into a phospholipid vesicle solution (previously diluted to the appropriate concentration) while simultaneously pulling the pipette out of the mixture. This was done to ensure an even mixing of peptide and vesicles.

4.4.7 Wimbley-White Calculations

The Wimbley-White Calculations were made using Membrane Protein Explorer (Stephen White Laboratory, UC Irvine). Sequences were input following the directions explicitly in the Totalizer portion of the program. Interfacial values reflect the input values with 0% helicity. The insertional values reflect the values generated using the octanol (Oct) parameter for membrane insertion. The *N*- and *C*-terminal selections are as indicated.

4.4.8 Circular Dichroism

CD spectra were collected using a Jasco J-810 CD spectropolarimeter (Easton, MD). Three spectra were recorded from 260 nm to 190 nm (step size = 0.2 nm, speed = 100 nm/s) using a 0.1 mm path length quartz slides at room temperature and averaged automatically. Each spectrum was background subtracted (using the same acquisition protocol) from the same conditions without peptide. Samples were heated using a peltier controller. Each sample was equilibrated at the desired temperature for 5 min before data acquisition.

4.4.9 Fluorescence Emission

Fluorescence emission measurements were acquired on a SPEX FluoroMax-3 and analyzed using DataMAX (Horiba Jobin Yvon, Edison, NJ). The excitation wavelength was 295 nm for tryptophan and 241 nm for Fcn. Tryptophan emission spectra were collected from 300 nm to 600 nm. Fcn emission spectra were acquired from 250 nm to 350 nm. The data pitch was 1 nm. The integration time was 0.5 sec. Data displayed is the average of three scans.

4.4.10 Steady-State Fluorescence Anisotropy

Fluorescence anisotropy measurements were acquired on a SPEX FluoroMax-3 and analyzed using DataMAX (Horiba Jobin Yvon, Edison, NJ). Diphenylhexatriene was at a molar ratio of 1:500 with a 10 mM phospholipid concentration. The excitation wavelength was 360 nm, and the emission wavelength was 426 nm.

4.4.11 Fluorescence Emission Measurements

Fluorescence emission measurements were acquired on a SPEX FluoroMax-3 and analyzed using DataMAX (Horiba Jobin Yvon, Edison, NJ). The excitation wavelength was 295 nm for tryptophan and 241 nm for Fcn. Tryptophan emission spectra were collected from 300 nm to 600 nm. Fcn emission spectra were acquired from 250 nm to 350 nm. The data pitch was 1 nm. The integration time was 0.5 sec. Data displayed is the average of three scans.

Chapter 5

Amyloid Assembly Mechanism in the Presence of Phospholipid Membranes

5.1 Introduction

Amyloid assembly in solution follows a complex pathway making its investigation in the context of membranes even more challenging (Dos Santos, Chandravarkar et al. 2005). The pathway of self-assembly is believed to proceed through ill-defined oligomeric species that subsequently transition into the observed β-sheet fibrils (Liang, Lynn et al. 2010).Chapter 3 presented data in support of this transition occurring though a conformation exchange mechanism at the oligomer-water interface. Hydrophobic and electrostatic interactions are two thermodynamic variables that influence this process (Liang, Pingali et al. 2008; Ahmed, Davis et al. 2010). Interestingly, these two properties also dictate peptide-membrane interactions (Seelig, Nebel et al. 1993). These similarities suggest that the phospholipid membrane might simply mimic the microenvironment believed to direct the conformational exchange mechanism that promotes amyloid assembly.

The exact peptide-membrane association remains a critical issue in the mechanism of amyloid assembly. Published data support both interfacial and insertional amyloid assemblies (Murphy 2007), and in order for the membrane-water interface to be the site of amyloid assembly, the peptide must be located on this surface. Furthermore, the actual mechanism controlling amyloid assembly in the context of membranes is inconclusive (Murphy 2007). Discrepancies in these data likely arise from the inability to control the assembly state in the absence of membranes (Dos Santos, Chandravarkar et al. 2005).

Probing amyloid assembly is further plagued by the transient nature of the species responsible for assembly initiation and the inability to control this process (Dos Santos,

Chandravarkar et al. 2005). I have developed methods to control the assembly of Aβ(13-21), a peptide derived from Aβ. At concentrations of 1 mM and lower, this peptide does not assemble into amyloid fibrils. This attribute removes any contributions from amyloid assembly in the absence of membranes. Studying the interactions of this peptide with membranes affords the opportunity to address many of these unsolved issues including the peptide-membrane association and the transition to amyloid. The work of this dissertation thus far has revealed several components of the membrane that are responsible for amyloid assembly but have not offered a molecular level description of the system.

5.2 Results and Discussion

5.2.1 Probing Aβ(13-21) Assembly using Tryptophan Fluorescence

Tryptophan fluorescence is sensitive to the polarity of it surrounding environment (Lakowicz 2006) should blue shift when associated with the membrane in either an interfacial or insertional orientation. If the indole ring is situated at the membrane interface, the emission maximum should appear around 340 nm, however it could shift to even lower wavelengths due to the changes in the dielectric constants. The wavelength range for a tryptophan inserted into the membrane hydrophobic core should be near 325 nm. Because the F19W and F20W peptide substitutions of Aβ(13-21) do not alter the assembly state, these peptides can be assembled in the presence of LUVs and analyzed using fluorescence and even initially explored with POPC, POPG, and POPS vesicles. These particular membranes were chosen because they exist in the fluid phase at room

temperature. This phase produces a clean β-sheet CD signature with the addition of Aβ(13-21) to POPG and POPS. POPC was explored as a control and to investigate peptide binding.

When Aβ(13-21)F19W and Aβ(13-21)F20W were added to POPC, the CD spectra do not indicate assembly (Figure 5.1A&C). The emission maximum in the presence of POPC is 360 nm while in the absence of POPC it is 361 nm. This shift is not significant; however, the fluorescence emission of each peptide does increase (Figure 5.1B&D). The tryptophan fluorescence emission intensity increases have been attributed to the indole ring being located in a more rigid environment. This suggests that the peptide binds to the POPC membrane, but this binding does not promote assembly.

When Aβ(13-21)F19W and Aβ(13-21)F20W were added to POPG, the CD spectra indicate assembly (Figure 5.2A&C). The spectra denote immediate assembly but appear to follow different trends. The F19W spectrum at 0 d appears somewhat helical and transitions into a predominant band at 203 nm. The F20W displays a more characteristic β-sheet CD signature albeit with the negative ellipticity that normally occurs at 215 nm occurring at 225 nm. This red shift is a direct result of scattering which likely comes from the assembly. The emission maxima for Aβ(13-21)F19W in the presence and absence of POPG is 346 nm and 361 nm correspondingly (Figure 5.2B). The emission maxima for Aβ(13-21)F20W in the presence and absence of POPG is 344 nm and 361 nm respectively (Figure 5.2D). The shift indicates that the indole ring is in a more hydrophobic environment. The emission maximum also increases when added to the LUVs signifying that the indole ring motion is restricted (Lakowicz 2006).

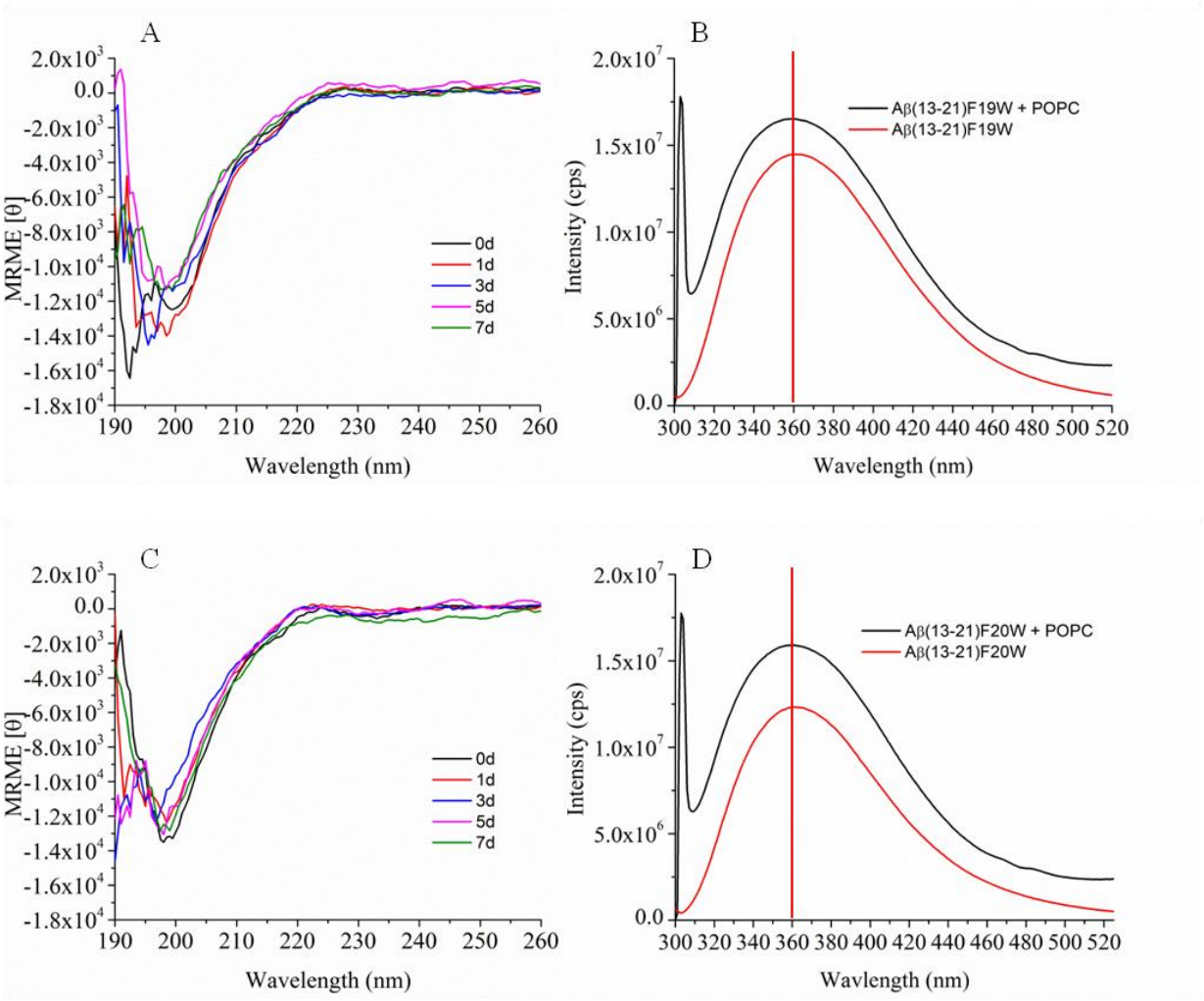

Figure 5.1 Probing the Membrane Association of Aβ(13-21)F19W and Aβ(13-21)F20W. A) CD spectra of Aβ(13-21)F19W + POPC, B) Tryptophan fluorescence emission of Aβ(13-21)F19W in the presence and absence of POPC, C) CD spectra of Aβ(13-21)F20W + POPC, B) Tryptophan fluorescence emission of Aβ(13-21)F20W in the presence and absence of POPC.

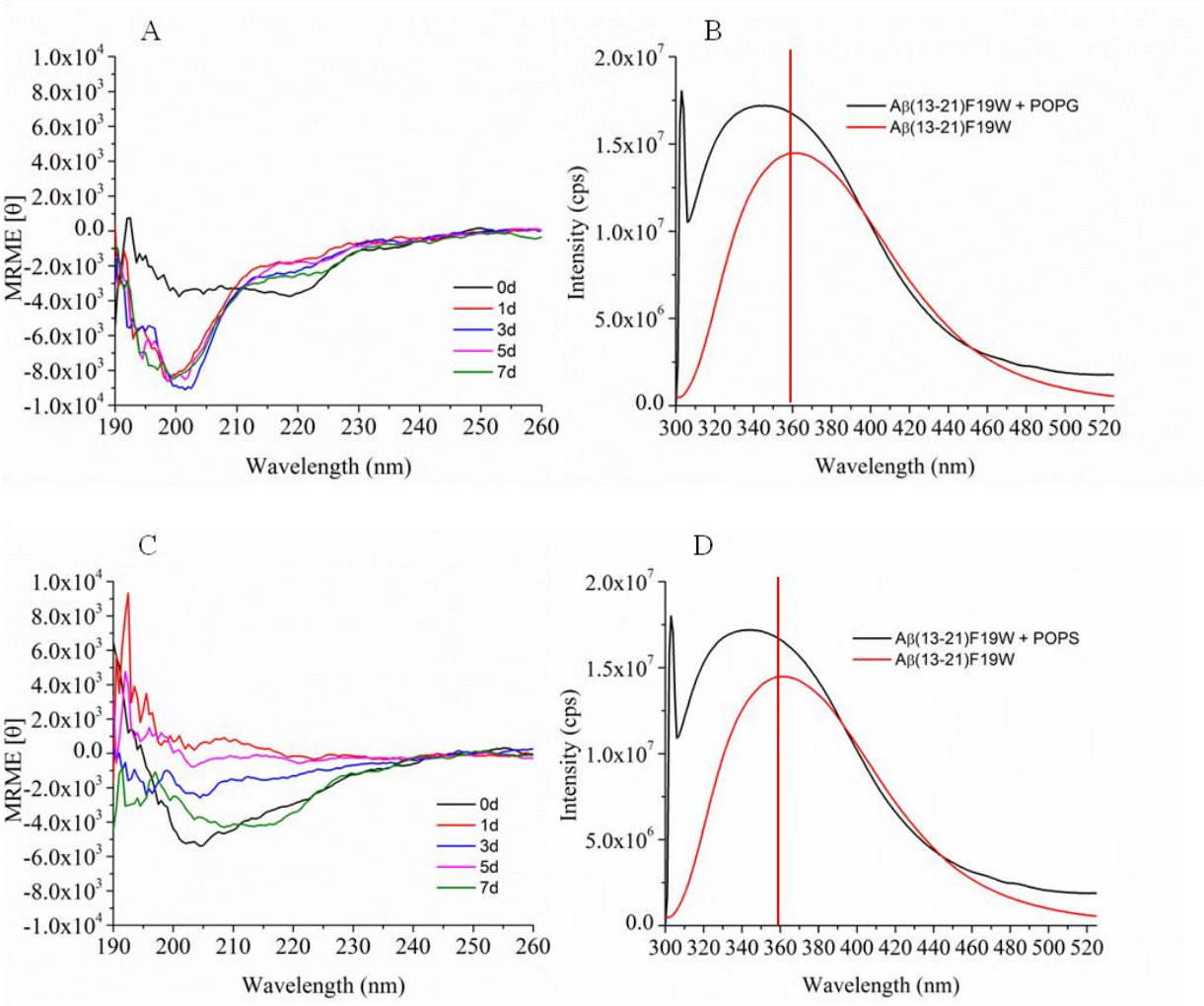

Figure 5.2 Probing the Membrane Association of Aβ(13-21)F19W. A) CD spectra of Aβ(13-21)F19W + POPG, B) Tryptophan fluorescence emission of Aβ(13-21)F19W in the presence and absence of POPG, C) CD spectra of Aβ(13-21)F19W + POPS, B) Tryptophan fluorescence emission of Aβ(13-21)F19W in the presence and absence of POPS.

When Aβ(13-21)F19W and Aβ(13-21)F20W were added to POPS, the CD spectra indicate assembly (Figure 5.3A&C). The spectra denote immediate assembly but appear to follow different trends again. The F19W spectrum at 0 d displays a predominate band at 203 nm which shifts towards the transition weakly indicating the presence of β-sheet. Again, the F20W displays a more characteristic β-sheet CD signature albeit with the negative ellipticity that normally occurs at 215 nm occurring at 225 nm. This red shift may be a direct result of scattering from the assembly or of a different secondary structure. The emission maxima for Aβ(13-21)F19W in the presence and absence of POPS is 345 nm and 361 nm respectively (Figure 5.3B) and for Aβ(13-21)F20W is 342 nm and 361 nm (Figure 5.3D), again suggesting a similar hydrophobic microenvironment and a restricted motion of the indole ring (Lakowicz 2006).

Tryptophan octylester (TOE) is commonly used as a control for the peptide-membrane association (Chattopadhyay, Mukherjee et al. 1997). The indole fluorescence emission for this compound ranges from 334-342nm depending on the pH of the solution (Chattopadhyay, Mukherjee et al. 1997). At a pH 7.5, which is the pH used here, the TOE emission maximum is ~338nm (Chattopadhyay, Mukherjee et al. 1997). The average location of the indole ring of TOE in POPC vesicles is 11Å from the center of the membrane (Chattopadhyay, Mukherjee et al. 1997), positioning the aromatic ring between the ester and methylene of the lipid tails (Mukhopadhyay, Monticelli et al. 2004). Since the emission intensity is red shifted relative to TOE, this places the tryptophan side chain closer to the membrane interface.

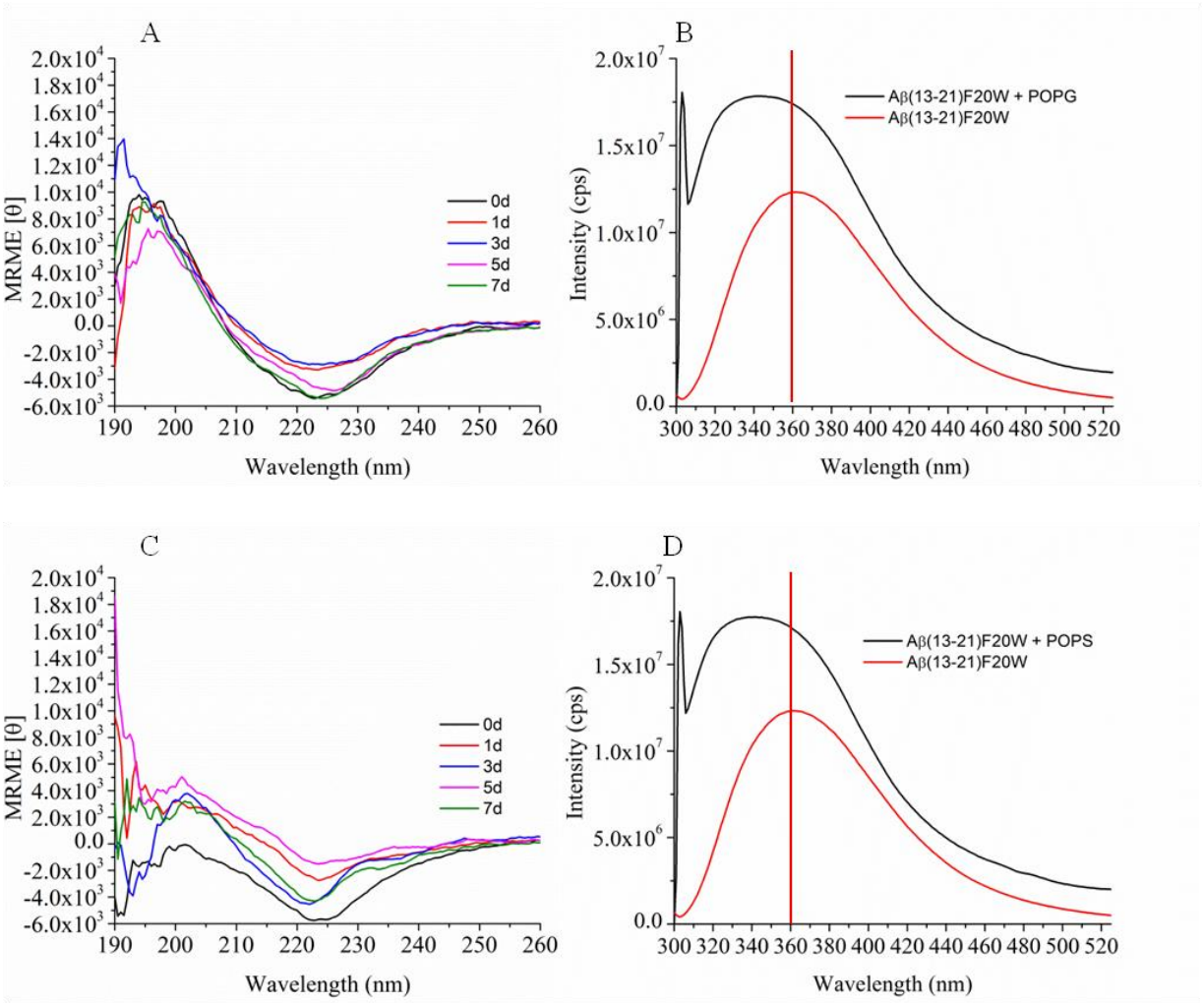

Figure 5.3 Probing the Membrane Association of Aβ(13-21)F20W. A) CD spectra of Aβ(13-21)F20W + POPG, B) Tryptophan fluorescence emission of Aβ(13-21)F20W in the presence and absence of POPG, C) CD spectra of Aβ(13-21)F20W + POPS, B) Tryptophan fluorescence emission of Aβ(13-21)F20W in the presence and absence of POPS.

5.2.2 Probing Aβ(13-21) Assembly in the Presence of DLPS LUVs using DSC

Differential scanning calorimetry (DSC) is regularly used to investigate protein stability via thermal denaturation and phospholipid membrane phase transitions (Heimburg and Biltonen 1994; Farber, Darmawan et al. 2010). During phospholipid gel-to-fluid phase transitions, the membrane absorbs heat resulting in a positive deflection (Lewis and McElhaney 2000). When the sample is cooled (fluid-to-gel transition), the membrane will release heat and produces a negative deflection (Lewis and McElhaney 2000). These phase transitions are lipid dependent. They predominantly depend on both the headgroup and the lipid tails. Because membrane transitions depend on the phospholipid molecular packing, any perturbations to the headgroup and/or the lipid chains results in a change in the thermal transition. External factors (*i.e.*, proteins, small molecules, metals) are known to change peak heights, broaden thermal transitions, shift the maximum (T_m) to higher or lower temperatures, and even induce the formation of new transitions (Heimburg and Biltonen 1994).

Changes in the phase transitions of phospholipid membranes have been exploited to investigate the location of peptides and proteins that interact with the phospholipid membrane (Heimburg and Biltonen 1994). For cytochrome c, a peripheral protein, the profile of the thermal transition changed depending on the degree of membrane surface coverage. With very little protein on the membrane surface, the profile was broad with the transition maximum (T_m) at the low temperature end of the transition, while at higher surface coverage, the T_m occurs at the high temperature side of the transition, and the higher melting temperatures were considered to be from the melting of lipid in direct contact with the protein. For an integral membrane protein that also shifts the C_p curve to

higher temperature, the T_m will remain at the low temperature end of the curve at the peptide-lipid ratio approaches unity. These distinctly different thermal profiles distinguish between peripheral and integral membrane proteins.

In order to determine the location of Aβ(13-21), the peptide was added to DLPS LUVs at the ratios indicated while the lipid concentration was held constant at 5 mM. In all samples, an increase in the phase transition temperature of this membrane was observed upon heating the sample from 5 ^{o}C to 25 ^{o}C (Figure 5.4A). More importantly, as the peptide concentration is increased a new transition appears at the back of the thermal profile. This new peak grows while the transition at the front decreases and at a lipid:peptide ratio of 5:0.5, the two peaks coalesce. These observed changes closely resemble that of calcium in the presence of phosphatidylserine membranes and support the idea that the peptide dehydrates the membrane (Silvius and Gagne 1984; Lewis and McElhaney 2000). This direct calorimetric support and comparative evidence positions the peptide at the membrane-water interface of the DLPS membrane.

When the Aβ(13-21)-DLPS samples are cooled, the DSC thermograms also contain a new transition (Figure 5.4B). This additional change suggests a lipid membrane structural change and/or a different peptide-membrane association. Given that the thermogram is similar in appearance to that of DMPG, it suggests that an extended phospholipid network is formed (Heimburg and Biltonen 1994; Schneider, Marsh et al. 1999), and a peptide structural change seems unlikely since the CD data gives the same signature at 5 ^{o}C and 25 ^{o}C (Figure 5.5A).

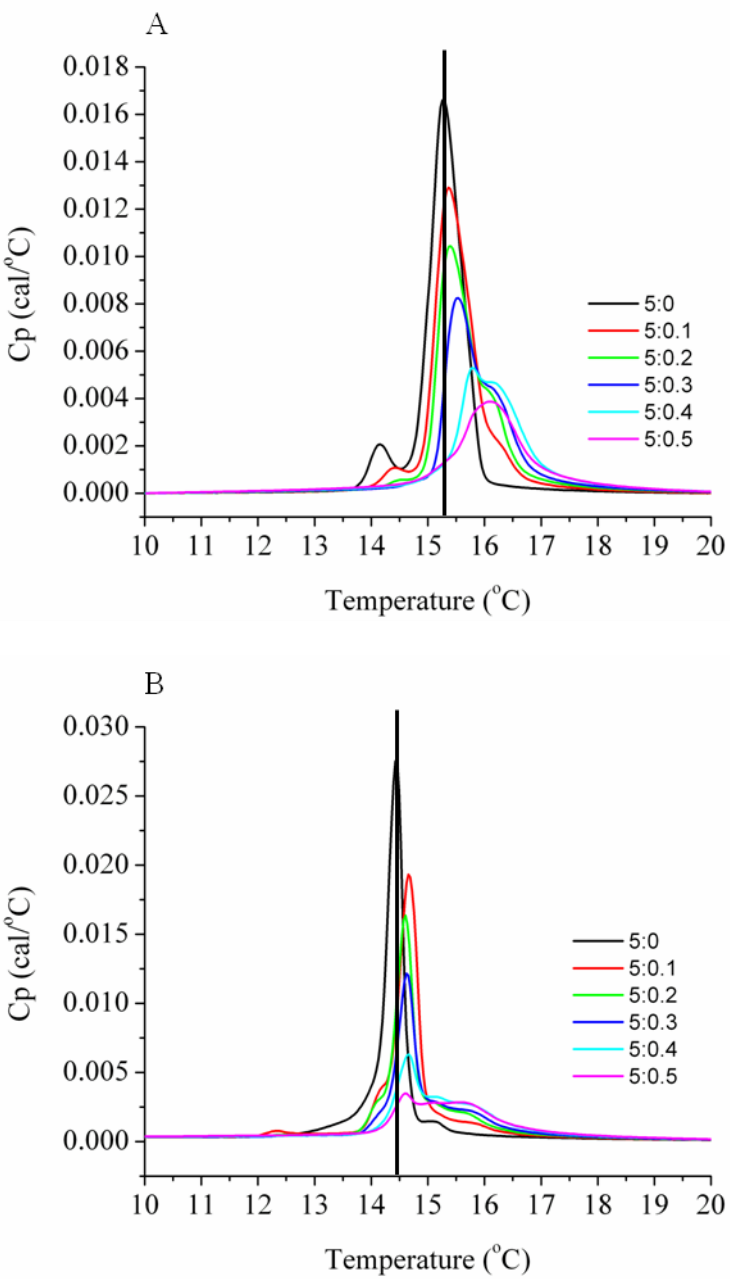

Figure 5.4 DSC thermograms of DLPS with increasing concentrations of Aβ(13-21). A) DSC heating thermograms of 5 mM DLPS in the presence of various concentrations of Aβ(13-21), B) DSC cooling thermograms of 5 mM DLPS in the presence of various concentrations of Aβ(13-21).

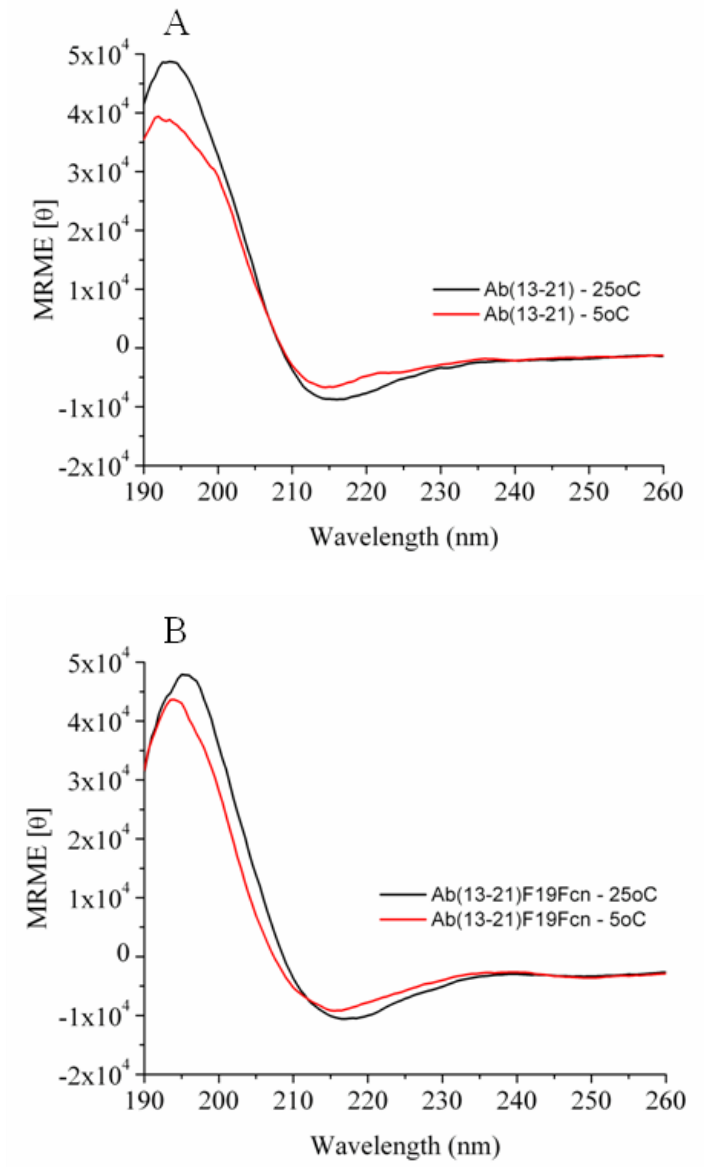

Figure 5.5 Aβ(13-21) and Aβ(13-21)F19Fcn produce a β-sheet CD signature independent of membrane phase. CD spectra at 5 ^{o}C and 25 ^{o}C of A) 0.5 mM Aβ(13-21) + 5 mM DLPS and B) 0.5 mM Aβ(13-21) Fcn+ 5 mM DLPS.

5.2.3 Probing DLPS Membrane Association of Aβ(13-21) using Fluorescence

The integration of fluorescent probes has offered insightful information about the amyloid assembly pathway (Liang, Lynn et al. 2010). Aβ(13-21)F19Fcn was used to probe whether the differences in the gel-to-liquid (heating) and liquid-to-gel (cooling) phase transitions in the DSC thermogram might be the result of peptide-membrane association changes. Both Aβ(13-21)F19Fcn and Aβ(13-21) require DLPS to assemble, and the first DSC downscan and upscan appear the same, however the relative intensities of the peaks relative to each other are different which is likely due to the inability to obtain the same peptide concentration for the two peptides (Figure 5.6). The variability arises from the purification process which adds differing amounts of salt to the peptide and the peptides are extremely flocculent which causes the peptide to stick to the pipette tip when initially dissolving the peptide sample. These two experimental complications make the concentrations approximately the same. Given that these two peptides behave similarly, the Fcn side chain fluorescence could be exploited as a reporter of membrane association and changes that may occur (Tang, Yin et al. 2009).

When Aβ(13-21)F19Fcn is added to DLPS, the fluorescence intensity of this molecule increases (Figure 5.7A). The lack of any intensity decrease suggests that the peptide does not insert into the membrane hydrophobic core, but rather binds to the membrane surface (Tang, Yin et al. 2009). However, the intensity increase is surprising and could stem from assembly itself and/or from the peptide-membrane association. To investigate whether the intensity increase is a result of a change in the fluorophore environment as a result of a change in the peptide-membrane association, the single amino acid (Fcn) was dissolved in 25 mM HEPES pH 7.5 or 25 mM phosphate pH 7.5 and analyzed for fluorescence

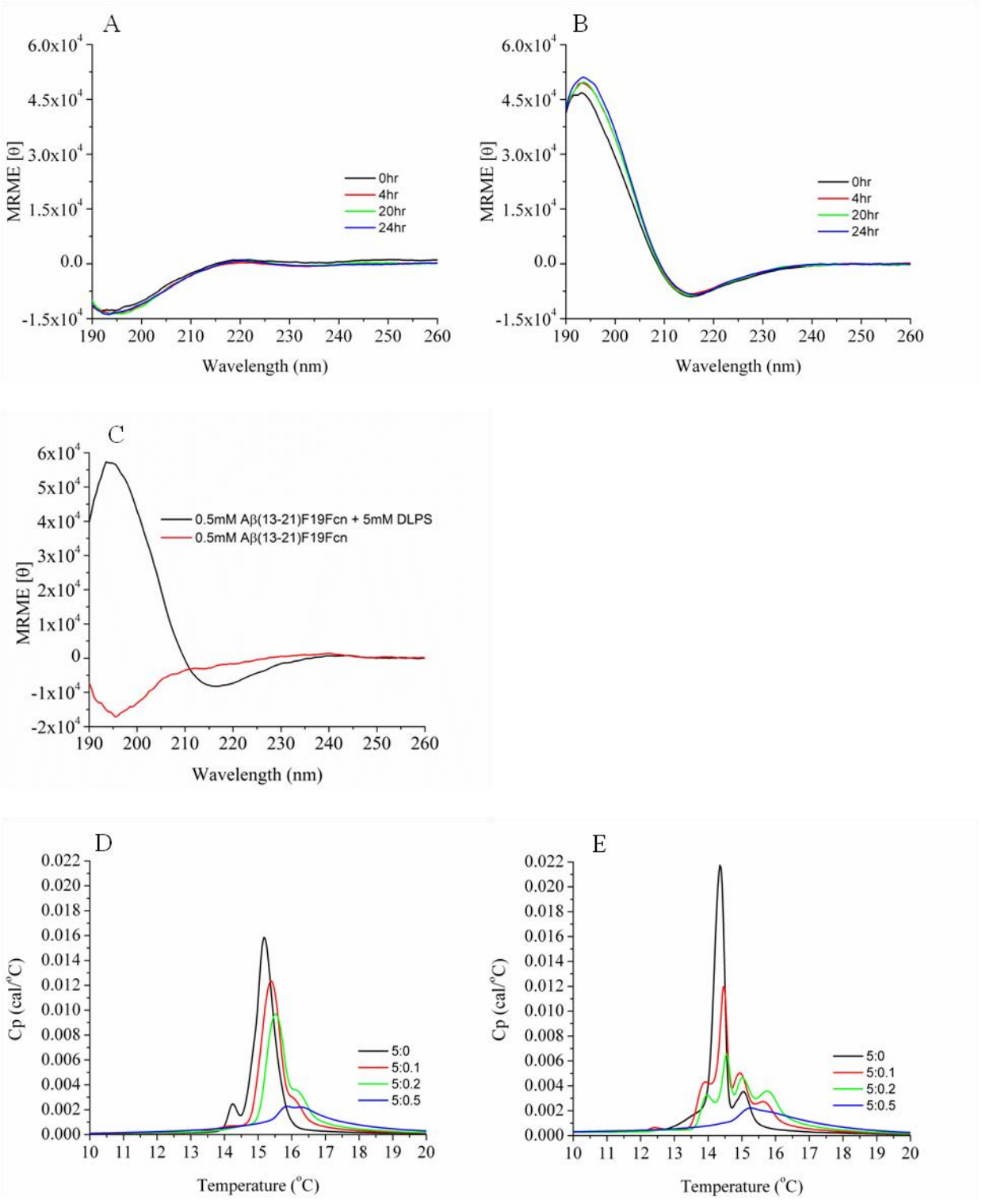

Figure 5.6 Ab(13-21)F19Fcn and Ab(13-21) Behave Similarly in the Presence of DLPS. A) CD spectra of 0.5 mM Aβ(13-21), B) CD spectra of 0.5 mM Aβ(13-21) + 5 mM DLPS LUVs, C) CD spectra in absence of DLPS and presence of DLPS, D) DSC heating

thermogram of Ab(13-21)F19Fcn+DLPS, E) DSC cooling thermogram of Ab(13-21)F19Fcn+DLPS. All samples are at pH 7.5 in 25 mM HEPES.

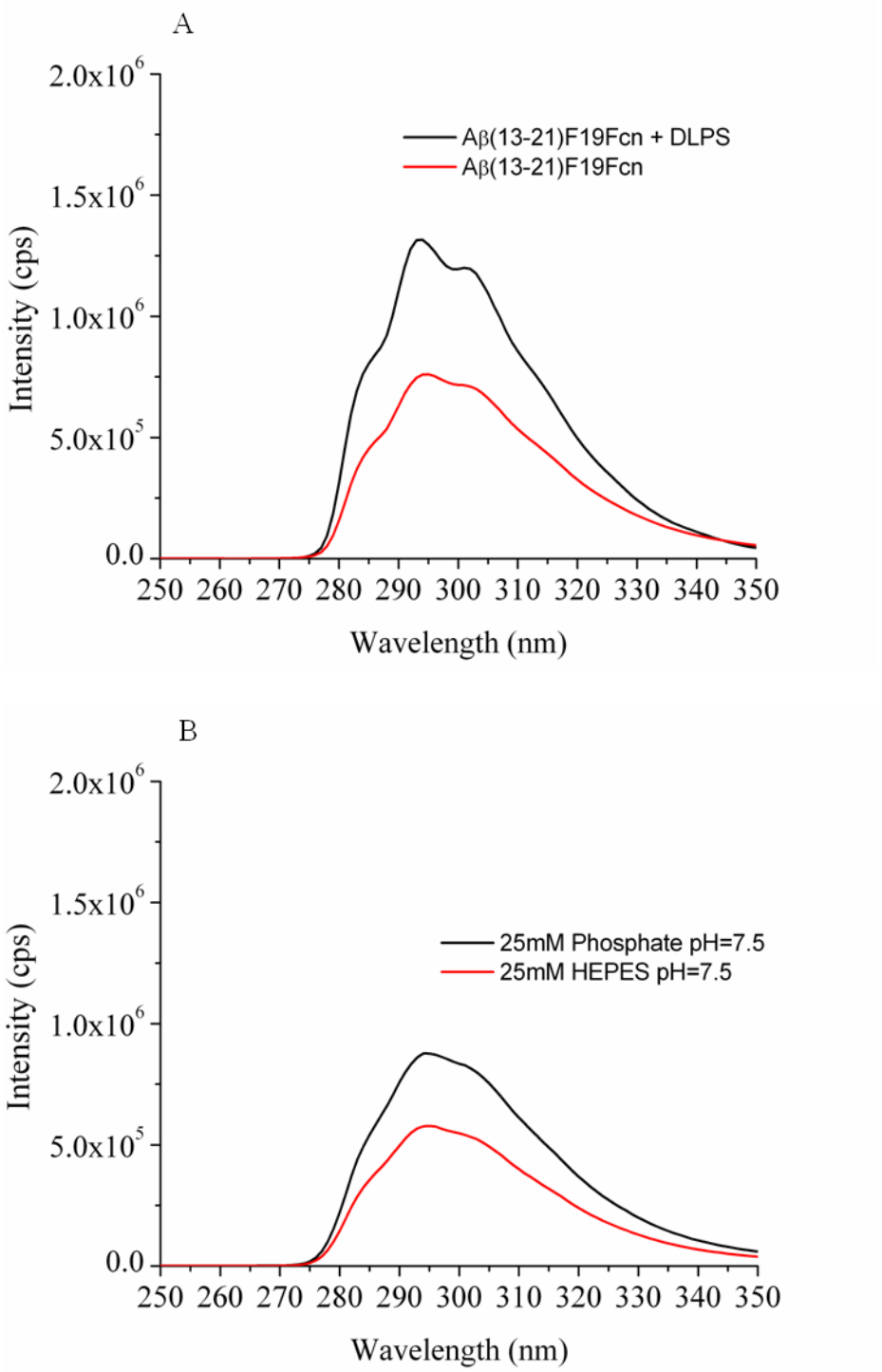

Figure 5.7 Fluorescence Emission Spectra of *para*-cyano-phenylalanine. A) 0.5mm Aβ(13-21)F19Fcn with and without 5mM DLPS, B) 0.5mM *para*-cyano-phenylalanine in 25mM HEPES pH=7.5 and 25mM phosphate pH=7.5 buffers.

emission changes (Figure 5.7B). Since the membrane association of Aβ(13-21)F19Fcn causes the fluorescence intensity to increase, any changes in the emission intensity should report on a change in membrane association upon changing the membrane phase because the thermal cycling of this sample does not change the secondary structure (Figure 5.5B&5.8A). No conformational changes are observed for Aβ(13-21)F19Fcn in the presence of DLPS when analyzed by CD thermal cycling (Figure 5.8A). Thus, there are no secondary structural changes. When Aβ(13-21)F19Fcn-DLPS is subjected to a thermal cycle in 5 ^{o}C increments, the fluorescence intensity of Fcn does not follow a linear temperature dependence as is observed for Fcn alone (Figure 5.8B-C), but the fluorescence intensity changes slope around the phase transition temperature. Since the CD control experiment reports that the amyloid assembly does not change structure, this fluorescence intensity change directly reflects a change in the peptide-membrane association. The decrease in fluorescence intensity could stem from scattering due to vesicle fusion.

5.2.4 Investigating the Aβ(13-21)-DLPS System by Thermal Cycling

Both Aβ(13-21) and Aβ(13-21)F19Fcn produce the characteristic β-sheet CD signature at 5 ^{o}C and 25 ^{o}C. These temperatures correspond to the gel and fluid phases of DLPS. To investigate the system over time, both Aβ(13-21) and Aβ(13-21)F19Fcn in the presence of DLPC were thermal cycled in the DSC at various ratios (Figure 5.9-5.12). In both peptide-membrane mixtures, the higher temperature transitions, which are assigned to the DLPS molecules that are affected by the presence of the peptide, continue to

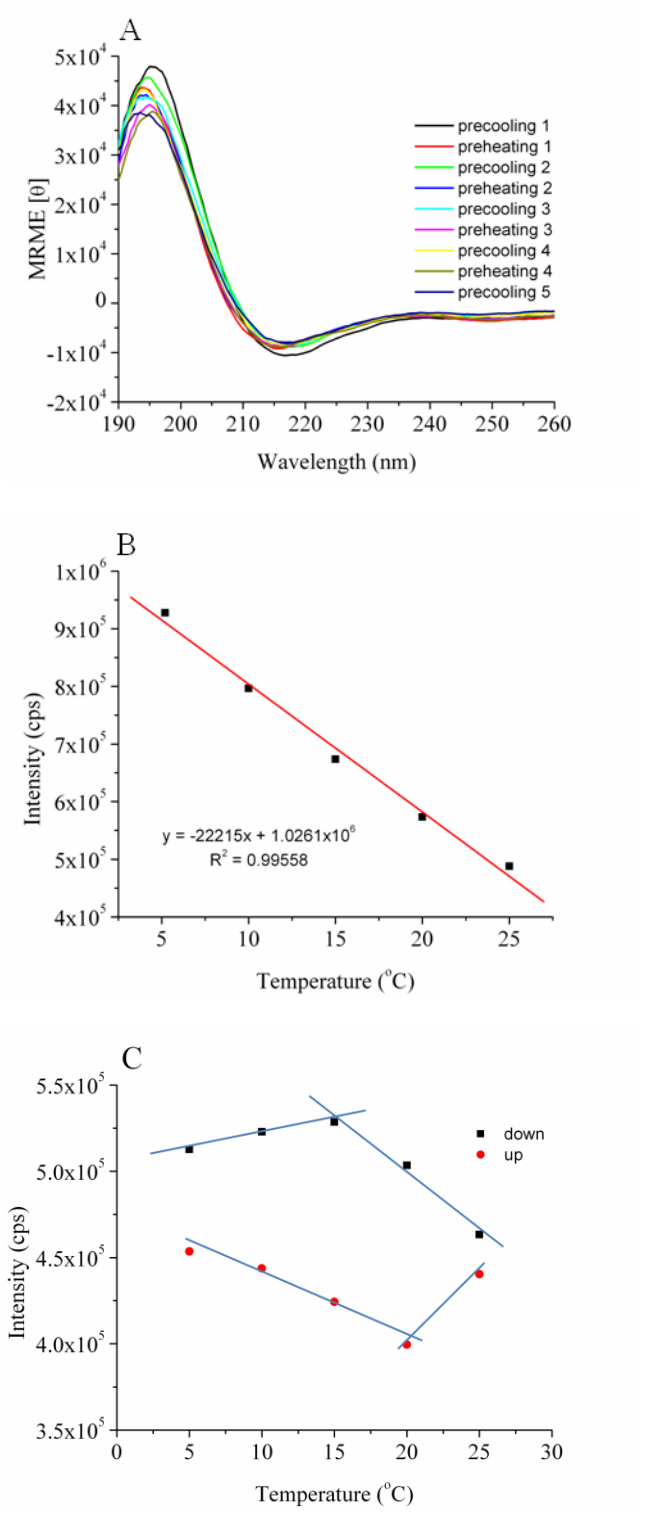

Figure 5.8 Thermal Cycling of *para*-cyano-phenylalanine. A) CD spectra of thermal cycling Ab(13-21)F19Fcn, B) Linear temperature dependence of Fcn fluorescence emission intensity between 5°C and 25°C, C) Fluorescence emission intensity of Aβ(13-21)F19Fcn with 5mM DLPS.

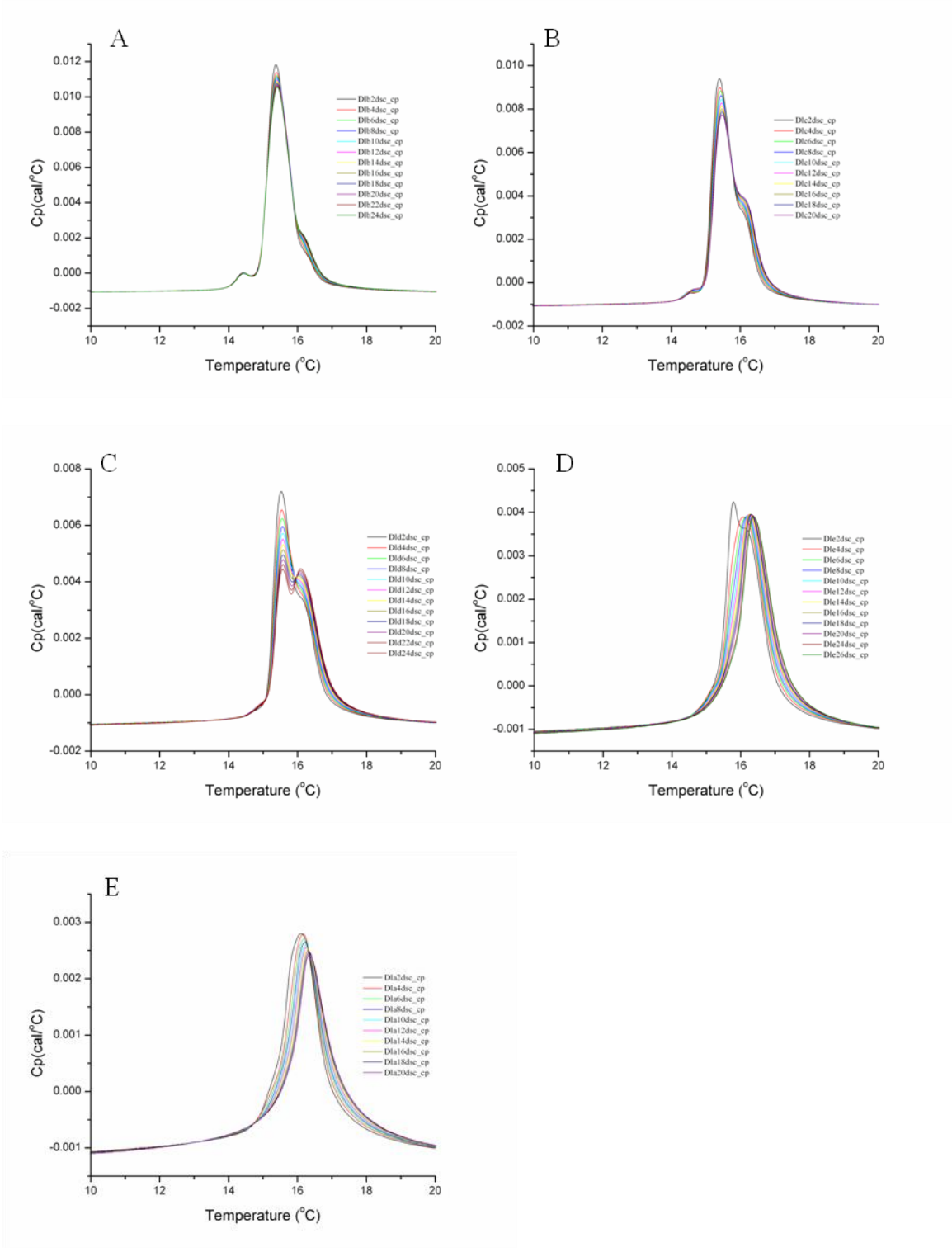

Figure 5.9 DSC thermal cycling of Ab(13-21)WT + DLPS heating scans. A) 5:0.1, B) 5:0.2, C) 5:0.3, D) 5:0.4, E) 5:0.5.

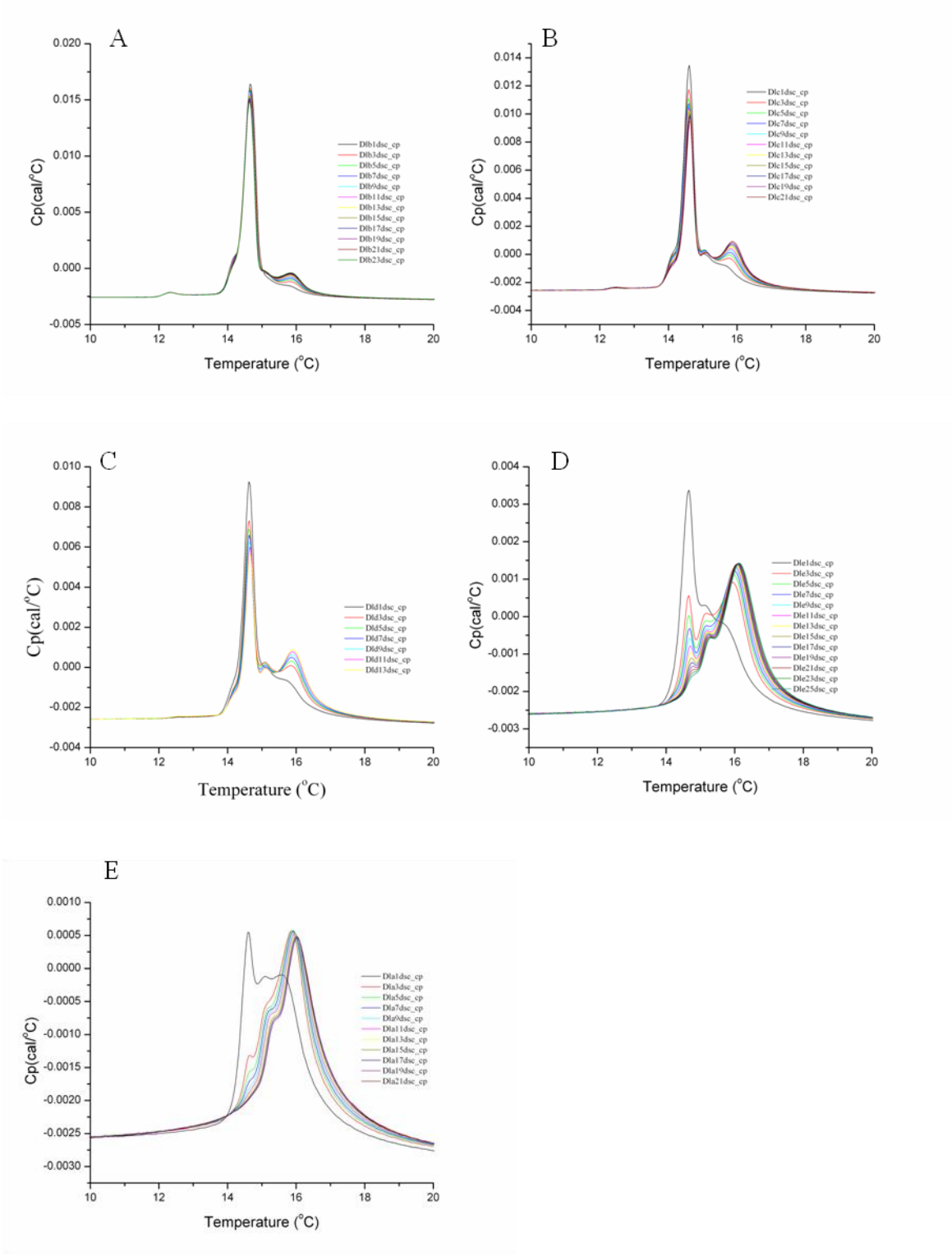

Figure 5.10 DSC thermal cycling of Ab(13-21)WT + DLPS cooling scans. A) 5:0.1, B) 5:0.2, C) 5:0.3, D) 5:0.4, E) 5:0.5.

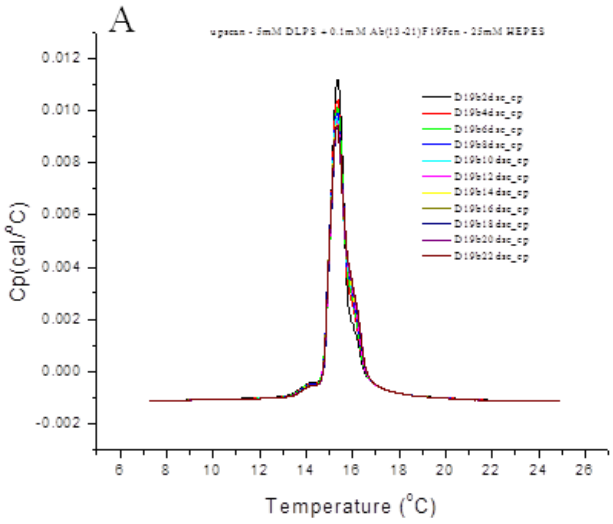
A
upscan - 5mM DLPS + 0.1mM Ab(13-21)F19Fen - 25mM HEPES
Cp(cal/°C)
Temperature (°C)

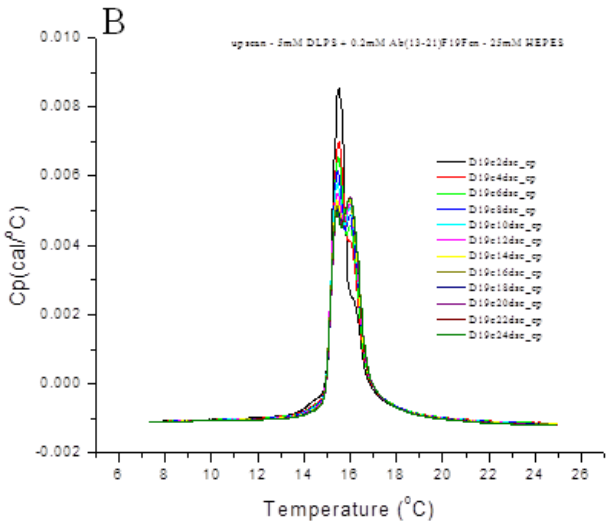
B
upscan - 5mM DLPS + 0.2mM Ab(13-21)F19Fen - 25mM HEPES
Cp(cal/°C)
Temperature (°C)

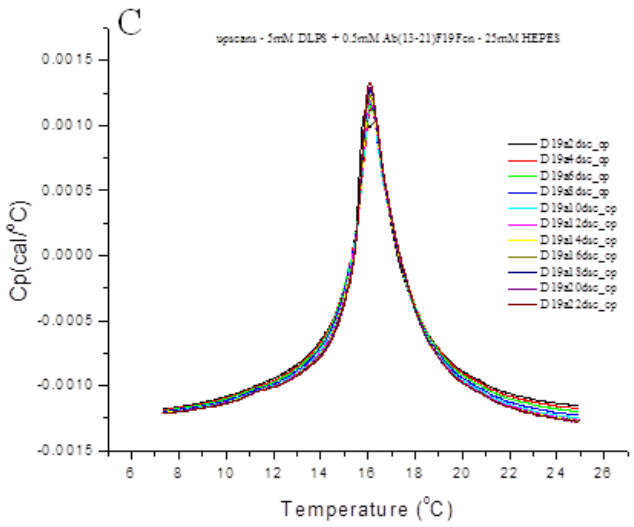

Figure 5.11 DSC thermal cycling of Ab(13-21)F19Fcn + DLPS heating scans. A) 5:0.1, B) 5:0.2, C) 5:0.5.

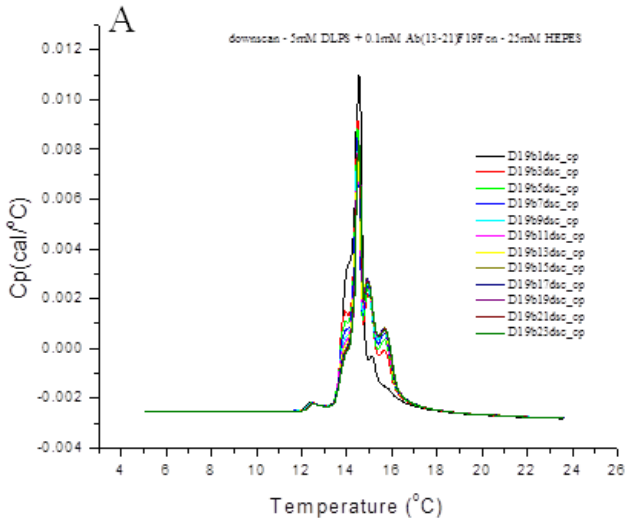
A
downscan - 5mM DLPS + 0.1mM Ab(13-21)F19Fcn - 25mM HEPES
Cp(cal/°C)
Temperature (°C)
D19b1dsc_cp
D19b3dsc_cp
D19b5dsc_cp
D19b7dsc_cp
D19b9dsc_cp
D19b11dsc_cp
D19b13dsc_cp
D19b15dsc_cp
D19b17dsc_cp
D19b19dsc_cp
D19b21dsc_cp
D19b23dsc_cp

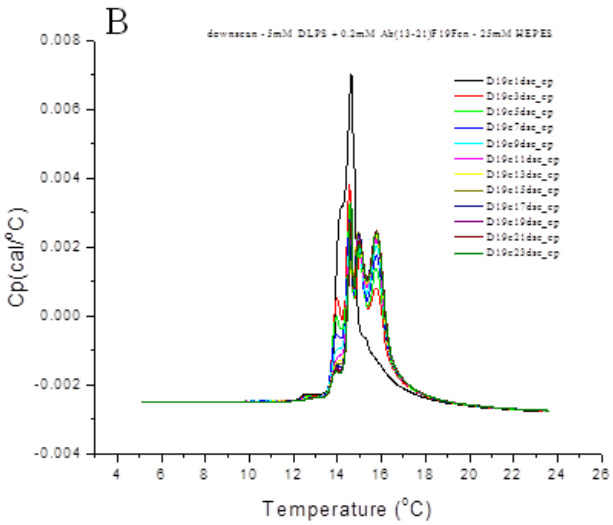
B
downscan - 5mM DLPS + 0.2mM Ab(13-21)F19Fcn - 25mM HEPES
Cp(cal/°C)
Temperature (°C)
D19c1dsc_cp
D19c3dsc_cp
D19c5dsc_cp
D19c7dsc_cp
D19c9dsc_cp
D19c11dsc_cp
D19c13dsc_cp
D19c15dsc_cp
D19c17dsc_cp
D19c19dsc_cp
D19c21dsc_cp
D19c23dsc_cp

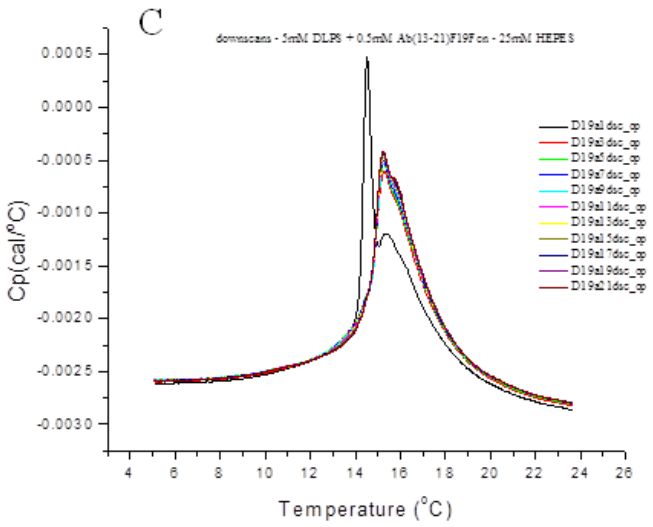

Figure 5.12 DSC thermal cycling of Ab(13-21)F19Fcn + DLPS cooling scans. A) 5:0.1, B) 5:0.2, C) 5:0.5.

increase over the timeframe of the experiment. This increase is accompanied by a continued decrease in the transition that has been assigned to the DLPS transition.

The heating scan for 5 mM DLPS and 0.2 mM Aβ(13-21)F19Fcn were processed to determine the rate of the transition increase and decrease observed in this particular system (Figure 5.13). The peak area integrations for the lipid only transition continually decrease as denoted by the closed black squares. The new transition that appears in the presence of the peptide grows (open red circles). These changes indicate the occurrence of a slow process occurring over the time course of the experiment. These continued transitions can be attributed to membrane fusion, amyloid assembly, and/or a combination of the two.

5.2.5 TEM Analysis of Aβ(13-21)-DLPS LUV Mixtures

To decipher the changes that occur in the peptide-DLPS system as observed by the DSC thermal cycling, Aβ(13-21)-DLPS mixtures were analyzed by transmission electron microscopy (TEM). Observation of 100 nm DLPS LUVs reveals the presence of predominately isolated LUVs and aggregated but predominately un-fused membranes (Figure 5.14A). Membrane ribbons and thin sheets are also observed occasionally, which is most likely due to the presence of Ca^{2+} ions in the water used to prepare the samples (Figure 5.15). The appearance of these structures complicates the examination of these samples, but comparison of the LUV and peptide-LUV samples reveals interesting insight into the amyloid assembly pathway.

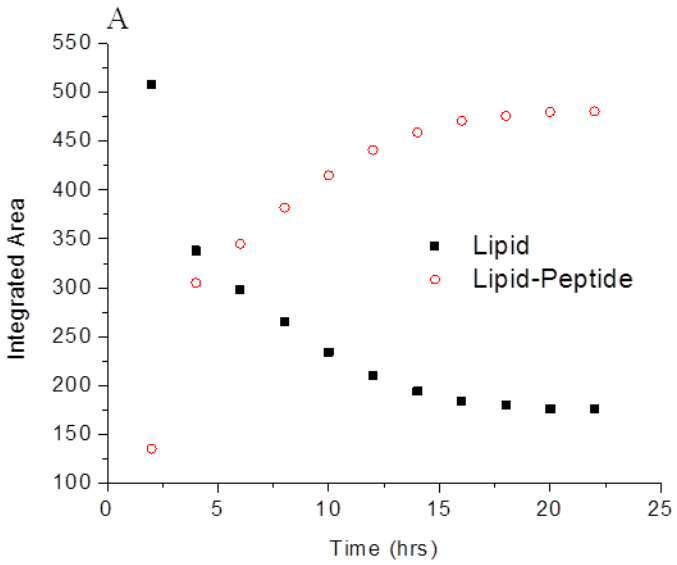

Figure 5.13 Thermal Cycling Analysis Suggests the Occurrence of a Slow Transition. A) Integrated areas for the 5 mM DLPS + 0.2 mM Ab(13-21)F19Fcn closed (black square – lipid only transition; open red circles – lipid-peptide transitions).

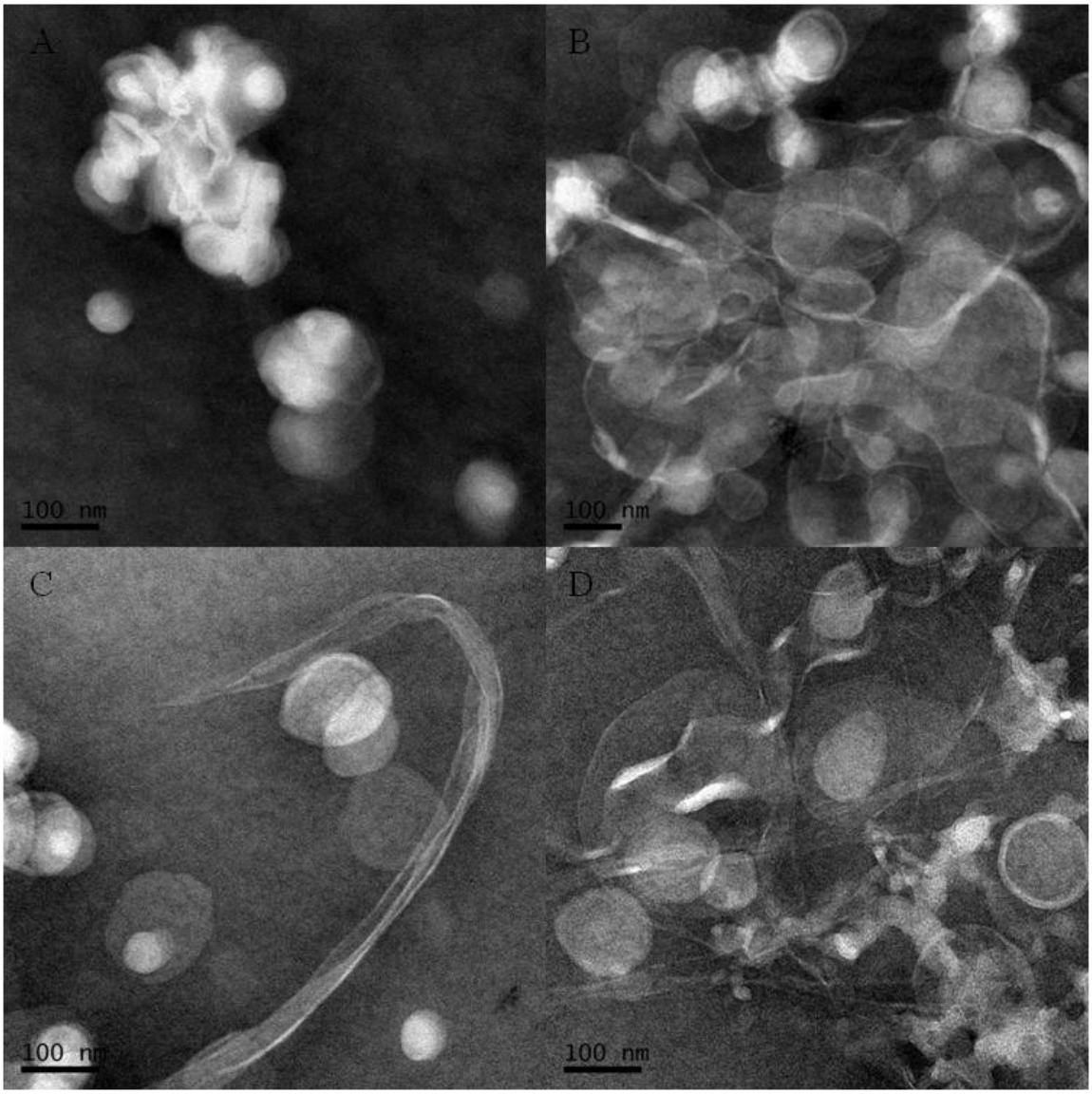

Figure 5.14 TEM images of 0.5 mM Aβ(13-21) added to 5 mM DLPS at various time points. A) no peptide, B) 0 hr, C) 3 hr, D) 24 hr.

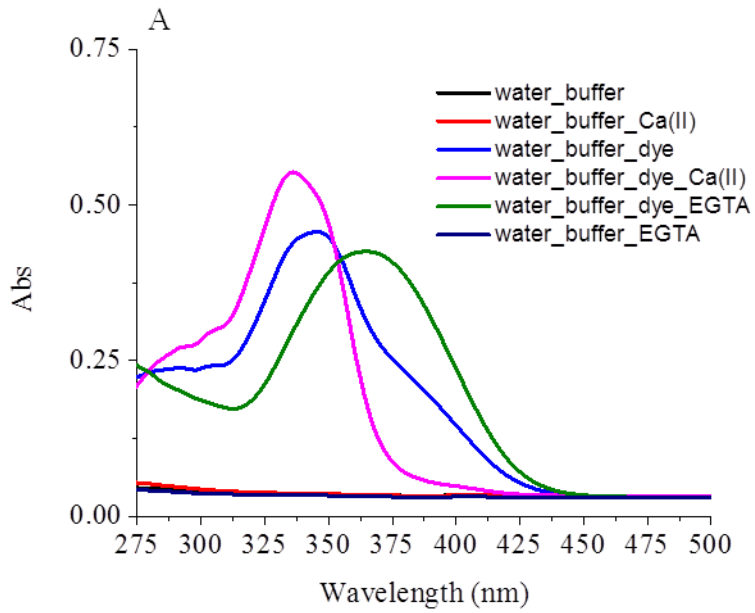

Figure 5.15 Fura-2 Ca^{2+} Induced UV shift. The water and/or the buffer contain trace amount of Ca^{2+}.

Three different time points were examined for the peptide-membrane mixtures – 0 hr, 3 hr, and 24 hr (Figure 5.14B-D). At 0hr, the presence of an extended phospholipid network is obvious, however any semblance of amyloid structures is not apparent even though CD measurements at these times do produce a β-sheet signature. It is possible that the peptide and membrane structures are conjoined and thus indistinguishable. Indeed at the 3 hr time point, striations that appear to be amyloid structures are associated with the extended membrane network. The formation of these striations possibly occurs though β-sheet growth to form the amyloid structure, and fibrils are clearly apparent in the 24 hr image in conjunction with the extended lipid network. These images likely explain the slow process detected in the DSC thermal scanning analysis and this interpretation suggests how amyloid fibrils grow and laminate. The phospholipid network may arise from the ability of an extended β-strand to interact with two opposing membranes given that this secondary structure has two distinct faces that may pull the membrane together.

5.3 Conclusions

5.3.1 Aβ(13-21) Membrane Association

Lipid-peptide interactions often involve a dynamic interplay between the two components. Eventually the system as a whole reaches a thermodynamically controlled equilibrium state. The data presented here postulates that amyloid propagation is the slow process that is observed in the DSC thermal cycling analysis. Protein-membrane associations can result in either phase transition temperature increases or decreases, thus concluding that the temperature shifts (higher or lower) observed are not specific

indicators of peptide-membrane associations (Heimburg and Biltonen 1996). However, the relative position of the transitions can reveal the peptide location on the membrane (Heimburg and Biltonen 1996). A peptide-lipid interfacial association results in a growing phospholipid transition located at the back of the phase transition as the relative protein concentration increases. These thermal profiles are seen with Aβ(13-21)-DLPS mixtures, therefore positioning the peptide in an interfacial orientation at the membrane-water interface (Figure 5.4). Furthermore, the thermal profiles of this system resemble that of Ca^{2+}-phosphatidylserine membranes where this ion binds at the membrane-water interface (Silvius and Gagne 1984).

The fluorescence intensity decrease observed for Aβ(13-21)F19Fcn-DLPS mixtures can be the result of two different types of membrane association changes: 1) peptide insertion or 2) peptide association changes. If the change in membrane association were due to insertion, then the CD signature should be accompanied by wavelength shifts and/or intensity changes (Park, Perczel et al. 1992), however these changes are not observed (Figure 5.8). Additionally, the DSC thermograms reflect peptide-membrane interactions in both gel and fluid phases. Therefore, these data suggest that the peptide is associated with the membrane, and given that a peptide in an extended conformation has two distinct faces, the question still remains as to the type of association.

Each of the two faces defined by the side chain orientation in an extended β-pleated sheet can interact with the membrane. The side chains on these two faces are HQLFcnA and HKVF (Figure 5.16), termed 5rf and 4rf, respectively (rf – residue face). If either of the faces is associated with the membrane, then dissociation would explain the increased

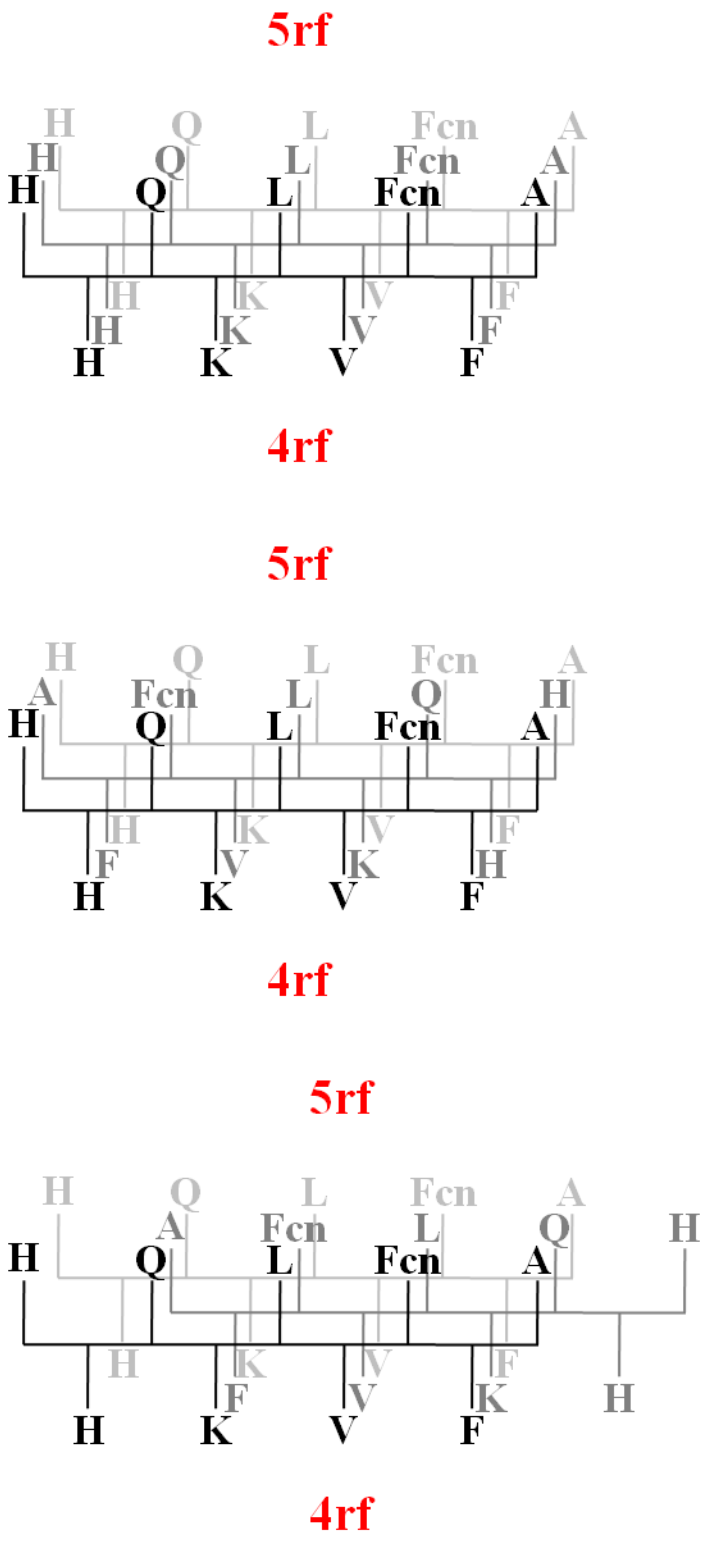

Figure 5.16 Defining β-sheet Faces. Defining Aβ(13-21)F19Fcn β-sheet with 5rf and 4rf.

fluorescence because F19Fcn would leave the phosphate environment and enter the HEPES buffer (Figure 5.17).

However, facial association does not support the DSC data which suggest Therefore, a double 5rf and 4rf association may be present in the liquid membrane phase whereby only one of the faces, 5rf or 4rf, dissociates from the membrane, explains both the DSC and fluorescence data. However, the question remains as to which face dissociates from the membrane interface. The Wimbley-White bilayer-to-water free energy transfer (ΔG) values are 2.85 kcal/mol and -0.1 kcal/mol for 5rf and 4rf, respectively, most consistent with the 4rf surface dissociating from the membrane. There are two types of double facial associations – 5rf /4rf and 5rf-4rf. The 5rf/4rf is simply a mixture of 5rf and 4rf associations while the 5rf-4rf association corresponds to an intermembrane association involving a single peptide (Figure 5.18). The fluorescence experiment in Figure 5.8 suggests that Figure 5.18B accurately describes the observed experimental changes. A revised membrane association must be drawn to explain the 5rf-4rf association because it does not "free" the Fcn side chain completely from the membrane (Figure 5.19). In a 5rf-4rf double association, the membrane wraps around the amyloid structure thereby pulling two opposing membranes together. This distorted membrane structure potentially leads to a closer peptide-membrane association. This type of membrane structure is similar to those proposed for membrane fusions (Martens and McMahon 2008), and the TEM images identify the presence of membrane fusions in the extended phospholipid network.

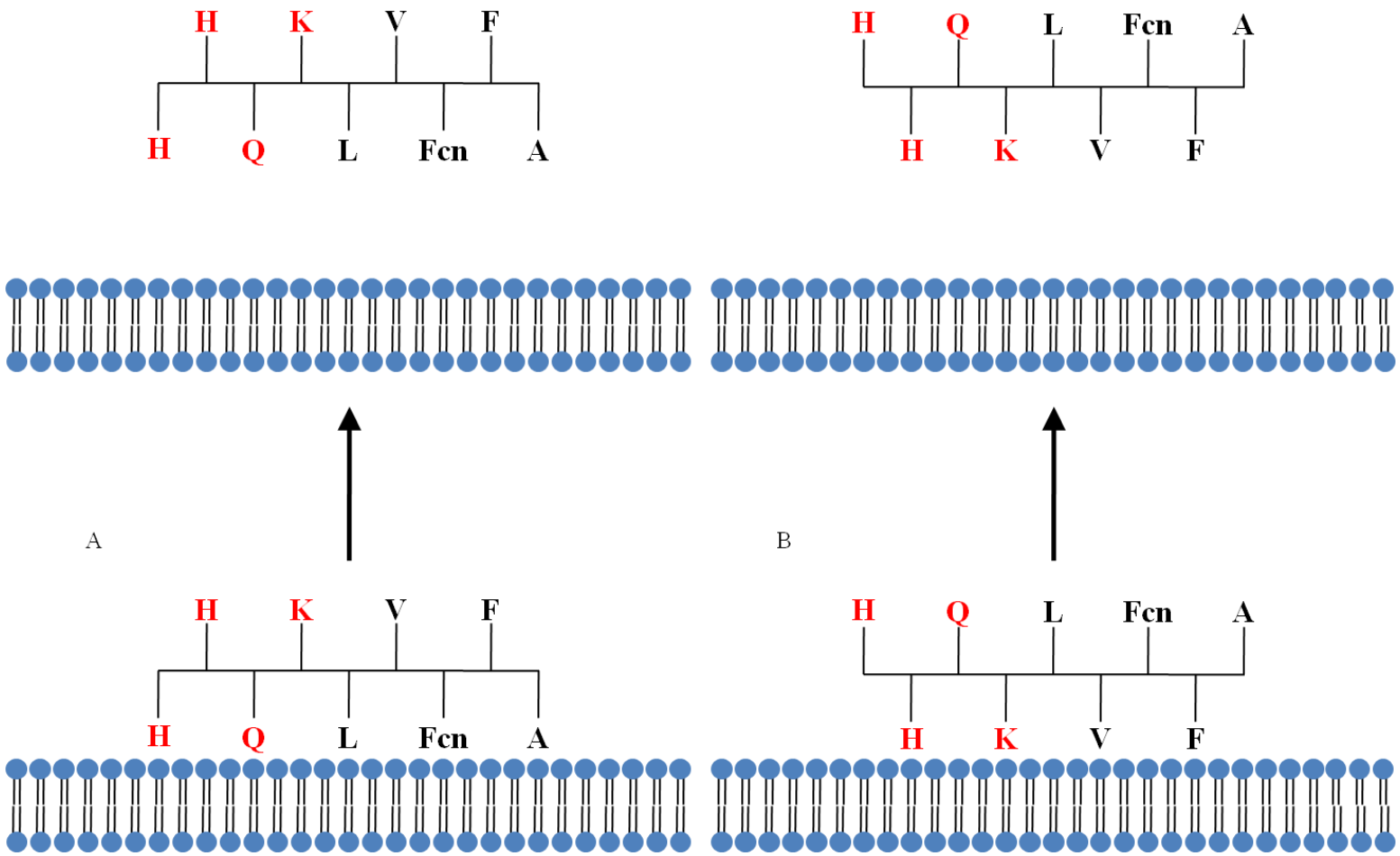

Figure 5.17 Single β-sheet Surface Membrane Association. A) Membrane dissociation of the 5rf β-sheet surface, B) Membrane dissociation of the 4rf β-sheet surface.

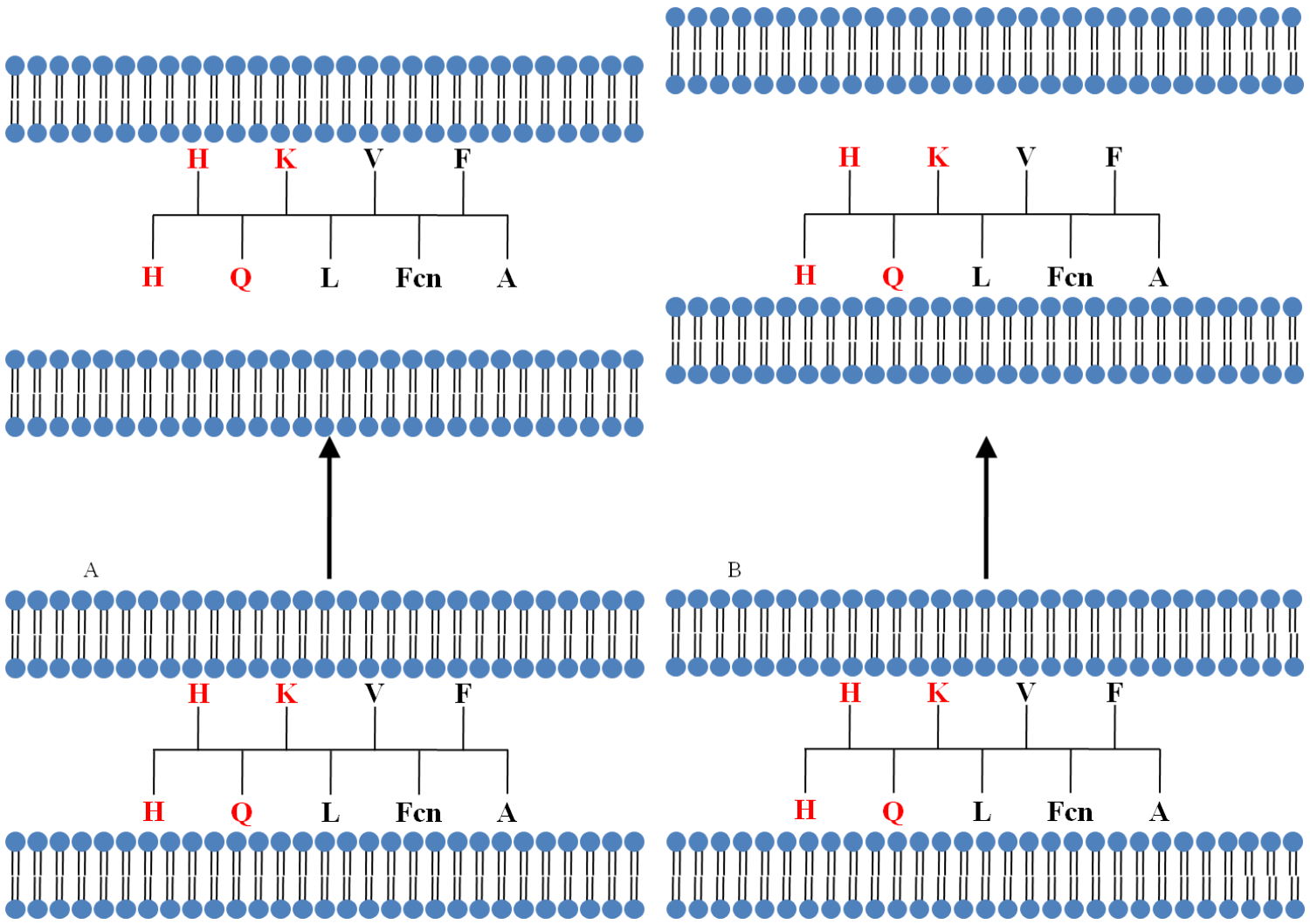

Figure 5.18 Double β-sheet Surface Membrane Association. A) Membrane dissociation of the 5rf β-sheet surface, B) Membrane dissociation of the 4rf β-sheet surface.

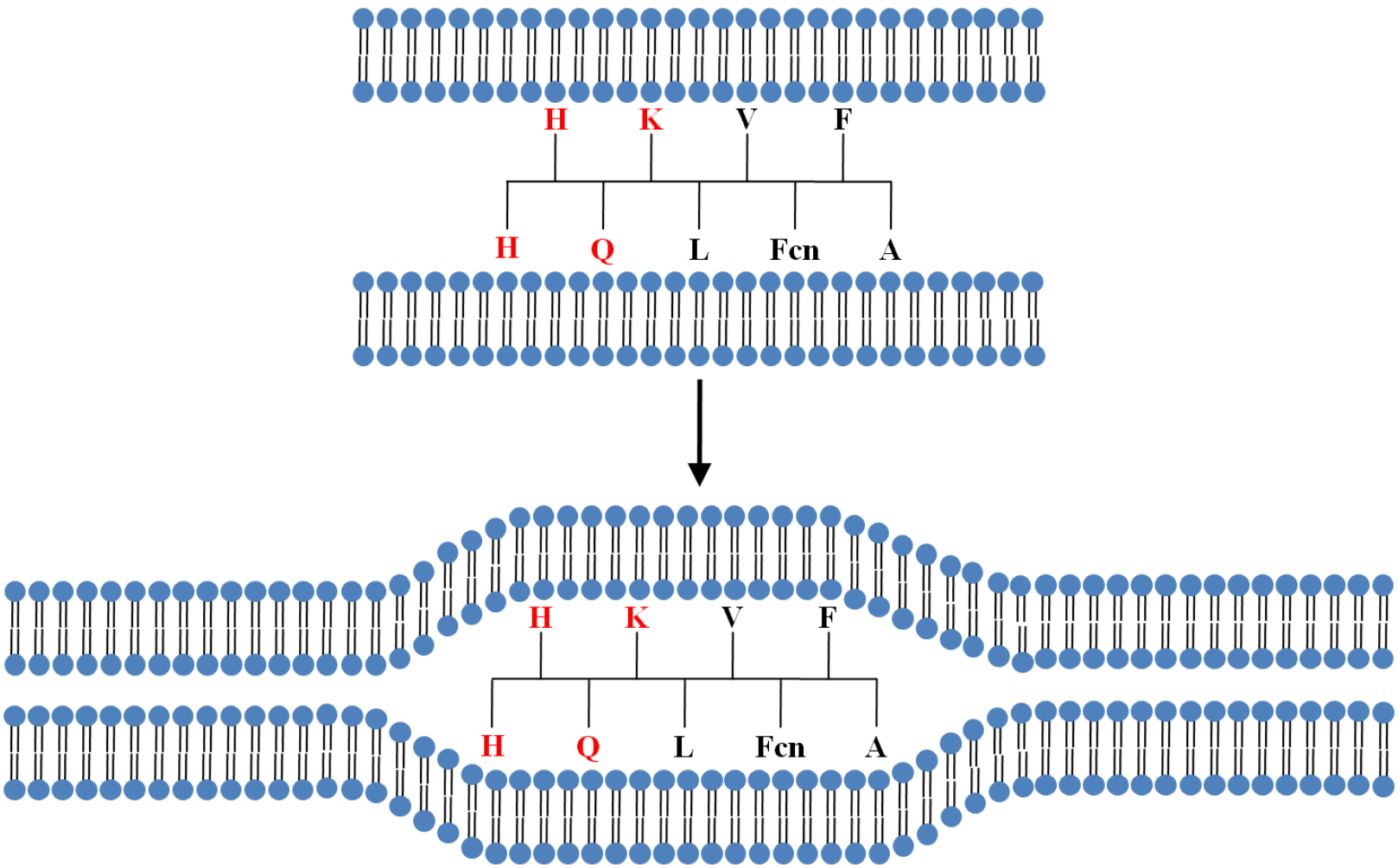

Figure 5.19 Revising the Double β-sheet Surface Membrane Association. A revision of the double membrane association generates a membrane-amyloid association that is strikingly similar to the proposed structures that occur during membrane fusion.

5.3.2 Mechanism and Pathway of Membrane-Induced Amyloid Assembly

The mechanism of amyloid assembly has long been investigated and a further comparison of the TEM images of DLPS and Aβ(13-21)-DLPS samples reveals clues about the amyloid assembly pathway. It is believed that amyloid formation entails the aggregation of peptide monomers into oligomeric species that transition into amyloidogenic species (Ahmed, Davis et al. 2010). Broadly speaking, these steps can be broken into initiation and propagation. Initiation describes the events responsible for β-sheet formation while propagation details amyloid growth. The specific structures and their location along the amyloid pathway are not well understood.

Initiation of amyloid structures is thought to involve ill-defined spherical oligomers (Murphy 2007). It is not clear whether initiation occurs on the surface or inside these species, but these structures are not present with Aβ(13-21) in solution. Presenting Aβ(13-21) with a membrane vesicle provides a spherical structure as well as a distinct microenvironment at the membrane-water interface. Is it possible that the membrane-water interface mimics the role of the oligomer-water interface?

The propagation steps depend on two growth dimensions – β-sheet and lamination. These two growth directions are orthogonal. The starting point, according to the CD data for Aβ(13-21) free in solution is a polyproline II helix conformation, and addition of DLPS membranes shows the immediate formation of a β-strand conformation. This conformational change appears to initiate amyloid formation by biasing the conformation into the required extended backbone conformation (Figure 5.20). If the peptide adopts a 3_{10}-helix, as seen with DPPG in the ripple phase, then assembly halts since this structure

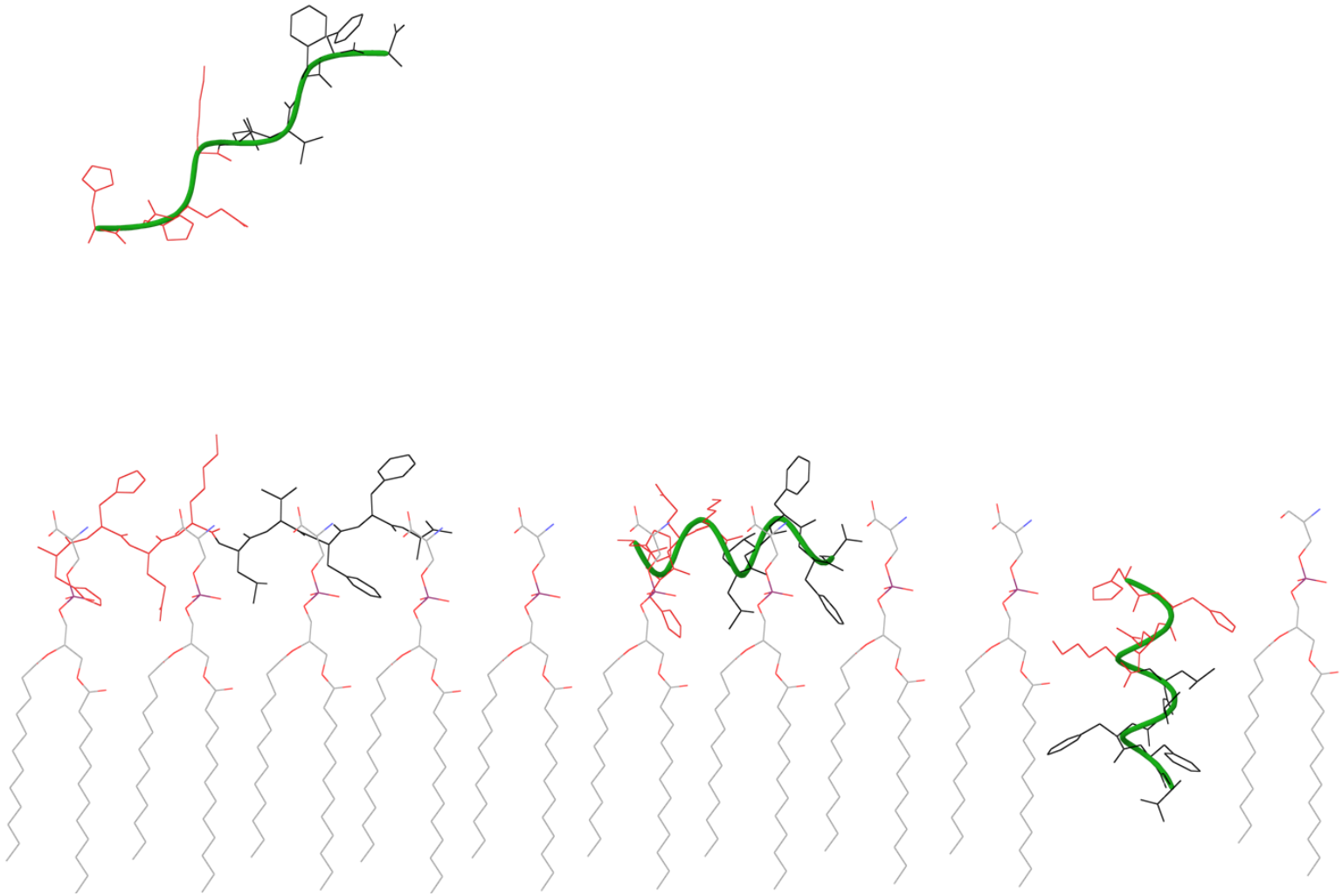

Figure 5.20 Amyloid assembly initiation. The membrane surface induces an extended conformation when peptide binds thereby initiating amyloid assembly. If the peptide imposes a high lateral pressure on the membrane, the peptide may adopt a 3_{10}-helix and possibly inserts as seen for the DPPG ripple phase. This structure would form under dehydration conditions.

cannot template the β-pleated sheet structure. It is unclear whether this helical structure is associated with the membrane interface or hydrophobic core. An energy barrier for insertion must be overcome in order for this to happen. This energy may stem from the lateral pressure that peptide association exerts on the membrane, however the membrane stress arising from peptide binding can also be reduced by adopting a 3_{10}-helix conformation because this structure is shorter than an extended conformation thereby reducing the number of affected lipids. Nevertheless, this mechanism is still driven by a change in the microenvironment to which the peptide is exposed.

Nature uses a similar mechanism to fold native and re-fold misfolded proteins as seen in the bacterial GroEL/GroES chaperone complex or the eukaryotic Hsp60/Hsp10 chaperone complex (Horwich, Fenton et al. 2007). However, peptides in an extended conformation must form intra-strand hydrogen-bonds in order to form amyloid structures. The data presented here allows peptide monomers to associate in either parallel or anti-parallel β-sheets that can be either in-register or out-of-register which results in the propagation of amyloid structures (Figure 5.21). The most thermodynamically stable or the faster kinetic product then propagates into an amyloid structure. DSC thermograms suggest that a slow thermodynamic equilibrium process is occurring during a 24 hr timeframe, a time where the most thermodynamically favored amyloid nucleus forms and competes for propagation.

Using membranes to mimic the microenvironment provides some structural insight into the surface of oligomers and the mechanism of amyloid assembly. The peptide is clearly located at the membrane-water interface in an extended conformation. These peptides then aggregate and compete to form amyloid nuclei for propagation. This

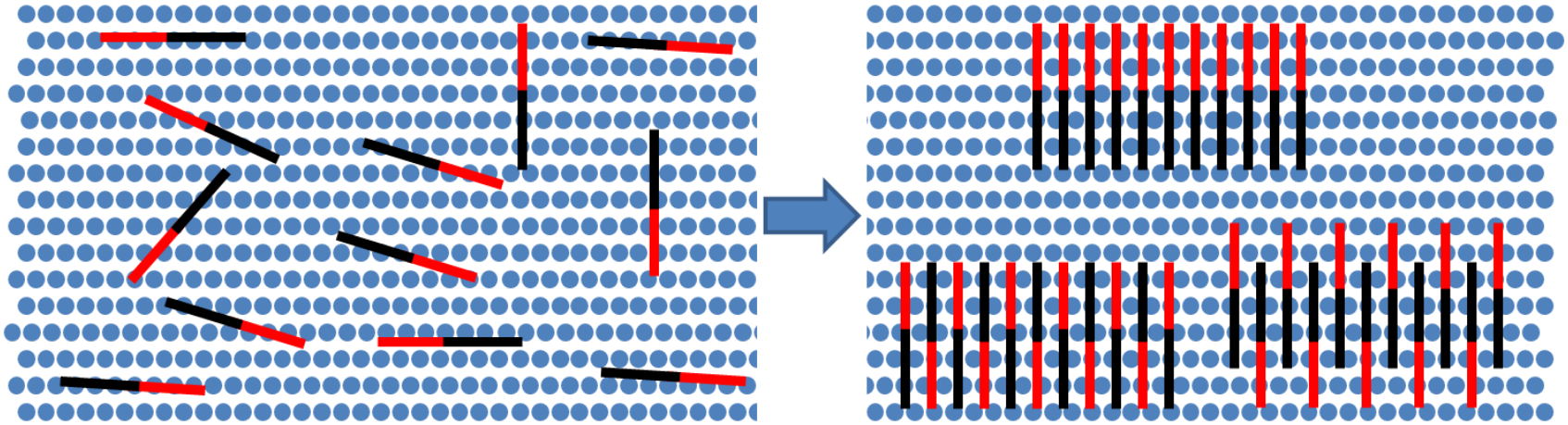

Figure 5.21 Amyloid assembly propagation. β-strands can form inter-strand hydrogen-bonds in either a parallel or anti-parallel orientation or associate in-register or out-of-register thereby producing the kinetic and/or thermodynamic amyloid structure which propagates along the membrane surface.

mechanism does not bias the peptide towards a particular strand orientation, peptide registry, or mixed assembly, but rather allows the kinetics and the thermodynamics of amyloid formation to dictate the final amyloid structure through propagation after its initiation by conformational exchange.

5.4 Methods

5.4.1 Materials

Solid-phase peptide synthesizer reagents (i.e., FMOC-amino acids, peptide resins) were obtained from Anaspec, Inc. (San Jose, CA). Distilled deionized water (ddH_2O) was purchased from EMD Chemicals, Inc. (Gibbstown, NJ) for sample preparations. All other reagents were acquired from Sigma-Aldrich Chemical Co. (Milwaukee, WI).

5.4.2 Peptide Synthesis and Purification

Peptide synthesis was performed using standard FMOC solid-phase peptide chemistry on a FMOC Rink-amide polystyrene resin (AnaSpec, Inc., sub. 0.4-0.6 meq/g) by a Rainin Symphony Quartet multiplex solid-phase peptide synthesizer (Protein Technologies, Tucson, AZ) or a Liberty Microwave solid-phase peptide synthesizer (CEM, Matthews, NC).

On the Rainin Symphony Quartet, HBTU and NMM were the coupling reagents. Each amino acid was coupled for 2 hours. His13, His14, Gln15, Lys16, Leu17, Val18 and Phe19 were double coupled. An acetylation reaction was performed after every coupling

reaction to eliminate deletion peptides. On the CEM Liberty, HBTU and NMP/DIEA were the coupling reagents. Each amino acid was single coupled following the standard coupling reaction conditions from CEM. An acetylation reaction was performed after every coupling reaction to eliminate deletion peptides.

The cleavage/deprotection reaction was carried out with trifluoroacetic acid/thiolanisole/EDT/anisole (95/5/3/2, v/v). The crude peptide was precipitated using cold ethyl ether and centrifuged at 6,500 rpm for 10 min at 4 ^{o}C. The crude product was then washed with cold ethyl ether and centrifuged four additional times. The crude peptide was kept under vacuum until purified.

All peptides were purified by RP-HPLC using a Waters Delta 600 and a Jasco LC2000 HPLC with a Zorbax 300SB-C18 preparative HPLC column (21.2mm x 25cm) and eluted at 10 mL/min. The peptide was dissolved in H_2O with 0.1% TFA. If the solution was cloudy, the crude mixture was filtered though a 0.2 μm filter (Whatman). A linear gradient from 15%/85% MeCN/H_2O with 0.1% TFA to 45%/55% MeCN/H_2O with 0.1% TFA was used. The HPLC peak was collected, condensed, frozen at -80 °C, and lyophilized (ATR FD3.0 freeze dryer or a Labconco FreeZone 12Plus freeze dryer). Lyophilized peptides were stored at -20 or -80 °C. MALDI-TOF MS analysis (Voyager-DE^{TM} STR Biospectrometry Workstation; 2,5-dihydroxybenzoic acid matrix) was collected on each peptide.

5.4.3 Peptide Sample Preparation

Peptide stock solutions were prepared by dissolving a known amount of peptide in ddH_2O at twice the desired concentration, sonicating for 10 min, and centrifuging at 13,200 x g for 10 min. The supernatant was collected and used as the peptide stock solution. 1 mM samples were prepared by diluting a 2 mM stock solution with 50 mM of the desired buffer and pH. 0.5 mM samples were further diluted with 25 mM of the desired buffer solution.

5.4.4 Multilamellar Vesicle (MLV) Preparation

Multilamellar vesicles were prepared using two different protocols. (1) Phospholipids were dissolved in buffer solution, vortexed for 1 min, and then stored at 4 ^{o}C until used. (2) Phospholipids were dissolved as monomers into a solution and dried on a rotary evaporator ≥12 hrs to form a thin lipid film. To hydrate the phospholipids, buffer solution, 10-15 ^{o}C above the phospholipid main transition temperature, was added to the thin lipid film to obtain the desired phospholipid concentration. The solution was spun on a rotary evaporator for agitation for >30 min while keeping the water bath above the main transition temperature of the phospholipid. The sample was then frozen by submerging the round bottom flask in an acetone-dry ice bath and was followed by melting the sample to a temperature above the main transition temperature of the phospholipid using the rotary evaporator as an agitator. Five cycles of this process (freeze-thaw) were completed.

5.5.5 Large Unilamellar Vesicles (SUV or LUV) Preparation by Extrusion

After the 5 freeze-thaw cycles, the sample was passed 19 times through a 100 nm single track-etch polycarbonate membrane (Avanti Polar Lipids) above the phospholipid main transition temperature using a mini-extruder (Avanti Polar Lipids, Alabaster, AL) to achieve the desired size (size = vesicle diameter).

5.5.6 Peptide-Vesicle Mixing

Peptide stock solutions were prepared as stated previously. Phospholipid vesicle stock solutions were prepared as stated in Phospholipid Vesicle Preparation. The peptide solution was added to the phospholipid vesicle solution by slowly ejecting the peptide stock solution into a phospholipid vesicle solution (previously diluted to the appropriate concentration) while simultaneously pulling the pipette out of the mixture. This was done to ensure an even mixing of peptide and vesicles.

5.5.7 Circular Dichroism

CD spectra were collected using a Jasco J-810 CD spectropolarimeter (Easton, MD). Three spectra were recorded from 260 nm to 190 nm (step size = 0.2 nm, speed = 100 nm/s) using a 0.1 mm path length quartz slides at room temperature and averaged automatically. Each spectrum was background subtracted (using the same acquisition protocol) from the same conditions without peptide. Samples were heated using a peltier controller. Each sample was equilibrated at the desired temperature for 5 min before data acquisition.

5.5.8 Fluorescence Emission

Fluorescence emission measurements were acquired on a SPEX FluoroMax-3 and analyzed using DataMAX (Horiba Jobin Yvon, Edison, NJ). The excitation wavelength was 295 nm for tryptophan and 241 nm for Fcn. Tryptophan emission spectra were collected from 300 nm to 600 nm. Fcn emission spectra were acquired from 250 nm to 350 nm. The data pitch was 1 nm. The integration time was 0.5 sec. Data displayed is the average of three scans.

5.5.9 Differential Scanning Calorimetry

The transition temperatures of phospholipid preparations were analyzed by measuring the heat change while scanning a temperature window from 5 ^{o}C to 25 ^{o}C at a scan rate of 0.5 ^{o}C/min using a VP-DSC microcalorimeter (Micro-Cal, Inc., Northhampton, MA). All solutions were degassed under vacuum and equilibrated at the appropriate starting temperature before scanning. The sample cell (0.5 mL) contained 25 mM HEPES buffer pH 7.5, with or without phospholipid preparations. An equal volume of buffer was used in the reference cell. Using the DSC analysis program in Origin supplied by MicroCal (Northampton, MA), the resulting thermograms were thermal transitions.

5.5.10 Transmission Electron Microscopy

Approximately 5 μL of the sample solution was placed on a Formvar/Carbon-coated 300 mesh copper grid (Electron Microscopy Science, Hatfield, PA) for 3 min. The excess solution was wicked away using triangular filter paper. 5 μL of 2% uranyl acetate or ammonium tungstate staining solution was applied to the TEM grid for 1.5 min, and the excess staining solution was wicked away. All grids were stored in a desiccator overnight. A Philips transmission electron microscope operating at 80 kV or a Hitachi H-7500 transmission electron microscope operating at 75 kV in the Robert P. Apkarian Integrated Electron Microscopy Core facility was used to obtain electron micrographs. Micrographs were digitally imaged used a Gatan BioScan 1K CCD camera with the accompanying imaging software (Gatan Inc., Pleasanton, CA).

5.5.11 UV-Vis Spectroscopy

UV-Vis spectra were collected in a 1 cm path length quartz cuvette using a Jasco V-530 UV/Vis spectrometer. The spectral window for each sample was 190 nm to 500 nm. The scan speed was 100 nm/min. The buffer concentration was 25 mM MOPS pH 7.1, and the EGTA was added to saturation. Spectra are the average values of three scans.

Chapter 6

Deciphering Amyloid Toxicity:

Effects of Amyloid Assembly on Phospholipid Membranes

6.1 Introduction

Alzheimer's disease has been associated with the presences of extracellular amyloid-β (Aβ) plaques and intracellular neurofibrillary tau tangles (Mattson 2004). Aβ is produced from the sequential cleavage of amyloid precursor protein (APP), a single-pass membrane protein (Thinakaran and Koo 2008). In Alzheimer's disease, APP is cleaved by β- and then γ-secretases producing peptide lengths of 38-43 amino acids with Aβ(1-40) and Aβ(1-42) being the predominate species (Thinakaran and Koo 2008). Aβ is believed to be the causative agent in neuronal toxicity observed in Alzheimer's disease under the amyloid hypothesis; however, the precise mechanism remains unclear (Bossy-Wetzel, Schwarzenbacher et al. 2004). Historically, Aβ toxicity has been linked to membrane pores, metal induced oxidative stress, receptor binding, and membrane leakage (Lashuel, Hartley et al. 2002; Dong, Canfield et al. 2007; LaFerla, Green et al. 2007; Friedman, Pellarin et al. 2009). More recently, Aβ oligomers have emerged as the leading contributory factor of toxicity (Kayed, Head et al. 2003). Interestingly, all of these proposed modes of toxicity involve the membrane in some fashion. However, the exact mechanism of membrane disruption that causes toxicity is much debated, and the exact membrane involved in leading to cell death is unknown.

Aβ affects the brain through an unknown mechanism. In neurons, Aβ(1-42) is generated in the endoplasmic reticulum (ER), and Aβ(1-40) is produced in the trans-Golgi network (TGN); however, these two amyloid peptides are predominately observed at the cell membrane of non-neuronal cells (Hartmann, Bieger et al. 1997). Furthermore, Aβ also is endocytosed by neuron cells (LaFerla, Green et al. 2007). Clifford *et al.* (2007) showed that Aβ accumulates in cerebral cortex neurons after injection into the tails of

mice (Clifford, Zarrabi et al. 2007), and Aβ is known to promote the internalization of several different receptors, thus giving it access to intracellular membranes (Yazawa, Yu et al. 2001; Nagele, D'Andrea et al. 2002). Additionally, Aβ has been localized at endosomes and to the lysosome (Cataldo, Peterhoff et al. 2000; Liu, Zhou et al. 2010). One striking difference between the extracellular face of the plasma membrane and intracellular membrane faces is the phospholipid composition. The extracellular membrane is predominately zwitterionic while the inner membrane contains negatively charged phospholipids in addition to zwitterionic lipids. Membranes are known to play a significant role in many cellular processes that include neurotransmitter exocytosis, signaling cascades, enzyme activity, and intracellular trafficking (Cabrera-Poch, Sanchez-Ruiloba et al. 2004; Andersen and Koeppe 2007; Korade and Kenworthy 2008; Murray and Tamm 2009). Any interaction with the negatively charged membrane lipids could affect these cellular processes deleteriously.

Mammalian cells are mostly comprised of phosphatidylcholine (PC), phosphatidylethanolamine (PE), and sphingomyelin (SM) lipids (Dodge and Phillips 1967). However, negatively charged phospholipids do exist, including phosphatidylinositol (PI), phosphatidylglycerol (PG), phosphatidic acid (PA), cardiolipin (CL), and phosphatidylserine (PS). Of particular interest is PS, which is the most abundant anionic phospholipid in mammals (Yeung, Gilbert et al. 2008). PS mainly remains on the cytosolic side of the plasma membrane of healthy cells; however, it is present on the extracellular leaflet of the plasma membrane in apoptotic cells (Yasin, Witting et al. 2003; Botto 2004; Vance and Steenbergen 2005). PS is also distributed asymmetrically across many organelle membranes and is found in a large number of

intracellular membranes like on the cytosolic face of the plasma membrane, in endosomes, and at the lysosome (Zachowski 1993; Vance and Steenbergen 2005; Yeung, Gilbert et al. 2008). Aβ is potentially exposed to PS membranes in these organelles through either its production or reuptake. Experimental data supports disruptions in endosomal, mitochondrial, and lysosomal in Alzheimer's disease (Cataldo, Peterhoff et al. 2000; Nixon and Cataldo 2006; Müller, Eckert et al. 2010). Furthermore, not only is PS associated with these membrane faces, but the brain also contains a higher concentration of PS (Calderon and Kim 2008). The fact that Aβ is selectively internalized in neural tissue and that the brain contains a higher amount of this negatively charged phospholipid necessitates the investigation of the interactions between amyloid peptides and PS membranes. Understanding how amyloid peptides interact with membranes composed of this phospholipid will provide greater insight for the mechanism responsible for amyloid toxicity.

Other intracellular organelles are known to contain PG, PA, and PI. PG and PA are present at the mitochondrial membranes and in the ER (Batenburg, Klazinga et al. 1985; Chakraborty, Vancura et al. 1999). The cytosolic face of the plasma membrane contains PI (Yeung, Gilbert et al. 2008). These negatively charged lipids are involved in several cellular processes including protein localization and synaptic vesicle exocytosis (Yeung, Gilbert et al. 2008). More importantly, malfunctions in cellular processes that involve these organelles have been shown in Alzheimer's disease, thus further necessitating a detailed investigation of the changes that occur in the presence of amyloid-forming peptides (Cataldo, Peterhoff et al. 2000; LaFerla, Green et al. 2007).

6.2 Results and Discussion

Several different properties of phospholipid membranes can be affected by the presence of amyloid peptides. Monomeric Aβ(13-21) was added to different LUVs to probe the effect this peptide has on phospholipid membrane properties. These properties include thickness, fluidity, hydration, and permeability.

6.2.1 Investigating Membrane Thickness using Small Angle Neutron Scattering (SANS)

Membrane thickness plays are role in biological systems and is often explained in terms of hydrophobic mismatch. Hydrophobic matching occurs when a protein hydrophobic stretch that spans the membrane (amino acids in α-helices or β-sheets) equals the membrane thickness (hydrophobic core of the membrane) (Andersen and Koeppe 2007). This situation is thermodynamically favorable, however when mismatches occur, subsequent changes in the overall membrane architecture or the protein structure occur. Lipids can lengthen, shorten, or tilt to compensate for any hydrophobic exposure, while proteins can tilt, change conformation, orient at the membrane interface, or aggregate to overcome the energetic penalty associated with exposure of hydrophobic residues (Fattal and Ben-Shaul 1993). Membrane thickness plays a biological role in exocytosis, endocytosis, and trafficking proteins through the Golgi as well as controlling protein activity (Fattal and Ben-Shaul 1993; Masibay, Balaji et al. 1993; Munro 1995; Mamdouh, Giocondi et al. 1996; Mitra, Ubarretxena-Belandia et al. 2004). Because disruptions in these cellular processes could potentially contribute to the progression of

Alzheimer's disease, amyloid-peptide induced membrane thickening or thinning needs further investigation.

Small angle neutron scattering (SANS) relies on scattering densities inherent in different atomic nuclei, and can provide information about peptide aggregation, micelle size, amyloid nanotube structure, and membrane thickness (Sadler, Rivas et al. 1984; Thiyagarajan and Tiede 1994; Burkoth, Benzinger et al. 2000; Thiyagarajan, Burkoth et al. 2000; Lu, Jacob et al. 2003). The data generated produces a scattering curve that can be processed using the Guinier equation to extract the radius of gyration (R_g). Alone this number is not of much value, however structural information can be obtained from this analysis when structures are known. These curves are fitted for known structural shapes (spheres, rod, tubes, etc.) and evaluated based on the quality of the fit with respect to R_g. Analysis of this raw data and the shape of the curve depend upon the number of scatters (concentration), particle size, the difference in the scattering length density, the selected form shape factor, interparticle interactions, the scattering angle and the wavelength.

Changes in membrane thickness were probed using SANS. A comparison of Aβ(13-21) to several phospholipids suggests that the peptide should orient itself at the membrane interface to the short hydrophobic stretch of this peptide relative to the hydrophobic thickness. Addition of Aβ(13-21) to POPC, POPG, and POPS did not produce any statistically significant membrane thickness changes (Figure 6.1A-C & 6.2A-C). The lack of membrane thickness changes for POPC is easily attributed to the lack of assembly with any PC membranes used. The absence of measurable membrane thickness changes observed for POPG and POPS suggest that the assembly of Aβ(13-21) occurs at the membrane interface or that the amyloid structure dissociates after assembly.

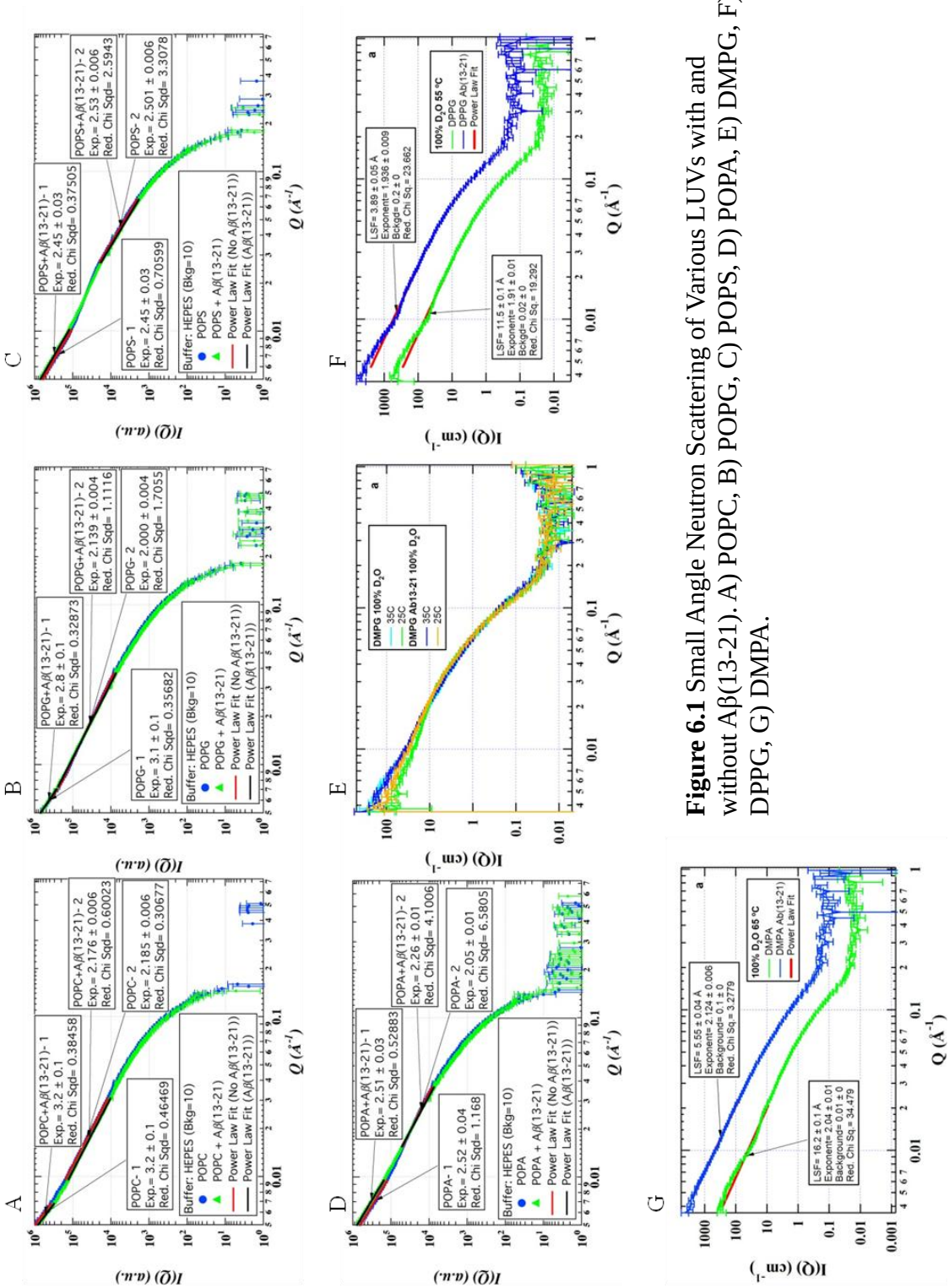

Figure 6.1 Small Angle Neutron Scattering of Various LUVs with and without Aβ(13-21). A) POPC, B) POPG, C) POPS, D) POPA, E) DMPG, F) DPPG, G) DMPA.

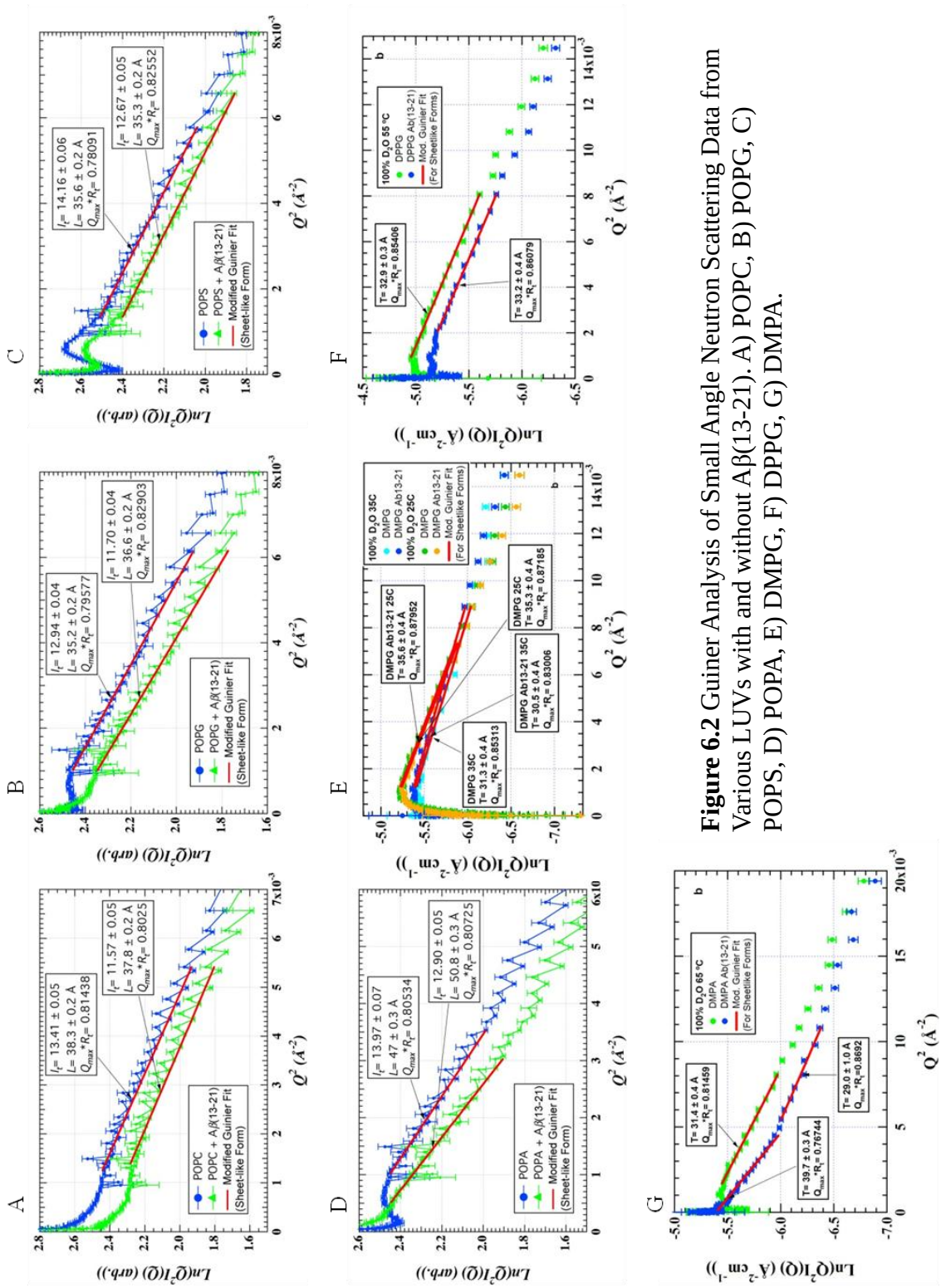

Figure 6.2 Guiner Analysis of Small Angle Neutron Scattering Data from Various LUVs with and without Aβ(13-21). A) POPC, B) POPG, C) POPS, D) POPA, E) DMPG, F) DPPG, G) DMPA.

However, addition of this peptide to POPA caused this membrane to thicken by approximately 3.8 Å. (Figure 6.1D & 6.2D). To determine whether this effect is dependent on the particular phospholipid headgroup, hydrocarbon chain, or a combination of the two, Aβ(13-21) association was evaluated with different phospholipid LUVs. Aβ(13-21) produced thickness changes for DMPA of approximately 8.3 Å but no significant changes in the membrane thickness of DMPG or DPPG could be detected (Figure 6.1E-G & 6.2E-G).

The absence of changes in scattering with PG or PS membranes suggests that the amyloid fibril assembly occurs at the membrane interface or is not associated with the membrane after assembly. The change in both PA membranes suggests that: 1) the amyloid assembly actually induces tighter packing of the phospholipid thus resulting in a greater membrane thickness or 2) the presence of the peptide dehydrates the membrane interface thus changing the scatter distance (D_2O) from the inside to the outside (artifical membrane thickening).

6.2.2 Membrane Fluidity – Fluorescence Anisotropy

Another important property of membranes is its fluidity. Membranes predominately exist in the fluid state; however, recent research suggests that membranes actually possess rigid microdomains called lipid rafts (Korade and Kenworthy 2008; Lingwood and Simons 2010). These domains have been associated with regulating protein function, endocytosis, protein sorting, and others (Simons and Ehehalt 2002; Pike 2009; Lingwood and Simons 2010). Furthermore, membrane fluidity has been shown to play a role in

nerve pulse propagation. It has been shown that reduced temperatures, which correlate to membrane stiffening, induce nerve pulses (Kobatake, Tasaki et al. 1971). Thus, any membrane fluidity changes that result of amyloid species could induce nerves pulse and lead to an increase risk of seizures and toxicity due to the hyperexcitability observed in Alzheimer's disease (Minkeviciene, Rheims et al. 2009).

To probe whether fluidity changes occur with the addition of Aβ(13-21), the membrane fluidity of POPG was investigated. Fluorescence anisotropy was selected to study membrane fluidity, and diphenylhexatriene (DPH), a commonly used membrane probe, provides a direct report of membrane fluidity where an increase in the anisotropy value reflects membrane stiffening.

One potential reason that Aβ(13-21) does not assemble in the presence of phosphatidylcholine membranes is that the peptide does not bind to PC membranes, that the binding of this peptide to the membrane does not allow aggregation, or that the peptide is sequestered in the membranes hydrophobic core. DPPC membranes in the presence of Aβ(13-21) show no changes in their fluidity (Figure 6.3). This lack of disruption could also be due to the high temperature used to investigate these effects.

In the absence of Aβ(13-21), the fluorescence anisotropy is 0.12. When Aβ(13-21) is present, the fluorescence anisotropy is approximately 0.24, suggesting that the membrane stiffens in the presence of the peptide (Figure 6.4A). To compare the assembly kinetics with rigidity kinetics, Aβ(13-21) was added to POPG, and the fluorescence anisotropy increase was followed over time (Figure 6.4B-C). Assembly as denoted by CD is significantly faster than the fluidity changes, thus suggesting that a slower process is

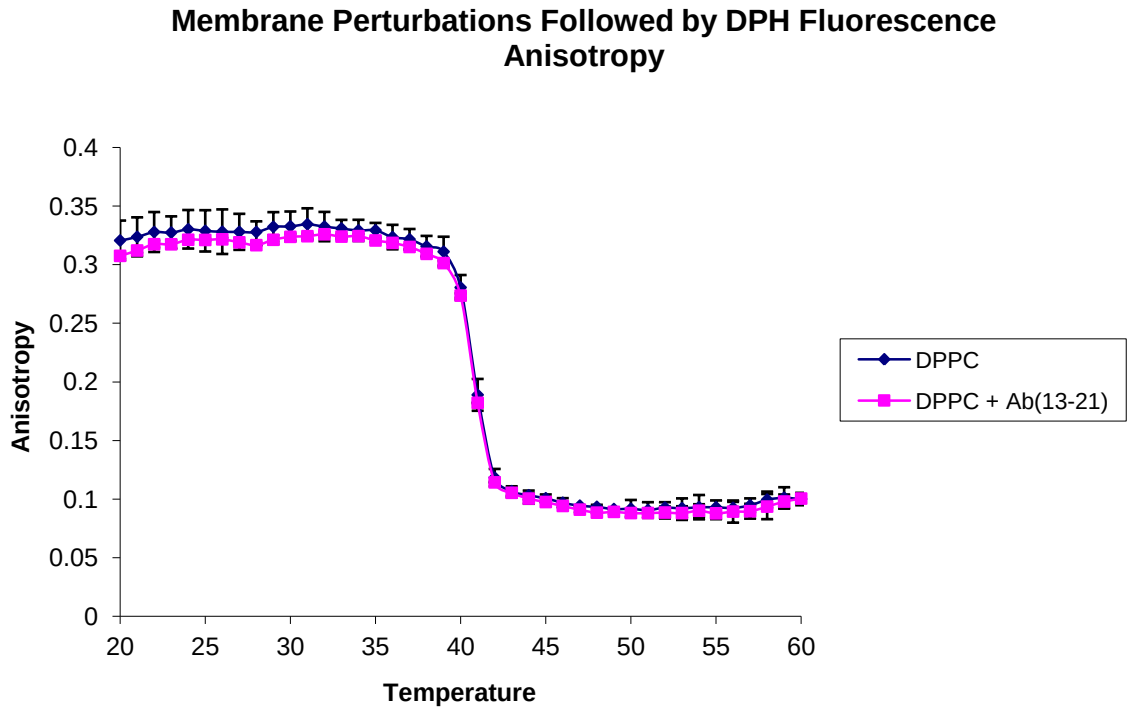

Figure 6.3 DPH Fluorescence Anisotropy in Aβ(13-21)-DPPC Mixtures. Probe:peptide:lipid = 1:55:1100.

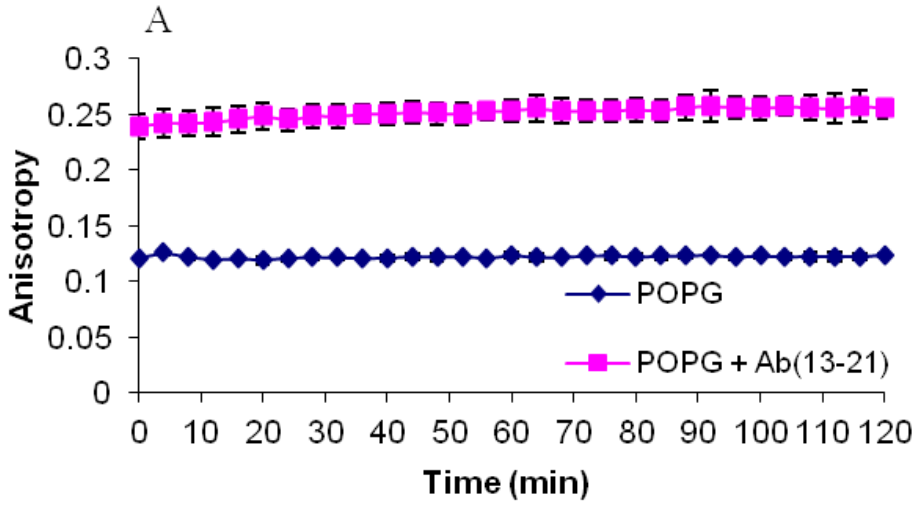
A
0.3
0.25
0.2
0.15
0.1
0.05
0
Anisotropy
POPG
POPG + Ab(13-21)
0 10 20 30 40 50 60 70 80 90 100 110 120
Time (min)

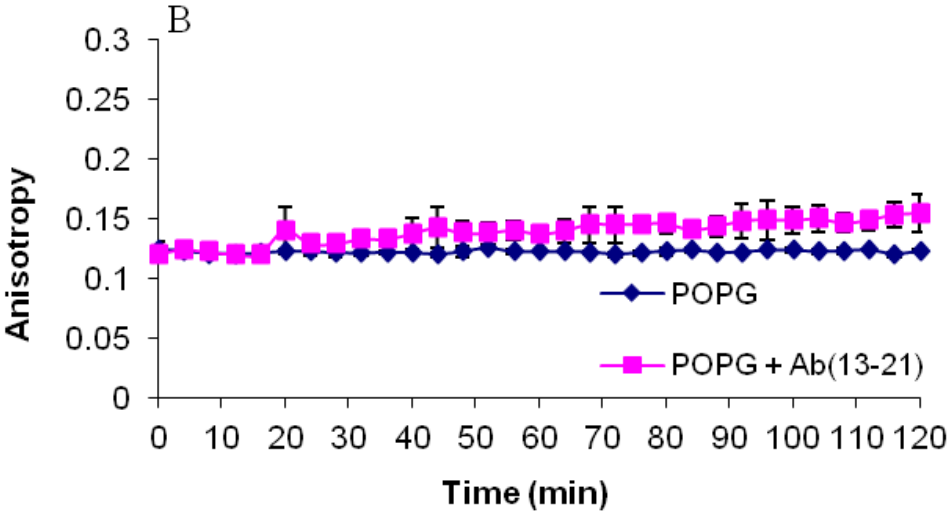
B
0.3
0.25
0.2
0.15
0.1
0.05
0
Anisotropy
POPG
POPG + Ab(13-21)
0 10 20 30 40 50 60 70 80 90 100 110 120
Time (min)

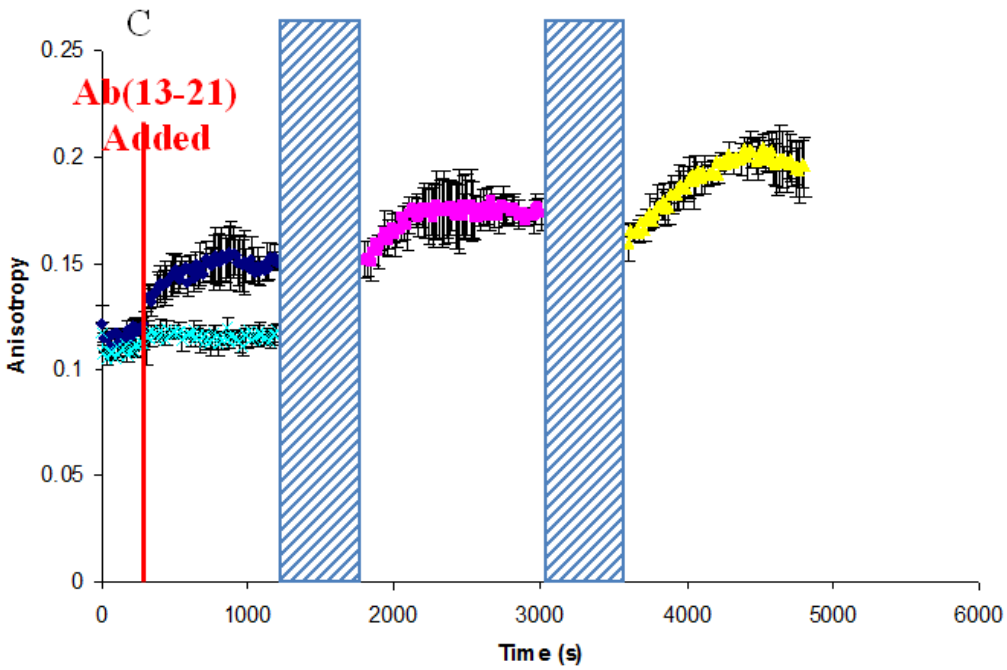

Figure 6.4 DPH Fluorescence Anisotropy in Aβ(13-21)-POPG Mixtures. A) Steady-state DPH fluorescence anisotropy, B) Time-resolved DPH fluorescence anisotropy. C) Time-resolved DPH fluorescence anisotropy.

occurring. These slower processes include membrane fusion or increased amyloid fibril formation. However, light scattering plagues fluorescence anisotropy, causing arbitrary increases or decreases in the anisotropy value, and thus making data interpretation difficult (Dorado, Llorente et al. 1994). This is a significant concern given that LUVs and fibrils scatter light.

6.2.3 Differential Scanning Calorimetry (DSC)

To overcome the scattering limitations inherent in fluorescence anisotropy measurements, differential scanning calorimetry (DSC) was employed. As in Chapter 5, calorimetry directly observes the phospholipid membrane phase transitions. This particular section will focus on thermogram interpretation with respect to the phospholipid membrane itself.

Thermograms of DLPS show multiple broad transitions. Additionally, the T_m shifts to higher temperatures as the peptide concentration is increased (5:0=15.25 ^oC, 5:0.1=15.36 ^oC, 5:0.2=15.40 ^oC, 5:0.3=15.53 ^oC, 5:0.4=15.78 ^oC, 5:0.5=16.09 ^oC), suggesting again that the membrane is becoming more rigid (Figure 6.5A). These results agree with the fluorescence anisotropy intensity increase observed for POPG and likely represent a general trend seen for amyloid-membrane interactions – membrane stiffening. Additionally, a new transition appears approximately 1 ^oC higher than the DLSP T_m in the absence of Aβ(13-21), suggesting that peptide assembly has facilitated the formation of a crystalline membrane (Lewis and McElhaney 2000). The gradual decrease and shift of the lipid only transition suggest that as the protein concentration is increased to a

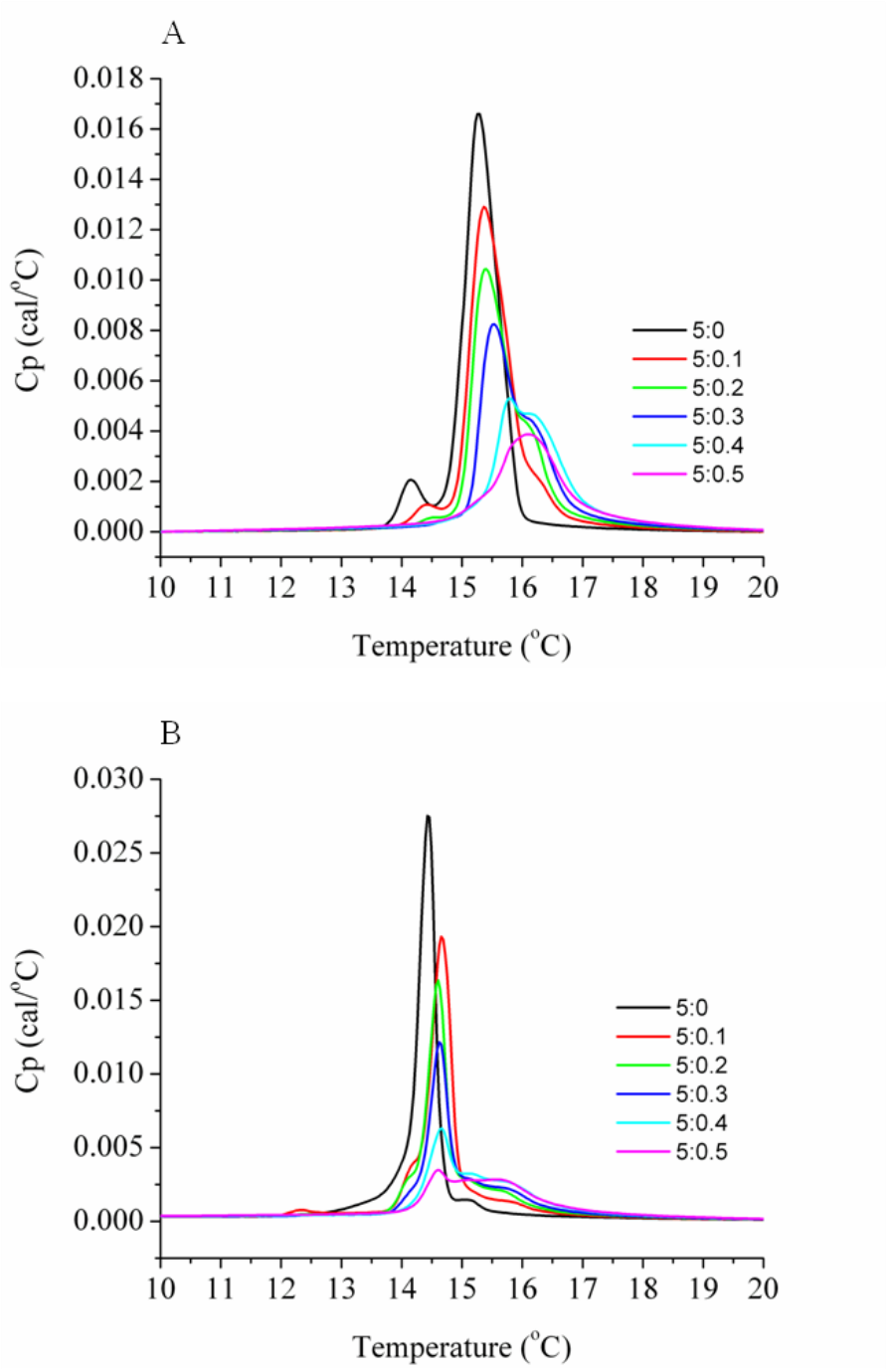

Figure 6.5 DSC thermograms of DLPS with increasing concentrations of Aβ(13-21). A) DSC heating thermograms of 5 mM DLPS in the presence of various concentrations of Aβ(13-21),B) DSC cooling thermograms of 5 mM DLPS in the presence of various concentrations of Aβ(13-21).

greater degree and the DLPS molecules are being affected, although they are not associated directly with the peptide β-sheet. It is known that lipids melt simultaneously in clusters of *n* lipids, therefore the force exerted on the membrane by the amyloid assembly is affecting nearby lipids (Heimburg 2007).

At a peptide:lipid ratio of 1:10, the thermal transition is broadened considerably with only one distinguishable maximum. It is unclear whether the lipid only transition has shifted to higher temperatures and is now overlapping with the amyloid-lipid transition or whether the lipid only transition has completely disappeared. Nevertheless, the changes observed for DLPS as the peptide concentration is increased resemble the trend observed for Ca^{2+} in the presence of DMPS (Silvius and Gagne 1984). This result suggests that the amyloid species in solution can mimic the role of Ca^{2+}, a metal ion which regulates multiple intracellular events including neurotransmitter exocytosis (Quetglas, Iborra et al. 2002). These similarities possibly explain amyloid-induced neuronal hyperexcitability (Minkeviciene, Rheims et al. 2009).

The downscan of each respective peptide-lipid combination contains multiple transitions (Figure 6.5B). These multiple peaks suggest that the DLPS membrane is undergoing a shape change when transiting from the gel to fluid phase (Ebel, Grabitz et al. 2001). The multiple transitions observed there could be a direct result of the two faces of the amyloid structure interacting with the membrane surface differently, as discussed in the previous chapter, or due to several other factors because these multiple transitions are strikingly similar to those observed for DMPG in the same buffer conditions (Figure 6.6). This particular DMPG thermal analysis has been investigated by several groups with

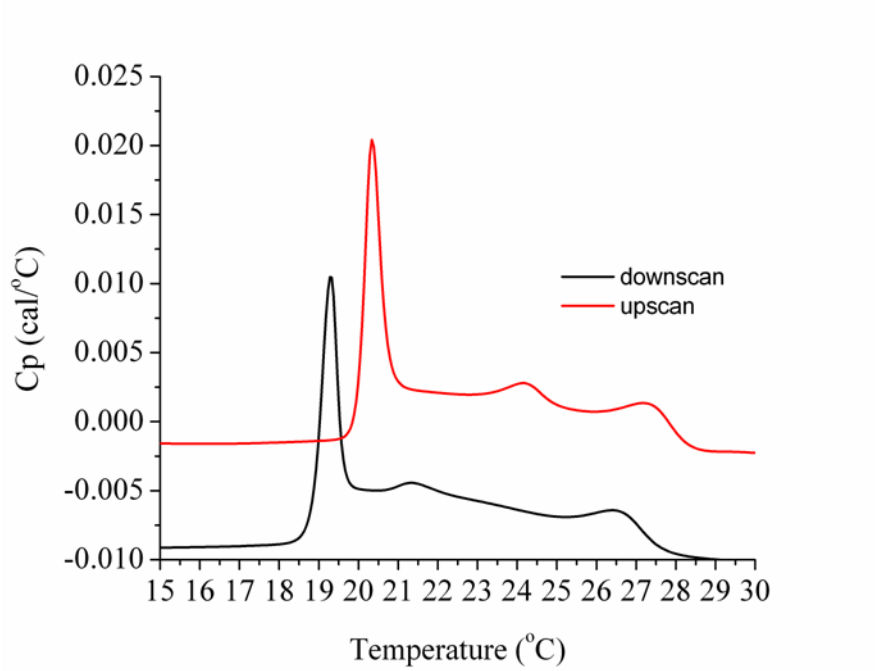

Figure 6.6 Heating and cooling DSC thermograms of DMPG.

each group presenting different experimental evidence to rationalize the cause of the three observed transitions seen in the DMPG melting regime.

Changes in membrane curvature during this thermal transition could also be responsible for these multiple transitions (Schneider, Marsh et al. 1999). TEM images find the DMPG LUVs to be spherical vesicles below and above this broad thermal transition, however imaging analysis of the sample at a temperature in the thermal transition show membrane sheets. TEM images, prepared when the sample is at room temperature, and above the DLPS transition temperature, contain an extended membrane network of fused membrane vesicle that do not appear in the DLPS only images.

This thermally induced membrane change was found to reflect the formation of membrane pores that are large enough to leak vesicle contents (Spinozzi, Paccamiccio et al. 2010). Such pores provide a plausible explanation because amyloid structures have consistently been shown to have membrane leakage capability, and most membrane leakage has been attributed to the formation of membrane pores. No membrane pores are however observed in TEM images, but pores smaller than the resolution of the TEM may be present.

Furthermore, Barroso *et al.* revisited the DMPG thermogram and provided evidence that the actual change observed in the DSC is a direct result of a change in the membrane charge from a different amount of salt present at the membrane-water interface (Barroso, Riske et al. 2010). Because the amyloid β-sheet contains positive charges from the *N*-terminus and the lysine-16 residue, this explanation may be more consistent with the

changes seen in these DSC thermograms. Again, this data best supports the positioning of the peptide at the membrane-water interface.

As Aβ(13-21)F19Fcn-DLPS sample are thermal cycled through the respective phase transitions, the temperature profile changes with time. In DLPS, the lower temperature transitions decrease while the higher temperature transitions increase. By integrating the thermal transition for the peptide:lipid ratio of 1:25, it is apparent that this slow process takes approximately 24 hr to occur when the temperature block is 5 ^{o}C to 25 ^{o}C (Figure 6.7). This equilibrium process appears to be a thermodynamically controlled event and suggests a slow process is occurring.

Similar trends are observed for DMPS as with DLSP. As the peptide concentration is increased, the transitions at the back of the thermogram grow while the transitions at the front shrink (Figure 6.8-6.10). However, the system contains many more transitions suggesting that several different changes are occurring in the system. CD spectra of the system using the same thermal cycling parameters as used in the DSC experiments definitely show that the peptide secondary structure is changing (Figure 6.8C). DSC upscans and downscan both show T_m shifts towards higher temperatures and multiple transitions over the melting profile. There are higher temperature transitions that increase and lower temperature ones that decrease for DMPS. However, the DSC thermal cycling is complicated by many different changes that make interpretation difficult, and these differences can be attributed to the change in either peptide secondary structure or to additional DMPS membrane changes.

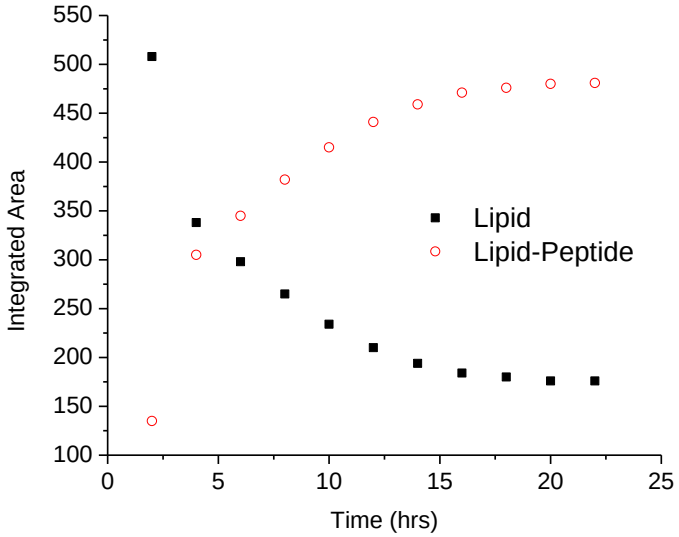

Figure 6.7 Thermal Cycling Analysis Suggests the Occurrence of a Slow Transition. Integrated areas for the 5 mM DLPS + 0.2 mM Ab(13-21)F19Fcn closed (black square – lipid only transition; open red circles – lipid-peptide transitions).

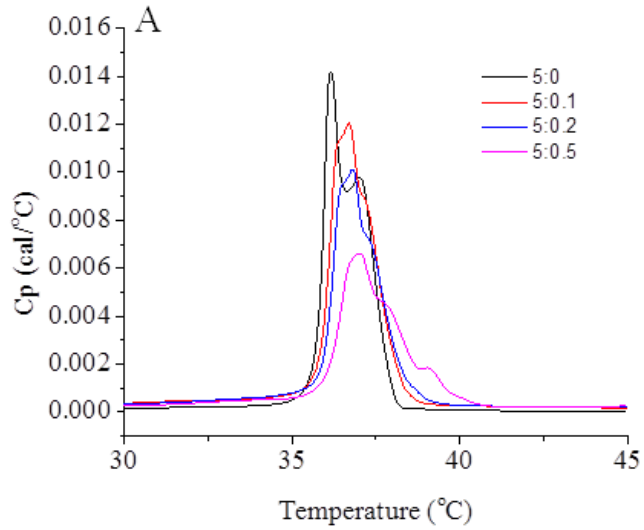
A
0.016
0.014
0.012
0.010
0.008
0.006
0.004
0.002
0.000
Cp (cal/°C)
30
35
40
45
Temperature (°C)
5:0
5:0.1
5:0.2
5:0.5

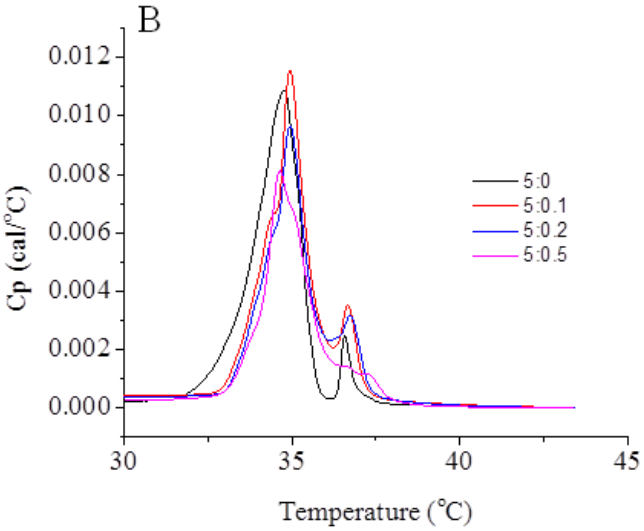
B
0.012
0.010
0.008
0.006
0.004
0.002
0.000
Cp (cal/°C)
30
35
40
45
Temperature (°C)
5:0
5:0.1
5:0.2
5:0.5

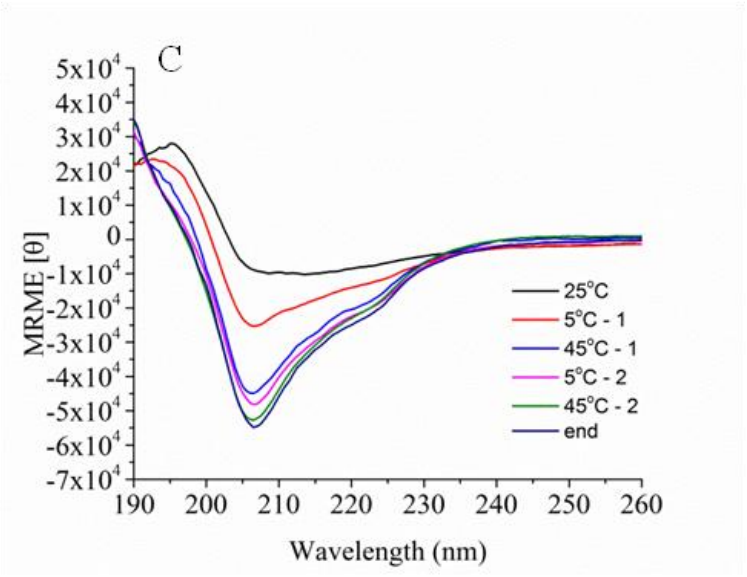

Figure 6.8 Investigating Aβ(13-21)-DMPS mixtures using DSC and thermal cycling CD. A) DSC heating thermograms of 5 mM DMPS in the presence of various concentrations of Aβ(13-21), B) DSC cooling thermograms of 5 mM DMPS in the presence of various concentrations of Aβ(13-21), C) Collective CD spectra of Aβ(13-21)-DMPS while cycling the sample using the same parameters as in the DSC.

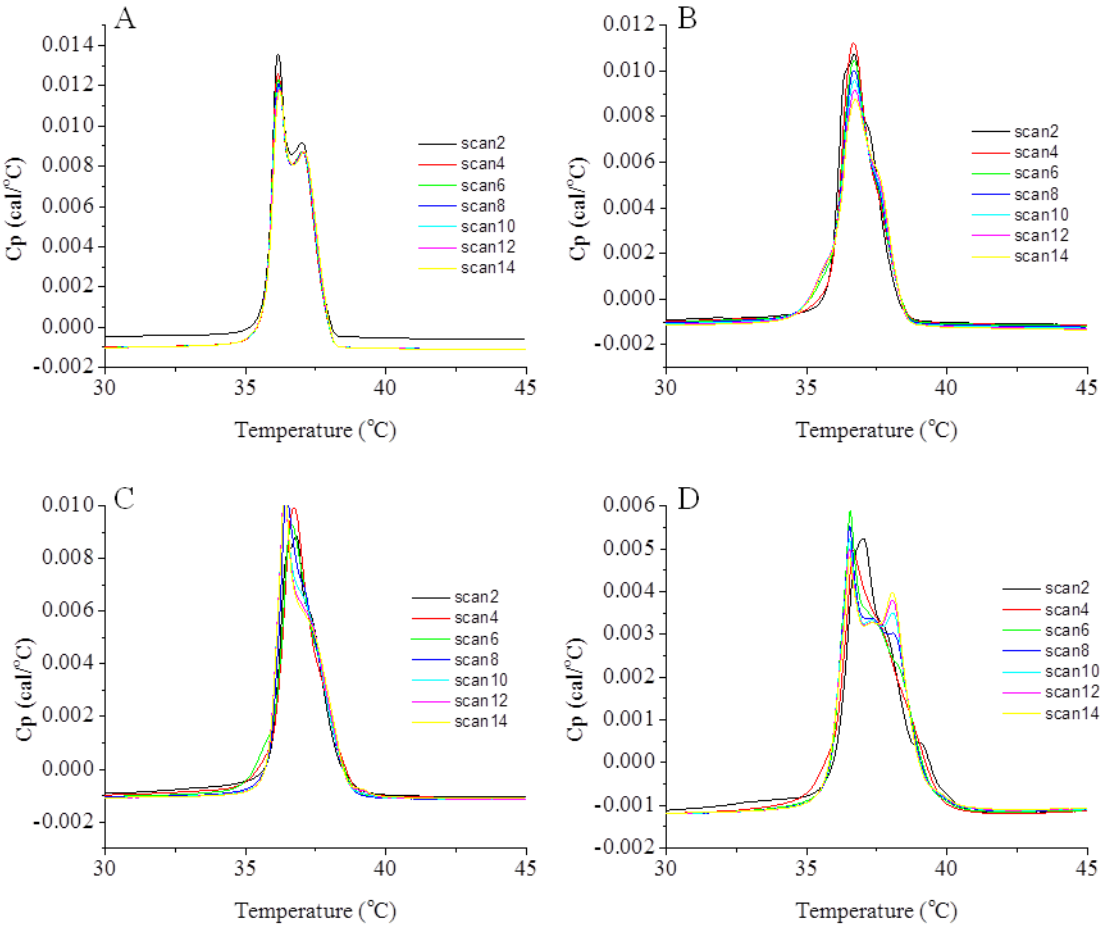

Figure 6.9 DSC Heating Scans of Aβ(13-21)-DMPS Mixtures. A) 5:0, B) 5:0.1, C) 5:0.2, D) 5:0.5.

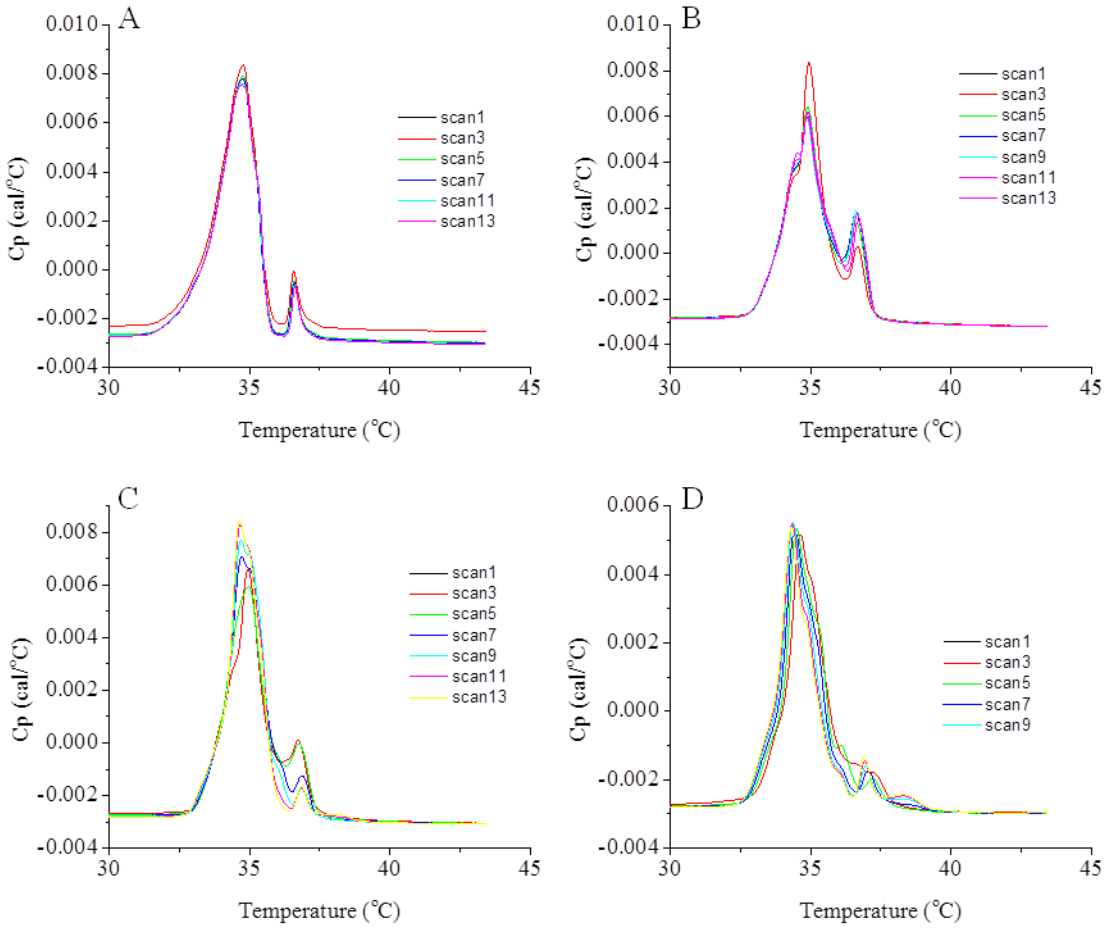

Figure 6.10 DSC Cooling Scans of Aβ(13-21)-DMPS Mixtures. A) 5:0, B) 5:0.1, C) 5:0.2, D) 5:0.5.

6.2.4 Membrane Fusion Assay

Both the fluorescence anisotropy and the DSC thermal cycle analysis suggest that a slow process, much slower than the rate of β-sheet assembly, is occurring. Membrane fusion could explain this slow thermodynamic event. Membrane fusion would be favored thermodynamically to distribute the membrane perturbations across a larger membrane surface. Another plausible explanation for membrane fusion is that the two surfaces of amyloid species interact with two membrane faces, thus bringing the two membranes in close enough proximity to promote fusion. Membrane fusion events occur constantly inside cells as it is involved in neurotransmitter release, protein sorting through the ER and Golgi, and endocytosis protein recycling through endosomes (Martens and McMahon 2008). All of these processes are disrupted in Alzheimer's disease and likely could contribute to cellular toxicity.

The fusion mechanism is believed to involve several steps (Chen and Scheller 2001; Martens and McMahon 2008). The first two steps in membrane fusion are tethering and docking. The two faces of the amyloid β-sheet have been shown to interact with two different membranes and can easily function in this manner for membrane fusion. The third step is fusion initiation, a step thought to involve changes in membrane curvature. Changes in membrane curvature are certainly plausible give the DSC analysis of these lipid-amyloid mixtures. Hemifusion is the fourth step of membrane fusion, a step that leads to membrane mixing without exchanging membrane contents. To complete the process of membrane fusion, the fusion pore opens and the membranes collapse into one larger membrane.

Probing membrane fusion traditionally entails the use of fluorescent probes (*i.e.*, pyrene eximer fluorescence intensity decrease) that report on the mixing of bilayer phospholipids or vesicle contents (Hoekstra, de Boer et al. 1984; Ellens, Bentz et al. 1985; Pal, Barenholz et al. 1988). A limitation of using probes to monitor membrane fusion is probe transfer in the absence of fusion (Arrastua, San Sebastian et al. 2003). Another drawback of these assays is the probe itself. The probes are normally highly conjugated ring structures, structures that are known to bind to amyloid, and such binding may be occurring with the membrane (Hoekstra, de Boer et al. 1984; Liang, Guo et al. 2008; Childers, Mehta et al. 2009). This binding could result in an artificial fusion event. The course taken here does not utilize any fluorescence probes, rather the membrane fusion assay uses two different membrane systems that when mixed will produce a drastic T_m shift in the DSC thermogram. The drawback of this assay is that it only can report on membrane phospholipid mixing confirming a hemifusion state.

Mixing DLPS and DMPS followed by the addition of Aβ(13-21) resulted in a drastic T_m shift as well as a considerable change in the appearance of the thermogram (Figure 6.11B&D), strong evidence of membrane mixing. However, when DLPS and DMPS were mixed in the absence of Aβ(13-21), the DSC profile also changes, albeit at a slower rate (Figure 6.11A&C). This result is possibly due to the presence of Ca^{2+}, a known inducer of PS membrane fusion (Silvius and Gagne 1984).The presence of Ca^{2+} was addressed in Chapter 5 by a Fura-2 absorbance shift assay (Figure 5.15). Nevertheless, the presence of Aβ(13-21) accelerates the membrane fusion of DLPS and DMPS.

To circumvent the problem with sample preparation incurred in DLPS and DMPS mixtures, two different LUV mixtures were used. These two mixtures consisted of

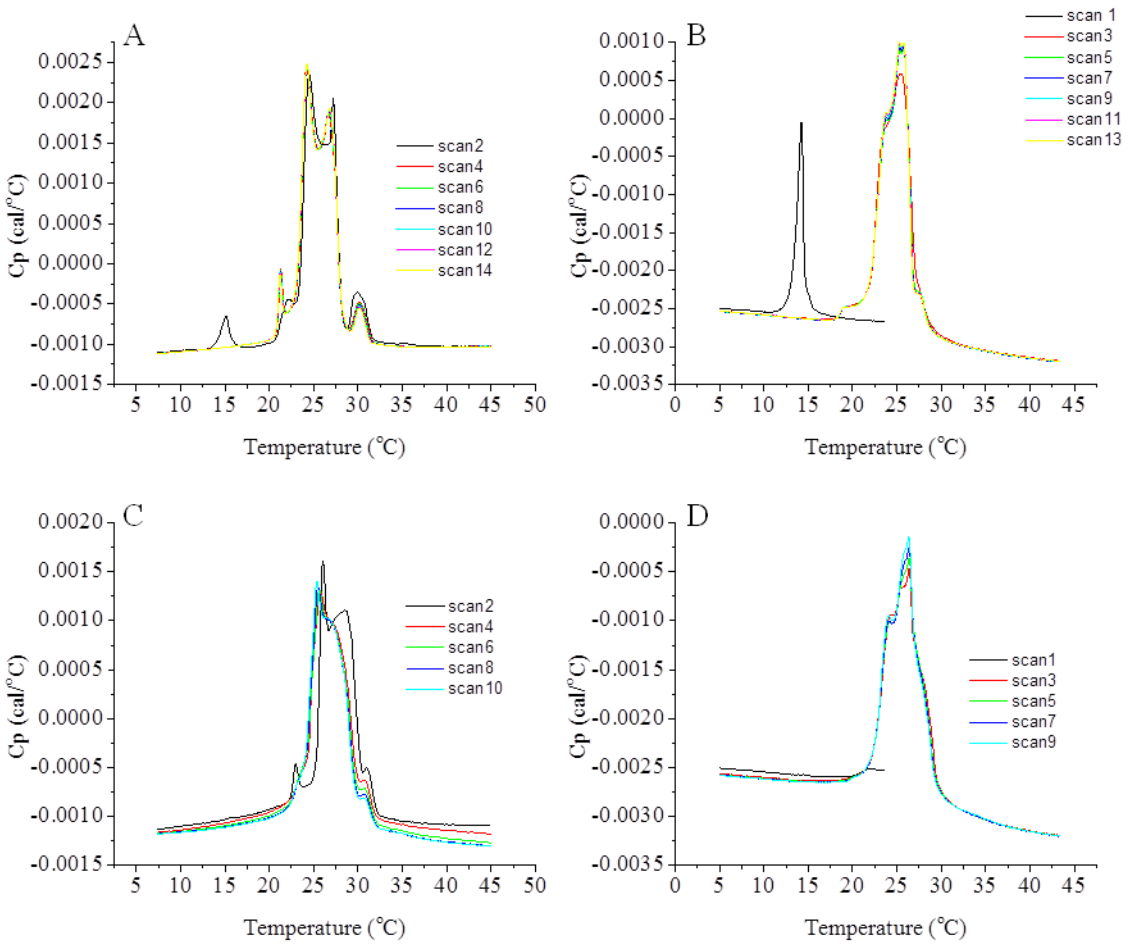

Figure 6.11 Membrane Fusion Assay. A) Compiled heating DSC thermograms of DLPS-DMPS LUVs without Aβ(13-21), B) Compiled heating DSC thermograms of DLPS-DMPS LUVs with Aβ(13-21), C) Compiled heating DSC thermograms of DLPS-DMPS LUVs without Aβ(13-21), D) Compiled cooling DSC thermograms of DLPS-DMPS LUVs with Aβ(13-21).

DOPC:DOPE:cardiolipin (DDC), at a ratio of 3:2:1, added to either DLPS or DMPS. In comparing DLPS LUVs with DDC LUVs in the presence and absence of Aβ(13-21), it is obvious that lipid mixing has occurred from the disappearance of the DLPS phase transition (Figure 6.12). This stems from the DOPC and DOPE phospholipids abolishing the DLPS transition upon lipid mixing. The transition disappears, more probably broadens, because DOPC and DOPE contain branched lipid tails that significantly reduce the membrane transition temperature due to disrupting DLPS lipid packing thereby eliminating the cooperative chain melting event that produces the thermal transitions of DLPS. When DLPS and DDC LUVs are mixed in the absence of Aβ(13-21), the DLPS transition is still present but shifts slightly.

Using a similar approach with DMPS, the phase transition is broadened but not at the same rate as is the case for DLPS (Figure 6.13). This possibly arises from two different sample preparations with varying time differences before the initialization of thermal scanning. However, this difference can also stem from sample preparation itself. Aβ(13-21) was added to the LUV combinations at room temperature. Therefore, DLPS is in the fluid phase while DMPS is in the gel phase. Since Aβ(13-21) in the presence of gel phase DMPS produces a β-sheet CD signature that changes to a non-classical signature over time, then Aβ(13-21) may exist in two different locations or possibly two different structures. If there are two different locations of Aβ(13-21), then membrane fusion can be promoted by one or the other. Given that the lipid combination using DLPS results in immediate disappearance of the transition and complete disappearance is seen after the downscan for DMPS, the fluid phase amyloid-membrane association likely promote

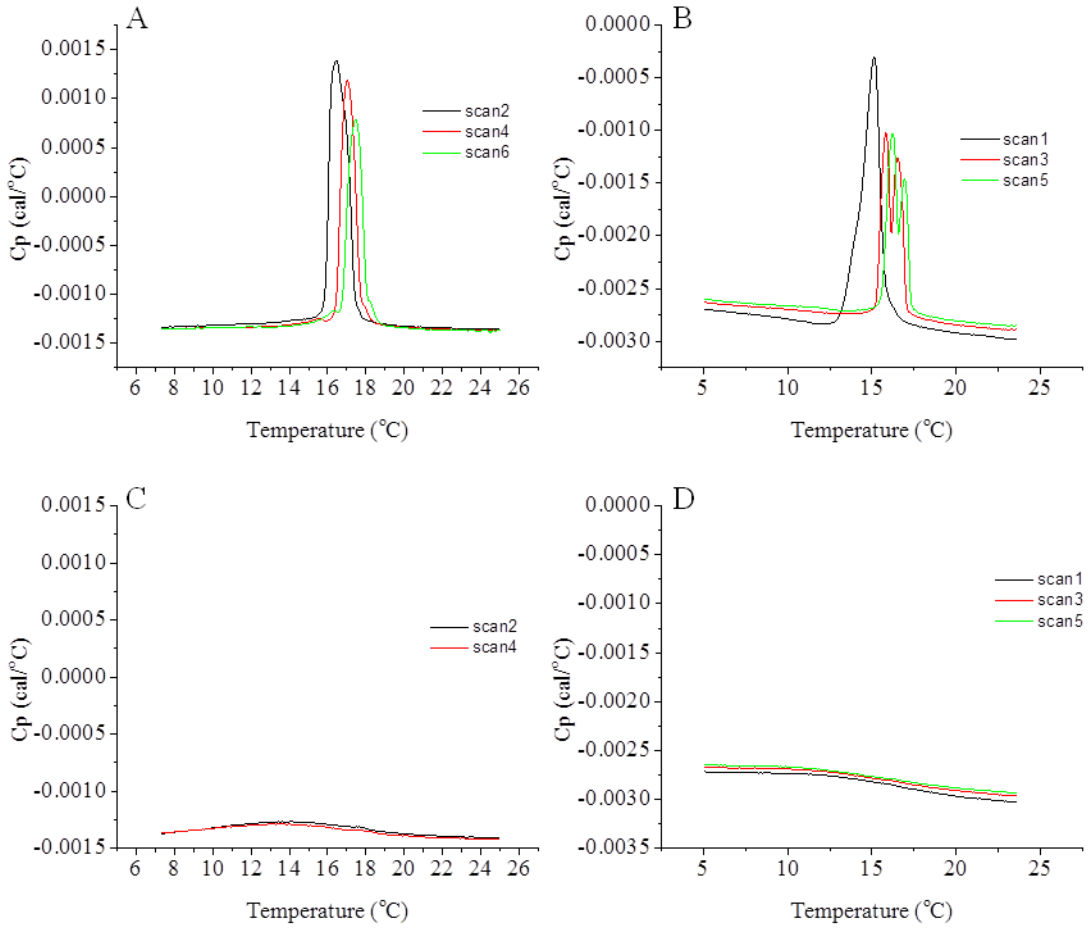

Figure 6.12 Membrane Fusion Assay. A) Compiled heating DSC thermograms of DLPS-DOPC:DOPE:cardiolipin LUVs without Aβ(13-21), B) Compiled heating DSC thermograms of DLPS-DOPC:DOPE:cardiolipin LUVs with Aβ(13-21), C) Compiled heating DSC thermograms of DLPS-DOPC:DOPE:cardiolipin LUVs without Aβ(13-21), D) Compiled cooling DSC thermograms of DLPS-DOPC:DOPE:cardiolipin LUVs with Aβ(13-21).

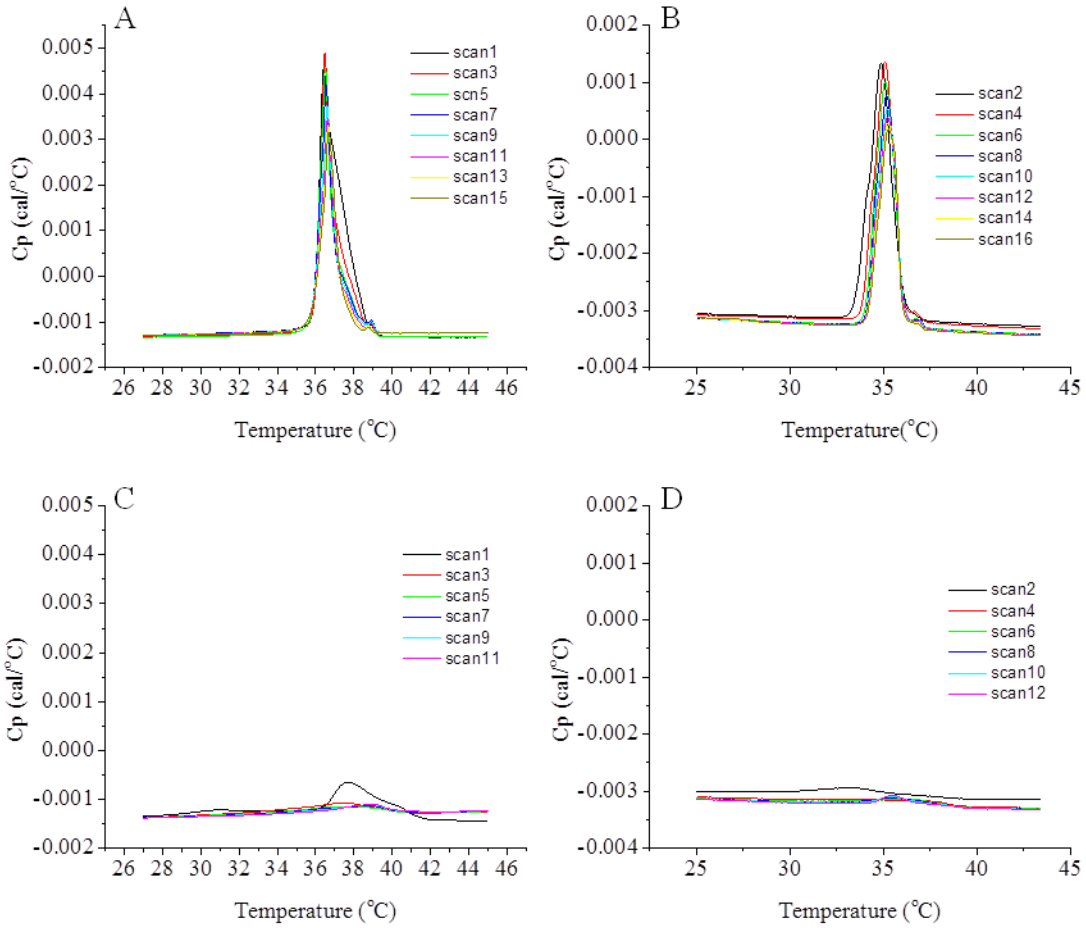

Figure 6.13 Membrane Fusion Assay. A) Overlay of downscan DSC thermograms of DMPS-DOPC:DOPE:cardiolipin LUVs with and witout Aβ(13-21), B) Overlay of upscan DSC thermograms of DMPS-DOPC:DOPE:cardiolipin LUVs with and witout Aβ(13-21).

membrane fusion while the non-classical association does not. Yet, another plausible explanation is that membrane fusion is best when membranes are in the fluid phase.

Membrane fusion has several proposed steps, and these DSC experiments provide insight to this mechanism with respect to amyloid-membrane interactions. It can clearly be stated that phospholipid membrane mixing does occur, but is only defined through the hemifusion state by DSC. To determine the step at which membrane fusion exists for the amyloid-membrane system, TEM images of these samples were acquired. The samples with and without peptide, appear the same for this phospholipid system and suggests that lipid mixing occurs without membrane fusion.

6.2.5 TEM Analysis of Aβ(13-21)-DLPS LUV Mixtures

A second difference is observed when contrasting the membrane only and peptide-membrane samples at any given time point. Although the Aβ(13-21)-DLPS mixtures contain similar structures as seen in the DLPS LUVs images, the appearance of a new structure – an extended phospholipid network – is often seen (Figure 6.14B-D). This structure resembles those for DMPG (Heimburg and Biltonen 1994; Schneider, Marsh et al. 1999). Strikingly, the DSC thermograms for these two samples appear similar, with the exception that the transitions occur at different temperatures, but this appears to be a direct result of the two different phospholipid membrane phase transitions. These images clearly reveal differences but are lacking the resolution to define any changes in the peptide-membrane association at early time points.

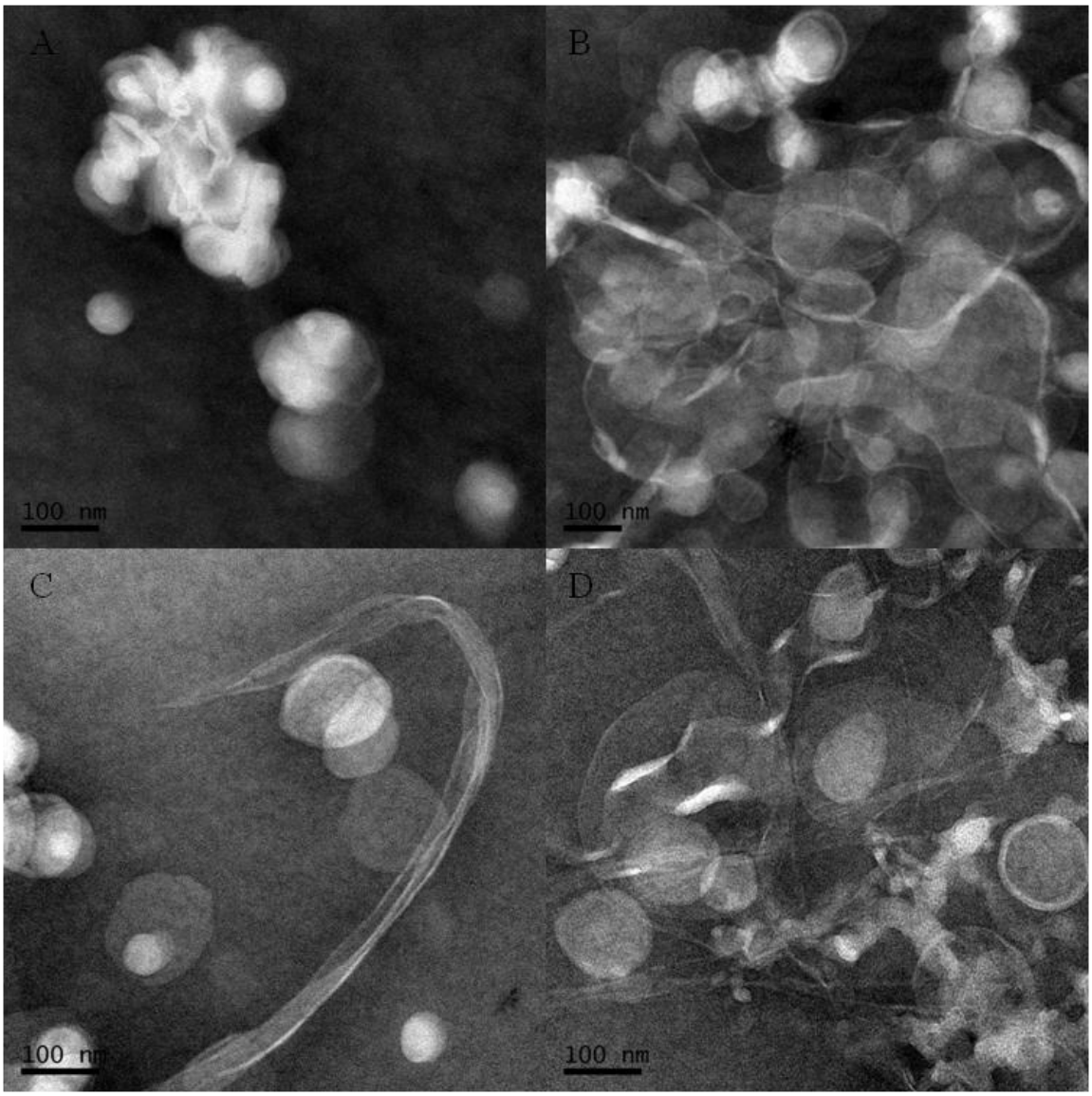

Figure 6.14 TEM images of 0.5 mM Aβ(13-21) added to 5 mM DLPS at various time points. A) no peptide, B) 0 hr, C) 3 hr, D) 24 hr.

T EM images contain phospholipid vesicles, sheets, and ribbons in the LUV only images in a greater number than in the DLPS scenario (Figure 6.15A-B). These are most likely due to a small amount of Ca^{2+} in the aqueous solution used for sample preparation as denoted by a Fura-2 UV shift in the previous chapter.TEM images show one difference between the LUV only sample and the LUV-peptide sample (Figure 6.15C-D); amyloid fibrils are associated with the membrane at 0 hr. After 24 hr, highly twisted assemblies are apparent in the images of the lipid-peptide mixtures (Figure 6.15E-F). Since these species are not observed in the LUV only images, it must be concluded that these structures are amyloid. It is extremely difficult to determine the differences in the phospholipid membrane structures that may or may not form, however the appearance of an extended phospholipid network is not observed. This absence may be attributed to the DMPS membrane forming different structures other than the extended phospholipid networks induced in DLPS in the presence of the peptide.

6.2.6 Toxicity Assay – MEF2

Continued debate exists over the toxic species in amyloid diseases. The possible species that exist in solution are: 1) monomer peptide, 2) oligomeric species, and 3) fibrils. Given that amyloid peptides can form a range of structures *in vitro*, there exists the possibility that other species may also exist (Dong, Canfield et al. 2007). Other biological molecules, metals, phospholipids, carbohydrates, *etc.*, are present, and the exact role in which Aβ exerts toxic effects remains unknown (Friedman, Pellarin et al. 2009). Our lab has created several structures *in vitro* and with the continued discussion

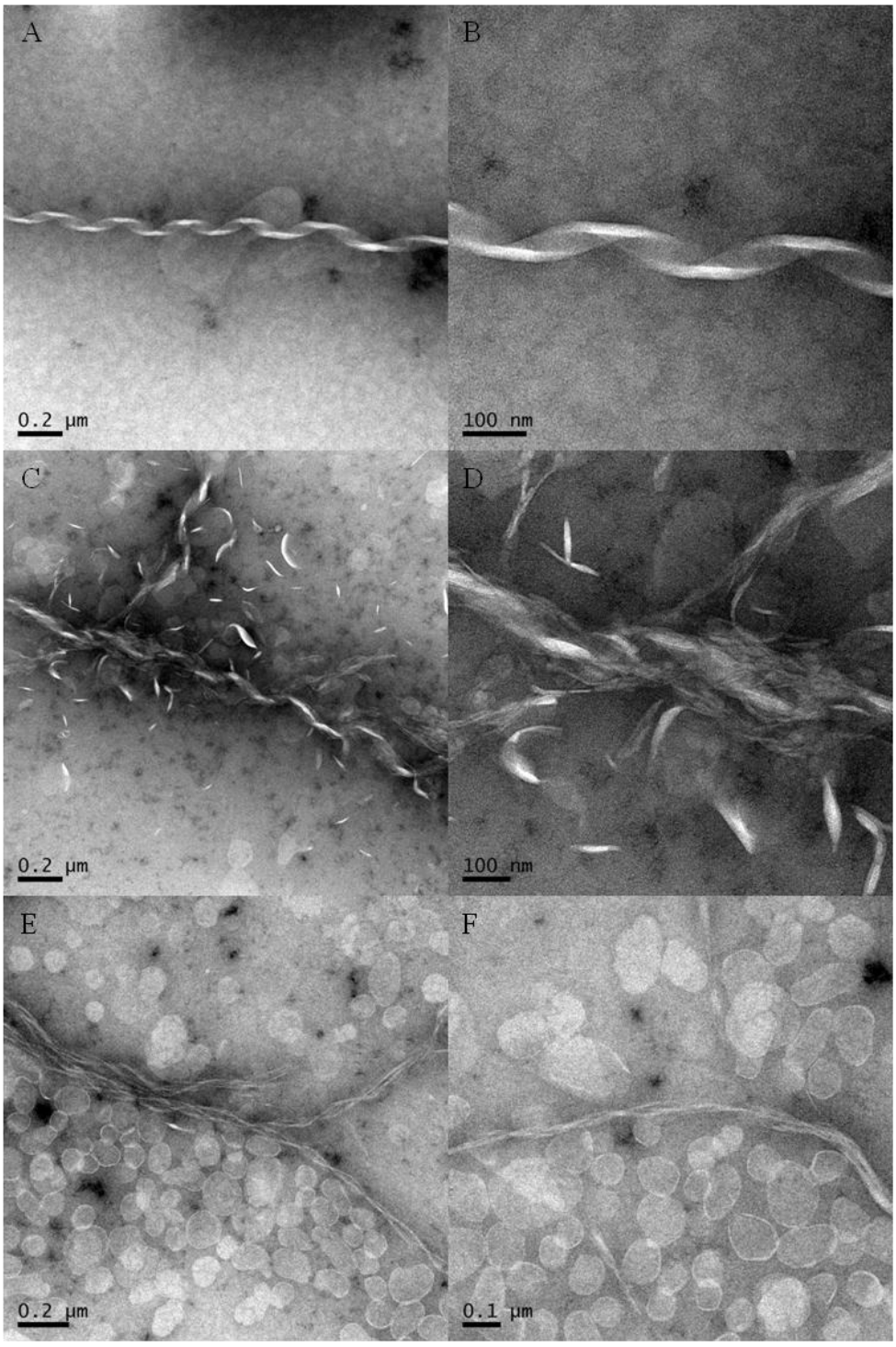

Figure 6.15 TEM of Aβ(13-21)-DMPS. A) 5 mM DMPS – 0 hr, B) 5 mM DMPS – 0 hr, C) 0.5 mM Ab(13-21) + 5 mM DMPS – 0 hr, D) 0.5 mM Ab(13-21) + 5 mM DMPS – 0 hr, E) 0.5 mM Ab(13-21) + 5 mM DMPS – 24 hr, F) 0.5 mM Ab(13-21) + 5 mM DMPS.

over the toxic species, we tested our amyloid assemblies in a myocyte enhancer factor 2 (MEF2) toxicity assay.

This assay follows the expression of MEF2. MEF2 is a transcription factor that is involved in neuronal cell survival (Mao, Bonni et al. 1999). Expression of this transcription factor initiates the cellular machinery for apoptosis (Gong, Tang et al. 2003; Tang, Wang et al. 2005). This particular assay was performed using a dopaminergic neuron cell line from the mouse midbrain (SN4741).

As a control, Aβ(1-42) was screen for toxicity at several different concentrations. It can be seen that toxicity of this peptide is concentration dependent (Figure 6.16). To control for the heterogeneity that exists with the full-length peptide, we screened our amyloid peptide truncations for toxicity. Aβ(10-35), which forms parallel in-register fibrils, is toxic as reported by MEF2 expression (Figure 6.16). This data suggests that amyloid truncations can recapitulate the toxic effects of the full-length peptide, opening the comparison of several different peptides.

Our peptide systems allow us to probe individual structures and begin to separate different structural aspects responsible for amyloid toxicity. These structural differences include peptide monomers, fibrils in the absences of metals, fibrils with zinc or copper, and amyloid nanotubes. The peptide monomer Aβ(13-21)K16A + Cu^{2+} was not toxic nor were any of the fibril truncations assembled in the absence of metal or in the presence of zinc (Aβ(13-21)K16A or Ac-Aβ(13-21)H14A) (Figure 6.16).

Ac-Aβ(13-21)H14A assembled in the presence of copper produced a toxic response (Figure 6.16). The response is not due to the fibril structure because similar fibrils formed

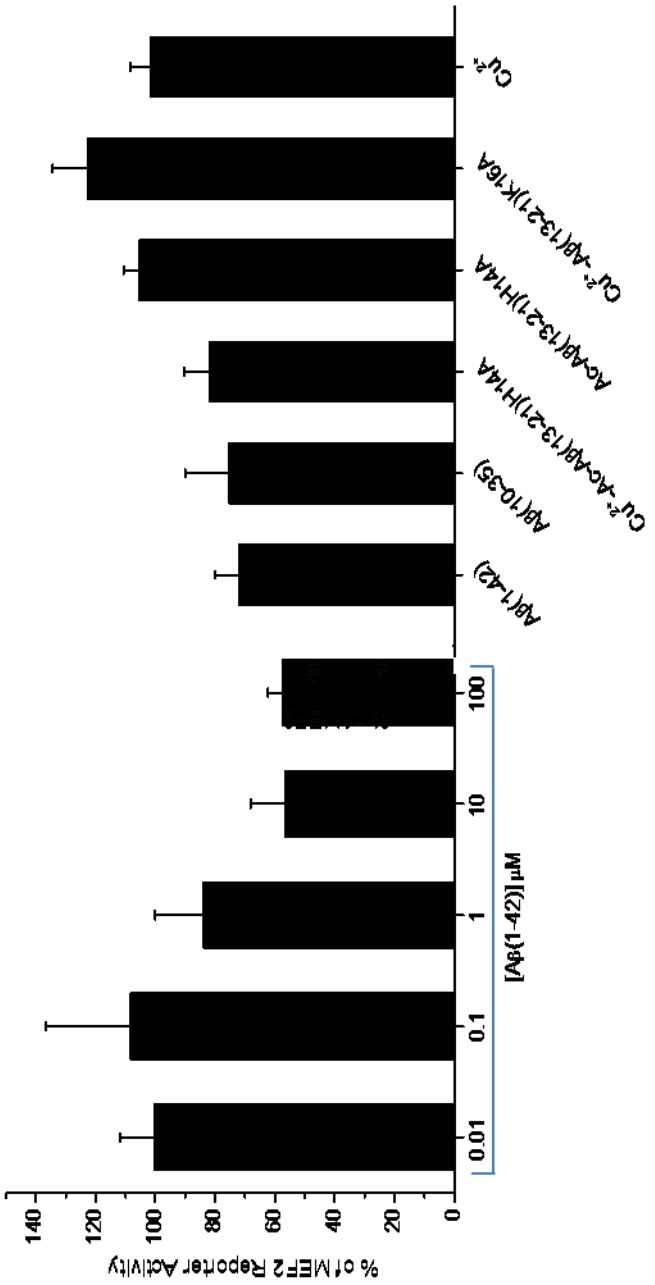

Figure 6.16 MEF2 Toxicity Assay. Dose dependent Ab(1-42) toxicity and comparison of amyloid truncations toxicity screening.

from this same peptide are not toxic in the absence of copper or presence of zinc. This response is also not due to copper alone as it is not toxic (Figure 6.16). Building upon previous catalytic data with Ac-Aβ(13-21)H14A + Cu^{2+}, which is capable of oxidizing 4-*tert*-butylcatechol (unpublished results), it was hypothesized that the toxic results stem from the redox potential of this copper-fibril complex affecting the membrane. Indeed, reactive oxygen species is a proposed method of amyloid induced toxicity observed in Alzheimer's disease because of the observed increase in neuronal oxidative damage and increased lipid oxidation has been correlated with several aspects of amyloid assembly and toxicity (Ellis, Fang et al. 2010). The toxicity studies in this section present the unique opportunity to probe amyloid catalyzed lipid oxidation because the copper-fibril structure possess the ability to perform redox chemistry as already observed with 4-*tert*-butylcatechol.

6.3 Conclusions

The membrane structure was first presented by Robertson in 1959 (Robertson 1959). Later, Singer and Nicolson proposed the "fluid mosaic" model stating that the membrane is composed of fluid phase lipids and freely diffusible integral and peripheral membrane proteins (Singer and Nicolson 1972). Over the past fifty years, significant advances in our understanding of membranes have led to the discovery that the membrane plays a more influential role than once portrayed. Apoptosis, endocytosis, exocytosis, ATP synthesis, organelle encasement, and cell migration all involve the membrane and have been shown to be dependent on specific phospholipids and proteins (Tamm 2005).

Aβ has been found in lysosomes (Liu, Zhou et al. 2010), and disruption of this normally compartmentalized organelle (*i.e.*, lysosome) can lead to apoptosis. This organelle could then serve as the site for membrane induced assembly due to the exposure of Aβ to PS phospholipid headgroups. If Aβ escapes the lysosome after being endocytosed, then it could interact with several membrane organelles that contain negatively charged lipid membranes. Cellular organelles bring another layer of complexity when dealing with membranes. Many organelles are composed of different phospholipid compositions but all contain some percentage of negative charged phospholipid which plays a role in membrane protein localization via electrostatic interactions (Murray and Honig 2002). Endosomes and lysosomes are known to contain phosphatidylserine (Zachowski 1993; Vance and Steenbergen 2005; Yeung, Gilbert et al. 2008). Phosphatidylglycerol and phosphatidic acid are present in mitochondrial and ER membranes (Batenburg, Klazinga et al. 1985; Chakraborty, Vancura et al. 1999). Disruptions in all of these membranes are observed in Alzheimer's disease.

Changes in membrane thickness have been shown to affect membrane protein function (Andersen and Koeppe 2007). Membrane fluidity controls protein localization (Andersen and Koeppe 2007). The membrane does serve as a tightly controlled semi-permeable barrier and disrupting this can result in the loss of cellular contents. In addition to membrane thickness, the membrane is also known to contain different membrane phases termed lipid rafts (Korade and Kenworthy 2008). Although still highly debated, these phases are believed to be present as detergent-resistant membrane microdomains (Brown and Rose 1992). They consist primarily of sphingomyelin, cholesterol, and GPI-anchored proteins and have been shown to play a role in signal transduction and protein trafficking

(Lingwood and Simons 2010). Any mimicking of this rigid domain could potentially result in unwanted cellular changes. Amyloid induced membrane stiffening can also mimic lipid raft domain formation, thus influencing or creating rigid domains. Lastly, membrane lipids are clearly organized within cells. The lipid mixing assay reported in this study shows that amyloid structures can promote lipid mixing. This type of biochemical response could disrupt the lipid sorting of organelles, and the data reported here and in Chapter 6 offer insight on the mechanism of membrane mixing. The double face of the amyloid assembly can easily bring different membranes together resulting in membrane mixing and thus a loss of control over lipid organization.

Clearly, amyloid assemblies affect membrane thickness, fluidity, hydration, and mixing, and changes in these variables are expected to impact cellular functions. The evidence presented here aids in explaining specific membrane changes that potentially lead to amyloid induced cellular toxicity.

6.4 Methods

6.4.1 Small Angle Neutron Scattering (SANS)

Data was collected at the Intense Pulsed Neutron Source of Argonne National Laboratory on the time-of-flight small-angle diffractometer (SAD). The 64 x 64 array position sensitive gas filled 20 x 20 cm^2 area detector was fixed 1.54 m from the sample. Pulsed neutrons with wavelengths of 0.5-14 Å were collected which provides a scattering vector ($Q = 4\pi \sin(\theta)/\lambda$) ranging from 0.005-0.25 Å in one experiment, where θ = half the scattering angle and λ = neutron wavelength. Aβ(13-21) (0.5 mM) was added to 10

mM 100 nm phospholipid LUV in 100% D_2O 25 mM HEPES buffer pH=7.5 in 1 mm quartz cells and measured for greater than 4 hours. Data were corrected for background scattering.

6.4.2 Steady-State Fluorescence Anisotropy

Fluorescence anisotropy measurements were acquired on a SPEX FluoroMax-3 and analyzed using DataMAX (Horiba Jobin Yvon, Edison, NJ). Diphenylhexatriene was at a molar ratio of 1:500 with a 10 mM phospholipid concentration. The excitation wavelength was 360 nm, and the emission wavelength was 426 nm.

6.4.3 Differential Scanning Calorimetry

DSC thermal cycling was performed using a VP-DSC (Microcal, Piscataway, NJ). Samples were cycled until equilibrium was reached. All samples were scanned at rate of 30 ^{o}C/min, with a filter period of 4 sec, and with the gain set to none. Before each scan the cells were equilibrated at the start temperature for each respective scan (upscan or downscan) for 15 min. For DLPS, the cells were scanned from 5 ^{o}C to 25 ^{o}C. The temperature was cycled between 5 ^{o}C and 45 ^{o}C for DMPS. The 100 nm phospholipid LUVs were at a constant concentration of 5 mM while the peptide concentration was at the indicated molar ratio. Samples were mixed and immediately degassed for 5 min before starting the experiment. Data was collected at approximately 26 p.s.i. to prevent evaporation.

6.4.4 Transmission Electron Microscopy (TEM)

Samples were first applied to 300 mesh FCF grids (Electron Microscopy Sciences, Hatfield, PA). A 2% solution of ammonium tungstate in 25 mM HEPES pH = 7.5 was used to stain the sample. Images were taken on a H-7500 transmission microscope (Hitachi High Technologies America, Pleasanton, CA) operated at 75 kV in the Robert Apakarian Microscopy Facility at Emory University.

6.4.5 Membrane Fusion Assay

Data were collected in a similar manner as with the single phospholipid LUVs. The peptide to lipid ratios were maintained; however, the overall concentrations were 2.5 mM for any phospholipids used and 0.25 mM for Aβ(13-21). All DSC scan parameters were kept constant. For samples containing DLPS and DMPS, the temperature window was 5 ^{o}C to 45 ^{o}C. For DDC samples, the temperature window depended on the use of DLPS (5 ^{o}C to 25 ^{o}C) or DMPS (25 ^{o}C to 45 ^{o}C).

6.4.6 MEF2 Toxicity Assay

Using the Lipofectamine 2000 transfection system (Invitrogen, Carlsbad, CA) to transfect a DNA construct with a gene encoding luciferase behind the MEF2 enhancer, SN4741 cells were screened for toxicity. Aβ peptides were added to these cells 24 hours

after transfection. Cells were lysed 24 hours later, and luciferase activity was analyzed using a luciferase reporter gene assay kit (Roche, Mannheim, Germany).

Chapter 7

Conclusions and Future Directions

Amyloid assembly has been investigated for over forty years and yet the molecular mechanism responsible for amyloid assembly remains elusive. From template assembly, monomer-directed conversion, nucleated polymerization, nucleated conformational conversion, and off-pathway micelle model, all of these mechanisms share similarities but none of them present a molecular level presentation of assembly. Certainly one limitation is the inability to control amyloid assembly initiation, and the data presented in this work provides an unprecedented ability to control amyloid assembly by manipulating a handful of experimental variables.

Aβ(13-21), a simple Aβ truncation, displays specific concentration dependent assembly characteristics that can be exploited thermodynamically and kinetically. In order to decipher the assembly mechanism, conditions were found where Aβ(13-21) remained in solution as a monomer. By comparing the CD spectral data with the work from the Kallenbach lab (Rucker and Creamer 2002; Shi, Chen et al. 2006; Shi, Chen et al. 2006), it was found that Aβ(13-21) exists dominantly as a polyproline II helix (P_{II}) in solution, consistent with other similar peptides (Eker, Griebenow et al. 2004).

The most recent assembly mechanisms require intermediate spherical particles and indeed no spherical particles can be detected under these conditions (Ahmed, Davis et al. 2010). These data then suggest that these particles are on-pathway, but it does not absolutely exclude an off-pathway contribution. The simplest model to understand the formation of these particles is a burial of hydrophobic side-chain residues through collapse. Indeed, *C*-terminal hydrophobicity increases amyloid assembly in A21V, A21L, and A21I of Aβ(13-21). The simplest model is, like the molten globule in protein folding (Liang, Lynn et al. 2010). The intermolecular particle reduces the water content to

facilitate secondary structure assembly, but one cannot rule out the possibility of creating microenvironments uniquely able to nucleate amyloid assembly.

Further structural insight emerged from attempts to minimize the effect β-branching. *C*-terminal substitutions that increased hydrophobicity without β-branching (Aβ(13-21)A21Abu, Aβ(13-21)A21Nva, Aβ(13-21)A21Nle) increased assembly. Indeed, Aβ(13-21)A21Abu clearly assembles at known concentrations and spherical aggregates appear at the lower concentrations. Such hydrophobic collapse is most well known in the context of lipid amphiphiles.

Significant literature now suggests that amyloid forming peptides possess lipid like properties. Considering the similarities with lipids and phospholipid membranes, I attempted to investigate the effects phospholipid membranes have on Aβ(13-21) assembly. Membrane charge and fluidity are shown to have dramatic effects on the secondary structure of Aβ(13-21). Surface charge affected the rate of amyloid assembly either by changing the number of bound Aβ(13-21) peptides or by changing peptide orientation on the surface. A more important finding is the effect membrane fluidity has on the secondary structure of Aβ(13-21). All the negatively charged membranes tested accelerated β-sheet assembly, and both interfacial and insertional membrane associations seem possible (Murphy 2007).

An interfacial association is strongly supported for the Aβ(13-21) peptide which initiates amyloid assembly by providing a microenvironment conducive for the formation of an extended β-strand conformation. Further dynamic interactions between peptide monomers and oligomers/membranes result in fibril propagation. The β-strands located at the oligomer/membrane-water interface can hydrogen bond with other β-strands at this

same location to form β-sheets by the fusion of additional oligomers/vesicles to the end of the fibril. This results in β-sheet growth in the hydrogen bonding dimension. The β-strands and/or β-sheets located at the interface of the oligomers/membrane can also associate with other β-sheets on different oligomers/vesicles for growth in the lamination dimension. Higher order fibril associations (fibril dimers, fibril trimers, etc.) stem from collisions of oligomers/vesicles containing β-strands and/or β-sheets that result in peptide termini associations. These dynamic interactions will be transient. They also do not bias the peptide towards a specific β-strand orientation or registry within the fibril not does it control the number of laminated β-sheets, but rather lets kinetics and thermodynamics to control amyloid assembly (Figure 7.1).

Future directions of this project are limitless. Still unanswered questions exist with respect to this proposed structure-based assembly mechanism. Can it be used to explain all amyloid assemblies? Do different spherical aggregates truly exist in solution? If so, then why do the different aggregates give rise to different initiation structures that result in different amyloid fibril structures? How do you shift the experimental variables to select for different thermodynamic spherical aggregates? Can manipulating β-sheet growth, lamination propensity, and other peptide surface associations give rise to new amyloid structures that offer insight into this mechanism?

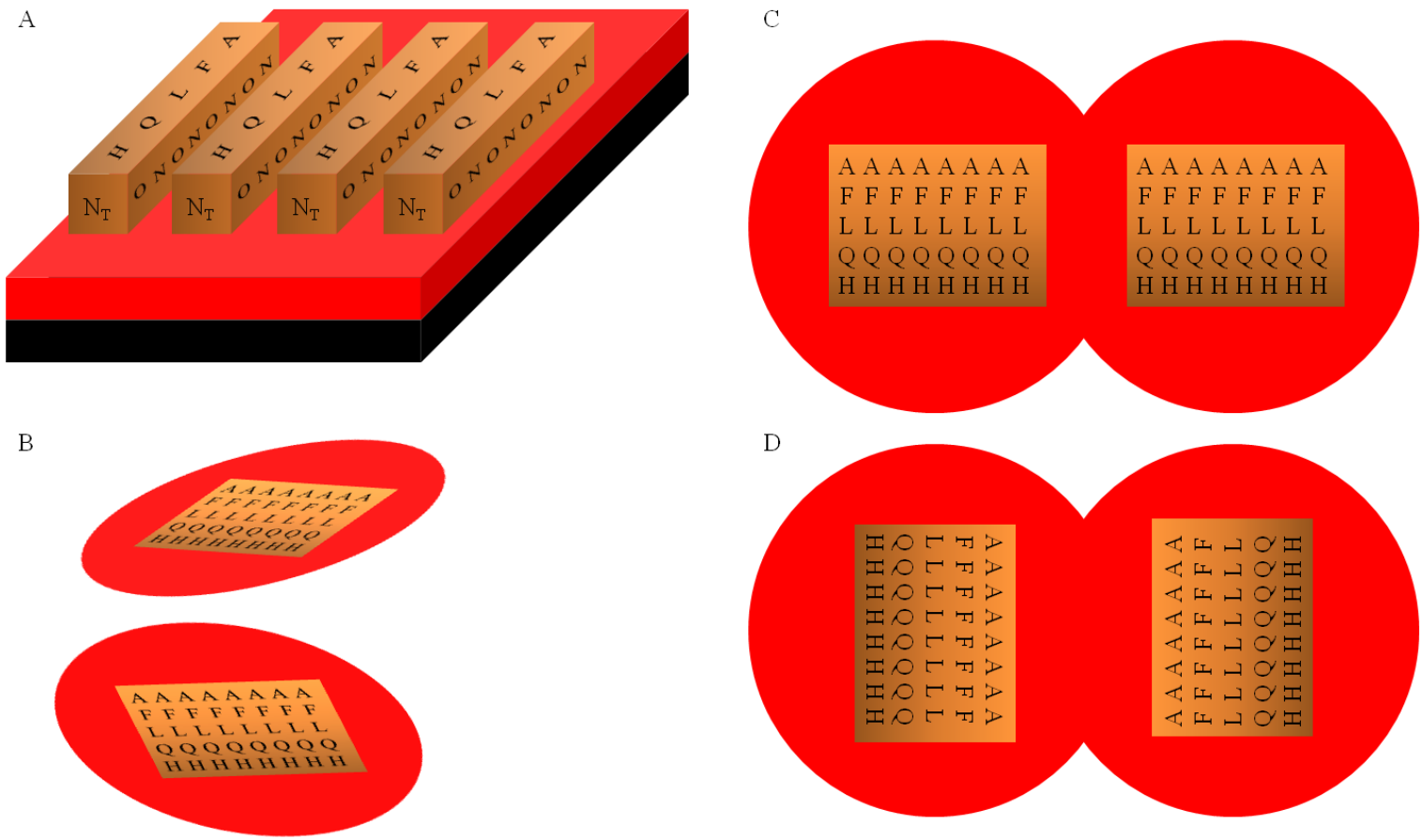

Figure 7.1 Proposed Amyloid Assembly Pathway Propagation. A) β-strand association to form β-sheets on oligomer surface which is initiated by conformational exchange, B) Oligomer fusion that orients the β-sheets that allows for the propagation of the β-sheet, C) Oligomer fusion that propagates fibril growth in the lamination dimension, D) Oligomer fusion that results in the N- and/or C-terminal association that results in fibril dimers.

Appendix A

Lipid Structures, Chemical Names, and Abbreviations

DHPC

06:0 PC (DHPC)

1,2-dihexanoyl-*sn*-glycero-3-phosphocholine

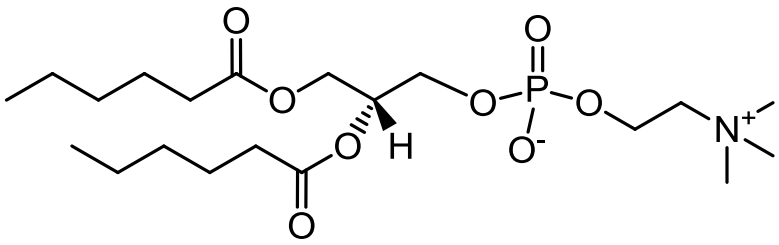

DCPC

10:0 PC

1,2-didecanoyl-*sn*-glycero-3-phosphocholine

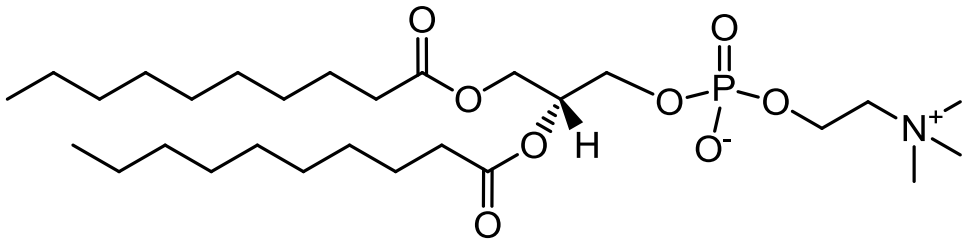

DLPC

12:0 PC

1,2-dilauroyl-*sn*-glycero-3-phosphocholine

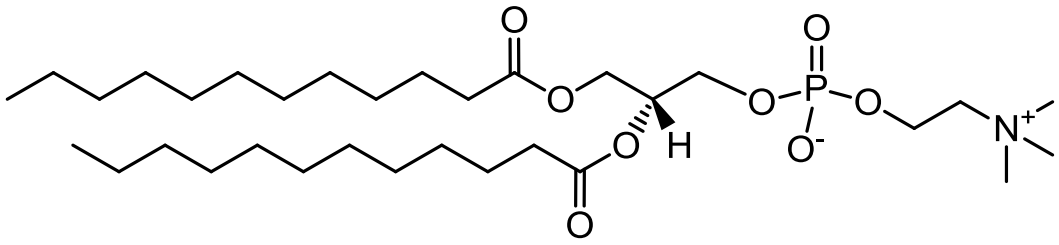

DMPC

14:0 PC

1,2-dimyristoyl-*sn*-glycero-3-phosphocholine

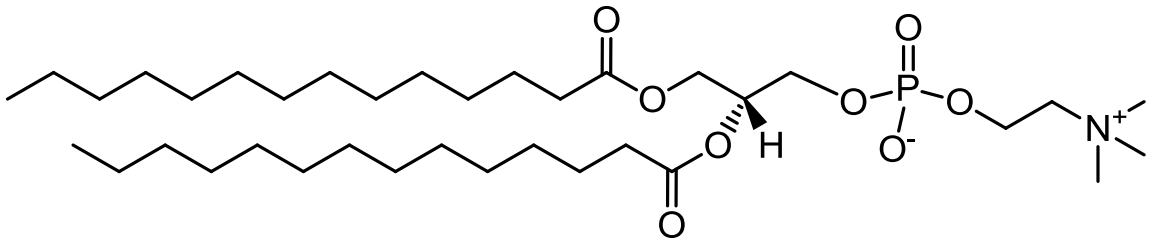

DPPC

16:0 PC

1,2-dipalmitoyl-*sn*-glycero-3-phosphocholine

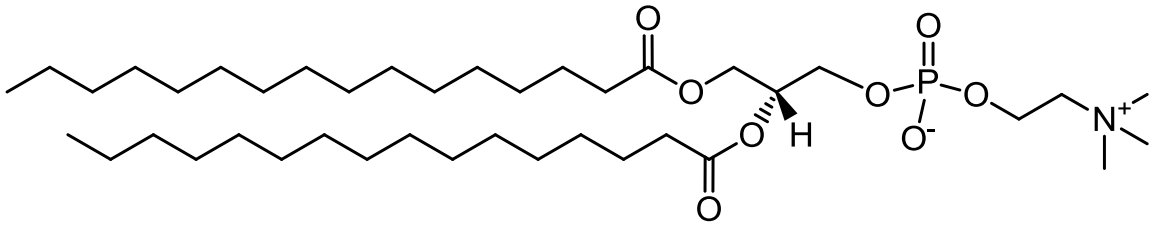

DOPC

18:1 (Δ9-Cis) PC

1,2-dioleoyl-*sn*-glycero-3-phosphocholine

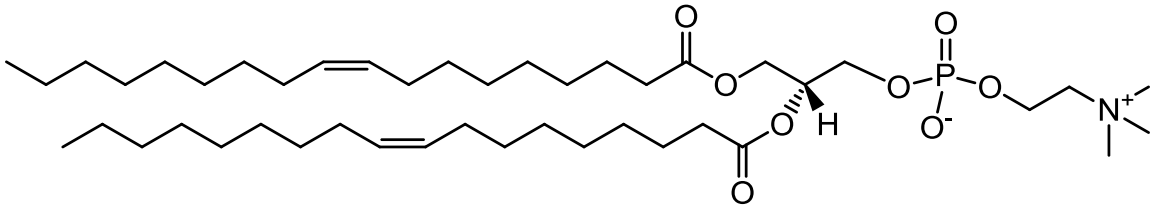

POPC

16:0-18:1 PC

1-palmitoyl-2-oleoyl-*sn*-glycero-3-phosphocholine

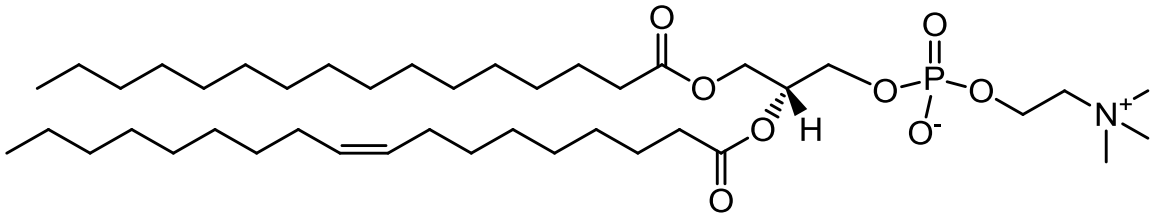

DCPG

10:0 PG

1,2-didecanoyl-*sn*-glycero-3-phospho-(1'-*rac*-glycerol) (sodium salt)

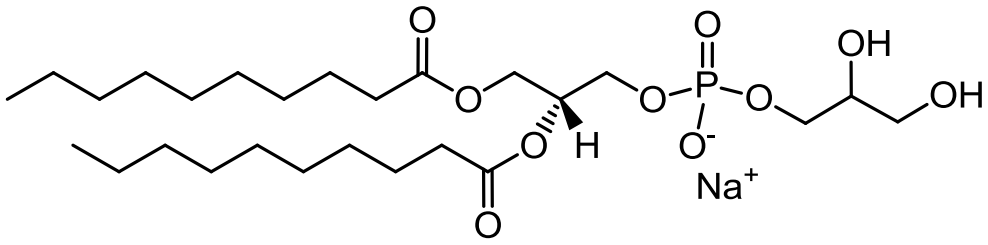

DLPG

12:0 PG

1,2-dilauroyl-*sn*-glycero-3-phospho-(1'-*rac*-glycerol) (sodium salt)

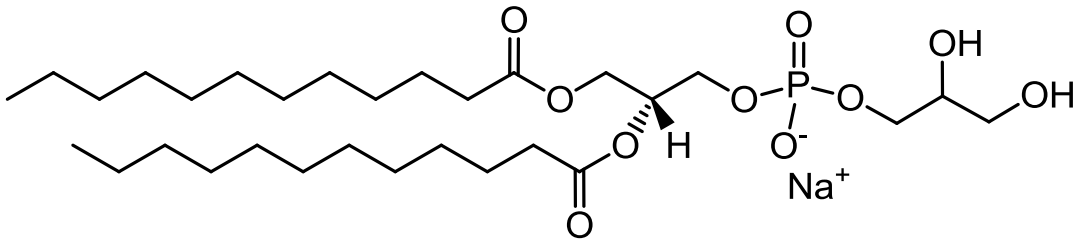

DMPG

14:0 PG

1,2-dimyristoyl-*sn*-glycero-3-phospho-(1'-rac-glycerol) (sodium salt)

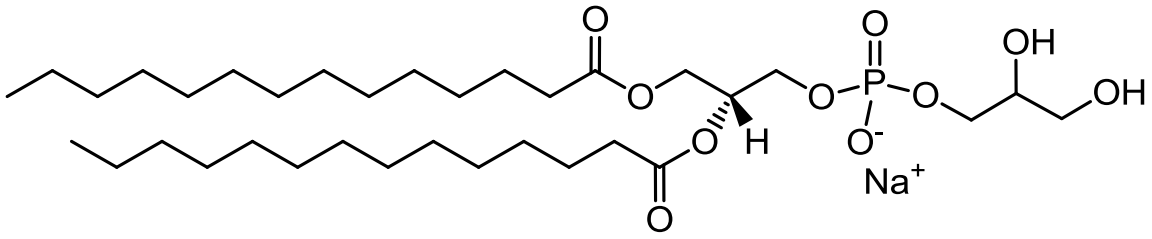

DPPG

16:0 PG

1,2-dipalmitoyl-*sn*-glycero-3-phospho-(1'-*rac*-glycerol) (sodium salt)

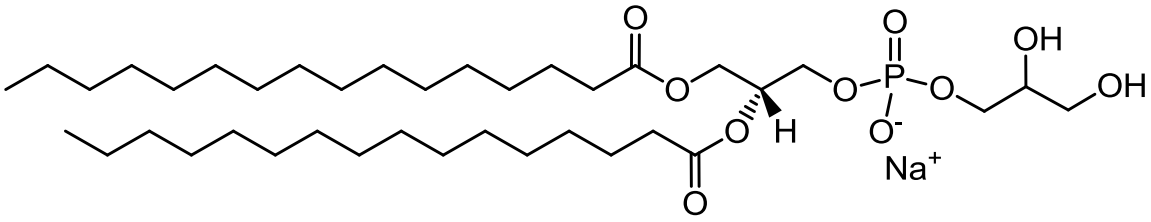

POPG

16:0-18:1 PG

1-palmitoyl-2-oleoyl-*sn*-glycero-3-phospho-(1'-*rac*-glycerol) (sodium salt)

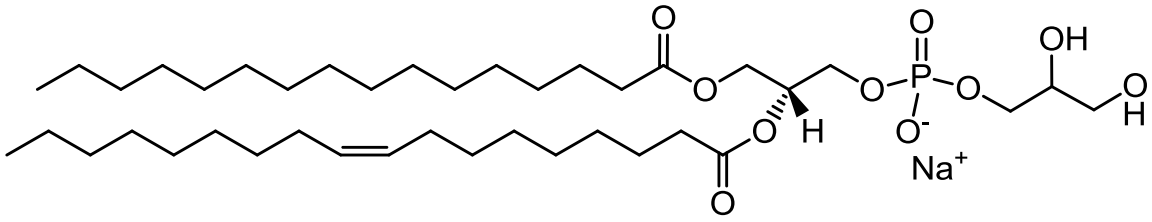

DCPS

10:0 PS

1,2-didecanoyl-*sn*-glycero-3-phospho-L-serine (sodium salt)

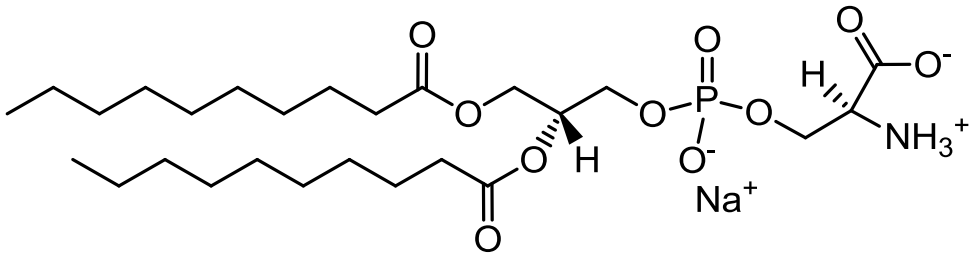

DLPS

12:0 PS

1,2-dilauroyl-*sn*-glycero-3-phospho-L-serine (sodium salt)

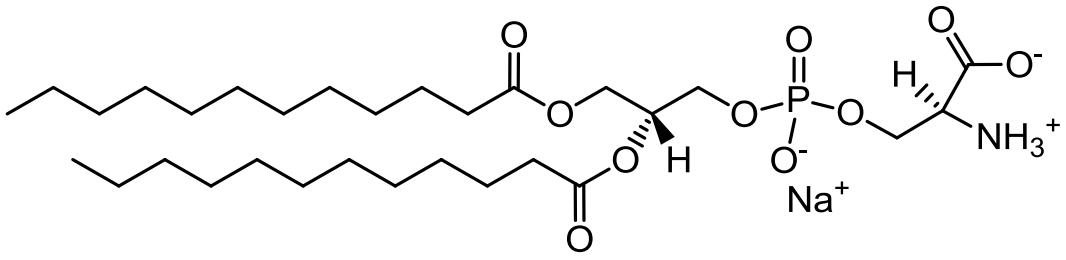

DMPS

14:0 PS

1,2-dimyristoyl-*sn*-glycero-3-phospho-L-serine (sodium salt)

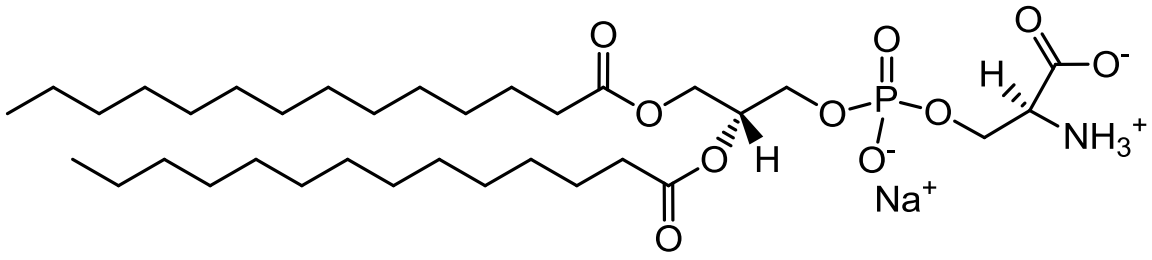

DPPS

18:0 PS

1,2-distearoyl-*sn*-glycero-3-phospho-L-serine (sodium salt)

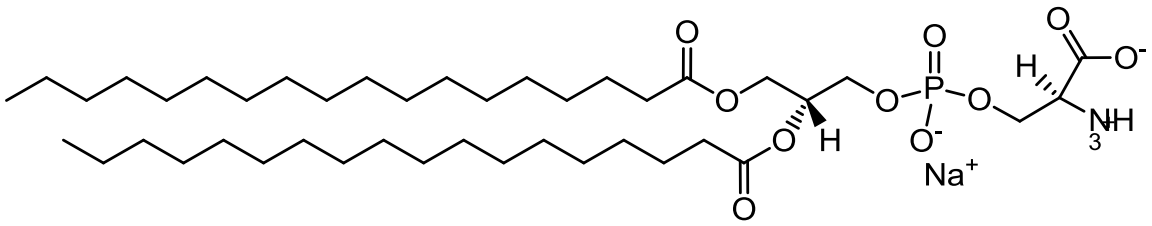

POPS

16:0-18:1 PS

1-palmitoyl-2-oleoyl-*sn*-glycero-3-phospho-L-serine (sodium salt)

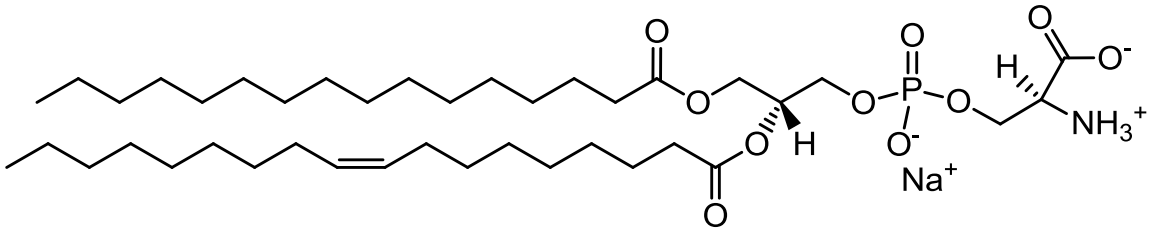

DCPA

10:0 PA

1,2-didecanoyl-*sn*-glycero-3-phosphate (sodium salt)

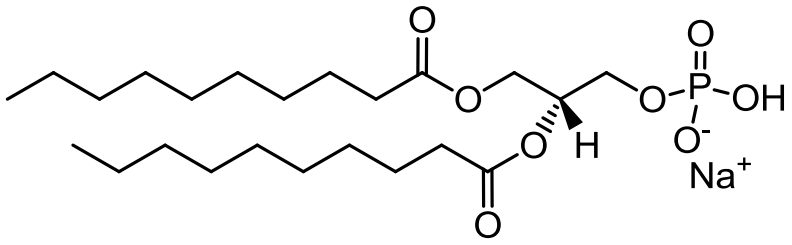

DLPA

12:0 PA

1,2-dilauroyl-*sn*-glycero-3-phosphate (sodium salt)

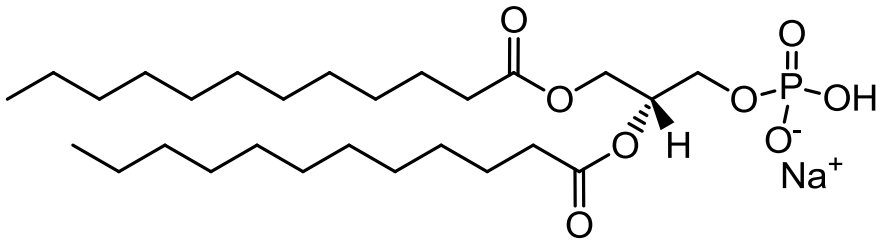

DMPA

14:0 PA

1,2-dimyristoyl-*sn*-glycero-3-phosphate (sodium salt)

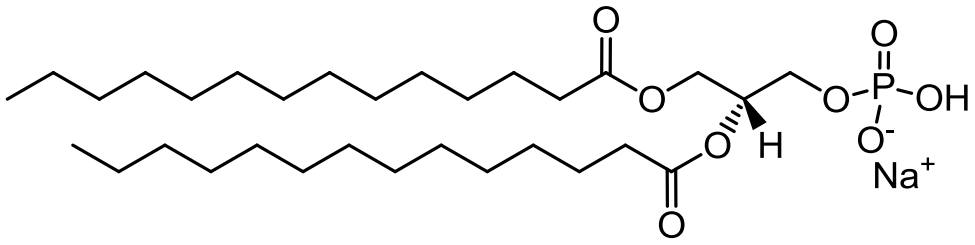

DOPE

18:1 (Δ9-Cis) PE

1,2-dioleoyl-*sn*-glycero-3-phosphoethanolamine

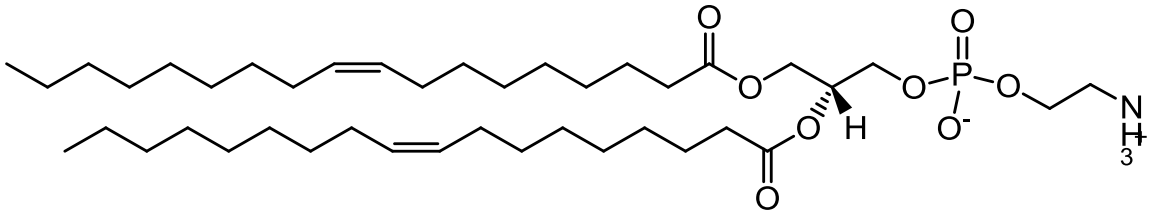

Cardiolipin

18:1 Cardiolipin

1',3'-bis[1,2-dioleoyl-*sn*-glycero-3-phospho]-*sn*-glycerol (sodium salt)

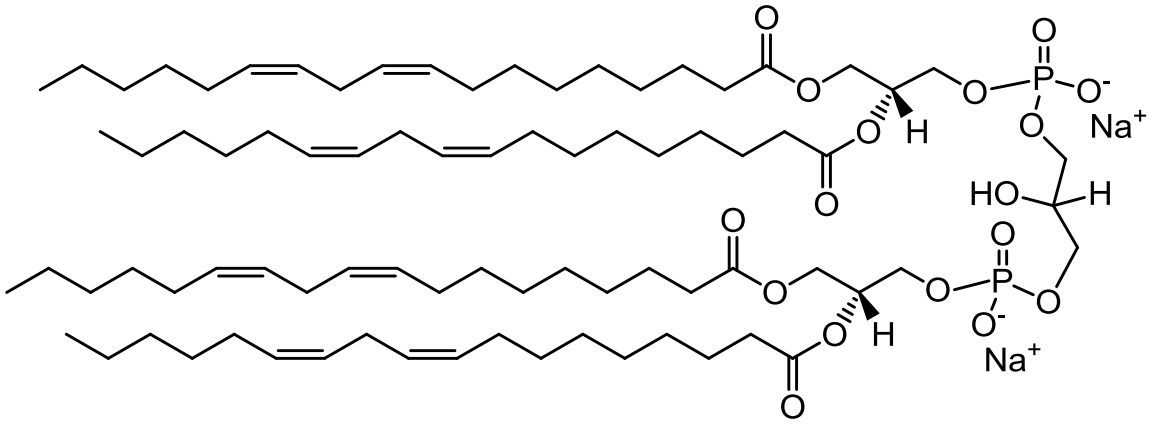

LPC-C14

14:0 Lyso PC

1-myristoyl-2-hydroxy-*sn*-glycero-3-phosphocholine

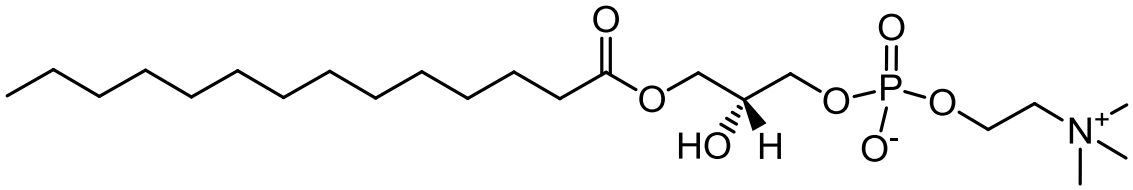

LPG-C14

14:0 Lyso PG

1-myristoyl-2-hydroxy-*sn*-glycero-3-phospho-(1'-*rac*-glycerol) (sodium salt)

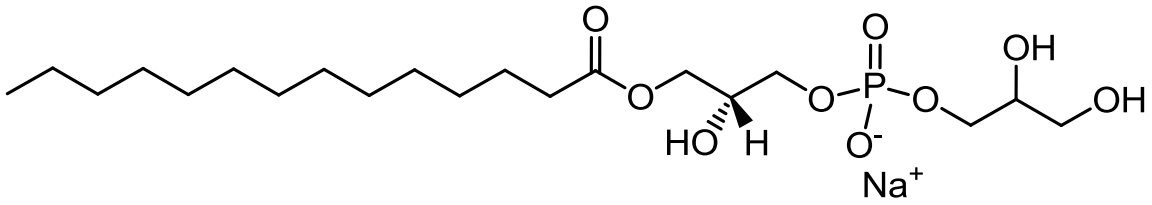

DPC

MAPCHO-12

n-dodecylphosphocholine

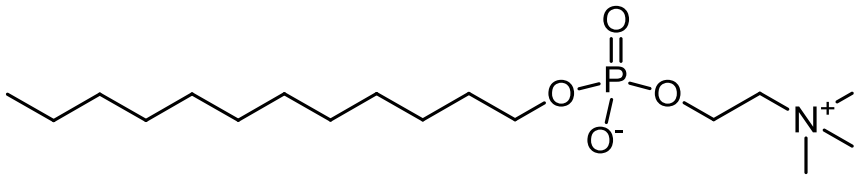

DTAB

Dodecyltrimethylammonium bromide

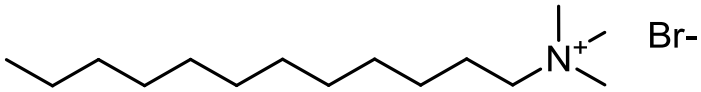

NLS

Sodium lauroyl sarcosinate

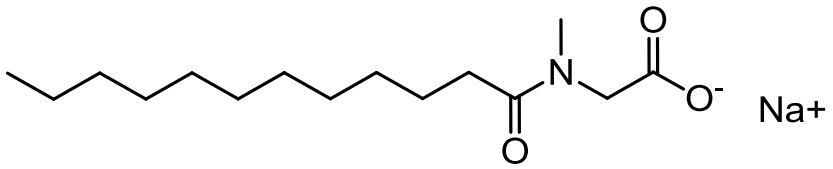

SDS

Sodium dodecyl sulfate

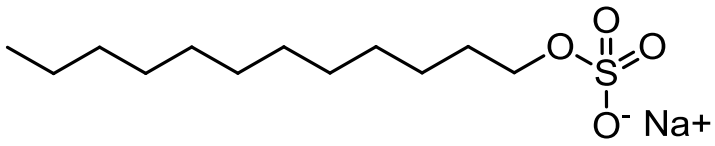

SOS

Sodium octyl sulfate

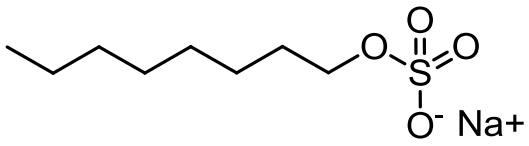

References

Ahmed, M., J. Davis, et al. (2010). "Structural conversion of neurotoxic amyloid-beta(1-42) oligomers to fibrils." Nat Struct Mol Biol **17**(5): 561-567.

Andersen, N. H., Z. Liu, et al. (1996). "Efforts toward deriving the CD spectrum of a 310 helix in aqueous medium." FEBS letters **399**(1): 47-52.

Andersen, O. S. and R. E. Koeppe (2007). "Bilayer Thickness and Membrane Protein Function: An Energetic Perspective." Annual Review of Biophysics and Biomolecular Structure **36**(1): 107-130.

Arrastua, L., E. San Sebastian, et al. (2003). "In vitro fusion between Saccharomyces cerevisiae secretory vesicles and cytoplasmic-side-out plasma membrane vesicles." Biochem J **370**(Pt 2): 641-649.

Barroso, R. P., K. A. Riske, et al. (2010). "Ionization and structural changes of the DMPG vesicle along its anomalous gel-fluid phase transition: a study with different lipid concentrations." Langmuir **26**(17): 13805-13814.

Barth, A., S. R. Martin, et al. (1998). "Resolution of Trp near UV CD spectra of calmodulin-domain peptide complexes into the 1La and 1Lb component spectra." Biopolymers **45**(7): 493-501.

Batenburg, J. J., W. Klazinga, et al. (1985). "Regulation and location of phosphatidylglycerol and phosphatidylinositol synthesis in type II cells isolated from fetal rat lung." Biochim Biophys Acta **833**(1): 17-24.

Bello, J., H. R. Bello, et al. (1982). "Conformation and aggregation of melittin: dependence on pH and concentration." Biochemistry **21**(3): 461-465.

Benzinger, T. L. S., D. M. Gregory, et al. (1998). "Propagating structure of Alzheimer's β-amyloid(10–35) is parallel β-sheet with residues in exact register." Proceedings of the National Academy of Sciences **95**(23): 13407-13412.

Bernstein, S. L., N. F. Dupuis, et al. (2009). "Amyloid-beta protein oligomerization and the importance of tetramers and dodecamers in the aetiology of Alzheimer's disease." Nat Chem **1**(4): 326-331.

Bohinc, K., A. Iglič, et al. (2005). "Self-assembly of linear aggregates on curved membranes." Europhys. Lett. **71**(1): 145-151.

Bokvist, M., F. Lindstrom, et al. (2004). "Two types of Alzheimer's beta-amyloid (1-40) peptide membrane interactions: aggregation preventing transmembrane anchoring versus accelerated surface fibril formation." J Mol Biol **335**(4): 1039-1049.

Bossy-Wetzel, E., R. Schwarzenbacher, et al. (2004). "Molecular pathways to neurodegeneration." Nat Med **10 Suppl**: S2-9.

Botto, M. (2004). "Phosphatidylserine receptor and apoptosis: consequences of a non-ingested meal." Arthritis Res Ther **6**(4): 147-150.

Brahms, S., J. Brahms, et al. (1977). "Identification of beta,beta-turns and unordered conformations in polypeptide chains by vacuum ultraviolet circular dichroism." Proc Natl Acad Sci U S A **74**(8): 3208-3212.

Brown, D. A. and J. K. Rose (1992). "Sorting of GPI-anchored proteins to glycolipid-enriched membrane subdomains during transport to the apical cell surface." Cell **68**(3): 533-544.

Bruque, S., M. Martinez-Lara, et al. (1987). "Characterization of the interlayer water in niobyl phosphate hydrates by IR and NMR spectroscopies." Inorganic Chemistry **26**(6): 847-850.

Burkoth, T. S., T. L. S. Benzinger, et al. (2000). "Structure of the β-Amyloid(10-35) Fibril." Journal of the American Chemical Society **122**(33): 7883-7889.

Cabrera-Poch, N., L. Sanchez-Ruiloba, et al. (2004). "Lipid raft disruption triggers protein kinase C and Src-dependent protein kinase D activation and Kidins220 phosphorylation in neuronal cells." J Biol Chem **279**(27): 28592-28602.

Calderon, F. and H. Y. Kim (2008). "Detection of intracellular phosphatidylserine in living cells." J Neurochem **104**(5): 1271-1279.

Cataldo, A. M., C. M. Peterhoff, et al. (2000). "Endocytic pathway abnormalities precede amyloid beta deposition in sporadic Alzheimer's disease and Down syndrome: differential effects of APOE genotype and presenilin mutations." Am J Pathol **157**(1): 277-286.

Chakraborty, T. R., A. Vancura, et al. (1999). "Phosphatidic acid synthesis in mitochondria. Topography of formation and transmembrane migration." J Biol Chem **274**(42): 29786-29790.

Chapman, M. R., L. S. Robinson, et al. (2002). "Role of Escherichia coli curli operons in directing amyloid fiber formation." Science **295**(5556): 851-855.

Chattopadhyay, A., S. Mukherjee, et al. (1997). "Ionization, partitioning, and dynamics of tryptophan octyl ester: implications for membrane-bound tryptophan residues." Biophys J **73**(2): 839-849.

Chen, Y. A. and R. H. Scheller (2001). "SNARE-mediated membrane fusion." Nat Rev Mol Cell Biol **2**(2): 98-106.

Childers, W. S. (2010). Amyloid: Merging the Properties of Membranes and Enzymes. Chemistry. Atlanta, Emory University. **Doctorate of Philosophy**.

Childers, W. S., A. K. Mehta, et al. (2009). "Templating molecular arrays in amyloid's cross-beta grooves." J Am Chem Soc **131**(29): 10165-10172.

Clifford, P. M., S. Zarrabi, et al. (2007). "Abeta peptides can enter the brain through a defective blood-brain barrier and bind selectively to neurons." Brain Res **1142**: 223-236.

Cox, D. L., R. R. Sing, et al. (2006). "Prion disease: exponential growth requires membrane binding." Biophys J **90**(11): L77-79.

Crisma, M., M. Saviano, et al. (2007). "Peptide α/310-Helix Dimorphism in the Crystal State." Journal of the American Chemical Society **129**(50): 15471-15473.

Dewald, A. H., J. C. Hodges, et al. (2011). "Physical determinants of beta-barrel membrane protein folding in lipid vesicles." Biophys J **100**(9): 2131-2140.

Ding, L., K. Chen, et al. (2003). "The pentapeptide GGAGG has PII conformation." J Am Chem Soc **125**(27): 8092-8093.

Dodge, J. T. and G. B. Phillips (1967). "Composition of phospholipids and of phospholipid fatty acids and aldehydes in human red cells." J Lipid Res **8**(6): 667-675.

Dong, J., J. M. Canfield, et al. (2007). "Engineering metal ion coordination to regulate amyloid fibril assembly and toxicity." Proceedings of the National Academy of Sciences **104**(33): 13313-13318.

Dong, J., J. M. Canfield, et al. (2007). "Engineering metal ion coordination to regulate amyloid fibril assembly and toxicity." Proc Natl Acad Sci U S A **104**(33): 13313-13318.

Dong, J., K. Lu, et al. (2006). "Controlling amyloid growth in multiple dimensions." Amyloid **13**(4): 206-215.

Dong, J., J. E. Shokes, et al. (2006). "Modulating amyloid self-assembly and fibril morphology with Zn(II)." J Am Chem Soc **128**(11): 3540-3542.

Dorado, A. P., M. A. Llorente, et al. (1994). "Influence of adventitious light scattering on fluorescence anisotropy measurements with front-face excitation. Simulation and correction." Journal of Photochemistry and Photobiology A: Chemistry **78**(3): 193-200.

Dos Santos, S., A. Chandravarkar, et al. (2005). "Switch-peptides: controlling self-assembly of amyloid beta-derived peptides in vitro by consecutive triggering of acyl migrations." J Am Chem Soc **127**(34): 11888-11889.

Ebel, H., P. Grabitz, et al. (2001). "Enthalpy and volume changes in lipid membranes. I. The proportionality of heat and volume changes in the lipid melting transition and its implication for the elastic constants." Journal of Physical Chemistry B **105**(30): 7353-7360.

Eichner, T. and S. E. Radford (2009). "A generic mechanism of beta2-microglobulin amyloid assembly at neutral pH involving a specific proline switch." J Mol Biol **386**(5): 1312-1326.

Eker, F., K. Griebenow, et al. (2004). "Abeta(1-28) fragment of the amyloid peptide predominantly adopts a polyproline II conformation in an acidic solution." Biochemistry **43**(22): 6893-6898.

Ellens, H., J. Bentz, et al. (1985). "H+-Induced and Ca-2+-Induced Fusion and Destabilization of Liposomes." Biochemistry **24**(13): 3099-3106.

Ellis, G., E. Fang, et al. (2010). "Lipid oxidation and modification of amyloid-beta (Abeta) in vitro and in vivo." J Alzheimers Dis **22**(2): 593-607.

Farber, P., H. Darmawan, et al. (2010). "Analyzing protein folding cooperativity by differential scanning calorimetry and NMR spectroscopy." J Am Chem Soc **132**(17): 6214-6222.

Fattal, D. R. and A. Ben-Shaul (1993). "A molecular model for lipid-protein interaction in membranes: the role of hydrophobic mismatch." Biophysical journal **65**(5): 1795-1809.

Feng, L., R. Orlando, et al. (2006). "Amide proton back-exchange in deuterated peptides: applications to MS and NMR analyses." Anal Chem **78**(19): 6885-6892.

Friedman, R., R. Pellarin, et al. (2009). "Amyloid aggregation on lipid bilayers and its impact on membrane permeability." J Mol Biol **387**(2): 407-415.

Gasymov, O. K., A. R. Abduragimov, et al. (2003). "Resolving near-ultraviolet circular dichroism spectra of single trp mutants in tear lipocalin." Anal Biochem **318**(2): 300-308.

Gomez, E. W., N. G. Clack, et al. (2009). "Like-charge interactions between colloidal particles are asymmetric with respect to sign." Soft Matter **5**(9): 1931-1936.

Gong, X., X. Tang, et al. (2003). "Cdk5-mediated inhibition of the protective effects of transcription factor MEF2 in neurotoxicity-induced apoptosis." Neuron **38**(1): 33-46.

Gorman, P. M. and A. Chakrabartty (2001). "Alzheimer beta-amyloid peptides: structures of amyloid fibrils and alternate aggregation products." Biopolymers **60**(5): 381-394.

Griffith, J. S. (1967). "Self-replication and scrapie." Nature **215**(5105): 1043-1044.

Griffiths, P. C., A. Paul, et al. (2005). "A small-angle neutron scattering study of biologically relevant mixed surfactant micelles comprising 1,2-diheptanoyl-sn-phosphatidylcholine and sodium dodecyl sulfate or dodecyltrimethylammonium bromide." Soft Matter **1**(2): 152-159.

Gryczynski, I., W. Wiczk, et al. (1988). "Lifetime distributions and anisotropy decays of indole fluorescence in cyclohexane/ethanol mixtures by frequency-domain fluorometry." Biophys Chem **32**(2-3): 173-185.

Haataja, L., T. Gurlo, et al. (2008). "Islet amyloid in type 2 diabetes, and the toxic oligomer hypothesis." Endocr Rev **29**(3): 303-316.

Haris, P. I. and F. Severcan (1999). "FTIR spectroscopic characterization of protein structure in aqueous and non-aqueous media." Journal of Molecular Catalysis B: Enzymatic **7**(1-4): 207-221.

Harper, J. D., S. S. Wong, et al. (1999). "Assembly of A beta amyloid protofibrils: an in vitro model for a possible early event in Alzheimer's disease." Biochemistry **38**(28): 8972-8980.

Hartmann, T., S. C. Bieger, et al. (1997). "Distinct sites of intracellular production for Alzheimer's disease A beta40/42 amyloid peptides." Nat Med **3**(9): 1016-1020.

He, W. and C. J. Barrow (1999). "The A beta 3-pyroglutamyl and 11-pyroglutamyl peptides found in senile plaque have greater beta-sheet forming and aggregation propensities in vitro than full-length A beta." Biochemistry **38**(33): 10871-10877.

Heimburg, T. (2007). Thermal biophysics of membranes. Weinheim, Wiley-VCH Verlag.

Heimburg, T. and R. L. Biltonen (1994). "Thermotropic behavior of dimyristoylphosphatidylglycerol and its interaction with cytochrome c." Biochemistry **33**(32): 9477-9488.

Heimburg, T. and R. L. Biltonen (1996). "A Monte Carlo simulation study of protein-induced heat capacity changes and lipid-induced protein clustering." Biophysical journal **70**(1): 84-96.

Hill, S. E., T. Miti, et al. (2011). "Spatial extent of charge repulsion regulates assembly pathways for lysozyme amyloid fibrils." PLoS One **6**(4): e18171.

Hoekstra, D., T. de Boer, et al. (1984). "Fluorescence method for measuring the kinetics of fusion between biological membranes." Biochemistry **23**(24): 5675-5681.

Horwich, A. L., W. A. Fenton, et al. (2007). "Two families of chaperonin: physiology and mechanism." Annual review of cell and developmental biology **23**: 115-145.

Jacobsen, N. E. (2007). NMR spectroscopy explained : simplified theory, applications and examples for organic chemistry and structural biology. Hoboken, N.J., Wiley-Interscience.

Jarrett, J. T. and P. T. Lansbury, Jr. (1993). "Seeding "one-dimensional crystallization" of amyloid: a pathogenic mechanism in Alzheimer's disease and scrapie?" Cell **73**(6): 1055-1058.

Ji, S. R., Y. Wu, et al. (2002). "Cholesterol is an important factor affecting the membrane insertion of beta-amyloid peptide (A beta 1-40), which may potentially inhibit the fibril formation." J Biol Chem **277**(8): 6273-6279.

Karplus, P. A. (1997). "Hydrophobicity regained." Protein Sci **6**(6): 1302-1307.

Kayed, R., E. Head, et al. (2003). "Common structure of soluble amyloid oligomers implies common mechanism of pathogenesis." Science **300**(5618): 486-489.

Keleti, T. (1970). "The excimer fluorescence of tryptophan, tyrosine and d-glyceraldehyde-3-phosphate dehydrogenase." FEBS Lett **7**(3): 280-282.

Killian, J. A. (1998). "Hydrophobic mismatch between proteins and lipids in membranes." Biochim Biophys Acta **1376**(3): 401-415.

Kim, J. and M. Lee (2004). "Observation of multi-step conformation switching in [beta]-amyloid peptide aggregation by fluorescence resonance energy transfer." Biochemical and Biophysical Research Communications **316**(2): 393-397.

Kim, W., K. I. Hardcastle, et al. (2006). "Fluoroproline Flip-Flop: Regiochemical Reversal of a Stereoelectronic Effect on Peptide and Protein Structures." Angewandte Chemie International Edition **45**(48): 8141-8145.

Kobatake, Y., I. Tasaki, et al. (1971). "Phase transition in membrane with reference to nerve excitation." Adv Biophys **2**: 1-31.

Korade, Z. and A. K. Kenworthy (2008). "Lipid rafts, cholesterol, and the brain." Neuropharmacology **55**(8): 1265-1273.

Kowalewski, T. and D. M. Holtzman (1999). "In situ atomic force microscopy study of Alzheimer's beta-amyloid peptide on different substrates: new insights into mechanism of beta-sheet formation." Proc Natl Acad Sci U S A **96**(7): 3688-3693.

Kremer, J. J. and R. M. Murphy (2003). "Kinetics of adsorption of beta-amyloid peptide Abeta(1-40) to lipid bilayers." J Biochem Biophys Methods **57**(2): 159-169.

Kremer, J. J., M. M. Pallitto, et al. (2000). "Correlation of beta-amyloid aggregate size and hydrophobicity with decreased bilayer fluidity of model membranes." Biochemistry **39**(33): 10309-10318.

LaFerla, F. M., K. N. Green, et al. (2007). "Intracellular amyloid-[beta] in Alzheimer's disease." Nat Rev Neurosci **8**(7): 499-509.

Lakowicz, J. R. (2006). Principles of fluorescence spectroscopy. New York, Springer.

Lashuel, H. A., D. Hartley, et al. (2002). "Neurodegenerative disease: amyloid pores from pathogenic mutations." Nature **418**(6895): 291.

Lee, G., H. B. Pollard, et al. (2002). "Annexin 5 and apolipoprotein E2 protect against Alzheimer's amyloid-beta-peptide cytotoxicity by competitive inhibition at a common phosphatidylserine interaction site." Peptides **23**(7): 1249-1263.

Lee, J., E. K. Culyba, et al. (2011). "Amyloid-β forms fibrils by nucleated conformational conversion of oligomers." Nat Chem Biol **7**(9): 602-609.

Lewis, R. N. and R. N. McElhaney (2000). "Calorimetric and spectroscopic studies of the thermotropic phase behavior of lipid bilayer model membranes composed of a homologous series of linear saturated phosphatidylserines." Biophys J **79**(4): 2043-2055.

Lewis, R. N. and R. N. McElhaney (2000). "Calorimetric and spectroscopic studies of the thermotropic phase behavior of lipid bilayer model membranes composed of a homologous series of linear saturated phosphatidylserines." Biophysical journal **79**(4): 2043-2055.

Liang, Y., P. Guo, et al. (2008). "Light harvesting antenna on an amyloid scaffold." Chem Commun (Camb)(48): 6522-6524.

Liang, Y., D. G. Lynn, et al. (2010). "Direct Observation of Nucleation and Growth in Amyloid Self-Assembly." Journal of the American Chemical Society **132**(18): 6306-6308.

Liang, Y., S. V. Pingali, et al. (2008). "Cross-Strand Pairing and Amyloid Assembly." Biochemistry **47**(38): 10018-10026.

Lingwood, D. and K. Simons (2010). "Lipid Rafts As a Membrane-Organizing Principle." Science **327**(5961): 46-50.

Liu, R.-Q., Q.-H. Zhou, et al. (2010). "Membrane Localization of β-Amyloid 1–42 in Lysosomes." Journal of Biological Chemistry **285**(26): 19986-19996.

Lu, K. (2006). Discovery of diverse peptide nanotube architecture from the self-assembly of designed amyloid cassettes. Chemistry. Atlanta, Emory University. **Doctorate of Philosophy**.

Lu, K., J. Jacob, et al. (2003). "Exploiting Amyloid Fibril Lamination for Nanotube Self-Assembly." Journal of the American Chemical Society **125**(21): 6391-6393.

Maekawa, H., C. Toniolo, et al. (2006). "Different spectral signatures of octapeptide 3(10)- and alpha-helices revealed by two-dimensional infrared spectroscopy." Journal of Physical Chemistry B **110**(12): 5834-5837.

Mamdouh, Z., M.-C. Giocondi, et al. (1996). "Temperature dependence of endocytosis in renal epithelial cells in culture." Biochimica et Biophysica Acta (BBA) - Biomembranes **1282**(2): 171-173.

Manning, M. C. and R. W. Woody (1991). "Theoretical CD studies of polypeptide helices: examination of important electronic and geometric factors." Biopolymers **31**(5): 569-586.

Mansour, H., D.-S. Wang, et al. (2001). "Comparison of Bilayer and Monolayer Properties of Phospholipid Systems Containing Dipalmitoylphosphatidylglycerol and Dipalmitoylphosphatidylinositol." Langmuir **17**(21): 6622-6632.

Mao, Z., A. Bonni, et al. (1999). "Neuronal activity-dependent cell survival mediated by transcription factor MEF2." Science **286**(5440): 785-790.

Martens, S. and H. T. McMahon (2008). "Mechanisms of membrane fusion: disparate players and common principles." Nat Rev Mol Cell Biol **9**(7): 543-556.

Masibay, A. S., P. V. Balaji, et al. (1993). "Mutational analysis of the Golgi retention signal of bovine beta-1,4-galactosyltransferase." J Biol Chem **268**(13): 9908-9916.

Matsumura, S., K. Shinoda, et al. (2011). "Two distinct amyloid beta-protein (Abeta) assembly pathways leading to oligomers and fibrils identified by combined fluorescence correlation spectroscopy, morphology, and toxicity analyses." J Biol Chem **286**(13): 11555-11562.

Mattson, M. P. (1997). "Cellular actions of beta-amyloid precursor protein and its soluble and fibrillogenic derivatives." Physiol Rev **77**(4): 1081-1132.

Mattson, M. P. (2004). "Pathways towards and away from Alzheimer's disease." Nature **430**(7000): 631-639.

McGlinchey, R. P., F. Shewmaker, et al. (2011). "Repeat domains of melanosome matrix protein Pmel17 orthologs form amyloid fibrils at the acidic melanosomal pH." J Biol Chem **286**(10): 8385-8393.

Mehta, A. K., K. Lu, et al. (2008). "Facial symmetry in protein self-assembly." J Am Chem Soc **130**(30): 9829-9835.

Minkeviciene, R., S. Rheims, et al. (2009). "Amyloid β-Induced Neuronal Hyperexcitability Triggers Progressive Epilepsy." The Journal of Neuroscience **29**(11): 3453-3462.

Mitra, K., I. Ubarretxena-Belandia, et al. (2004). "Modulation of the bilayer thickness of exocytic pathway membranes by membrane proteins rather than cholesterol." Proceedings of the National Academy of Sciences of the United States of America **101**(12): 4083-4088.

Morgan, D. M., J. Dong, et al. (2002). "Metal switch for amyloid formation: insight into the structure of the nucleus." J Am Chem Soc **124**(43): 12644-12645.

Mukhopadhyay, P., L. Monticelli, et al. (2004). "Molecular dynamics simulation of a palmitoyl-oleoyl phosphatidylserine bilayer with Na+ counterions and NaCl." Biophys J **86**(3): 1601-1609.

Müller, W., A. Eckert, et al. (2010). "Mitochondrial Dysfunction: Common Final Pathway in Brain Aging and Alzheimer’s Disease—Therapeutic Aspects." Molecular Neurobiology **41**(2): 159-171.

Munro, S. (1995). "An investigation of the role of transmembrane domains in Golgi protein retention." EMBO J **14**(19): 4695-4704.

Murphy, R. M. (2007). "Kinetics of amyloid formation and membrane interaction with amyloidogenic proteins." Biochimica et biophysica acta **1768**(8): 1923-1934.

Murray, D. and B. Honig (2002). "Electrostatic control of the membrane targeting of C2 domains." Mol Cell **9**(1): 145-154.

Murray, D. H. and L. K. Tamm (2009). "Clustering of syntaxin-1A in model membranes is modulated by phosphatidylinositol 4,5-bisphosphate and cholesterol." Biochemistry **48**(21): 4617-4625.

Nagele, R. G., M. R. D'Andrea, et al. (2002). "Intracellular accumulation of beta-amyloid(1-42) in neurons is facilitated by the alpha 7 nicotinic acetylcholine receptor in Alzheimer's disease." Neuroscience **110**(2): 199-211.

Naslund, J., A. Schierhorn, et al. (1994). "Relative abundance of Alzheimer A beta amyloid peptide variants in Alzheimer disease and normal aging." Proc Natl Acad Sci U S A **91**(18): 8378-8382.

Nixon, R. A. and A. M. Cataldo (2006). "Lysosomal system pathways: genes to neurodegeneration in Alzheimer's disease." J Alzheimers Dis **9**(3 Suppl): 277-289.

O'Nuallain, B., A. K. Thakur, et al. (2006). "Kinetics and thermodynamics of amyloid assembly using a high-performance liquid chromatography-based sedimentation assay." Methods Enzymol **413**: 34-74.

Pal, R., Y. Barenholz, et al. (1988). "Pyrene phospholipid as a biological fluorescent probe for studying fusion of virus membrane with liposomes." Biochemistry **27**(1): 30-36.

Pande, A. H., S. Qin, et al. (2005). "Membrane fluidity is a key modulator of membrane binding, insertion, and activity of 5-lipoxygenase." Biophys J **88**(6): 4084-4094.

Parbhu, A., H. Lin, et al. (2002). "Imaging real-time aggregation of amyloid beta protein (1-42) by atomic force microscopy." Peptides **23**(7): 1265-1270.

Park, K., A. Perczel, et al. (1992). "Differentiation between transmembrane helices and peripheral helices by the deconvolution of circular dichroism spectra of membrane proteins." Protein science : a publication of the Protein Society **1**(8): 1032-1049.

Petkova, A. T., Y. Ishii, et al. (2002). "A structural model for Alzheimer's beta -amyloid fibrils based on experimental constraints from solid state NMR." Proc Natl Acad Sci U S A **99**(26): 16742-16747.

Pike, L. J. (2009). "The challenge of lipid rafts." Journal of Lipid Research **50**(Supplement): S323-S328.

Poirier, M. A., H. Li, et al. (2002). "Huntingtin spheroids and protofibrils as precursors in polyglutamine fibrilization." J Biol Chem **277**(43): 41032-41037.

Prusiner, S. B. (1982). "Novel proteinaceous infectious particles cause scrapie." Science **216**(4542): 136-144.

Quetglas, S., C. Iborra, et al. (2002). "Calmodulin and lipid binding to synaptobrevin regulates calcium-dependent exocytosis." EMBO J **21**(15): 3970-3979.

Robbins, R. J., G. R. Fleming, et al. (1980). "Photophysics of aqueous tryptophan: pH and temperature effects." Journal of the American Chemical Society **102**: 6271-6279.

Robertson, J. D. (1959). "The ultrastructure of cell membranes and their derivatives." Biochem Soc Symp **16**: 3-43.

Roux, S., E. Zekri, et al. (2008). "Elimination and exchange of trifluoroacetate counter-ion from cationic peptides: a critical evaluation of different approaches." J Pept Sci **14**(3): 354-359.

Rucker, A. L. and T. P. Creamer (2002). "Polyproline II helical structure in protein unfolded states: lysine peptides revisited." Protein Sci **11**(4): 980-985.

Sabate, R., M. Gallardo, et al. (2005). "Spontaneous incorporation of beta-amyloid peptide into neutral liposomes." Colloids and Surfaces a-Physicochemical and Engineering Aspects **270**: 13-17.

Sachs, J. N. and D. M. Engelman (2006). "Introduction to the membrane protein reviews: the interplay of structure, dynamics, and environment in membrane protein function." Annu Rev Biochem **75**: 707-712.

Sadler, D. M., E. Rivas, et al. (1984). "Measurements of membrane thickness by small-angle scattering of suspensions: results for reconstituted Rhodopseudomonas sphaeroides reaction-center protein and for lipids." Biochemistry **23**(12): 2704-2712.

Safarzadeh-Amiri, A., M. Thompson, et al. (1989). "Trans-4-Dimethylamino-4'-(1-oxobutyl)stilbene: a new fluorescent probe of the bilayer lipid membrane." Journal of Photochemistry and Photobiology A: Chemistry **47**(3): 299-308.

Saido, T. C., T. Iwatsubo, et al. (1995). "Dominant and differential deposition of distinct beta-amyloid peptide species, A beta N3(pE), in senile plaques." Neuron **14**(2): 457-466.

Santini, S., G. Wei, et al. (2004). "Pathway complexity of Alzheimer's beta-amyloid Abeta16-22 peptide assembly." Structure **12**(7): 1245-1255.

Saupe, S. J. (2007). "A short history of small s: a prion of the fungus Podospora anserina." Prion **1**(2): 110-115.

Schneider, A. S., M. J. Schneider, et al. (1970). "Optical activity of biological membranes: scattering effects and protein conformation." Proc Natl Acad Sci U S A **66**(3): 793-798.

Schneider, M. F., D. Marsh, et al. (1999). "Network formation of lipid membranes: triggering structural transitions by chain melting." Proc Natl Acad Sci U S A **96**(25): 14312-14317.

Seelig, J., S. Nebel, et al. (1993). "Electrostatic and nonpolar peptide-membrane interactions. Lipid binding and functional properties of somatostatin analogues of charge z = +1 to z = +3." Biochemistry **32**(37): 9714-9721.

Senguen, F. T., N. R. Lee, et al. (2011). "Probing aromatic, hydrophobic, and steric effects on the self-assembly of an amyloid-beta fragment peptide." Mol Biosyst **7**(2): 486-496.

Serio, T. R., A. G. Cashikar, et al. (2000). "Nucleated conformational conversion and the replication of conformational information by a prion determinant." Science **289**(5483): 1317-1321.

Serrano, A. L., T. Troxler, et al. (2010). "Photophysics of a Fluorescent Non-natural Amino Acid: p-Cyanophenylalanine." Chem Phys Lett **487**(4-6): 303-306.

Seubert, P., C. Vigo-Pelfrey, et al. (1992). "Isolation and quantification of soluble Alzheimer's beta-peptide from biological fluids." Nature **359**(6393): 325-327.

Sharp, J. S., J. A. Forrest, et al. (2002). "Surface denaturation and amyloid fibril formation of insulin at model lipid-water interfaces." Biochemistry **41**(52): 15810-15819.

Shi, Z., K. Chen, et al. (2006). "Conformation of the backbone in unfolded proteins." Chem Rev **106**(5): 1877-1897.

Shi, Z., K. Chen, et al. (2006). "PII structure in the model peptides for unfolded proteins: studies on ubiquitin fragments and several alanine-rich peptides containing QQQ, SSS, FFF, and VVV." Proteins **63**(2): 312-321.

Shi, Z., C. A. Olson, et al. (2002). "Polyproline II structure in a sequence of seven alanine residues." Proc Natl Acad Sci U S A **99**(14): 9190-9195.

Shi, Z., R. W. Woody, et al. (2002). "Is polyproline II a major backbone conformation in unfolded proteins?" Adv Protein Chem **62**: 163-240.

Silvius, J. R. and J. Gagne (1984). "Lipid Phase-Behavior and Calcium-Induced Fusion of Phosphatidylethanolamine-Phosphatidylserine Vesicles - Calorimetric and Fusion Studies." Biochemistry **23**(14): 3232-3240.

Simakova, O. and N. J. Arispe (2007). "The cell-selective neurotoxicity of the Alzheimer's Abeta peptide is determined by surface phosphatidylserine and cytosolic ATP levels. Membrane binding is required for Abeta toxicity." J Neurosci **27**(50): 13719-13729.

Simons, K. and R. Ehehalt (2002). "Cholesterol, lipid rafts, and disease." The Journal of Clinical Investigation **110**(5): 597-603.

Singer, S. J. and G. L. Nicolson (1972). "The fluid mosaic model of the structure of cell membranes." Science **175**(23): 720-731.

Smith, D. G., G. D. Ciccotosto, et al. (2010). "Histidine 14 modulates membrane binding and neurotoxicity of the Alzheimer's disease amyloid-beta peptide." J Alzheimers Dis **19**(4): 1387-1400.

Smith, D. P., S. E. Radford, et al. (2010). "Elongated oligomers in beta2-microglobulin amyloid assembly revealed by ion mobility spectrometry-mass spectrometry." Proc Natl Acad Sci U S A **107**(15): 6794-6798.

Souillac, P. O., V. N. Uversky, et al. (2002). "Elucidation of the molecular mechanism during the early events in immunoglobulin light chain amyloid fibrillation. Evidence for an off-pathway oligomer at acidic pH." J Biol Chem **277**(15): 12666-12679.

Spinozzi, F., L. Paccamiccio, et al. (2010). "Melting regime of the anionic phospholipid DMPG: new lamellar phase and porous bilayer model." Langmuir **26**(9): 6484-6493.

Sreerama, N. and R. W. Woody (2003). "Structural composition of betaI- and betaII-proteins." Protein Sci **12**(2): 384-388.

Strickland, E. H. (1974). "Aromatic contributions to circular dichroism spectra of proteins." CRC Crit Rev Biochem **2**(1): 113-175.

Tamm, L. K. (2005). Protein-lipid interactions : from membrane domains to cellular networks. Weinheim, Wiley-VCH.

Tang, J., H. Yin, et al. (2009). "Using Two Fluorescent Probes to Dissect the Binding, Insertion, and Dimerization Kinetics of a Model Membrane Peptide." Journal of the American Chemical Society **131**(11): 3816-3817.

Tang, X., X. Wang, et al. (2005). "Cyclin-dependent kinase 5 mediates neurotoxin-induced degradation of the transcription factor myocyte enhancer factor 2." J Neurosci **25**(19): 4823-4834.

Thinakaran, G. and E. H. Koo (2008). "Amyloid precursor protein trafficking, processing, and function." J Biol Chem **283**(44): 29615-29619.

Thiyagarajan, P., T. S. Burkoth, et al. (2000). "pH dependent self assembly of [beta]-amyloid(10-35) and [beta]-amyloid(10-35)-PEG3000." Journal of Applied Crystallography **33**(3 Part 1): 535-539.

Thiyagarajan, P. and D. M. Tiede (1994). "Detergent micelle structure and micelle-micelle interactions determined by small-angle neutron scattering under solution conditions used for membrane protein crystallization." The Journal of Physical Chemistry **98**(40): 10343-10351.

Toniolo, C., A. Polese, et al. (1996). "Circular Dichroism Spectrum of a Peptide 310-Helix." Journal of the American Chemical Society **118**(11): 2744-2745.

Torrent, J., P. Rubens, et al. (2001). "Pressure versus temperature unfolding of ribonuclease A: an FTIR spectroscopic characterization of 10 variants at the carboxy-terminal site." Protein Sci **10**(4): 725-734.

Tsai, H. H., J. B. Lee, et al. (2010). "Folding and membrane insertion of amyloid-beta (25-35) peptide and its mutants: implications for aggregation and neurotoxicity." Proteins **78**(8): 1909-1925.

Uratani, Y., S. Asakura, et al. (1972). "A circular dichroism study of Salmonella flagellin: evidence for conformational change on polymerization." J Mol Biol **67**(1): 85-98.

Vance, J. E. and R. Steenbergen (2005). "Metabolism and functions of phosphatidylserine." Prog Lipid Res **44**(4): 207-234.

Volles, M. J., S. J. Lee, et al. (2001). "Vesicle permeabilization by protofibrillar alpha-synuclein: implications for the pathogenesis and treatment of Parkinson's disease." Biochemistry **40**(26): 7812-7819.

Wimley, W. C. and S. H. White (1996). "Experimentally determined hydrophobicity scale for proteins at membrane interfaces." Nat Struct Biol **3**(10): 842-848.

Wosten, H. A. and M. L. de Vocht (2000). "Hydrophobins, the fungal coat unravelled." Biochim Biophys Acta **1469**(2): 79-86.

Wright, E. R. and V. P. Conticello (2002). "Self-assembly of block copolymers derived from elastin-mimetic polypeptide sequences." Advanced Drug Delivery Reviews **54**(8): 1057-1073.

Wu, J., J. T. Yang, et al. (1992). "Beta-II conformation of all-beta proteins can be distinguished from unordered form by circular dichroism." Anal Biochem **200**(2): 359-364.

Yasin, Z., S. Witting, et al. (2003). "Phosphatidylserine externalization in sickle red blood cells: associations with cell age, density, and hemoglobin F." Blood **102**(1): 365-370.

Yazawa, H., Z. X. Yu, et al. (2001). "Beta amyloid peptide (Abeta42) is internalized via the G-protein-coupled receptor FPRL1 and forms fibrillar aggregates in macrophages." FASEB J **15**(13): 2454-2462.

Yeung, T., G. E. Gilbert, et al. (2008). "Membrane phosphatidylserine regulates surface charge and protein localization." Science **319**(5860): 210-213.

Zachowski, A. (1993). "Phospholipids in animal eukaryotic membranes: transverse asymmetry and movement." Biochem J **294 (Pt 1)**: 1-14.

Zhou, H. and Y. Zhou (2004). "Quantifying the effect of burial of amino acid residues on protein stability." Proteins **54**(2): 315-322.

Zhu, L., M. D. Kemple, et al. (1995). "N-terminus and lysine side chain pKa values of melittin in aqueous solutions and micellar dispersions measured by 15N NMR." Biochemistry **34**(40): 13196-13202.

Zuckermann, M. J. and T. Heimburg (2001). "Insertion and pore formation driven by adsorption of proteins onto lipid bilayer membrane-water interfaces." Biophys J **81**(5): 2458-2472.